Technische Universität München
TUM School of Engineering and Design

OME als Wegbereiter klimaneutraler und schadstofffreier Dieselmotoren

Alexander Daniel Gelner

Vollständiger Abdruck der von der TUM School of Engineering and Design der Technischen Universität München zur Erlangung eines

Doktors der Ingenieurwissenschaften (Dr.-Ing.)

genehmigten Dissertation.

Vorsitz: Prof. Dr. rer. nat. Oliver Lieleg

Prüfer*innen der Dissertation:

1. Prof. Dr.-Ing. Georg Wachtmeister
2. Prof. Dr.-Ing. Michael Günthner

Die Dissertation wurde am 08. 11. 2022 bei der Technischen Universität München eingereicht und durch die TUM School of Engineering and Design am 18. 02. 2023 angenommen.

Vorwort und Danksagung

Die vorliegende Forschungsarbeit basiert auf Ergebnissen und Erkenntnissen, die ich während meiner Tätigkeit als wissenschaftlicher Mitarbeiter am Lehrstuhl für Nachhaltige Mobile Antriebssysteme (vormals: Lehrstuhl für Verbrennungskraftmaschinen) der Technischen Universität München von Oktober 2018 bis März 2022 erlangt habe.

Ich möchte meinem Doktorvater, Herrn Prof. i.R. Dr.-Ing. Georg Wachtmeister, herzlich für die Betreuung dieser Arbeit danken. Besonders hervorzuheben sind hier seine unzähligen Lektionen mit dem Ziel, mein Auge fürs Detail zu schärfen. Außerdem bedanke ich mich für die Übernahme des Korreferates bei Herrn Prof. Dr.-Ing. Michael Günthner sowie bei Herrn Prof. Dr. rer. nat. Oliver Lieleg für die Übernahme des Vorsitzes der Prüfungskommission.

Mein besonderer Dank gilt meinem Mentor, Herrn Dr.-Ing. Dominik Pélerin, der als mein Vorgänger am Lehrstuhl nicht nur durch die Betreuung meiner Studienabschlussarbeiten, sondern auch durch seine ununterbrochene fachliche und überfachliche Unterstützung während meiner Promotion maßgeblichen Anteil an meiner wissenschaftlichen Ausbildung hat.

Dem kollegialen Umfeld am Lehrstuhl bin ich für die Zusammenarbeit und tausendfachen Hilfestellungen innerhalb der letzten Jahre dankbar, ohne welche das Zustandekommen der vorliegenden Arbeit nicht möglich gewesen wäre. Dieser Dank umfasst neben den wissenschaftlichen Angestellten ebenso die Beschäftigten in der mechanischen Werkstatt, im technischen Dienst, im Gebäudemanagement und im Elektroniklabor, sowie die Damen im Sekretariat. Eine Nennung jeder einzelnen dieser Personen sprengt den Rahmen dieser Danksagung. Ich möchte aber betonen, dass sämtliche Beschäftigten des Lehrstuhls über unterschiedliche Wege einen Teil zu dieser Arbeit beigetragen haben, wofür ich sehr dankbar bin. Besonders hervorheben möchte ich dennoch meinen Bürokollegen, den Tribologieexperten Herrn Dr.-Ing. Jürgen Binder, für sämtliche interdisziplinäre Diskussionen und die zahlreichen Ratschläge zu strategischen Vorgehensweisen. Meinem Oberingenieur und OME-Pionier, Herrn Dr.-Ing. habil. Martin Härtl, danke ich für die Co-Autorenschaft zahlreicher Publikationen, welche durch seine scharfsinnigen Verbesserungsvorschläge zweifellos an Qualität gewonnen haben. Mein Dank gilt darüber hinaus Herrn Prof. Dr. Malte Jaensch, der mich als Prof. Wachtmeisters Nachfolger in der Organisation meines Auslandsaufenthalts unterstützt hat.

Da die Forschungsergebnisse größtenteils im Rahmen des von der Bayerischen Forschungsstiftung geförderten Projektes „Sub-Zero-Emissions Dieselmotor“ entstanden sind, möchte ich allen Projektbeteiligten meinen Dank für die Zusammenarbeit und Unterstützung des Vorhabens aussprechen: Herrn Prof. Dr. rer. nat. habil. Christoph Haisch und dem Lehrstuhl für Analytische Chemie und Wasserchemie der TUM für die Entwicklung des Massenspektrometersystems, Vitesco Technologies Emitec GmbH für die Bereitstellung des Abgasnachbehandlungssystems, der MAN Truck & Bus SE für die Eingliederung in das Unternehmen während des Projektzeitraums sowie für die Bereitstellung der Versuchsträger und Prüfstandperipherie, der ASG Analytik Service AG für die Lieferung von Kraftstoff und projektbegleitende Analysen zur Qualitätssicherung der bereitgestellten OME-Mischungen.

Über den Kreis der Projektbeteiligten hinaus danke ich der Firma Catalytic Instruments GmbH & Co. KG für die freundliche Leihgabe eines Catalytic Strippers und die Zusammenarbeit während der Erstellung der Publikation über Nanopartikelemissionen im OME-Betrieb. Außerdem möchte ich meinen Dank all jenen aussprechen, die außerhalb des Projektrahmens durch ihre wertvollen fachlichen Hilfestellungen Anteil an dieser Arbeit haben. Insbesondere Frau Prof. Lisa Pfefferle, Ph.D., Herrn Charles McEnally, Ph.D., und Herrn Junqing (Peter) Zhu, Ph.D., für die herzliche Aufnahme an der Yale University für einen dreimonatigen Forschungsaufenthalt und für die Möglichkeit, mit solch bedeutenden Rußbildungskoryphäen zusammenzuarbeiten.

Innerhalb der MAN Truck & Bus SE danke ich allen Personen, die durch ihre großzügige Unterstützung zum Gelingen des Forschungsvorhabens beigetragen haben. Stellvertretend nennen und danken möchte ich hier Herrn Andreas Sommermann in seiner Funktion als Abteilungsleiter für die großen Freiräume zur Organisation und Abwicklung des Projektes im Nürnberger Motorenwerk und das entgegengebrachte Vertrauen. Besonderer Dank gilt meinem Sachbearbeiter-Kollegen, Herrn Christian Pastötter, für die MAN-seitige Initiierung und Betreuung des Forschungsprojekts und die zahlreichen Lektionen während meiner Zeit in Nürnberg. Den Herren Dr. rer. nat. Harald Beck und Dr. rer. nat. Dieter Rothe danke ich für ihr außerordentliches Engagement und die Möglichkeit zur Teilhabe an ihrer grenzenlosen Expertise im Bereich Emissionen, Messtechnik und Abgasnachbehandlung. Ebenso danke ich Herrn Florian Lindner für die wertvolle Unterstützung bei der Erarbeitung der Betriebsstrategie des Abgasnachbehandlungssystems, ohne welche die in dieser Arbeit vorgestellten Demonstrationen nicht möglich gewesen wären.

Allen Studierenden und Schülern, deren Arbeiten ich während meiner Lehrstuhlzeit betreuen durfte, danke ich für ihren Beitrag zu meinem Forschungsvorhaben und die Möglichkeit, Führungserfahrung zu sammeln und mich damit persönlich weiterzuentwickeln. Besonders hervorheben möchte ich hier die Herren Alessandro Sommer und Rudolf Höß aufgrund ihrer herausragenden Unterstützung.

Der Bayerischen Forschungsstiftung danke ich für die Finanzierung des Forschungsvorhabens; der Hanns-Seidel-Stiftung danke ich für die ideelle Förderung von Oktober 2020 bis September 2022 und für die finanzielle Unterstützung meines Auslandsaufenthalts.

Meiner Familie und meinen Freunden danke ich für die Unterstützung während der Anstrengungen der letzten Jahre. Ihr wart die emotionale Basis und Quell aller Resilienz.

Meinen Eltern danke ich für ihre werteorientierte Erziehung zur Authentizität und der Ermöglichung meines Bildungswegs: Meiner Mutter Sylvia insbesondere für ihre altruistische Aufopferung zum Wohle ihrer Kinder, meinem Vater Harald für seinen strengen, aber tugendhaften Unterricht. Meiner Schwester Daniela danke ich für ihre Zuneigung und den geschwisterlichen Zusammenhalt.

Abschließend gehört mein Dank meiner Frau Stephanie für ihre unbezahlbare Unterstützung: Inhaltlich in der Rolle der Lektorin sowie als kritische Gutachterin der statistischen und semantischen Zusammenhänge, emotional in schweren Zeiten durch ihre Rücksicht und bedingungslose Liebe.

„Was ich geschrieben habe, habe ich geschrieben.“

Pontius Pilatus

Kurzzusammenfassung

Polyoxymethylendimethylether (OME) sind vielversprechende alternative Dieselkraftstoffe, hergestellt über einen Syntheseprozess aus den Edukten Wasserstoff und Kohlenstoffdioxid. Sie ermöglichen daher einen klimaneutralen Betrieb von Verbrennungskraftmaschinen. OME stechen aus anderen e-Fuels aufgrund ihrer rußfreien Verbrennung hervor, welche den Zielkonflikt zwischen Stickoxid- und Rußemissionen auflöst. Dies eröffnet Freiheitsgrade im Einspritzsystem, in der Abgasrückführung und in der Betriebsstrategie von Abgasnachbehandlungssystemen. Diese Dissertation präsentiert neuartige Untersuchungen zu einer pareto-optimalen Betriebsstrategie mit OME, zur Charakterisierung der Nanopartikelemissionen und zur Effizienz und Selektivität der Komponenten im Abgasnachbehandlungssystem. Weiterer Bestandteil dieser Arbeit ist die Demonstration von Niedrigstemissionen bezüglich limitierter sowie nichtlimitierter Schadstoffe und Treibhausgasen in abgasgesetztechnisch relevanten Testzyklen. Da diese Demonstration ein warmes Abgasnachbehandlungssystem voraussetzt, ist diese Dissertation durch eine Untersuchung zu Emissionen während des Kaltstarts und zwei Aufheizmaßnahmen des Abgasnachbehandlungssystems abgerundet, welche sich auf den Vorteil der rußfreien Verbrennung von OME in diesem Kontext fokussieren.

Abstract

Polyoxymethylene dimethyl ethers (OME) are promising alternative diesel fuels with a synthetic production via hydrogen and carbon dioxide, which therefore enable carbon-neutral operation of internal combustion engines. Among other e-fuels, OME stand out because of soot-free combustion, which resolves the trade-off between nitrogen oxide and soot emissions. This opens up degrees of freedom in the injection system, in the exhaust gas recirculation and in the operation strategy of exhaust after-treatment systems. This thesis presents novel investigations on pareto-optimal engine operation with OME, on the characterization of nanoparticle emission, and on the efficiency and selectivity of several components of the after-treatment system. Furthermore, the thesis contains the demonstration of ultra-low emissions regarding limited and non-limited pollutants and greenhouse gases in exhaust gas legislation relevant test cycles. As this demonstration requires a hot after-treatment system, the thesis is rounded with an investigation on the emissions during cold-start operation and on two methods for after-treatment system heating which focus on the advantage of the soot-free combustion of OME in this context.

Inhaltsverzeichnis

Abkürzungsverzeichnis

Variable	Bedeutung
AGN	Abgasnachbehandlung
AGR	Abgasrückführung
ASC	Ammoniaksperrkatalysator (engl.: Ammonia Slip Catalyst)
C	Atomarer Kohlenstoff
CH_2O	Formaldehyd (IUPAC-Bezeichnung: Methanal)
$-CH_2O-$	Oxymethylen-Gruppe
CH_2O_2	Ameisensäure (IUPAC-Bezeichnung: Methansäure)
CH_3OH	Methanol
CO	Kohlenstoffmonoxid
CO_2	Kohlenstoffdioxid
CRT	Kontinuierlicher Regenerationsfilter (engl.: Continous Regeneration Trap)
DMM	Dimethoxymethan (OME_1)
DOC	Dieseloxidationskatalysator (engl.: Diesel Oxidation Catalyst)
DPF	Dieselpartikelfilter (engl.: Diesel Particulate Filter)
Ed.	Edelgase und CO_2
e-DOC	Elektrisch beheizbarer Dieseloxidationskatalysator (engl.: electrically heatable Diesel Oxidation Catalyst)

Variable	Bedeutung
EVI	Einspritzverlaufsindikator
FT-IR	Fourier-Transform-Infrarot-Spektrometer
H	Wasserstoff (Element)
H_2	Wasserstoff (Molekül)
H_2O	Wasser
HC	Kohlenwasserstoffe (engl. Hydrocarbons)
HCN	Blausäure (IUPAC-Bezeichnung: Cyanwasserstoff)
HNCO	Isocyansäure
HVO	Hydriertes Pflanzenöl (engl. Hydrogenated Vegetable Oil)
MS	Massenspektrometer
N_2	Stickstoff
N_2O	Lachgas (IUPAC-Bezeichnung: Distickstoffmonoxid)
NCN	Cyanonitren
NH_3	Ammoniak (IUPAC-Bezeichnung: Azan)
NMHC	Kohlenwasserstoffemission, ausgenommen Methan (engl. Non-Methane-Hydrocarbons)
NO	Stickstoffmonoxid
NO_2	Stickstoffdioxid

Variable	Bedeutung
NO_x	Stickoxide
O	Sauerstoff (Element)
O_2	Sauerstoff (Molekül)
OME	Polyoxymethylendimethylether
OME_n	Polyoxymethylendimethylether der Kettenlänge n
PAK	Polyzyklische aromatische Kohlenwasserstoffe
Pd	Palladium
PM	Partikelmasse
PMP	Particle Measurement Programme (Arbeitsgruppe der UN/ECE)
PN_{10}	Partikelanzahl, ermittelt mit einem Kondensationspartikelzähler mit einer 50 %-Detektionsgrenze bei 10 nm
PN_{23}	Partikelanzahl, ermittelt mit einem Kondensationspartikelzähler mit einer 50 %-Detektionsgrenze bei 23 nm
PNA	Passiver NO_x-Absorber
Pt	Platin
R	Rest
SCR	Selektive katalytische Reduktion (engl.: Selective Catalytic Reduction)
T	Trägertemperatur des SCR-Systems

Variable	Bedeutung
TEM	Transmissionselektronenmikroskop
THC	Gesamtheit der Kohlenwasserstoffemissionen (engl.: Total Hydrocarbons)
TWC	Drei-Wege-Katalysator (engl.: Three Way Catalyst)
UDP	Universelles Dekompositionsrohr (engl.: Universal Decomposition Pipe)
UN/ECE	Wirtschaftskommission für Europa der Vereinten Nationen
UN/ECE R49	Regelung Nr. 49 der UN/ECE
WHSC	World Harmonised Steady State Cycle
WHTC	World Harmonised Transient Cycle
YSI	Yield Sooting Index

Formelzeichen

Variable	Einheit	Bedeutung
h_N	mm	Nadelhub
$H_{U,n}$	MJ/kg	Unterer Heizwert der Komponente n
$L_{min,molar}$	mol/mol	Molarer Mindestluftbedarf
$L_{min,OME}$	mol/mol	Molarer Mindestluftbedarf der verwendeten OME-Mischung
$M_{Luft,tr}$	kg/kmol	Molare Masse trockener Luft
M_{OME}	kg/kmol	Molare Masse der verwendeten OME-Mischung
m_x	kg	Atomare Masse des Elements x
mt_{KS}	g/s	Kraftstoffmassenstrom
$n_{O2,Luft}$	–	Molarer Anteil von O_2 in Luft
p_S	bar	Steuerraumdruck
λ	kg/kg	Verbrennungsluftverhältnis
μ	$kg/m^{-1}s^{-1}$	Dynamische Viskosität
ξ_x	–	Massenanteil des Elements x im Molekül
$\rho_{(n)}$	kg/m^3	Dichte (der Komponente n)
Φ	kg/kg	Kraftstoff-Luft-Verhältnis

1. Einleitung und Motivation

Das Ziel des Pariser Klimaabkommens der Vereinten Nationen ist es, die globale Erderwärmung zu begrenzen [1]. Es ist allgemein anerkannt, dass dazu eine Reduktion der anthropogenen Treibhausgasemissionen notwendig ist, insbesondere der Ausstoß von Kohlenstoffdioxid (CO_2) [2]. Ein wesentlicher Aspekt hiervon ist die Substitution fossiler Brennstoffe durch erneuerbare Energien aus regenerativen Quellen, insbesondere aus Wind- und Solarenergie. Zeitliche Schwankungen und lokale Unterschiede bei der Verfügbarkeit von Solarenergie und Windkraft erschweren die vollständige Umstellung des Energieverbrauchs auf erneuerbaren Strom [3], obwohl Photovoltaik- und Windkraftanlagen teilweise ein Überangebot produzieren [4]. Für eine klimaneutrale und nachhaltige globale Energieversorgung ist es notwendig, dieses Überangebot zu speichern, um sonnen- und windschwache Phasen auszugleichen. Die strombasierte Synthese flüssiger Energieträger [5] – sogenannter e-Fuels – dient als eine solche Speichermöglichkeit.

Beginnend mit CO_2, ermöglicht die sukzessive Hydrierung über Wasserstoff (H_2) aus Elektrolyse die Synthese verschiedener Kohlenwasserstoffverbindungen mit unterschiedlichen Oxidationsstufen [6, 7]. Beispiele hierfür sind Oxygenate wie Aldehyde, Ketone, Alkohole, Ester und Ether, wie auch paraffinische Kraftstoffe im Allgemeinen. Diese synthetischen Kraftstoffe ermöglichen die Reduktion des Treibhausgasausstoßes bestehender Verbrennungsmotoren, da im Gegensatz zu fossilen Kraftstoffen die bei der Verbrennung ausgestoßene CO_2-Menge zuvor im Syntheseprozess gebunden wurde. Läuft die Herstellung und Verteilung dieser Kraftstoffe ohne CO_2-Ausstoß ab, ergibt sich ein CO_2-neutraler Betrieb. Im Jahr 2018 verursachten Verbrennungsmotoren im Verkehrssektor etwa 25 % des globalen anthropogenen CO_2-Ausstoßes [8]. Damit bieten e-Fuels ebenso wie batterieelektrische Anwendungen einen Lösungsansatz für klimaneutrale Energieversorgung und Mobilität [7, 9]. Darüber hinaus erlauben e-Fuels größtenteils die Nutzung bestehender Infrastruktur zur Speicherung und Verteilung [10].

Während manche dieser e-Fuels ähnliche Verbrennungseigenschaften aufweisen wie ihr fossiles Gegenstück, bieten Oxygenate den Vorteil neuer Freiheitsgrade zur Schadstoffreduktion. Für Dieselmotoren, welche neben dem Pkw-Bereich besonders bei schweren Nutzfahrzeugen, in der Schifffahrt und im Energiesektor Anwendung finden, gilt eine Mischung aus langkettigen Polyoxymethylendimethylethern (OME) als vielversprechender Kandidat zur Substitution fossilen Dieselkraftstoffs [11]. OME verbrennt rußfrei und löst damit den für Dieselmotoren typischen, innermotorischen Zielkonflikt zwischen Stickoxid- (NO_x) und

Rußemissionen auf. Dies ermöglicht eine gleichzeitige Reduktion des Rohemissionslevels beider Schadstoffkomponenten [12]. CO_2-neutral hergestelltes OME trägt somit sowohl zum Klimaschutz als auch zur Luftreinhaltung bei. Das Potenzial von OME für den Einsatz in Dieselmotoren mit niedrigsten Schadstoffemissionen ist Gegenstand zahlreicher Publikationen, die sich bisher auf Laborbedingungen oder Forschungsmotoren im vorkonditionierten und stationären Betrieb beschränken [12–30].

Auf deren Ergebnissen basieren Hypothesen, welche das Potenzial von mit OME betriebenen Serienmotoren bis hin zu Schadstoffemissionen unterhalb des Umgebungsniveaus urbaner Regionen postulieren [31–36]. Ein Emissionsniveau in dieser Größenordnung setzt eine Abgasnachbehandlung (AGN) voraus [37]. Wechselwirkungen von Abgas aus einer OME-Verbrennung mit den Komponenten einer für einen Dieselmotor entwickelten AGN sind unzureichend untersucht. Studien dazu beschränken sich auf Hypothesen [19], Versuche am Einzylinderforschungsmotor [20, 30] oder auf stationäre Betriebspunkte mit geringer Motorlast [26]. Eine Studie zu Messungen am Vollmotor mit Abgasnachbehandlung im Straßenbetrieb reduziert sich auf die isolierte Betrachtung aktuell reglementierter, fester Partikelemissionen [38].

Aus diesem Grund ist es das Ziel der vorliegenden Arbeit, das Potenzial von OME hinsichtlich niedrigster Schadstoffemissionen zu bewerten. Als Versuchsträger dienen zwei seriennahe Nutzfahrzeugmotoren mit Abgasnachbehandlung. Um eine realitätsnahe Demonstration zu gewährleisten, finden Fahrzyklen aus der Homologation im Bereich straßenbetriebener schwerer Nutzfahrzeuge Anwendung. Die Anpassung der Einspritzstrategie auf den Betrieb mit OME erfolgt anhand der Ergebnisse eines am Einzylinderforschungsmotor validierten 0D-/1D-Simulationsmodells. Darüber hinaus betrachtet diese Arbeit die Auswirkungen von OME auf die Effizienz und Selektivität der Komponenten der Abgasnachbehandlung. Neben den bisher vom Gesetzgeber reglementierten Schadstoffemissionen enthält diese Arbeit ebenfalls eine Untersuchung weiterer klima- und potenziell gesundheitsschädlicher Emissionen unter Zuhilfenahme neu entwickelter Abgasmesstechnik. Da ein schadstofffreier Betrieb eine betriebswarme Abgasnachbehandlung voraussetzt, beinhaltet diese Arbeit außerdem eine Untersuchung einiger Maßnahmen zur Verkürzung der Aufheizphase nach einem Kaltstart des Motors. Diese Untersuchung berücksichtigt insbesondere die Vorteile der rußfreien Verbrennung von OME gegenüber fossilem oder paraffinischem Dieselkraftstoff.

2. Stand der Wissenschaft und Technik

2.1 Emissionen am Dieselmotor

2.1.1 Abgaszusammensetzung

Fossile Kraftstoffe zur Energieumwandlung in Verbrennungskraftmaschinen bestehen vorwiegend aus Verbindungen von Kohlenstoff (C) und Wasserstoff (H). Im Falle von Estern, Alkoholen, Ethern oder Ketonen, welche aus biologischen Quellen oder aus synthetischer Herstellung stammen, enthalten Kraftstoffe außerdem molekular gebundenen Sauerstoff (O).

Die idealisierte Verbrennung eines nur aus C-, H- und O-Atomen bestehenden Kraftstoffes läuft im stöchiometrischen Fall gemäß folgender Reaktionsgleichung ab:

$$\mathrm{C_xH_yO_z} + \left(x + \frac{y}{4} - \frac{z}{2}\right)\mathrm{O_2} \rightarrow x\ \mathrm{CO_2} + \frac{y}{2}\ \mathrm{H_2O} \tag{1}.$$

Da Dieselmotoren in der Regel mit Luftüberschuss betrieben werden, ist die Reaktionsgleichung einer idealisierten Verbrennung im Dieselmotor abhängig vom Verbrennungsluftverhältnis λ, welches das Verhältnis von vorhandener Luft und für die stöchiometrische Verbrennung benötigte molare Luftmenge $L_{\mathrm{min,molar}}$ beschreibt. Formel (2) und Formel (3) basieren dabei auf der vereinfachenden Annahme folgender molarer Luftbestandteile nach *Giacomo* [39]: 78 % molekularer Stickstoff (N_2), 21 % molekularer Sauerstoff (O_2) und 1 % Edelgase und CO_2 (Ed.).

$$\mathrm{C_xH_yO_z} + \lambda \cdot L_{\mathrm{min,molar}}$$

$$\rightarrow x\ \mathrm{CO_2} + \frac{y}{2}\ \mathrm{H_2O} + 0{,}78 \cdot \lambda \cdot L_{\mathrm{min.molar}} \cdot \mathrm{N_2} + 0{,}01 \cdot \lambda \cdot L_{\mathrm{min.molar}} \cdot \mathrm{Ed.} + (\lambda - 1) \cdot L_{\mathrm{min,molar}} \cdot\ \mathrm{O_2} \tag{2}.$$

$$L_{\mathrm{min,molar}} = \frac{x + \frac{y}{2} - \frac{z}{2}}{0{,}21}\ \frac{\text{mol Luft}}{\text{mol Brennstoff}} \tag{3}.$$

Abgas einer idealisierten dieselmotorischen Verbrennung besteht somit aus den Verbrennungsprodukten CO_2 und Wasserdampf (H_2O), sowie überschüssigem O_2 und den Bestandteilen der Luft, die nicht an der Verbrennung teilnehmen.

Die reale Verbrennung im Dieselmotor weicht von dieser idealisierten Verbrennung ab. Aus diesem Grund enthält Abgas einige weitere Stoffe:

- CO und HC: Unterschiedliche Faktoren verhindern die vollständige Umsetzung aller Kraftstoffbestandteile. Hierzu zählen Gemischinhomogenitäten zwischen Kraftstoff und Luft, lokaler Luftmangel und Ablöschen der Flamme durch lokale Abkühlung im Brennraum [40]. Eine unvollständige Verbrennung erzeugt Kohlenstoffmonoxid (CO) und nicht- oder teiloxidierte Kraftstofffragmente [41]. Der Begriff Kohlenwasserstoffemissionen (HC-Emissionen) fasst diese Fragmente zusammen.

- Ruß und andere Partikel: Produkte einer unvollständigen Verbrennung wirken teilweise als Rußvorläufer, welche kohlenstoffhaltige Agglomerate bilden. Diese wachsen im weiteren Verlauf der Verbrennung zu Rußpartikeln heran. Oxidieren diese nicht mehr vollständig, bilden sie als Feststoffe einen Bestandteil des ausgeschobenen Abgases. [41] Darüber hinaus ist es möglich, dass Spuren von Elementen wie Schwefel und Metallen, welche aus Verunreinigungen oder Rückständen des Rohöls stammen, an der Verbrennung teilnehmen, ebenso wie Bestandteile des Schmieröls und Kraftstoffadditive. Die daraus gebildeten Oxide und Carbonate finden sich dann als Aschepartikel im Abgas. Insbesondere Schwefel führt über Schwefelsäurebildung und Sulfatisierung mit Bestandteilen des Motorenöls ebenfalls zu Partikeln im Abgas [42]. Einen zusätzlichen Anteil haben außerdem metallischer Abrieb und bereits in der Ansaugluft enthaltene Festpartikel [43]. Rekondensierte Tröpfchen unverbrannter und teiloxidierter Kraftstoffanteile und des Motorenöls sowie Wassertröpfchen zählen ebenfalls zu den Partikelemissionen.

- Stickoxide: Die hohen Verbrennungstemperaturen im Brennraum verändern das chemische Gleichgewicht und regen die Dissoziation des in der Ansaugluft vorhandenen Stickstoffs an. Es bilden sich Stickoxide, die im weiteren Verlauf der Verbrennung nicht ausreichend schnell zerfallen und im ausgeschobenen Abgas verbleiben. Der Begriff „nitroses Gas“ beschreibt ein Gasgemisch dieser Stickoxide, welches sich in motorischen Abgas im Wesentlichen aus Stickstoffmonoxid (NO) und Stickstoffdioxid (NO_2) zusammensetzt. [44]

Abbildung 2-1 stellt eine repräsentative massenbezogene Abgaszusammensetzung eines Dieselmotors dar.

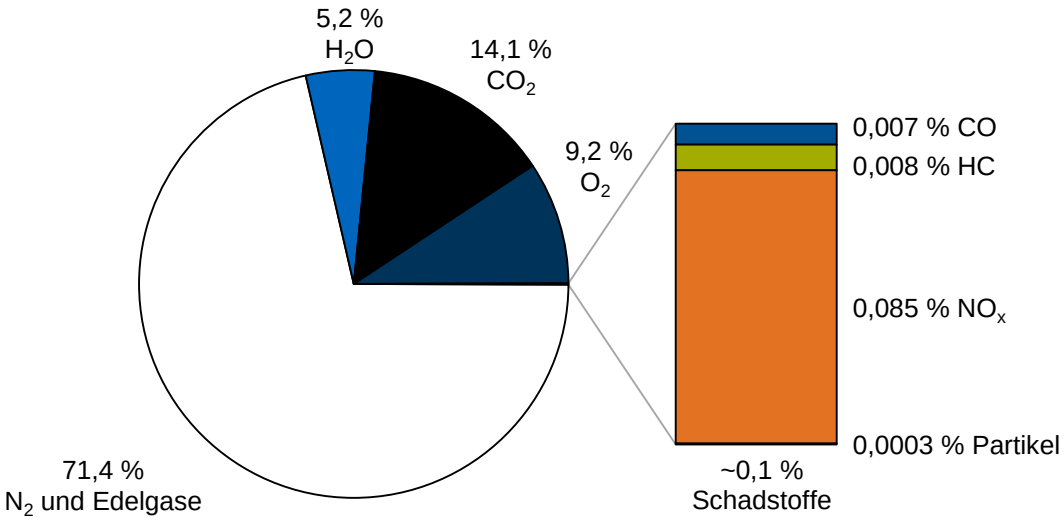

Abbildung 2-1: Repräsentative massenbezogene Zusammensetzung des Rohabgases eines Dieselmotors nach eigener Messung am Nutzfahrzeugdieselmotor; Stoffwerte aus [45].

Die aufgeführten Schadstoffe machen zwar nur einen Anteil von etwa 0,1 Massenprozent des Abgases aus, sie erfahren aber aufgrund ihrer umwelt- und gesundheitsschädlichen Wirkung [46–48] großes gesellschaftliches Interesse. Mit dem Ziel der Luftreinhaltung beschränken sukzessiv strengere Abgasgesetzgebungen daher ihren Ausstoß. Innerhalb der Europäischen Union bilden die Abgasvorschriften der Stufe Euro VI/6 die aktuelle Limitierung [49]; Grenzwerte für Euro 7/VII befinden sich derzeit in Diskussion [50]. Neben der Reduktion der Grenzwerte verschärft eine kontinuierliche Erweiterung der Testprozeduren die Herausforderungen der Emissionsreduktion. Der Gesetzgeber ist motiviert, Prüfzyklen vorzuschreiben, welche den realen Betrieb des Motors im Anwendungsfall besser abbilden als Prüfzyklen vorangegangener Abgasgesetzgebungen [51]. Damit erhöht sich im Allgemeinen mit fortschreitender Entwicklungsstufe der Emissionsgesetzgebung der für die Homologation relevante Betriebsbereich des Verbrennungsmotors. Während frühere Testverfahren eine thermische Vorkonditionierung des Motors vor Beginn der Prüfläufe vorsehen, berücksichtigen heutige Testverfahren den Schadstoffausstoß auch in der Kaltstartphase direkt nach Anlassen des Motors [49].

Darüber hinaus erfassen für die Zukunft diskutierte Abgasgesetzgebungen neue Spezies, welche frühere Stufen nicht reglementieren. So umfasst die Stufe Euro 7/VII zum heutigen Zeitpunkt (Juni 2022) voraussichtlich erstmals Lachgas (N_2O) und Formaldehyd (CH_2O). Des Weiteren wird die Anforderung der Detektionssensitivität von 50 % der Partikelanzahlemission zu einem Durchmesser von 10 nm (PN_{10}) verschoben. Die bisherige Erfassung setzt dieses Detektionslimit auf eine Partikelgröße von 23 nm (PN_{23}). [50]

2.1.2 Schadstoffentstehung

CO und HC:

CO tritt bei der Verbrennung von Kohlenwasserstoffen als Zwischenprodukt auf. *Bowman* fasst die CO-Bildung über nicht näher spezifizierte Reste (R) schematisch zusammen:

$$RH \rightarrow R \rightarrow RO_2 \rightarrow RCHO \rightarrow RCO \rightarrow CO \quad (4)\ [40].$$

Das gebildete CO oxidiert im Verbrennungsprozess über vorhandene Hydroxylradikale zu CO_2, allerdings mit einer geringeren Reaktionsrate als in der Bildungsreaktion. Die CO-Oxidation über O_2 zu CO_2 hat im Vergleich dazu geringere Reaktionsraten [40]. Aufgrund der verfügbaren Wasserstoffradikale dominiert während der Verbrennung daher die Oxidationsreaktion über Hydroxylradikale [52]. Die CO-Oxidation ist maßgeblich von der Temperatur abhängig, weshalb sie in der Expansionsphase abnimmt. Unvollständige Verbrennung durch lokalen Sauerstoffmangel oder Ablöschen der Flamme in wandnahen oder zu mageren Bereichen, führt zu CO-Emissionen im Abgas [40]. CO gilt als für den Menschen giftiges Gas, da es durch eine höhere Hämoglobinaffinität den Sauerstoffgehalt im Blut reduziert [53].

Ebenso wie CO entstehen HC-Emissionen bei unvollständiger Verbrennung durch lokalen Luftmangel und Ablöschen der Flamme [40]. Darüber hinaus führen Verdunstungsemissionen von Kraftstoff aus dem Injektorsackloch zum Verbrennungsende oder benetzten Wandregionen im Brennraum zu HC-Emissionen im Abgas [54].

HC-Emissionen sind in aktuellen Abgasgesetzgebungen nur in ihrer Gesamtheit reglementiert und nicht in einzelne Bestandteile unterteilt. Der in der europäischen Gesetzgebung für schwere Dieselnutzfahrzeuge verwendete Begriff der „Total Hydrocarbons“ (THC) enthält Methan (CH_4) [45], während die Gesetzgebung für erdgasbetriebene Fahrzeuge den Begriff „Non-Methane Hydrocarbons“ (NMHC) verwendet, CH_4 damit explizit ausschließt und separat berücksichtigt. Insbesondere den in HC-Emissionen enthaltenen Carbonylverbindungen wird ein Gefährdungspotenzial für den menschlichen Körper zugeschrieben [55]. Darüber hinaus sind sie an der Ozonbildung mit Stickoxiden beteiligt, was zum sogenannten fotochemischen Smog führt [56]. Einen Anteil der in Dieselabgas vorhandenen Carbonylgruppen bildet CH_2O ab [57]. CH_2O gilt als für den Menschen toxischer Stoff [58] und ist darüber hinaus von der Weltgesundheitsorganisation als karzinogen eingestuft [59].

Ruß und andere Partikel:

Rußpartikel bestehen aus vorwiegend kugelförmigen Kohlenstoffpartikeln, sogenannter Primärpartikel, welche sich durch Koagulation zu Agglomeraten verbinden [41]. Zur Rußbildung gibt es zwei wesentliche Hypothesen, die versuchen, die zugrundeliegenden Mechanismen zu beschreiben:

Die Acetylenhypothese besagt, dass durch Aufspaltung von Kohlenwasserstoffen in Molekülfragmente mit einem oder zwei C-Atomen, insbesondere Ethin/Acetylen, und deren Rekombination durch Dimerisation und Polymerisation zyklische und polyzyklische aromatische Kohlenwasserstoffe (PAK) entstehen. Durch sukzessive Anlagerung weiterer Acetylenmoleküle und Dehydrierung bilden sich graphitähnliche Nukleationskeime, welche im weiteren Verlauf der Rußbildung zu meist sphärischen Primärpartikeln anwachsen. Diese Primärpartikel verbinden sich durch Koagulation zu Rußpartikelagglomeraten. [41]

Die Elementarkohlenstoffhypothese hingegen betrachtet die diffusionskontrollierte Bildung von Primärpartikeln aufgrund der unterschiedlichen Diffusionsgeschwindigkeiten von Kohlenstoff und Wasserstoff. Letzterer diffundiert wegen seiner geringeren Masse und Größe bei den vorherrschenden Verbrennungstemperaturen schneller zur sauerstoffreichen Umgebung als Kohlenstoff. Die Reaktion der einzelnen Spezies mit Sauerstoff ist damit von der Diffusionsgeschwindigkeit abhängig. Aufgrund der dadurch stattfindenden Dehydrierung der Kohlenwasserstoffe schließen sich die verbleibenden Kohlenstoffatome zu Gerüsten mit pentagonalen und hexagonalen Strukturen zusammen. Fullerenartige sphärische Schalen führen dann zur Entstehung von Primärpartikeln. Parallel dazu bilden sich PAK, welche an Rußpartikeln adsorbieren. Partikel, die aus der Kraftstoffverbrennung hervorgehen, beinhalten daher immer einen festen Kern aus elementarem Kohlenstoff und darauf angelagerten PAK-Hüllen. [41, 60]

Die beiden Rußbildungshypothesen widersprechen sich im chemischen Sinne nicht. Während die Acetylenhypothese den Fokus auf den Zerfall zu Ethin als entscheidenden Rußvorläufer legt, fügt die Elementarkohlenstoffhypothese dem Mechanismus eine zeitliche und örtliche Komponente hinzu. Oxidieren die gebildeten Rußteilchen im Laufe der Verbrennung aufgrund von zu geringer Temperatur oder lokalem Sauerstoffmangel nicht mehr vollständig, verbleiben sie als Partikelemission im Abgas.

Abbildung 2-2 fasst die Rußbildungshypothesen schematisch zusammen.

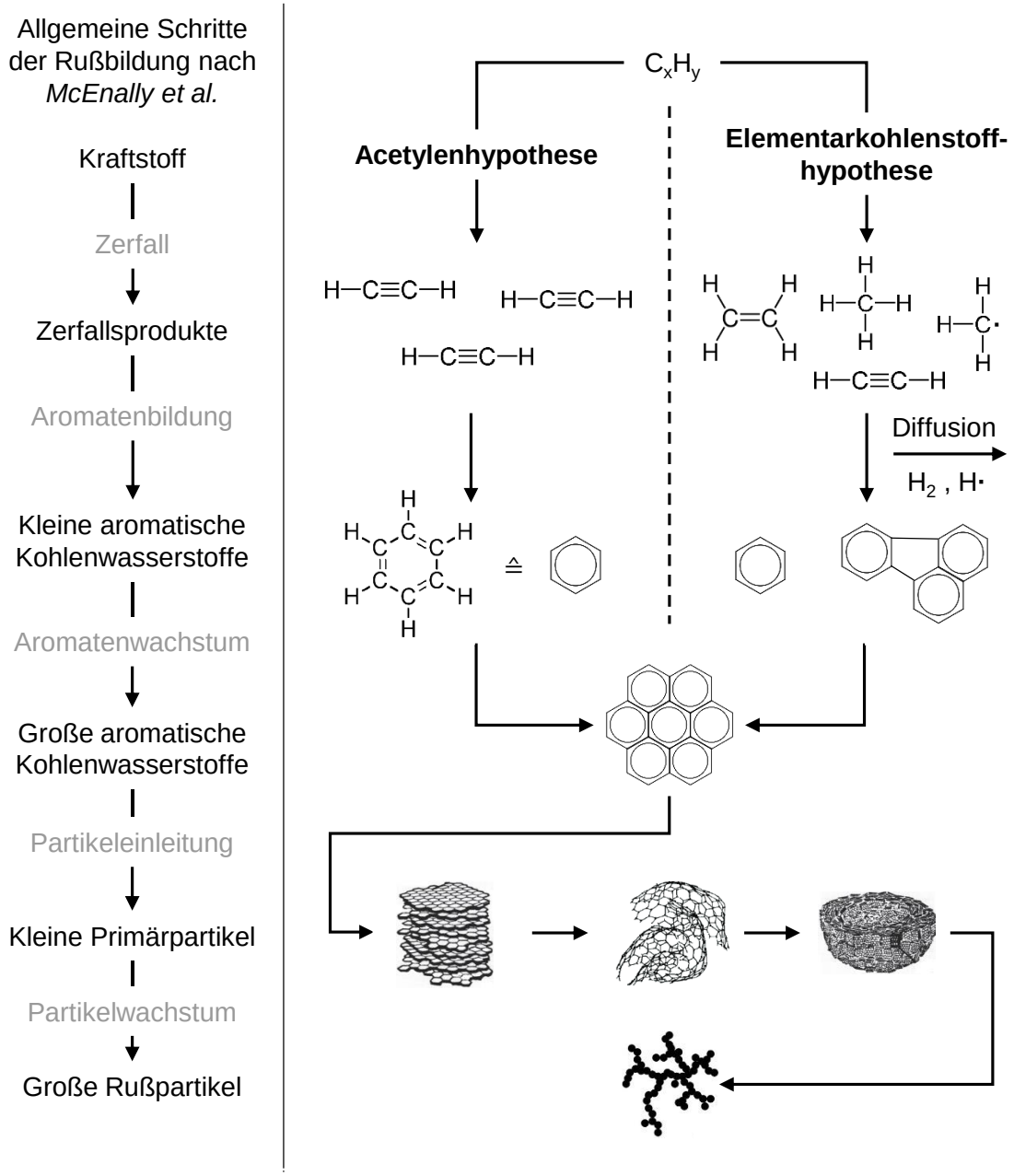

Abbildung 2-2: Schematische Darstellung der Rußbildung nach Goldanskii et al. [41], Beck [61] und McEnally et al. [62].

Rußpartikel gelten allgemein als gesundheitsschädlich [63] und weisen einen beschleunigenden Effekt auf den Klimawandel auf [64]. Sie machen den Großteil der Partikelemissionen im Abgas von Dieselmotoren aus; *Kweon et al.* quantifizieren in ihrer Arbeit diesen Anteil abhängig vom Betriebspunkt auf etwa 40 – 95 % [43].

Aufgrund ihrer unterschiedlichen Oberflächenstrukturen findet eine Einteilung von Partikeln häufig anhand ihres elektrischen Mobilitätsdurchmessers statt. Diese Größe beschreibt den Durchmesser einer Kugel, welche in einem elektrischen Feld dieselbe Mobilität wie der betrachtete Partikel aufweist.

Nach *Kittelson* bilden Partikel im Dieselabgas eine trimodale Größenverteilung: Die Nukleationsmode mit einem Durchmesser von 5 bis 50 nm besteht vorwiegend aus volatilen organischen Verbindungen und schwefelhaltigen Komponenten, die sich während der Verdünnung und Abkühlung des Abgases bilden. Darüber hinaus enthält sie Kohlenstoff- sowie Metallverbindungen. Die Akkumulationsmode mit Partikeln zwischen 100 und 300 nm enthält kohlenstoffhaltige Agglomerate und darauf angelagerte organische Komponenten. Diese Mode macht 40 – 94 % der Partikelmasse aus. Die Grobstaubmode enthält Partikel der Akkumulationsmode, welche sich an Oberflächen im Abgassystem angelagert haben, nach kontinuierlichem Wachstum ablösen und zurück ins Abgas eindringen. [42]

Abbildung 2-3 zeigt eine qualitative Partikelgrößenverteilung im Dieselabgas.

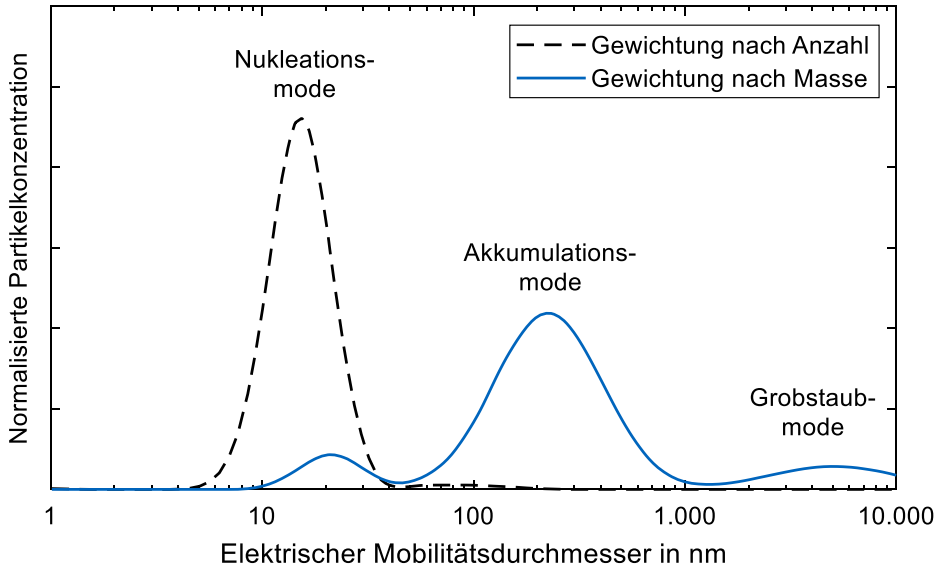

Abbildung 2-3: Repräsentative Partikelgrößenverteilung im Dieselabgas nach Kittelson [42].

Die aktuelle Abgasgesetzgebung der Stufe Euro 6/VI setzt die 50 %-Detektionssensitivität auf einen Partikeldurchmesser von 23 nm. Vorschläge für zukünftige Gesetzgebungen verschieben diese Detektionsschwelle hin zu 10 nm [65, 66]. Um motorische Partikelemissionen unabhängig von äußeren klimatischen Randbedingungen vergleichbar zu machen, empfiehlt das Particle Measurement Programme (PMP) der Wirtschaftskommission für Europa der Vereinten Nationen (UN/ECE) die Entfernung volatiler Bestandteile vor Bestimmung der Partikelkonzentration. Dies geschieht entweder durch Verdampfung oder katalytische Konvertierung. Partikel der Grobstaubmode bleiben ebenfalls unberücksichtigt; ein Impaktor oder Zyklonabscheider entfernt sie vor dem Messgerät. Darüber hinaus spielt die Methodik der Probenahme eine wichtige Rolle bei der Untersuchung der Partikelemissionen, weshalb das PMP hier genaue Vorgaben macht. [67]

Stickoxide:

Die Stickoxidbildung läuft nach bisherigem Kenntnisstand über vier wesentliche Pfade ab:

1. Die Bildung von thermischem NO: Bei hohen Temperaturen stammt der Großteil des aus Luftstickstoff gebildeten NO aus dem Mechanismus nach *Zeldovich* [68], später erweitert von *Lavoie et al.* [44]:

$$O + N_2 \leftrightarrow NO + N \quad (5)\ [68].$$

$$N + O_2 \leftrightarrow NO + O \quad (6)\ [68].$$

$$N + OH \leftrightarrow NO + H \quad (7)\ [44].$$

   Die Hinreaktion in Formel (6) setzt aufgrund der stabilen Dreifachbindung im Stickstoffmolekül eine vergleichsweise hohe Aktivierungsenergie voraus und ist deshalb der geschwindigkeitsbestimmende Schritt. Der Geschwindigkeitskoeffizient dieser Hinreaktion hängt maßgeblich von der Temperatur ab [69]. Der Zeldovich-Mechanismus gilt als wichtigster Bildungsmechanismus von Stickoxidemissionen in der dieselmotorischen Verbrennung [70].

2. Die Bildung von Prompt-NO: *Fenimore* beschreibt erstmals einen Pfad in der Flammenfront über die Reaktion von CH-Radikalen mit Stickstoff zu Blausäure (HCN), welche zu NO weiterreagiert [71]:

$$CH + N_2 \rightarrow HCN + N \quad (8)\ [71].$$

   Moskaleva et al. [72] hingegen postulieren einen Prompt-NO-Pfad über Cyanonitren (NCN) als Zwischenspezies, welches *Glarborg et al.* [73] als Ausgangsstoff für Reaktionen mit unterschiedlichen Spezies zu NO beschreiben. Aufgrund der relativ zum Zeldovich-Mechanismus geringeren Aktivierungsenergie läuft die Prompt-NO-Bildung schon bei niedrigeren Temperaturen ab. Bezüglich des genauen Ablaufs der Mechanismen und die zugehörigen Reaktionsraten besteht weiterhin Forschungsbedarf.

3. Die Bildung von NO aus dem N_2O-Mechanismus: Bei tiefen Temperaturen gewinnt außerdem der von *Wolfrum* beschriebene N_2O-Mechanismus an Bedeutung [74]:

$$O + N_2 + M \rightarrow N_2O + M \quad (9)\ [74].$$

$$O + N_2O \rightarrow 2\,NO \quad (10)\ [74].$$

   Der in Formel (10) beschriebene Dreierstoß zwischen N_2, O und dem unverändert hervorgehenden Stoßpartner M läuft bevorzugt bei hohen Drücken ab [74].

4. Die Bildung von Brennstoff-NO: *Miller & Bowman* [70] beschreiben die Bildungsreaktionen von NO mit aus dem Brennstoff stammenden Stickstoff über HCN und Ammoniak (NH_3). Diese Mechanismen spielen bei der dieselmotorischen Verbrennung keine Rolle, da bisher eingesetzte Kraftstoffe praktisch keinen gebundenen Stickstoff enthalten [54]. Sie werden aber mit der Verwendung von NH_3 als kohlenstofffreie Kraftstoffalternative an Bedeutung gewinnen [75].

   Teilweise bildet entstandenes NO in weiteren Reaktionen nach *Miller & Bowman* NO_2 [70]:

$$NO + HO_2 \leftrightarrow NO_2 + OH \quad (11)\ [70].$$

$$NO + OH \leftrightarrow NO_2 + H \quad (12)\ [70].$$

$$NO + O_2 \leftrightarrow NO_2 + O \quad (13)\ [70].$$

   Bei niedrigen Flammentemperaturen findet die Bildung von NO_2 vorwiegend über Reaktion (12) statt; gegenläufig dazu erhöhen steigende Temperaturen einen Abbau über Reaktion (13). Der Anteil von NO_2 an der Gesamtkonzentration der Stickoxide im Rohabgas eines Dieselmotors ist abhängig von unterschiedlichen Betriebsparametern [76], jedoch im Allgemeinen geringer als 20 % [69].

   Stickoxide gelten als gesundheitsschädlich, da sie die Lungenfunktion negativ beeinträchtigen [77]. Sie führen in der Atmosphäre ebenso wie Schwefeloxide zum sogenannten sauren Regen [78]. In Kombination mit Kohlenwasserstoffen tragen sie zur Smogbildung bei, da sie die Ozonbildung in Bodennähe beschleunigen [56]. Stickoxide in der Stratosphäre, vorwiegend aus der Luftfahrt stammend, verstärken darüber hinaus den Ozonabbau [79, 80].

2.2 Maßnahmen zur Emissionsreduktion

2.2.1 Innermotorische Maßnahmen

Die Entstehungsmechanismen von Schadstoffen hängen von unterschiedlichen Faktoren ab; maßgeblich sind die Temperatur und die lokale Sauerstoffverfügbarkeit. Konstruktive und applikative Ansätze zur Emissionsreduktion zielen darauf ab, die Verbrennung hinsichtlich dieser Einflussgrößen zugunsten einer geringeren Schadstoffentstehung zu beeinflussen.

Applikation und Konstruktion des Einspritzsystems:

Im dieselmotorischen Brennverfahren finden Gemischbildung und Verbrennung zeitgleich statt. Eine Erhöhung der Gemischbildungsenergie und eine Reduktion der Kraftstofftröpfchendurchmesser führen zu einer optimierten Verbrennung mit reduzierter Bildung der Schadstoffe Ruß, CO und HC-Emissionen [54]. Des Weiteren beeinflusst die Steuerung des Druck- und Brennverlaufs den Verbrennungsprozess. Beispielhafte innermotorische Maßnahmen zur Emissionsreduktion sind:

1. Applikation der Einspritzung: Insbesondere Common-Rail-Injektoren bieten Freiheitsgrade über Mehrfacheinspritzungen und den Einspritzzeitpunkt [81].

2. Konstruktive Gestaltung der Injektor-/Düsengeometrie: Sacklochvolumen, Gestaltung der Einspritzlöcher und des Steuerraums im Injektor beeinflussen den Kraftstoffstrahl und den Einspritzverlauf [82–85].

3. Einspritzdruck: Dieser ist Einflussgröße für den Tröpfchenzerfall infolge der Turbulenz, höherer Scherkräfte an den Kraftstofftröpfchen und Kavitation in der Kraftstoffströmung [83].

Aufladung und Ladungsbewegung:

Eine Aufladung über einen Kompressor oder einen Abgasturbolader erhöht das globale Sauerstoffangebot im Brennraum und hat somit direkten Einfluss auf die Schadstoffemissionen eines Dieselmotors [86]. Daneben definiert die Zylinderinnenströmung das lokale Sauerstoffangebot am Kraftstoffstrahl, insbesondere durch eine Drallbewegung um die Zylinderachse. Maßnahmen zur Beeinflussung dieser sind unter Anderem die konstruktive Gestaltung der Einlasskanäle und eine Variabilität der Ventilsteuerzeiten [87]. Darüber hinaus beeinflusst die Geometrie der Kolbenmulde die Strömungsrichtung des Kraftstoffstrahls und der umgebenden Luftschicht; und damit ebenso Partikel- und Stickoxidemissionen [88].

Abgasrückführung (AGR):

Die AGR über eine Änderung der Ventilsteuerzeiten oder über eine Klappe zwischen Abgas- und Ansaugtrakt hat eine Reduktion der Stickoxidbildung zum Ziel. Die AGR erhöht den Anteil an CO_2 und Wasserdampf im Frischgas und reduziert damit den Sauerstoffgehalt. *Ladommatos et al.* führen die stickoxidsenkende Wirkung auf drei Effekte zurück [89–92]:

1. Verdünnungseffekt: Eine geringere Sauerstoffkonzentration reduziert die Verbrennungstemperatur, die maßgebliche Einflussgröße der Stickoxidbildung [89].
2. Chemischer Effekt: CO_2 und H_2O dissoziieren in einem endothermen Prozess und reduzieren somit die Verbrennungstemperatur [90, 91].
3. Thermischer Effekt: CO_2 und H_2O erhöhen die Wärmekapazität des Frischgases, was wiederum zu niedrigeren Verbrennungstemperaturen führt [92].

Ruß-NO_x-Zielkonflikt:

Da die Einflussgrößen Temperatur und Sauerstoffverfügbarkeit entgegengesetzt auf die Bildungsmechanismen von Ruß- und Stickoxidemissionen wirken, ergibt sich für Dieselmotoren der sogenannte Ruß-NO_x-Zielkonflikt [93–97]. Abbildung 2-4 stellt diesen Zielkonflikt schematisch dar. Das Kraftstoff-Luft-Äquivalenzverhältnis ϕ ist dabei indirekt proportional zum Verbrennungsluftverhältnis λ. Die diffusive Flamme der Dieselverbrennung enthält unterschiedliche Zonen, die von fett bis mager sowie kalt und heiß variieren und somit eher NO_x- oder Rußemissionen bilden.

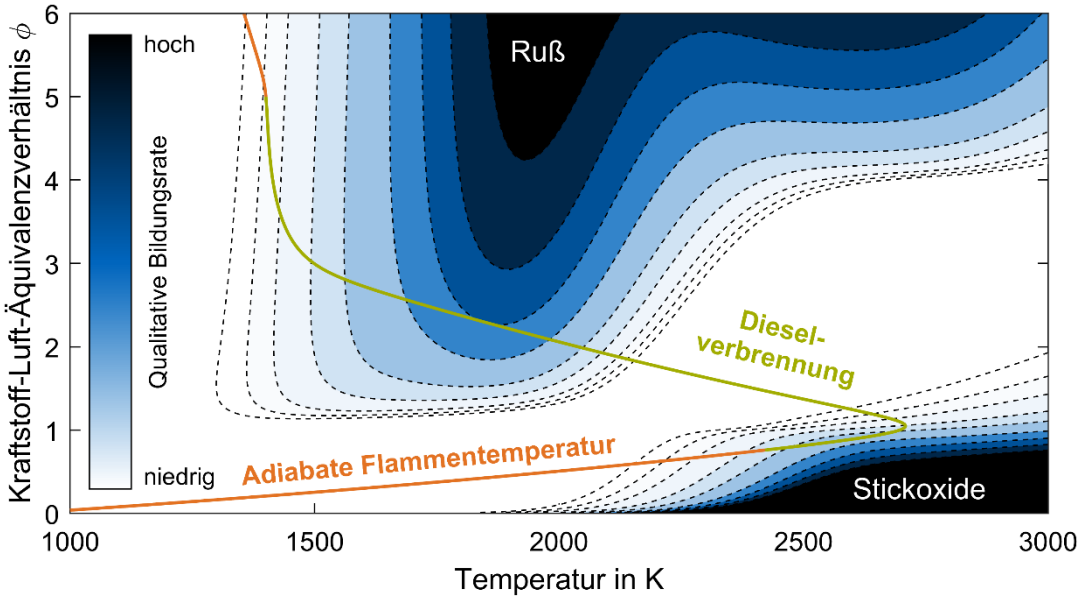

Abbildung 2-4: Qualitative Darstellung des Ruß-NO_x-Zielkonflikts nach Neely et al. [98] mit eigenen berechneten Bildungsraten der adiabaten Verbrennung von n-Heptan als Dieselreferenz.

Je nach Emissionsreduktionsmaßnahme verschieben sich die Bedingungen in den Verbrennungszonen in einen Bereich mit höherer Bildungsrate der jeweils anderen Schadstoffspezies. Auch eine Kombination unterschiedlicher Maßnahmen, wie hohe Einspritzdrücke, hohe Aufladung und hohe AGR-Rate lösen diesen Zielkonflikt nicht auf [99]. Die sich aus diesem Zielkonflikt bildende Paretofront führt dazu, dass die Grenzwerte der aktuellen Abgasgesetzgebung für Dieselmotoren nicht allein durch innermotorische Maßnahmen zu erreichen sind [100]. Abbildung 2-5 verdeutlicht dies schematisch anhand einer beispielhaften Paretofront zwischen NO_x und der Partikelmasse (PM).

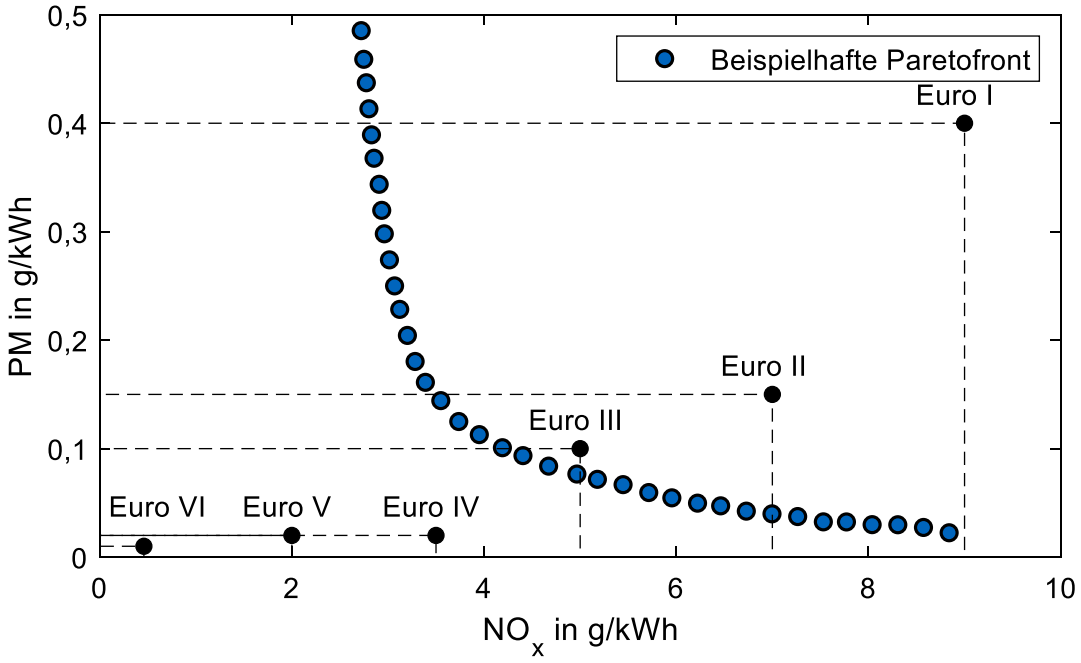

Abbildung 2-5: Beispielhafte Paretofront des Ruß-NO_x-Zielkonflikts nach eigener Messung am Nutzfahrzeugdieselmotor und Grenzwerte unterschiedlicher Stufen der Abgasgesetzgebung für schwere Nutzfahrzeuge in Europa aus [49, 101, 102].

Stattdessen erfordert die Emissionsreduktion bis unterhalb aktueller und zukünftiger Grenzwerte die außermotorische AGN. Katalytisch beschichtete Träger und Filtersysteme ermöglichen die Oxidation oder Reduktion der bei der Verbrennung gebildeten Schadstoffemissionen. Innermotorische Maßnahmen dienen daher mittlerweile dem Zweck, die Rohemissionen zu reduzieren, um die Belastung des AGN-Systems zu minimieren. Bei steigender Performanz des AGN-Systems ist eine zunehmende Entkopplung des Motors und der AGN möglich. Hierbei besteht das Entwicklungsziel der Motorapplikation in einer wirkungsgradoptimalen Verbrennung. Ziel ist dabei die Minimierung innermotorischer Maßnahmen zur Emissionsreduktion, welche den Kraftstoffverbrauch erhöhen. Das AGN-System kompensiert die dadurch steigenden Rohemissionen.

2.2.2 Abgasnachbehandlung

Dieseloxidationskatalysator (DOC):

Ein DOC unterstützt die Oxidation von Abgasbestandteilen, insbesondere der CO-, HC- und NO-Emissionen, aufgrund seiner katalytischen Beschichtung mit Elementen aus der Gruppe der Platinoide. Hier haben sich vor allem Platin (Pt) und eine Legierung mit Palladium (Pd) bewährt. Während eine Pt-Beschichtung höhere Aktivität hinsichtlich der CO- und HC-Oxidation aufweist [103], wirkt der Pd-Anteil vorwiegend als Stabilisator, indem es die Agglomeration der Pt-Partikel bei hohen Temperaturen ab ca. 500 °C hemmt [104]. Ein solcher irreversibler Sintervorgang reduziert die Anzahl der aktiven Zellen auf der Oberfläche und führt zu sinkender Aktivität [105]. Neben der Oxidation von CO- und HC-Emissionen unterstützt der DOC außerdem die Oxidation von NO zu NO_2 [103].

Die wesentlichen Reaktionsgleichungen sind [54]:

$$2\,CO + O_2 \rightarrow 2\,CO_2 \qquad (14)\ \text{nach [54]}.$$

$$C_xH_y + \left(x + \frac{y}{2}\right) O_2 \rightarrow x\,CO_2 + y\,H_2O \qquad (15)\ \text{nach [54]}.$$

$$2\,NO + O_2 \leftrightarrow 2\,NO_2 \qquad (16)\ \text{nach [54]}.$$

Die NO_2-Konzentration ist dabei allerdings durch ein thermodynamisches Gleichgewicht begrenzt, sodass über einer gewissen Temperatur zwischen 300 °C und 350 °C – abhängig von der Sauerstoffkonzentration – gebildetes NO_2 wieder zu NO zerfällt [103].

Eine Cordierit-Keramik oder ein metallischer Monolith bilden das DOC-Trägersubstrat. Um bei dem vorhandenen Trägervolumen des Katalysators eine möglichst große Oberfläche zu generieren, findet eine Beschichtung des Trägermaterials mit einem sogenannten „Washcoat“ Anwendung, meist auf Aluminiumdioxidbasis. Auf dessen poröse Oberfläche erfolgt dann der Auftrag der Edelmetallpartikel. Je nach Ausführung geschieht diese Beschichtung gleichmäßig oder gezont. [106]

Abbildung 2-6 stellt eine repräsentative Umsatzrate eines DOC in Abhängigkeit der Abgastemperatur dar.

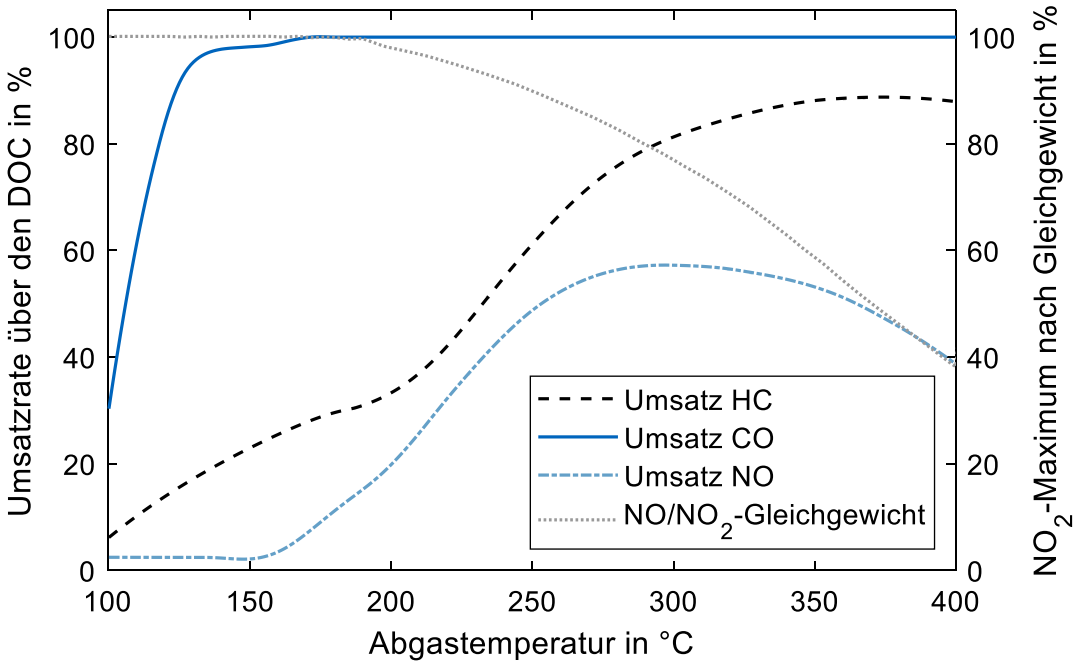

Abbildung 2-6: Repräsentative Umsatzrate eines DOC in Abhängigkeit der Abgastemperatur nach eigener Messung am Nutzfahrzeugdieselmotor; Gleichgewicht nach Epling et al. [107].

Eine Besonderheit stellt der Drei-Wege-Katalysator (TWC) dar. Dieser enthält zusätzlich zu Pt und Pd noch einen Anteil an Rhodium zur Reduktion von Stickoxiden. Für diese Reaktion ist allerdings ein stöchiometrisches Luftverhältnis erforderlich, weshalb dieser Katalysator bei konventionellen Dieselmotoren nicht zum Einsatz kommt [106].

Die Alterung und Deaktivierung des Katalysators geschieht im Wesentlichen über die folgenden Mechanismen:

- Thermische Alterung: Durch temperaturinduzierte Sintervorgänge verändert sich die Struktur der katalytischen Beschichtung, hauptsächlich durch Agglomeration der Edelmetallpartikel oder des Washcoats. Die resultierende Verkleinerung der katalytischen Oberfläche führt zur Reduktion der Katalysatoraktivität. [106]

- Vergiftung: Katalysatorgifte wie Phosphor, Zink oder Schwefel reagieren mit Edelmetallen und führen damit zur Blockade der aktiven Zentren [106].

- Maskierung: Spezies legen sich auf dem Washcoat oder den Edelmetallen ab und führen zur Blockade durch Verglasung oder Verkokung [108].

- Mechanische Schädigung: Aufgrund unterschiedlicher Wärmeausdehnung kommt es zur Reduktion der Adhäsion des Washcoats an der Substratoberfläche [108].

Katalysator für selektive katalytische Reduktion (SCR):

Katalysatoren für die Reduktion von NO_x-Emission über SCR erfahren mittlerweile breite Anwendung als Maßnahme zur Erfüllung der sukzessiv strenger werdenden Abgasgesetzgebungen [109]. Als Reduktionsmittel für die Reaktion dient NH_3 [110], eingedüst in Form wässriger Harnstofflösung, bekannt unter dem Handelsnamen „AdBlue®“ gemäß ISO 22241 [111]. In manchen SCR-Systemen bildet ein mit Titandioxid beschichteter Hydrolysekatalysator das vorderste Element, welcher die Harnstoffzersetzung durch Thermolyse und Hydrolyse in NH_3 und CO_2 über Isocyansäure (HNCO) als Zwischenprodukt unterstützt [112]. Da dafür ein homogenes Gemisch notwendig ist, kommen entweder spezielle Dosiermodule oder Mischer im Abgastrakt zum Einsatz [113].

Auf einem mit Kupferzeolith, Eisenzeolith oder Vanadiumoxid beschichteten Substrat findet die NO_x-Reduktion mit NH_3 über drei wesentliche Mechanismen statt, weitläufig bezeichnet als „Standard-“, „NO_2-“ und „Fast-SCR“:

$$4\,NO + 4\,NH_3 + O_2 \rightarrow 4\,N_2 + 6\,H_2O \qquad (17)\ [110].$$

$$6\,NO_2 + 8\,NH_3 \rightarrow 7\,N_2 + 12\,H_2O \qquad (18)\ [114].$$

$$NO + NO_2 + 2\,NH_3 \rightarrow 2\,N_2 + 3\,H_2O \qquad (19)\ [114].$$

Abbildung 2-7 stellt die Konvertierungsrate der NO_x-Emissionen unterschiedlich beschichteter SCR-Katalysatoren dar.

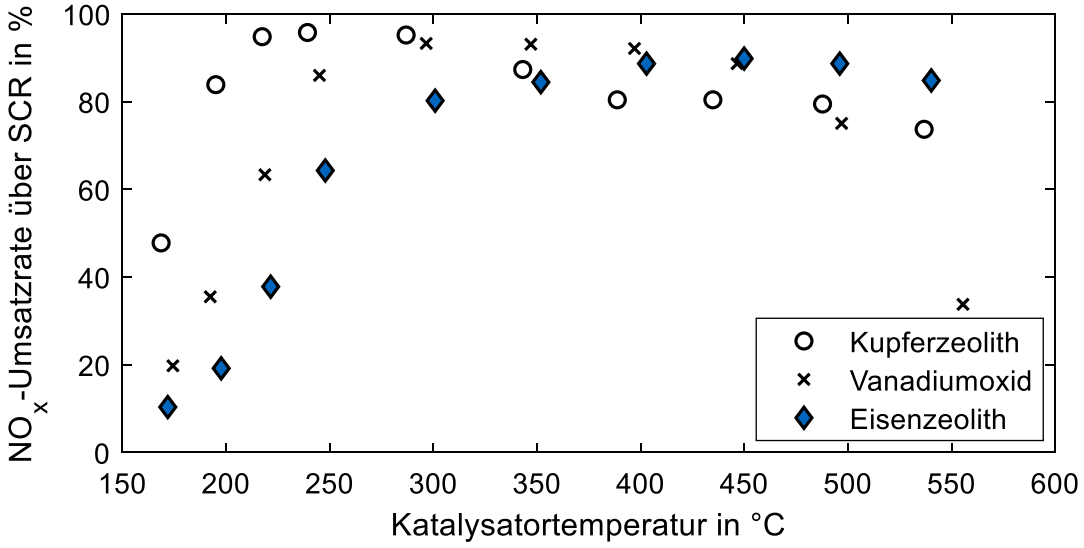

Abbildung 2-7: Repräsentative NO_x-Umsatzrate unterschiedlicher SCR-Katalysatoren in Abhängigkeit der Temperatur nach Girard et al. [115].

Bei der Auswahl der Beschichtungskonfiguration des SCR-Katalysators spielen neben der Umsatzrate über die Katalysatortemperatur noch weitere Faktoren eine Rolle: So etwa die Beständigkeit gegenüber Katalysatorgiften, die hydrothermale Stabilität, das Ammoniak-Speichervermögen und die Selektivität der Reduktionsmechanismen. [109]

Bei niedriger Selektivität des Katalysators kommt es zur Bildung unerwünschter Nebenprodukte, etwa von N_2O durch die unselektive katalytische Reduktion. Darüber hinaus begünstigen hohe Konzentrationen an NO_2 die unselektive Bildung von N_2O über NH_3 über folgende Konproportionierungsreaktion:

$$2\,NH_3 + 2\,NO_2 \rightarrow N_2O + N_2 + 3\,H_2O \qquad (20)\ [116].$$

N_2O gilt als besonders klimaschädlich und hat gegenüber CO_2 ein um den Faktor 265 erhöhtes Treibhauspotenzial über einen Betrachtungzeitraum von 100 Jahren [2]. Da der Reaktionsmechanismus der Fast-SCR ein stöchiometrisches Verhältnis von NO zu NO_2 voraussetzt, ein NO_2-Überschuss aber zur Bildung von N_2O führt, erfolgt die Auslegung des DOC bezüglich der NO-Oxidation auf ein optimales NO_2-NO_x-Verhältnis von 50 %.

Als letztes Element des SCR-Systems verhindert ein Ammoniaksperrkatalysator (ASC) einen Schlupf an überschüssigem NH_3 [109]. Dieser Schlupf geschieht aufgrund kurzfristiger Überdosierung des Reduktionmittels im transienten Motorbetrieb oder durch eine Auslagerung des auf der SCR-Katalysatoroberfläche eingespeicherten NH_3, da die Speicherfähigkeit mit zunehmender Temperatur abnimmt [117]. Während ein DOC über die unselektive Oxidation von überschüssigem NH_3 wiederum zur N_2O-Bildung führt [118], verfügt ein ASC über eine höhere Selektivität aufgrund einer zusätzlichen SCR-Beschichtung [119]. Dadurch erfolgt die Umwandlung von NH_3 zu N_2 und H_2O.

Neben SCR-Systemen bieten auch NO_x-Speicherkatalysatoren oder passive NO_x-Absorber (PNA) Alternativen zur NO_x-Reduktion von Dieselmotoren. Während NO_x-Speicherkatalysatoren über geringere Umsatzraten als SCR-Systeme verfügen [120], sind PNA aufgrund der höheren Systemkosten derzeit wenig verbreitet. Das Konzept eines AGN-Systems mit PNA sieht vor, dass diese im Kaltstart emittierte NO_x einspeichern, bis das SCR-System seine Betriebstemperatur erreicht. Dies gewinnt aufgrund der steigenden Anforderungen der Emissionsgesetzgebung und zukünftig stärkeren Gewichtung des Kaltstarts an Bedeutung. Diese Systeme befinden sich derzeit noch in einem frühen Entwicklungsstadium und erfahren bisher keinen Einsatz in der Serienanwendung. Grund hierfür sind die mangelnde thermische Stabilität, die N_2O-Bildung und die zu frühe Freigabe von NO_x ab einer Temperatur von bereits 150 °C. [109]

Dieselpartikelfilter (DPF):

DPF sind auf keramischen oder metallischen Substraten basierende Monolithen, die durch diffusive, impaktive, interzeptive und elektrostatische Abscheidung feste Partikel aus dem Abgasstrom filtrieren [121]. Sie unterscheiden sich dabei durch ihren Aufbau und ihre Wirkungsweise:

- Wandstromfilter: Diese keramischen Filter mit einer Bienenwabenstruktur sind abwechselnd auf der Einlass- und Auslassseite verschlossen. Der Abgasstrom passiert somit die porösen Wände zwischen den Kanälen, wodurch sich Partikel durch Oberflächenfiltration abscheiden [54]. Der durch die damit kontinuierliche Beladung anwachsende sogenannte „Rußkuchen“ erhöht dabei den Abscheidegrad [122], führt aber nach einiger Zeit zur Verblockung des Filters.

- Nebenstromfilter: Diese metallischen Filter lenken einen Teil des Abgasstroms durch Leitbleche in Richtung eines Filtermediums, wie etwa ein Sintermetallvlies [123]. Dieses fängt die Partikel in diesem Nebenstrom durch Diffusion oder elektrostatische Abscheidung ab [124]. Im Gegensatz zum Wandstromfilter besteht bei diesem System aufgrund seiner offenen Geometrie keine Gefahr der Verblockung.

Abbildung 2-8 vergleicht die Filtrationseffizienz der beiden Filtersysteme.

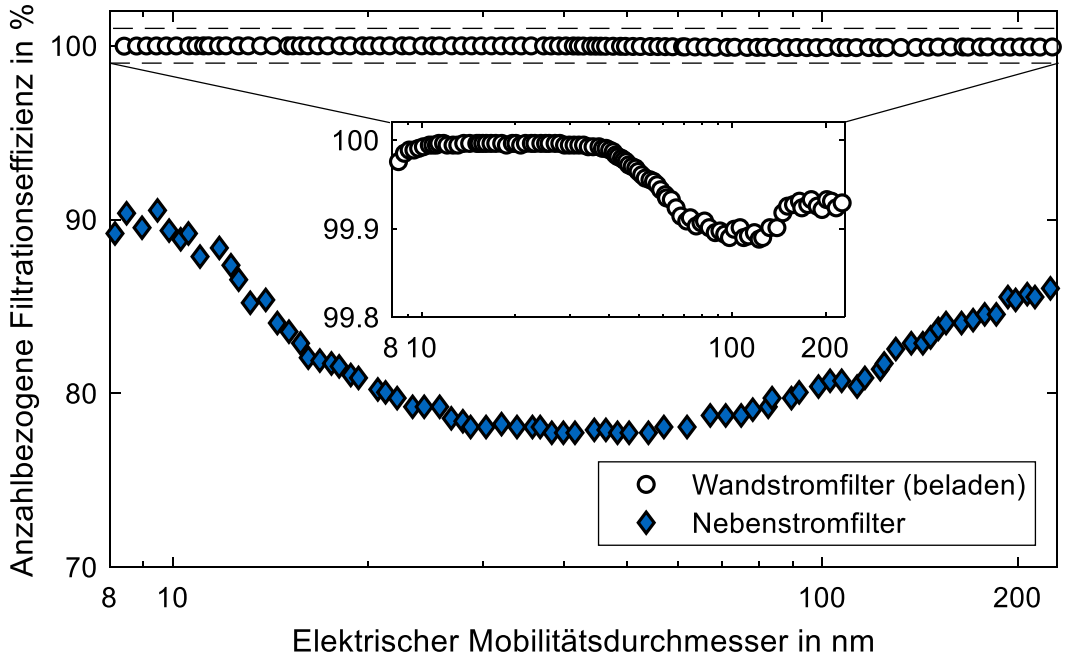

Abbildung 2-8: Repräsentative Filtrationseffizienz unterschiedlicher DPF in Abhängigkeit der Partikelgröße, Messwerte nach Rothe [100].

Beide Filtersysteme erfordern die Regeneration durch Abbrennen des filtrierten Rußkuchens. Während ein Anwachsen des Rußkuchens im Nebenstromfilter dafür sorgt, dass weniger Abgas durch das filtrierende Vlies strömt, resultiert es im Wandstromfilter zur vollständigen Verblockung. Diese hat eine Abgasgegendruckerhöhung zur Folge, die ohne Gegenmaßnahme bis zum Motorschaden führt. Die Regeneration läuft über zwei Mechanismen ab [54]:

1. Aktive Regeneration: Durch hohe Abgastemperaturen im Bereich ab 550 °C erfolgt ein „Freibrennen“ des Filters. Durch eine nachgelagerte Einspritzung von Kraftstoff, der nicht mehr im Brennraum, sondern auf dem DOC exotherm oxidiert, erhöht sich die Abgastemperatur vor dem DPF so weit, dass sie die Aktvierungsenergie der thermischen Kohlenstoffoxidation nach Formel (21) im DPF bereitstellt [125]. Diese Regenerationsart erfolgt periodisch je nach Beladungsgrad des DPF.

$$\mathrm{C} + \mathrm{O_2} \rightarrow \mathrm{CO_2} \qquad (21)\ [125].$$

2. Passive Regeneration: Eine kontinuierliche Reaktion ab 250 °C mit NO_2 führt zur Oxidation des Kohlenstoffs und ist unter dem Namen CRT-Effekt (CRT: Continuously Regeneration Trap) nach Formel (22) bekannt. Diese Regenerationsart erfordert eine ausreichende NO_2-Konzentration im Abgas in Abhängigkeit des Kohlenstoffgehalts im Filter [125]:

$$\mathrm{C} + 2\ \mathrm{NO_2} \rightarrow 2\ \mathrm{NO} + \mathrm{CO_2} \qquad (22)\ [125].$$

Um die Regeneration zu unterstützen, kommen teilweise katalytische Beschichtungen mit Pt und Pd auf dem DPF zum Einsatz, die wie beim DOC die Oxidation beschleunigen. Dies unterstützt den CRT-Effekt durch Erhöhung des NO_2-Anteils durch die Oxidation von NO [54].

Ein Teil der im Filter abgeschiedenen Partikel bestehen aus Ascherückständen, welche aus dem Schmieröl stammen. Diese setzen sich ebenfalls im Filter ab, eine Regeneration ist hier allerdings nicht möglich. Die kontinuierlich anwachsende Beladung sorgt für eine Steigerung der Filtrationseffizienz, erhöht aber über die Lebensdauer des DPF auch den Abgasgegendruck. Dies ist in Wartungsintervallen zu berücksichtigen [54].

Darüber hinaus ist eine SCR-Beschichtung des DPF möglich. Die Kombination der beiden AGN-Komponenten in einem Bauteil reduziert die Aufheizdauer im Kaltstart [54], den benötigten Bauraum und den Abgasgegendruck. Nachteile dieser Anwendung sind die höheren Systemkosten und die Reduktion des CRT-Effekts, da die SCR-Beschichtung hierfür notwendiges NO_2 bereits reduziert.

Aktuelle Herausforderungen in der Abgasnachbehandlung:

Die Abgasnachbehandlung über Katalysatoren setzt voraus, dass die Katalysatoroberfläche die jeweils spezifische Anspringtemperatur, den sogenannten „Light-Off“ erreicht. Um den Schadstoffausstoß während des Motorbetriebs gering zu halten, ist es zielführend, mit entsprechenden Maßnahmen die Aufheizphase bis zum Light-Off der Katalysatoren zu verkürzen. Solche Maßnahmen sind:

- Applikation der Einspritzung: Eine oder mehrere Nacheinspritzungen stellen Kraftstoff bereit, welcher nicht der Erhöhung der mechanischen Kolbenarbeit, sondern der Erhöhung der Abgastemperatur dient. Dies geschieht durch späte Umsetzung im Brennraum oder am DOC, sobald dieser seinen Light-Off erreicht [54, 126]. Im weiteren Verlauf dieser Arbeit wird diese Methode als „Fuel Dosing“ bezeichnet.

- Drosselklappe und Stauklappe im Abgasstrang: Durch Androsseln des Motors oder Aufstauen des Abgases erhöht sich die Abgastemperatur.

- Elektrische Heizung oder Abgasbrenner: Zusatzheizungen durch Heizstäbe/–scheiben oder Brenner im Abgasstrang erhöhen die Abgastemperaturen [127]. Je größer der Abgasstrom durch den Motor, desto geringer fällt die Erhöhung aus.

- Motornahe Katalysatoren: Je nach verfügbarem Bauraum findet eine Anordnung des ersten Katalysators in unmittelbarer Nähe des Abgaskrümmers statt, um die Aufheizdauer zu verkürzen [54].

Diese Maßnahmen gehen zu Lasten des Kraftstoffverbrauchs und führen teilweise zu höheren Rohemissionen. Über einen gesamten Fahrzyklus kompensiert die kürzere Anspringzeit der AGN idealerweise die höheren Schadstoffemissionen im Kaltstart.

Darüber hinaus kommt es im Kaltstart oder beim Einsatz von Fuel Dosing bei den vordersten Elementen der AGN zum Phänomen des sogenannten „Face Plugging“, bei dem im Rohabgas vorhandene Rußpartikel in Verbindung mit unverbrannten Kohlenwasserstoffen zur Maskierung der Katalysatoroberfläche führen [128].

Da im Kaltstart die Rußemissionen insbesondere im AGR-Kühler zur Versottung führen, erfolgt die Abschaltung der AGR im Kaltstart, was zu höheren NO_x-Emissionen führt.

Analog zum Ruß-NO_x-Zielkonflikt erzeugt die SCR-Technologie einen N_2O-NO_x-Zielkonflikt. Je höher die NO_x-Rohemissionen des Motors sind, desto höher ist der Ausstoß an im SCR-System gebildeten N_2O, je nach Selektivität des Katalysators.

2.3 OME als kraftstoffbasierter Ansatz zur Emissionsreduktion

2.3.1 Überblick und Kraftstoffeigenschaften

Aufgrund des bei innermotorischen Maßnahmen zur Emissionsreduktion auftretenden Ruß-NO_x-Zielkonflikts und des hohen Kosten- und Systemaufwands einer dieselmotorischen Abgasnachbehandlung bieten sich Ansätze an, den Kraftstoff selbst als Stellschraube zur Emissionsreduktion zu behandeln. Die Bezeichnung „Tailored Fuels“ beschreibt synthetische Kraftstoffe, die gegenüber ihrem fossilen Gegenstück günstigere Eigenschaften für die Verbrennung im Motor aufweisen [129]. Im Falle von Dieselmotoren gelten Oligomere aus der Reihe der OME aufgrund ihrer rußfreien Verbrennung als vielversprechende Kandidaten, fossilen Dieselkraftstoff zu ersetzen [11]. OME besitzen die Strukturformel CH_3-O-$(CH_2O)_n$-CH_3, wobei n die Anzahl der Oxymethylengruppen (-CH_2O-) innerhalb des Moleküls angibt. In der Literatur hat sich die Abkürzung OME_n zur Spezifizierung der Kettenlänge des jeweiligen Ethers etabliert. OME_0 entspricht der Substanz Dimethylether, welche in der Industrie den großflächigen Einsatz als Treibmittel erfährt [130]; OME_1 entspricht Dimethoxymethan (DMM), großflächig eingesetzt als Lösungsmittel [131]. Längerkettige OME mit n > 6 finden Anwendung in der Polymertechnik [132]. Die rußfreie Verbrennung von OME resultiert *nach Ogawa* aus der Abwesenheit innermolekularer C-C-Bindungen, welche nach den Rußbildungstheorien die Formierung von Rußvorläufern wie Acetylen verhindert [133]. Dies löst den innermotorischen Ruß-NO_x-Zielkonflikt bei mit OME_n betriebenen Motoren auf. Unter Anwendung entsprechender Maßnahmen wie Erhöhung der AGR-Rate oder Reduktion des Einspritzdrucks unterschreiten die Konzentrationen an NO_x und Partikeln im Rohabgas deutlich die eines mit fossilem oder paraffinischem Dieselkraftstoff betriebenen Aggregats [12, 13, 20, 21, 134]. Aus diesem Grund formulierten mehrere Autoren die Hypothese, dass mit OME_n betriebene Dieselmotoren in Kombination mit AGN das Potenzial zu derart niedrigen Schadstoffkonzentrationen im Abgas bieten, dass diese die Hintergrundkonzentration urbaner Gebiete unterschreiten könnten oder sogar einen schadstofffreien Betrieb ermöglichen [31–33, 35, 36, 135].

Um den physikalischen Eigenschaften von fossilem Dieselkraftstoff zu entsprechen oder diese zu übertreffen, sind Mischungen mit vorwiegend OME_n der Kettenlänge 3 – 5 notwendig. Kürzere OME_n sind leichtflüchtiger, längere OME_n liegen bei Raumtemperatur im festen Aggregatszustand vor. Der Normentwurf für OME-Kraftstoff M DIN TS 51699 orientiert sich an den Werten der DIN EN 590 für Dieselkraftstoff, definiert aber für manche Eigenschaften strengere Grenzwerte: So etwa eine höhere Cetanzahl für die Erhöhung der Zündwilligkeit und

einen höheren Flammpunkt für die einfachere Lagerung des Kraftstoffs. Tabelle 2-1 stellt die beiden Kraftstoffe gemäß ihrer Normen gegenüber.

Tabelle 2-1: Gegenüberstellung der Stoffwerte von handelsüblichem Dieselkraftstoff nach DIN EN 590 [136] und OME-Kraftstoff entsprechend des Normentwurfs M DIN TS 51699 [137].

Eigenschaft	**Diesel**	**OME**
Spezifiziert in beiden Normen	*DIN EN 590*	*M DIN TS 51699*
Cetanzahl	≥ 51	≥ 65
Dichte bei 15 °C	820 – 845 kg/m³	1045 – 1070 kg/m³
Kinematische Viskosität bei 40 °C	2,000 – 4,500 mm²/s	0,900 – 1,500 mm²/s
Schmierfähigkeit	≤ 460 µm	≤ 460 µm
Flammpunkt	≥ 55 °C	≥ 60 °C
Cold Filter Plugging Point (CFFP)	≤ -20 – 0 °C *	Ist anzugeben**
Oxidationsstabilität	≥ 20 h	≥ 240 min (bei 120 °C)
Schwefelgehalt	≤ 10 mg/kg	≤ 5 mg/kg
Wassergehalt	≤ 0,020 vol-%	≤ 0,020 vol-%
Gesamtverschmutzung	≤ 24 mg/kg	≤ 15 mg/kg
Nicht spezifiziert in der Norm DIN EN 590		
Formaldehydgehalt	-	≤ 200 mg/kg
Trioxangehalt	-	≤ 1000 mg/kg
Peroxidzahl	-	≤ 10 meq O/g
Säurezahl	-	≤ 10 mg KOH/g
Gefrierpunkt	-	≤ -20 °C
Unterer Heizwert	-	Ist anzugeben**

* Je nach Jahreszeit, festgelegt in DIN EN 590. | ** Ist anzugeben, aber nicht beschränkt.

In den nachfolgenden Kapiteln dieser Arbeit bezieht sich die Abkürzung OME auf eine Mischung nach der Norm M DIN TS 51699, sofern nicht anderweitig spezifiziert.

2.3.2 Herstellung

Die von *Burger et al.* [138–140] und *Schmitz et al*. [141] beschriebenen Syntheseprozesse von OME basieren auf den Edukten Methanol (CH_3OH) und CH_2O. Erfolgt die Herstellung dieser beiden Komponenten aus CO_2 und regenerativ gewonnenem H_2, gleicht die bei der Synthese von OME gebundene CO_2-Menge die bei der Verbrennung ausgestoßene Menge aus. Dies führt zum Potenzial der Klimaneutralität. Voraussetzung dafür ist zum einen die Gewinnung von CO_2 aus der Umgebungsluft [142, 143] oder aus Abfallprodukten industrieller Prozesse, entweder durch direkte Abscheidung oder durch Abgaswäsche [144, 145]. Zum anderen setzt die Einordnung als klimaneutraler Syntheseprozess H_2 aus nachhaltigen Quellen voraus, beispielsweise aus Elektrolyse mittels erneuerbaren Stroms. Aus den Edukten CO_2 und H_2 erfolgt die Synthese zu CH_3OH; die Gewinnung von CH_2O läuft mithilfe eines Silberkatalysators ab [146]. Im Druckschwingprozess bildet CH_2O im nächsten Schritt Trioxan, CH_2O und CH_3OH synthetisieren in wässriger Lösung zu DMM respektive OME_1 [140]. Dieses OME_1 und das gewonnene Trioxan bilden die Syntheseedukte von langkettigen OME_n. Die von *Schmitz et al.* konzeptionierte Route der OME_n-Synthese läuft direkt über CH_2O und CH_3OH ab [141]. Abbildung 2-9 stellt den Syntheseprozess langkettiger OME_n schematisch dar.

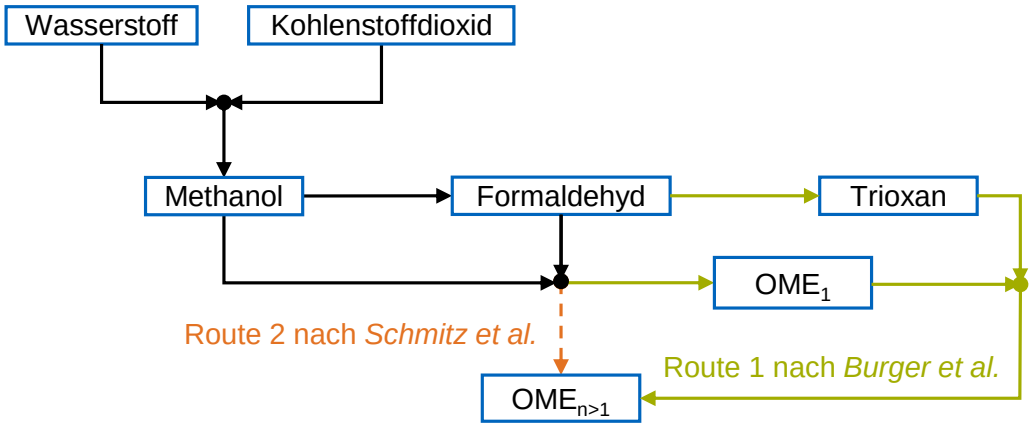

Abbildung 2-9: Schematische Darstellung der Syntheserouten von $OME_{n>1}$ nach Held et al. [147].

Held et al. geben für die Energieeffizienz der OME_n-Synthese je nach Gewinnungsart von CO_2 und H_2 sowie in Abhängigkeit des Prozessdesign Werte von 24,3 % bis 36,7 % an, wobei auf die Hydrolyse von H_2 ein Wirkungsgrad von 60 % entfällt [147].

2.4 Forschungsbedarf und Zielsetzung dieser Arbeit

Die einschlägige Fachliteratur bietet ein breites Spektrum an Forschungsarbeiten, die sich mit der Verbrennung und der motorischen Nutzung von OME_n befassen. Die jeweiligen OME_n liegen dabei sowohl in Form von Reinstoffen, einer Mischung von OME_n unterschiedlicher Kettenlänge, als auch in Mischungen mit fossilem Dieselkraftstoff, sogenannten „Blends“, vor. *Pélerin* gibt einen Überblick über einige dieser Arbeiten [148]. Abbildung 2-10 fasst aktuelle Arbeiten [17–20, 22–24, 26–30, 37, 38, 149–166] in Bezug auf den Kraftstoff und den Versuchsträger zusammen.

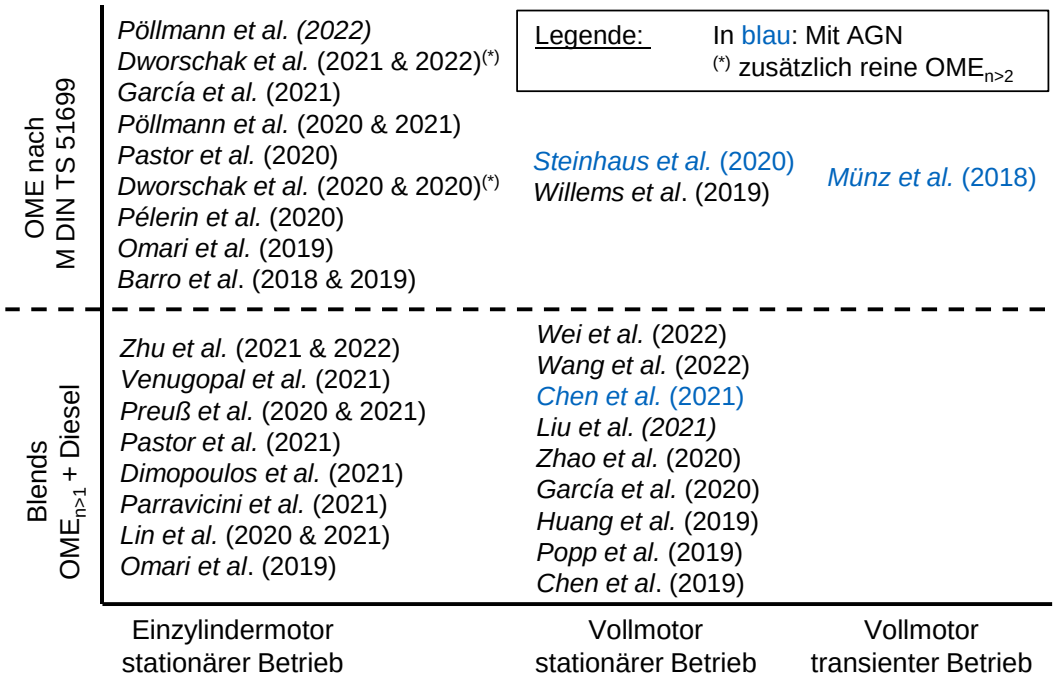

Abbildung 2-10: Chronologische Übersicht einiger aktuell publizierter Untersuchungen zur motorischen Verbrennung von OME nach M DIN TS 51699, reinen OME_n unterschiedlicher Kettenlänge und in Blends mit Diesel.

Die Übersicht in Abbildung 2-10 macht deutlich, dass die publizierten Arbeiten mit im Vergleich zu Serienmotoren vereinfachten Versuchsträgern und Blends dominieren, während für längerkettige OME_n bisher keine Veröffentlichungen zum ganzheitlichen Emissionspotenzial von Serienmotoren in Kombination mit Abgasnachbehandlung vorliegen. Mit Ausnahme der Arbeit von *Münz et al*. gehen die aufgeführten Arbeiten nicht über Versuchsträger unter stationären Laborbedingungen hinaus; *Münz et al.* betrachten allerdings nur isoliert die Emission an PN_{23} [38]. Eine Anpassung der Betriebsstrategie des Motors, die Wechselwirkungen von OME mit den Komponenten des AGN-Systems, bisher nicht reglementierte Emissionen und der Schadstoffausstoß im Kaltstart sind nicht Gegenstand der aufgeführten Veröffentlichungen.

Um die Hypothese eines klimaneutralen und schadstofffreien OME-Motors zu überprüfen, sind über die bereits veröffentlichten Arbeiten hinaus Untersuchungen zu folgenden Themen notwendig, welche die vorliegende Dissertation behandelt:

- Anpassung der Betriebsstrategie des Motors an die physikalisch-chemischen Eigenschaften und die rußfreie Verbrennung von OME: Die in den bisher publizierten Arbeiten gewonnenen Erkenntnisse sind auf ihre Wirksamkeit in Bezug auf niedrigste Rohemissionen am Nutzfahrzeugmotor zu überprüfen. Der Fokus liegt dabei auf der Einspritzstrategie und der AGR-Regelung, um die NO_x-Konzentration im Rohabgas für eine vollständige Umsetzung im AGN-System gering zu halten.

- Anpassung der Betriebsstrategie der AGN auf die rußfreie Verbrennung von OME: Die rußfreie Verbrennung bietet Freiheitsgrade für innermotorische Maßnahmen sowie in der AGN. Insbesondere die Harnstoffdosierregelung im SCR-System ist auf diese veränderte Rahmenbedingung anzupassen, um den NO_x-Umsatz zu maximieren.

- Wechselwirkungen des AGN-Systems mit Abgas aus der OME-Verbrennung: Die für fossilen Dieselkraftstoff entwickelte Abgasnachbehandlung ist hinsichtlich Effizienz und Selektivität zu untersuchen, um neue Zielkonflikte oder die Entstehung neuer Schadstoffe zu detektieren.

- Beschaffenheit von Nanopartikeln im Abgas von OME-Motoren: Partikelemissionen sind über die Betrachtungsgrenzen bisheriger Abgasgesetzgebung hinaus zu untersuchen. Kriterien sind Beschaffenheit, Konzentration und Wechselwirkungen mit der AGN.

- Schadstoffkonzentrationen reglementierter und nicht reglementierter Spezies im realitätsnahen Motorbetrieb: Ein schadstofffreier Betrieb ist an einem seriennahen Motor mit Abgasnachbehandlung in homologationsrelevanten Fahrzyklen zu demonstrieren.

Eine solche Demonstration setzt nach bisherigen Erkenntnissen eine betriebswarme AGN voraus [37]. Aus diesem Grund umfasst die vorliegende Dissertation über die oben genannten Punkte hinaus folgende Betrachtung:

- Heizmaßnahmen und Schadstoffemissionen im Kaltstart: Die im Kaltstart auftretenden Emissionen sind ebenso wie Maßnahmen zur Reduktion der Warmlaufphase inaktiver AGN zu untersuchen.

3. Angewandte Methodik

3.1 Versuchsträger

Im Rahmen der Forschungsarbeit kommen unterschiedliche Versuchsträger zum Einsatz:

- Einspritzverlaufsindikator (EVI): Dieser basiert auf dem Prinzip des Bosch-Rohrs [167] und wurde im Rahmen der Dissertation von *Schuckert* [168] am Lehrstuhl für Verbrennungskraftmaschinen entwickelt. Er dient zur Bestimmung zeitlicher Verläufe der Einspritzraten der verwendeten Injektoren im OME-Betrieb, welche als Eingangsgröße für das 0D-/1D-Simulationsmodell zur Arbeitsprozessrechnung benötigt werden. Darüber hinaus zeigt er Unterschiede im hydraulischen Verhalten der Injektoren zwischen Diesel- und OME-Betrieb auf.

- Einzylinderforschungsmotor: Dieser im Rahmen der Dissertation von *Pflaum* [99] am Lehrstuhl für Verbrennungskraftmaschinen entwickelte Versuchsträger ist von einem Nutzfahrzeugmotor abgeleitet. Die Druckverlaufsanalyse eines an diesem Motor vermessenen Kennfelds im OME-Betrieb dient als Grundlage für die Kalibrierung des prädiktiven Verbrennungsmodells in einer 0D-/1D-Simulationsumgebung.

- MAN D0834LFL79: Dieser Nutzfahrzeugmotor dient als Versuchsträger für die Untersuchungen zu Wechselwirkungen von OME-Abgas mit dem DOC. Der Fokus liegt hierbei auf Heizstrategien des AGN-Systems durch Kraftstoffumsetzung am DOC.

- MAN D2676LF51: Dieser Nutzfahrzeugmotor dient als Versuchsträger für die Untersuchungen zu Wechselwirkungen von OME-Abgas mit dem SCR-System und dem Partikelfilter. Darüber hinaus erfolgt die Charakterisierung der Nanopartikelemissionen an diesem Versuchsträger, ebenso wie die Fahrzyklen zur Demonstration des schadstofffreien Betriebs. Zusätzlich basieren die Untersuchungen der Kaltstartemissionen sowie die Bewertung unterschiedlicher Aufheizstrategien auf diesem Versuchsträger.

Die detaillierte Beschreibung der jeweiligen Versuchsträger, der angewandten Messmethodik und die Spezifikation der Messgeräte findet in den für diese Dissertation als Grundlage dienenden Publikationen statt.

3.2 Testkraftstoffe

ASG Analytik-Service AG stellt die im Rahmen dieser Arbeit verwendeten OME-Mischungen in zwei unterschiedlichen Chargen bereit. Charge 1 findet Anwendung in den Untersuchungen am EVI sowie am Einzylinderforschungsmotor und den darauf aufbauenden 0D-/1D-Simulationen. Charge 2 dient der Bestimmung der Wechselwirkungen mit dem AGN-System, der Charakterisierung der Nanopartikel im Abgas, der Demonstrationen der Fahrzyklen sowie den Untersuchungen im Kaltstart. Als Referenzkraftstoff dient fossiler Dieselkraftstoff (B7) nach DIN EN 590 [136], im Folgenden vereinfachend als Diesel referenziert.

Tabelle 3-1 zeigt die ermittelten Stoffwerte der beiden Chargen unter Angabe der jeweiligen Messmethode. Beide Kraftstoffmischungen erfüllen die Norm M DIN TS 51699.

Da sich bei beiden Chargen die über die Gaschromatographie ermittelten Anteile unterschiedlicher OME_n nicht zu 100 % addieren, basiert die Berechnung von $L_{min,OME}$ auf der folgenden Annahme: Mit Berücksichtigung der Messgenauigkeit der verwendeten Methodik [169] erfolgt die Abschätzung der fehlenden Massenanteile derart, dass die eine Hälfte auf OME_7 zurückgeht, die andere auf OME_8. Die zur Berechnung des stöchiometrischen gravimetrischen Mindestluftbedarfs $L_{\mathrm{min,OME}}$ in Formel (23) benötigten C-, H- und O-Massenanteile ξ_C, ξ_H und ξ_O stammen aus den in Tabelle 3-1 angegebenen Anteilen an OME_n, ebenso wie die molare Masse des Ersatzmoleküls der Mischung M_{OME}. Formel (24) leitet sich aus Formel (3) in Kapitel 2.1.1 ab. Die molare Masse trockener Luft $M_{\mathrm{Luft,tr}}$ von 28,9635 kg/kmol stammt von *Giacomo* [39], ebenso wie der molare Anteil an Sauerstoff in Luft $n_{\mathrm{O2,Luft}}$ von 0,2094. Die Atommassen m_x stammen von *Wieser et al.* [170] und *Audi & Wapstra* [171].

$$L_{\mathrm{min,OME}} = \frac{M_{\mathrm{Luft,tr}}}{n_{\mathrm{O2,Luft}}} \cdot \left(\frac{\xi_{\mathrm{C}}}{m_{\mathrm{C}}} + \frac{\xi_{\mathrm{H}}}{4 \cdot m_{\mathrm{H}}} - \frac{\xi_{\mathrm{O}}}{2 \cdot m_{\mathrm{O}}} \right) \quad (22).$$

Das volumetrische Dieseläquivalent berechnet sich über die Heizwerte $H_{u,n}$ und Dichten ρ_n von OME und Diesel nach Formel (24), unter Annahme des unteren Heizwerts von Diesel in Höhe von 42,6 MJ/kg nach *Lautenschütz et al.* [172]:

$$\frac{\rho_{\mathrm{Diesel}} \cdot H_{\mathrm{u,Diesel}}}{\rho_{\mathrm{OME}} \cdot H_{\mathrm{u,OME}}} \quad (23).$$

Dieser Wert variiert in Tabelle 3-1 aufgrund des angegebenen Intervalls in der Dichte von Diesel nach DIN EN 590.

Tabelle 3-1: Stoffwerte der verwendeten OME-Mischungen. Die jeweilige Bestimmungsmethode der Stoffwerte findet sich in den Appendizes der zugehörigen Publikationen.

Eigenschaft	**OME (Charge 1)**	**OME (Charge 2)**
OME_1- / OME_2-Gehalt in %*	- | 0,01	0,01 | 0,01
OME_3-Gehalt in %*	47,11	57,90
OME_4-Gehalt in %*	29,48	28,87
OME_5-Gehalt in %*	16,70	10,07
OME_6-Gehalt in %*	5,56	1,91
Cetanzahl	74,1	68,6
Dichte bei 15 °C in kg/m³	1067,0	1057,1
Kinematische Viskosität bei 40 °C in mm²/s	1,183	1,082
Schmierfähigkeit bei 60 °C in µm	350	320
Flammpunkt in °C | CFPP in °C	68,0 | -23	65,0 | -40
Oxidationsstabilität in h	> 12	> 48
Wasser-/ Schwefelgehalt in mg/kg	150 / < 5	146 / < 5
Gesamtverschmutzung in mg/kg	1	2
Formaldehydgehalt in mg/kg	300	233
Molare Masse in kg/kmol**	156,75	150,77
Unterer Heizwert in MJ/kg	19,2	19,2
Volumetrisches Dieseläquivalent**	1,71 – 1,76	1,72 – 1,77
Stöchiometrischer Mindestluftbedarf in kg/kg**	5,9	5,9

*Oberflächenprozent, vereinfachend gleich Massenprozent [169] | **Eigene Berechnung

Darüber hinaus enthalten beide Kraftstoffmischungen 300 ppm Butylhydroxytoluol zur Erhöhung der Oxidationsstabilität, um die Zersetzung des Kraftstoffs zu CH_2O zu verhindern [173]. Die zusätzliche Additivierung mit 300 ppm Tallölfettsäuren, eingesetzt als „Flow Improver“, erhöht die Schmierfähigkeit.

3.3 Betriebsstrategie des zweistufigen SCR-Systems

Die Demonstration des schadstofffreien Betriebs am Versuchsträger MAN D2676LF51 erfordert die vollständige Umsetzung der NO_x-Emissionen im zweistufigen SCR-System. Hierfür ist eine dynamische Regelung zur Dosierung des Reduktionsmittels AdBlue notwendig. Um den Zielkonflikt NH_3-Schlupf bei Überdosierung und NO_x-Schlupf bei Mangeldosierung auszugleichen, enthält die Dosierstrategie eine Verschränkung der beiden SCR-Stufen. Abbildung 3-1 stellt die eingesetzte Dosierstrategie schematisch dar. α beschreibt dabei das Verhältnis zu dosierter und für einen vollständigen NO_x-Umsatz benötigter AdBlue-Menge, in Analogie zum Verbrennungsluftverhältnis λ.

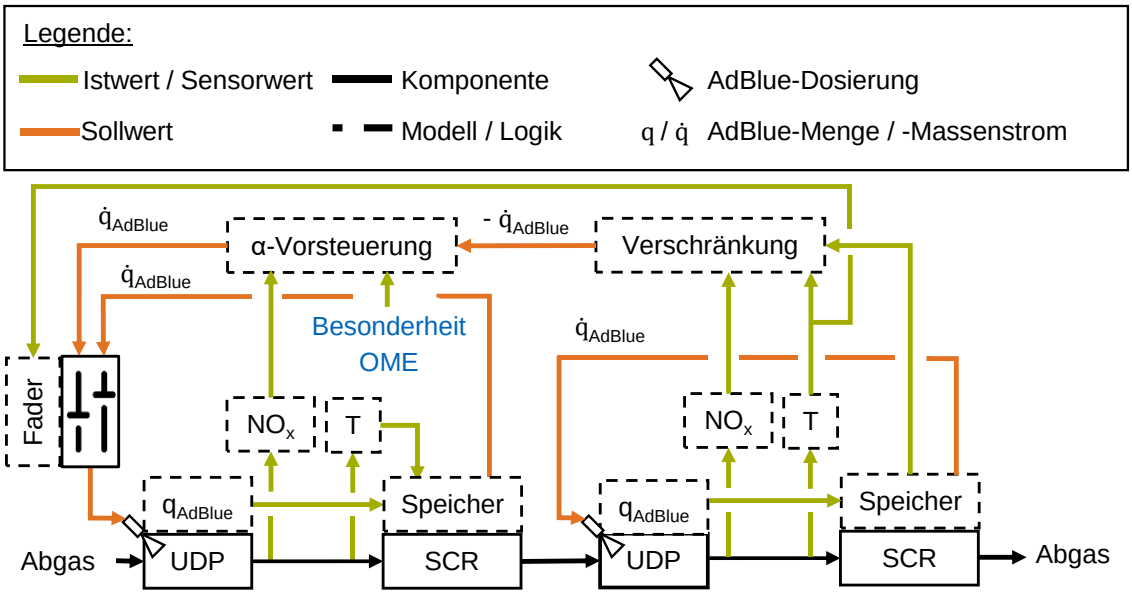

Abbildung 3-1: Übersicht der verwendeten Dosierstrategie am zweistufigen SCR-System.

Das NH_3-Speichermodell der SCR-Katalysatoren ist abhängig vom jeweiligen Volumen, der Trägertemperatur (T) und der bereits dosierten AdBlue-Menge. Bevor das hintere SCR-System seine Betriebstemperatur erreicht, erfolgt die Dosierung an der vorderen Stufe über die Speicherregelung. In Abhängigkeit von T der zweiten Stufe wechselt diese Regelung über eine Kennlinie („Fader“) in die α-Vorsteuerung, welche für die erste Stufe eine Dosierung in Abhängigkeit des Soll-α einstellt. Im Dieselbetrieb ist die Limitierung von α notwendig, um genügend NO_2 für die passive Regeneration des DPF zwischen den SCR-Stufen vorzuhalten. Im OME-Betrieb ist aufgrund der rußfreien Verbrennung ein höheres α möglich, was zu einer höheren NO_x-Gesamtreduktion führt. Eine Dosierung mit $\alpha = 1$ ist allerdings auch hier zu vermeiden: Um NH_3-Ausspeicherung bei steigender Temperatur aus der zweiten SCR-Stufe zu verhindern, ist stattdessen die Verschränkung der beiden Speichermodelle notwendig, welche wiederum zu einer Reduktion der Dosiermenge an der ersten Stufe führt.

4. Ergebnisse

4.1 Betriebsstrategien am OME-Motor

OME weist gegenüber fossilem Dieselkraftstoff unterschiedliche chemische und physikalische Eigenschaften auf. Physikalische Eigenschaften wie die höhere Dichte und verringerte dynamische Viskosität beeinflussen die Einspritzcharakteristik eines Magentventilinjektors. *Peter et al.* demonstrierten den veränderten Einspritzverlauf zweier Pkw-Injektoren im Betrieb mit OME [174]. Chemische Eigenschaften wie die rußfreie Verbrennung, eine höhere Zündwilligkeit und der geringere Heizwert führen zu mehr Freiheitsgraden in der Verbrennungssteuerung, wie geringere Einspritzdrücke oder Verzicht auf die Voreinspritzung. Darüber hinaus erfordert insbesondere der geringere Heizwert eine Anpassung der Düsengeometrie zur Vergrößerung der gesamten Einspritzlochquerschnittsfläche, um der Notwendigkeit längerer Einspritzdauern bei Betriebspunkten mit hoher Last entgegenzuwirken [18]. *Röll et al.* untersuchten den hydraulischen Einspritzverzug und den Einspritzverlauf von OME als Pilotkraftstoff in Dual-Fuel-Motoren und erklärten die Unterschiede zu Diesel aufgrund der geringen Kraftstoffmengen in dieser Anwendung als vernachlässigbar [175]. *Pélerin et al*. beobachteten die Auswirkungen einer Düsengeometrieanpassung auf die Emissionen und den Wirkungsgrad, ebenso wie den Einfluss der Voreinspritzung auf den Brennverlauf [20]. Diese Untersuchung beschränkt sich auf einen einzelnen repräsentativen Betriebspunkt, verspricht aber das Potenzial zur Vereinfachung des Einspritzsystems eines OME-Motors durch den Verzicht auf eine Voreinspritzung und die Absenkung des Raildrucks. Um die Notwendigkeit der Düsengeometrieanpassung und deren Auswirkung auf die NO_x-Emissionen und den Wirkungsgrad zu bewerten, sind umfassende Untersuchungen über das gesamte Motorbetriebskennfeld zielführend.

Gelner, A. D.; Höß, R.; Zepf, A.; Härtl, M.; Wachtmeister, G.: *Engine Operation Strategies with the Alternative Diesel Fuel Oxymethylene Ether (OME): Evaluation Using Injection Rate Analyzer and 0D-/1D-Simulation*; SAE Technical Paper 2021-0050; 2021. [176]

Diese Publikation präsentiert eine pareto-optimale Motorbetriebsstrategie für OME hinsichtlich Wirkungsgrad und NO_x-Emissionen mittels 0D-/1D-Simulation. Zur Kalibrierung des Strömungs-, Verbrennungs- und Emissionsmodells dienen Druckverlaufsanalysen mehrerer Betriebspunkte des Kennfelds eines mit OME betriebenen Einzylinderforschungsmotors mit zwei unterschiedlichen Injektoren, sowie derer am EVI ermittelten Einspritzverläufe. Die Arbeit zeigt damit erstmals die Kalibrierung eines prädiktiven OME-Verbrennungsmodells in Kombination mit der Erstellung eines Fluidobjekts von OME in der Bibliothek der Simulationsumgebung mit dafür ermittelten Stoffwerten. Die Veröffentlichung untersucht den Einfluss der im Vergleich zu fossilem Diesel unterschiedlichen physikalischen Stoffwerte von OME auf den Einspritzverlauf des Injektors und zeigt, dass der Einspritzverzug im Betrieb mit OME größer ist, die Schließgeschwindigkeit der Düsenadel geringer ist und der Massenstrom bei vollständig geöffnetem Injektor höher ist als im Dieselbetrieb. Bei energetischer Betrachtung kompensieren diese Effekte aber bei beiden Injektoren nicht den geringeren Heizwert von OME. Die Simulation der Motorbetriebspunkte ergibt, dass aufgrund der höheren Zündwilligkeit von OME die im Dieselmotor übliche Voreinspritzung obsolet wird und ein Verzicht darauf den Wirkungsgrad erhöht. Das Verbrennungsgeräusch und die NO_x-Emissionen steigen im Vergleich dazu nur marginal an. Der Injektor mit größeren Einspritzlochdurchmessern zeigt den höheren Wirkungsgrad und verbessert in Kombination mit Verzicht auf die Voreinspritzung die Wirkungsgrad-NO_x-Paretofront. Ein pareto-optimaler Betrieb setzt hohe Raildrücke voraus, während die AGR-Rate eine Bewegung auf der Paretofront je nach Auslegungsziel ermöglicht. Der Einspritzzeitpunkt dient als Werkzeug zur Annäherung an die Paretofront, der optimale Wert ist vom jeweiligen Betriebspunkt abhängig.

Eigener Beitrag zur Publikation:

Mein Beitrag zur Publikation liegt in der Idee der Untersuchung, Konzeptionierung der Methodik für die Untersuchungen am Einspritzverlaufsindikator, der Kennfeldervermessung am Motorenprüfstand und der Modellerstellung in der Simulationsumgebung. Darüber hinaus führte ich die Datenerhebung zur Vermessung des Motorenkennfelds beider Injektoren durch und unterstützte bei der Ermittlung der Einspritzraten sowie der Simulation der Betriebsstrategien, und leitete die Auswertung der Ergebnisse an. Ich erstellte die Abbildungen im Methodikteil der Publikation und leitete die Erstellung der restlichen an. Das Manuskript der Publikation wurde von mir geschrieben und gemäß den Anmerkungen der Co-Autoren und Reviewer angepasst.

Weiterführende Untersuchung: Injektorsimulation mit Viskositäts- und Dichtevariation

Peter et al. formulieren die Hypothese, die in der Publikation beobachtete geringere Öffnungs- und Schließgeschwindigkeit des Injektors im OME-Betrieb resultiere aus der höheren Dichte von OME im Vergleich zur Dichte von Diesel [174]. Um diese Hypothese zu überprüfen, dient eine Simulation der (fluid-)mechanischen Vorgänge innerhalb des Injektors mithilfe des in der Arbeit von *Schuckert et al*. vorgestellten Injektormodells [177]. Um den Einfluss der Kraftstoffdichte und –viskosität zu bewerten, erfolgt der Import des in der vorgestellten Publikation [176] erstellten Kraftstoffobjekts von OME in die Simulationsumgebung GT Suite 2019 (Gamma Technologies Inc.) des Injektormodells. Zusammen mit dem vorhandenen Dieselobjekt, mit dem die Validierung des Modells erfolgte, und einer Kombination der beiden Objekte bezüglich Dichte ρ und dynamische Viskosität μ ergeben sich vier Kraftstoffmodelle, anhand derer der Einfluss von ρ und μ auf das Injektorverhalten darstellbar ist. Abbildung 4-1 zeigt die Ergebnisse der Kraftstoffvariation hinsichtlich Nadelhub h_N, Steuerraumdruck p_S und Einspritzverlauf mt_{KS} für einen Betriebspunkt mit vollständig geöffnetem Injektor. Die Kurven des Steuerraumdrucks und daraus resultierend die Nadelhubkurven bestätigen die Hypothese des Dichteeinflusses, nach der die Nadelgeschwindigkeit im Schließvorgang aufgrund der höheren Dichte von OME geringer ist. Darüber hinaus ergibt sich auch ein Einfluss durch die niedrigere dynamische Viskosität, die diese Wirkung verstärkt. Im Öffnungsprozess hingegen verhalten sich die Einflüsse von ρ und μ gegenläufig. Während eine höhere Dichte die Nadelgeschwindigkeit reduziert, sorgt eine höhere Viskosität für eine niedrigere Öffnungsgeschwindigkeit. Im direkten Vergleich öffnet der Injektor im OME-Betrieb schneller und schließt langsamer als im Dieselbetrieb. Diese Ergebnisse bestätigen die Hypothese von *Peter et al*. hinsichtlich der niedrigeren Schließgeschwindigkeit aufgrund der höheren Dichte von OME und erweitern diese Erklärung um den Einfluss der niedrigeren dynamischen Viskosität. Bezüglich des Öffnungsprozesses widersprechen die Ergebnisse der Hypothese. Bezüglich des Einspritzmassenverlaufs bestätigt sich der höhere Kraftstoffdurchsatz im OME-Betrieb bei vollständig geöffnetem Injektor. Für den bei OME steileren Anstieg von mt_{KS} ist im Öffnungsprozess die dynamische Viskosität ausschlaggebend, im Schließprozess zeigen sich analoge Einflüsse zum Nadelhub und Steuerraumdruck. Zusammenfassend ergibt die Injektorsimulation, dass neben der höheren Dichte auch die niedrigere Viskosität von OME den Einspritzverlauf beeinflusst.

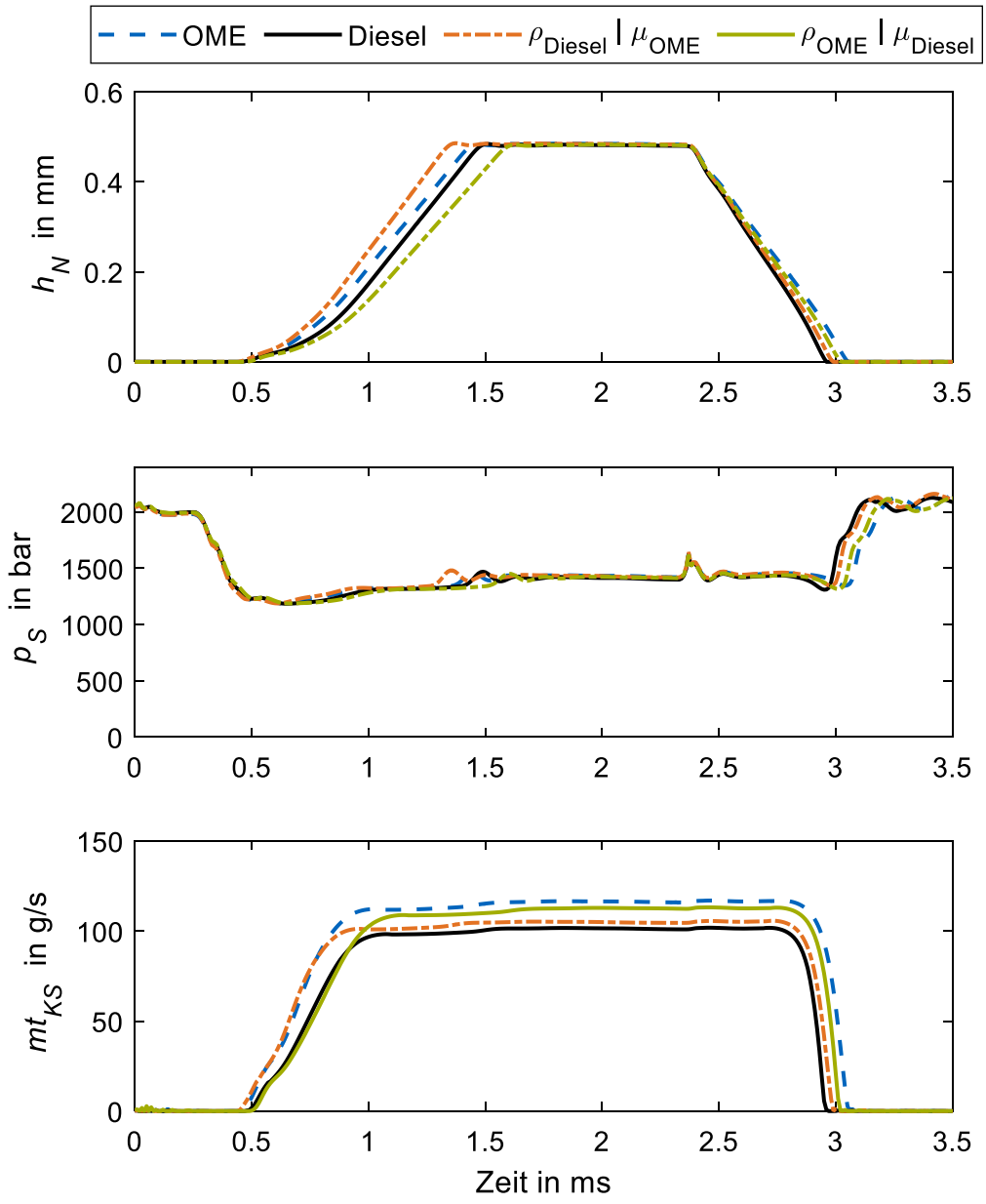

Abbildung 4-1: Einfluss von Dichte ρ und dynamischer Viskosität μ der Kraftstoffe auf Nadelhub h_N, Steuerraumdruck p_S und Einspritzverlauf mt_{KS} des Injektors; berechnet mit dem Injektormodell nach Schuckert et al. [177].

4.2 Nanopartikelemissionen

Während die rußfreie Verbrennung von OME hinreichend demonstriert ist [12, 13, 16, 134], ist die Emission von Nanopartikeln im OME-Betrieb unzureichend charakterisiert. *Lin et al.* [178] und *Liu et al.* [162] untersuchten den Einfluss der Zugabe von OME zu fossilem Diesel bis zu 30 % (v/v) und beobachteten unterschiedliche Effekte auf die Akkumulationsmode, abhängig vom Einspritzdruck und der Motorlast. *Popp et al.* [158] und *Preuß et al.* [154] zeigten die Verschiebung des Konzentrationsmaximums in der Partikelgrößenverteilung hin zu kleineren Durchmessern bei Erhöhung des OME-Anteils in Blends mit Diesel oder hydriertem Pflanzenöl (HVO) am Nutzfahrzeugmotor. *Ferraro et al.* bestätigten diesen Effekt bei Erhöhung der Zugabe von OME_3 in einem vorgemischten Ethylenbrenner [179]. *Richter & Zellbeck* [15], *Omari et al.* [19] und *Barro et al.* [17] untersuchten die Partikelgrößenverteilungen eines reinen OME-Mixes mit einer deutlich ausgeprägten Nukleationsmode im Größenbereich um 10 nm. Die verwendeten Probenahmesysteme sind in den genannten Publikationen sind nicht näher beschrieben, weshalb eine Unterscheidung zwischen volatilen und festen Partikelemissionen in den Ergebnissen nicht möglich ist. *Barro et al.* untersuchten feste Partikel in Abgasproben unter einem Transmissionselektronenmikroskop (TEM) und formulierten daraufhin die Hypothese, dass der Großteil der im OME-Betrieb ausgestoßenen Nanopartikel nichtvolatilen Ursprungs seien [17]. *Dworschak et al.* führten Messungen der Partikelgrößenverteilungen von reinen OME_3, OME_4 und OME_5 [22] sowie einem Mix aus $OME_{2\text{-}6}$ [23] mit HVO als Dieselreferenzkraftstoff durch. Das in den Arbeiten von *Dworschak et al.* beschriebene Probenahmesystem enthält eine PMP-konforme Einheit zur Entfernung volatiler Partikel und die Ergebnisse zeigen keine Nukleationsmode, weder im OME- noch im HVO-Betrieb. Eine Unterscheidung zwischen volatilen und festen Partikeln ist in keiner der bisher genannten Publikationen möglich. Ob die im Sub-23-nm-Bereich im OME-Betrieb auftretenden Nanopartikelemissionen volatilen oder nichtvolatilen Ursprungs sind, ist für die Bewertung der Zukunftsfähigkeit hinsichtlich der Grenzwerte zukünftiger Abgasgesetzgebungen [65] ausschlaggebend.

Gelner, A. D.; Rothe, D.; Kykal, C.; Irwin, M.; Sommer, A.; Pastoetter, C.; Härtl, M.; Jaensch, M.; Wachtmeister, G.: *Particle Emissions of a Heavy-Duty Engine Fueled with Polyoxymethylene Dimethyl Ethers (OME)*; Environmental Science: Atmospheres (2), 2022, pp. 291-304. [180]

Diese Publikation präsentiert den Vergleich der Partikelgrößenverteilungen im OME- und Dieselabgas eines Nutzfahrzeugmotors, sowie eine Unterscheidung zwischen volatilen und nichtvolatilen Nanopartikeln. Sie enthält die Beschreibung eines für diese Untersuchung konzeptioniertes Abgasprobenahmesystems, welches sich an den Anforderungen des PMP orientiert und erstmals die detaillierte Untersuchung der Partikelgrößenverteilungen sowohl im OME- als auch im Dieselbetrieb ermöglicht. Die im OME-Betrieb im Bereich der Nukleationsmode auftretenden Partikelkonzentrationen sind größtenteils volatilen Ursprungs. Nach der abgasgesetzrelevanten Entfernung dieser volatilen Partikel liegt die Konzentration in der Nukleationsmode unter derer im Dieselbetrieb. Messungen am Endrohr zeigen, dass das Abgasnachbehandlungssystem sowohl die volatile als auch nichtvolatile Partikel mit einer Effizienz von bis zu 99,99 % entfernt. Im Bereich der Akkumulationsmode bestätigt sich die rußfreie Verbrennung von OME über ebenfalls geringere Partikelkonzentrationen. Die Harnstoffdosierung zur NO_x-Reduktion über SCR bringt Partikel insbesondere im Größenbereich unter 23 nm hervor. Dennoch unterschreiten die Partikelemissionen im OME-Betrieb in den homologationsrelevanten Fahrzyklen „World Harmonised Steady State Cycle“ (WHSC) und „World Harmonised Transient Cycle“ (WHTC) nach der Regelung Nr. 49 der UN/ECE (UN/ECE R49) [45] den Grenzwert der Emissionsstufe Euro VI, ebenso wie den derzeit diskutierten Grenzwert der zukünftigen Stufe Euro VII [50], selbst ohne die Verwendung eines DPF. Mithilfe eines DPF unterschreiten die Partikelkonzentrationen das durchschnittliche Hintergrundniveau urbaner und regionaler Gebiete in Deutschland.

Eigener Beitrag zur Publikation:

Mein Beitrag zur Publikation liegt in der Idee der Untersuchung, Konzeptionierung der Methodik für die Untersuchungen der Partikelgrößenverteilungen am Motorenprüfstand und Aufbau des Probenahmesystems. Darüber hinaus führte ich die Datenerhebung am Versuchsträger und die Auswertung der Ergebnisse durch. Ich entwarf und implementierte den Programmcode für die Berechnungen der zu berücksichtigenden Partikelverluste. Ich erstellte die Abbildungen für die Publikation. Das Manuskript der Publikation wurde von mir geschrieben und gemäß den Anmerkungen der Co-Autoren und Reviewer angepasst.

Weiterführende Untersuchung: Rußneigung von OME-Diesel-Blends

Das in der Publikation demonstrierte niedrige Partikelemissionsniveau ist auf die rußfreie Verbrennung von OME zurückzuführen. Die Beimischung von OME in fossilen oder paraffinischen Dieselkraftstoff verspricht die Reduktion der Rußemissionen, der genaue Zusammenhang zwischen der ausgestoßenen Rußmenge und dem OME-Anteil in einem Blend mit Diesel ist aber weitgehend ungeklärt. Der an der Yale University von *McEnally et al.* entwickelte Yield Sooting Index (YSI) ist eine Kenngröße zur Beschreibung der Rußneigung eines Kraftstoffes [181]. *Xiang et al.* formulierten darauf aufbauend eine lineare Mischungsregel, die ausgehend vom YSI der Einzelkomponenten die zu erwartende Rußneigung des Blends angibt [182]. Abbildung 4-2 zeigt die nach dieser Mischungsregel berechnete Rußneigung von OME-Blends in einem Dieselsurrogat nach *Fiorino et al.* [183] in Abhängigkeit der Blendrate sowie die experimentelle Validierung.

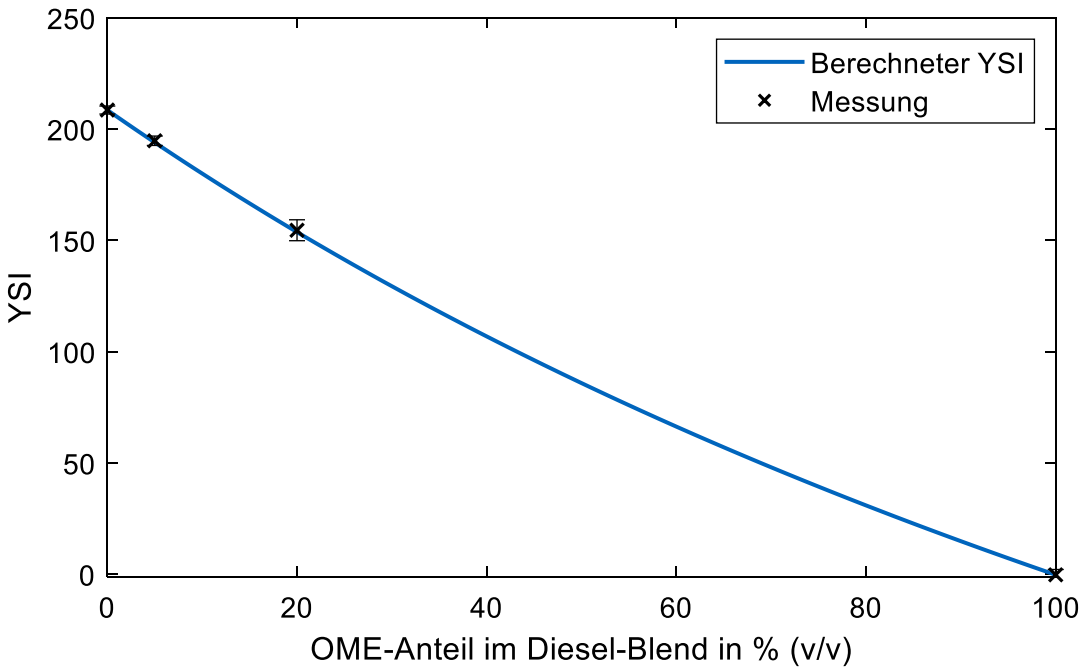

Abbildung 4-2: Nach Xiang et al. [182] berechnete Rußneigung von OME-Diesel-Blends und experimentelle Validierung durch eigene Messung mit Angabe der Standardabweichung. Dieselsurrogat nach Fiorino et al. [183] und Stoffwerte der OME-Charge 2.

Im Motorbetrieb ist die Rußemission neben dem OME-Anteil im Blend noch von anderen Parametern wie etwa der Einspritzstrategie, Ladungsbewegung oder der AGR-Rate abhängig. Die Untersuchung des Zusammenhangs zwischen Blendrate und YSI zeigt aber, dass mit steigendem Dieselanteil die Rußneigung stetig zunimmt und somit ein schadstofffreier Motorbetrieb eine reine OME-Mischung als Kraftstoff voraussetzt.

4.3 SCR-System und Demonstration der Fahrzyklen

Während das Rohemissionsspektrum von OME hinreichend untersucht ist [12, 13, 15–17, 19, 20], sind Wechselwirkungen von OME-Abgas mit Komponenten des AGN-Systems weitgehend unbekannt. *Münz et al.* untersuchten das Potenzial eines stöchiometrischen OME_1-Betriebs in Kombination mit einem TWC [184]. *Pélerin et al.* untersuchten die Oxidationseffizienz eines DOC mit Abgas aus der Verbrennung von OME_1 und $OME_{3\text{-}6}$ [20]. *Pöllmann et al.* untersuchten eine Kombination aus TWC und DOC im stöchiometrischen Betrieb mit OME nach M DIN TS 51699 [30]. *Steinhaus et al.* demonstrierten darüber hinaus das Emissionspotenzial eines mit OME betriebenen Pkw-Motors mit zweistufigem SCR-System [26]. Diese Publikationen beschränken sich bezüglich der Emissionsdemonstration auf stationäre Betriebspunkte. Eine Untersuchung der Selektivität und Effizienz der oxidierenden und reduzierenden Katalysatoren im direkten Vergleich zum Dieselbetrieb erfolgt nicht. Insbesondere die Bildung von CH_2O im OME-Abgas führt zu neuen Herausforderungen in der Konzeptionierung und Auslegung der AGN, da sich dadurch neue Formationsmechanismen von Sekundäremissionen wie beispielsweise HCN im SCR-System [185, 186] ergeben. Aus diesem Grund ist neben der Untersuchung bereits reglementierter Schadstoffe auch die Berücksichtigung weiterer, nicht reglementierter Emissionen notwendig. Dies gilt insbesondere im Hinblick auf die derzeitigen Diskussionen zur zukünftigen Emissionsstufe Euro 7/VII [50]. Eine Einordnung des Emissionsniveaus im OME-Betrieb setzt den Vergleich mit homologationsrelevanten Fahrzyklen voraus. Da die Emissionsauswertung für Nutzfahrzeugmotoren nach UN/ECE R49 [45] eine gravimetrische Betrachtungsweise in g/kWh vorschreibt, ist die Berücksichtigung der gegenüber dem Dieselbetrieb veränderten Abgasdichte notwendig. Die von *Härtl et al.* [134] und *Pélerin et al.* [20] beobachtete CH_4-Bildung bei Verbrennungsluftverhältnissen von $\lambda < 1{,}1$ begrenzt die AGR-Rate im stationären Motorbetrieb. Im transienten Betrieb ist für die NO_x-Reduktion eine hohe AGR-Klappendynamik notwendig. Damit ist eine kurzzeitige Unterschreitung dieser Lambda-Grenze nicht auszuschließen. Aus diesem Grund ist zu untersuchen, ob im transienten Motorbetrieb ein CH_4-NO_x-Zielkonflikt auftritt.

Gelner, A. D.; Beck, H. A.; Pastötter, C.; Härtl, M.; Wachtmeister, G.: *Ultra-Low Emissions of a Heavy-Duty Engine Powered with Oxymethylene Ether in Stationary and Transient Driving Conditions*; International Journal of Engine Research Vol. 23 (5), 2022, pp. 738-753. [187]

Diese Publikation präsentiert erstmals die Berechnung der u-Werte für OME, welche für die spezifische Emissionsauswertung der Fahrzyklen WHSC und WHTC nach UN/ECE R49 [45] notwendig sind. Die u-Werte sind die Koeffizienten, die sich aus den Dichteverhältnissen der Analyten zur Abgasdichte ergeben. Darüber hinaus enthält die Publikation einen Vergleich der Selektivität und Effizienz eines SCR-Systems im OME- und Dieselbetrieb. Die NO_x-Reduktionseffizienz ist im Teillastbetrieb bei OME geringer als bei Diesel. Dies ist auf geringere Abgastemperaturen und einen parallel zu den SCR-Reaktionen ablaufenden Reduktionspfad von CH_2O über NH_3 zurückzuführen. Da die rußfreie Verbrennung eine höhere AGR-Rate, AGR-Dynamik und Harnstoffdosierung an der ersten SCR-Stufe ermöglicht, erfolgt eine Überkompensation dieses Nachteils. Somit unterschreiten die NO_x-Emissionen in beiden Fahrzyklen die Nachweisgrenzen der homologationsrelevanten Messtechnik. Außerdem demonstriert die Publikation in den genannten Fahrzyklen ebenso Niedrigstemissionen aller anderen reglementierten Schadstoffe. Deren Konzentrationsniveaus liegen ebenso unter der Nachweisgrenze der Abgasmesstechnik. Ausnahme bildet die Partikelanzahlemission, welche – wie in der vorangehenden Publikation demonstriert [180] – allerdings unter dem Hintergrundniveau liegen. Die Konzentrationen der bisher nicht reglementierten Emissionen von CH_2O, HNCO, HCN und OME_n liegen ebenfalls unter der Nachweisgrenze der verwendeten Messtechnik. Die Strategie zur Vermeidung von HCN-Emissionen durch oxidative Komponenten vor und nach dem SCR-System erweist sich als effektiv. Bezüglich der Treibhausgase N_2O und CH_4 ergibt sich ein Zielkonflikt mit der NO_x-Reduktion über SCR und AGR: Die für die verwendeten Kupferzeolithe typische unselektive Reduktion von NO_2 zu N_2O erfordert eine Reduktion des NO_x-Rohniveaus; die erhöhte AGR-Dynamik führt zu CH_4-Emissionen im transienten Motorbetrieb. Ein sowohl klimaneutraler als auch schadstofffreier Motorbetrieb setzt – neben klimaneutralem Kraftstoff – ebenso eine SCR-Beschichtung mit ausreichender Selektivität und Effizienz sowie die Begrenzung der AGR-Dynamik voraus.

Eigener Beitrag zur Publikation

Mein Beitrag zur Publikation liegt in der Idee der Untersuchung, Konzeptionierung der Methodik für die Alphatitration und die Demonstration der Fahrzyklen. Darüber hinaus führte ich die Datenerhebung am Versuchsträger und die Auswertung der Ergebnisse durch. Ich berechnete die für OME benötigten Kenngrößen zur Zyklusauswertung. Ich erstellte die Abbildungen für die Publikation. Das Manuskript der Publikation wurde von mir geschrieben und gemäß den Anmerkungen der Co-Autoren und Reviewer angepasst.

Weiterführende Untersuchung: CH_4-NO_x-Zielkonflikt

Abbildung 4-3 stellt die NO_x- und CH_4-Emissionen im heißen WHTC bei unterschiedlichen AGR-Strategien gegenüber.

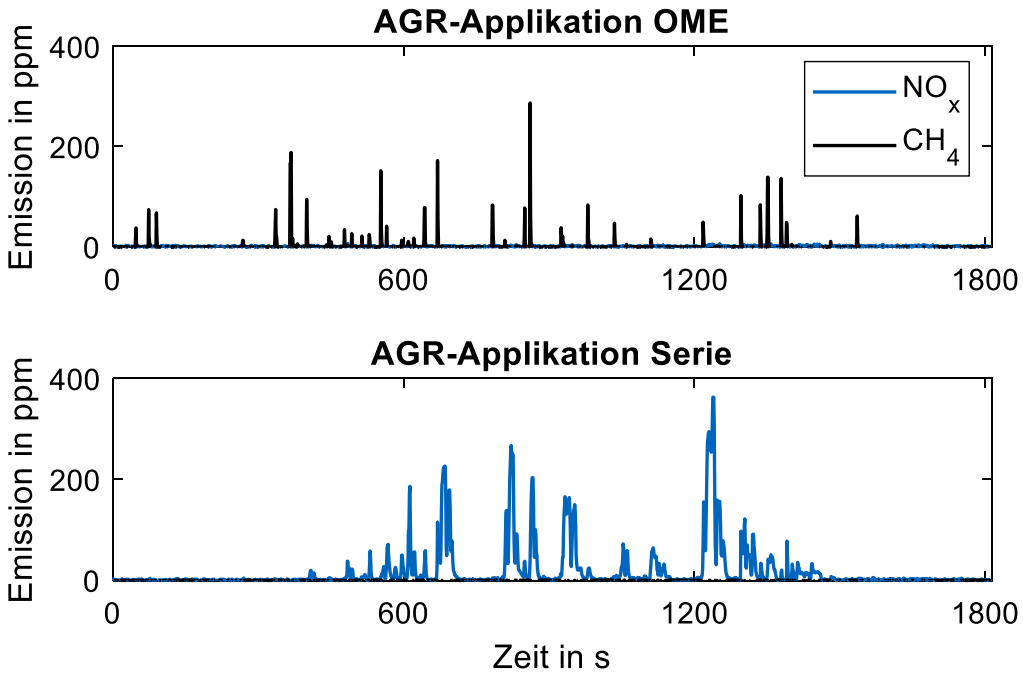

Abbildung 4-3: Darstellung des CH_4-NO_x-Zielkonflikt im OME-Betrieb im heißen WHTC-Lauf durch Gegenüberstellung der Endrohrkonzentrationen bei zwei unterschiedlichen AGR-Strategien.

Bei dem in der Publikation gewählten Ansatz der NO_x-Reduktion über hohe AGR-Dynamik und -Raten im OME-Betrieb ergeben sich die vorgestellten CH_4-Konzentrationspeaks [187]. Das NO_x-Rohemissionsniveau liegt durch diese Strategie über den Zyklus gemittelt bei 2,4 g/kWh und wird in der AGN vollständig umgesetzt. Bei Einsatz der im Serienbetrieb verwendeten Dieselapplikation mit geringeren AGR-Raten sowie einer Reduktion der Klappendynamik aufgrund der Begrenzung durch das sogenannte Rauchkennfeld treten im OME-Betrieb keine CH_4-Konzentrationspeaks auf. Das dadurch höhere NO_x-Rohemissionsniveau von 5,2 g/kWh sorgt für NO_x-Schlupf über die AGN. Daraus ergibt sich ein Zielkonflikt der innermotorischen Reduktion von CH_4 und NO_x, welcher den durch die rußfreie Verbrennung von OME gewonnenen Freiheitsgrad in der AGR-Applikation einschränkt.

4.4 Fuel Dosing als Heizmaßnahme des AGN-Systems

Die in der vorangehenden Publikation demonstrierten Niedrigstemissionen [187] setzen eine betriebswarme Abgasnachbehandlung voraus. Die Light-Off-Temperaturen von DOC und SCR-Katalysatoren liegen bei ca. 150 °C [115], ebenso wie die Mindesttemperatur für eine ausreichende Aufbereitung des für die SCR benötigten Harnstoffs. Aus diesem Grund sind Aufheizmaßnahmen notwendig. Für Pkw-Motoren eingesetzte elektrische Heizscheiben mit Leistungen im einstelligen Kilowattbereich nach *Maus et al.* [127] verfügen im Nutzfahrzeugbereich aufgrund der höheren Abgasmassenströme über eine geringere Effizienz. *Gao et al*. geben einen Überblick über verschiedene Maßnahmen und diskutieren deren Effizienz [188]. Den größten Wärmeleistungseintrag verspricht das Fuel Dosing, bei dem eine späte Nacheinspritzung über den Brennrauminjektor oder ein separates Dosiermodul im Abgasstrang Kraftstoff für die exotherme Umsetzung am DOC bereitstellt. Die dabei freiwerdende Wärme heizt sowohl die DOC-Oberfläche als auch die nachfolgenden Komponenten des SCR-Systems auf. Fuel Dosing ist im Dieselbetrieb durch die Rußbildung und anschließendem Face Plugging im Kaltstart der DOC-Oberfläche limitiert. Durch die rußfreie Verbrennung von OME ergibt sich hier ein Freiheitsgrad, welcher die im OME-Betrieb niedrigeren Abgastemperaturen ausgleicht oder überkompensiert. Hardware- und applikationsseitig eignet sich für das Fuel Dosing die Strategie der aktiven DPF-Regeneration. Damit sorgt die Implementierung für keinen zusätzlichen Aufwand am Dieselmotor. Die Effizienz des DOC bezüglich der Oxidation von OME-Kraftstoffmolekülen oder Zerfallsprodukten wie CH_2O ist bisher unbekannt. Eine Bewertung des Katalysatorverhaltens setzt einen Vergleich mit Diesel unter den gleichen für die Oxidation maßgebenden Betriebsbedingungen voraus. Dazu zählen insbesondere die Abgastemperatur und die Raumgeschwindigkeit. Letztere berechnet sich aus dem Abgasvolumenstrom und dem Katalysatorvolumen und ist somit eine Maßzahl für die Verweildauer der Spezies auf der Katalysatoroberfläche. Neben der Oxidationseffizienz sind ebenso Wechselwirkungen mit anderen auf dem Katalysator ablaufenden Reaktionen zu untersuchen. Eine Belegung der aktiven Zentren im DOC durch unverbrannten Kraftstoff oder dessen Fragmente verringert im Allgemeinen parallele DOC-Prozesse wie die Oxidation von CO und NO.

Gelner, A. D.; Pastötter, C.; Beck, H. A.; Härtl, M.; Wachtmeister, G.: *Fuel Dosing on a Diesel Oxidation Catalyst for After-Treatment System Heating on a Heavy-Duty Engine Powered by Polyoxymethylene Dimethyl Ethers*; SAE Technical Paper 2020-0050; 2020. [189]

Diese Publikation enthält die detaillierte Untersuchung des Zusammenhangs zwischen dosierter Kraftstoffmenge und dem Schlupf von Zerfallsprodukten über den DOC im OME- und Dieselbetrieb bei der Anwendung von Fuel Dosing als Aufheizmaßnahme für das AGN-System. Eine Versuchsmethodik mit Berücksichtigung der auftretenden Abgastemperatur und Raumgeschwindigkeit ermöglicht einen direkten Vergleich zwischen OME- und Dieselbetrieb. Eine Emissionsmessung vor und nach dem DOC ergibt, dass die im OME-Betrieb auftretenden Zerfallsprodukte CH_2O und CH_4 beim Fuel Dosing bereits im Brennraum und nicht auf der DOC-Oberfläche entstehen. Das Verhältnis zwischen dosierter Kraftstoffmenge und HC-Schlupf im Dieselbetrieb bzw. CH_2O-Schlupf im OME-Betrieb ist gegensätzlich: Während im Dieselbetrieb mit steigender Kraftstoffmenge auch der HC-Schlupf ansteigt, zeigt der CH_2O-Schlupf im OME-Betrieb ein reziprokes Verhalten. Je höher die bereitgestellte Kraftstoffmenge und somit die freiwerdende Wärmemenge, desto geringer fällt das Konzentrationsniveau von CH_2O nach dem DOC aus. Eine Untersuchung der Sprungantwort liefert den Erklärungsansatz, dass die durch die CO- und CH_2O-Oxidation freiwerdende Wärme die DOC-Effizienz durch Anhebung der Oberflächentemperatur erhöht. Damit reduziert eine höhere Kraftstoffmenge trotz steigender CH_2O-Konzentration im Rohabgas das Endrohrniveau. Bei Betrachtung des CO- und NO-Umsatzes zeigt sich ein analoges Verhalten: Im Dieselbetrieb führt Fuel Dosing zu einer Reduktion, im OME-Betrieb führt es zu einer Erhöhung der CO- und NO-Oxidation.

Eigener Beitrag zur Publikation:

Mein Beitrag zur Publikation liegt in der Idee der Untersuchung und Konzeptionierung der Methodik für das Fuel Dosing. Darüber hinaus führte ich die Datenerhebung am Versuchsträger teilweise selbst durch oder leitete sie an. Ich wertete die Ergebnisse aus und erstellte die Abbildungen für die Publikation. Das Manuskript der Publikation wurde von mir geschrieben und gemäß den Anmerkungen der Co-Autoren und Reviewer angepasst.

4.5 Kaltstartemissionen und Aufheizmaßnahmen am OME-Motor

Durch sukzessive Anpassung der Abgasgesetzgebung gewinnen die im Kaltstart ausgestoßenen Emissionen zunehmend an Bedeutung [190]. In dieser Phase sind die Katalysatoren im AGN-System inaktiv, da die dortige Umsetzung von der Temperatur abhängt und eine jeweilige Anspringtemperatur, den sogenannten „Light-Off", voraussetzt. Aus diesem Grund ist der Großteil des Schadstoffausstoßes im Motorbetrieb auf diese Kaltstartphase zurückzuführen [191]. Während die dort auftretenden Emissionen im Betrieb mit fossilem oder Biodiesel Gegenstand zahlreicher Publikationen sind [192–196], sind die im OME-Betrieb auftretenden Kaltstartemissionen bisher unbekannt. *Härtl et al*. [134], *Barro et al*. [18] und *Pélerin et al*. [20] beobachteten Emissionen von CH_2O und CH_4 bei unvollständiger OME-Verbrennung unter stationären Laborbedingungen am vorkonditionierten Einzylinderforschungsmotor. Daher sind diese Spezies ebenso im Kaltstart zu erwarten. *Zengel et al.* [185] und *Elsener et al.* [186] wiesen die Bildung von HCN über NH_3 im SCR-System unter der Präsenz von CH_2O nach. Die Ergebnisse der vorangehenden Publikation zeigen im betriebswarmen Zustand keine HCN-Emissionen in den stationären und transienten Prüfläufen WHSC und WHTC [187] und demonstrieren somit die Effektivität der eingesetzten Vermeidungsstrategie mit oxidativen Katalysatoren vor und nach der ersten SCR-Stufe. Die Effektivität dieser Strategie ist im Kaltstart ebenfalls zu überprüfen. Darüber hinaus ist unbekannt, welche Emissionen neben den bereits beobachteten Spezies CH_2O, CH_4 und OME_n bei der OME-Verbrennung und den Konvertierungsprozessen im AGN-System entstehen. Koinzidenzen der Absorptionsbanden im Infrarotspektrum erschweren das sogenannte Non-Target-Screening mittels Fourier-Transform-Infrarot-Spektrometer (FT-IR) zur Detektion von bisher nicht in den Berechnungsmethoden enthaltenen Spezies [197]. Ein alternativer Ansatz zur Abgasanalyse ist daher zur Beantwortung der Frage nach weiteren Emissionen zielführend. Da ein schadstofffreier Motorbetrieb eine betriebswarme AGN voraussetzt, sind Ansätze zur Reduktion der Kaltstartphase notwendig. Das in der vorangehenden Publikation vorgestellte Fuel Dosing im OME-Betrieb liefert die höchste Wärmeeintragsleistung, bringt gleichzeitig aber eine Erhöhung der CH_2O-Emission mit sich [189]. Aufgrund des beobachteten reziproken Verhaltens der CH_2O-Konzentration und der Einspritzmenge ist diese Maßnahme bei Vermeidung der Sprungantwort in Form eines CH_2O-Peaks vielversprechend. Ein elektrisch beheizbarer DOC (e-DOC) enthält eine dem beschichteten Monolithen vorgeschaltete Heizscheibe, die die Abgastemperatur erhöht und somit die Dauer der Aufheizphase des Trägers verkürzt. Die Bestromung des e-DOC reduziert den durch Fuel Dosing induzierten CH_2O-Peak, weshalb eine Kombination beider Aufheizmaßnahmen eine Reduktion der Kaltstartphase ohne Erhöhung der CH_2O-Emission verspricht.

Gelner, A. D.; Pang, G. A.; Weber, M.; Haisch, C.; Beck, H. A.; Härtl, M.; Jaensch, M.; Wachtmeister, G.: *Gaseous Emissions in Transient Cold-Start Operation of a Heavy-Duty Engine Fueled with Polyoxymethylene Dimethyl Ethers and Methods for After-Treatment System Heating*; Environmental Science: Advances (1), 2022, pp. 470-482. [198]

Diese Publikation präsentiert den Schadstoffemissionsvergleich im transienten Fahrzyklus zwischen kaltem und heißem Motorbetrieb. Hierzu finden sowohl konventionelle Abgasmesstechnik mittels FT-IR als auch ein neu entwickeltes System mittels Time-of-Flight-Massenspektrometer (MS) Anwendung. Darüber hinaus enthält die Publikation die Bewertung zu Aufheizmethoden des AGN-Systems in Form eines e-DOC in Kombination mit Fuel Dosing. Die gemessenen Konzentrationen von OME_n unterschiedlicher Kettenlänge im Rohabgas finden sich aufgrund von Hydrolyse- und Adsorptionsvorgängen in der AGN-Strecke nicht im Abgas am Endrohr wieder. Dort liegen sie sowohl im kalten aus auch heißen Prüflauf unterhalb der Nachweisgrenze des FT-IR; nach den Messungen des nachweisstärkeren und für OME_{3-5} kalibrierten MS-Systems liegen sie im ppb-Bereich. Den größten Anteil der im Kaltstart auftretenden Emissionen machen CH_2O und Ameisensäure (CH_2O_2) aus. Die HCN-Konzentration liegt im kalten und heißen Prüflauf unterhalb der FT-IR-Nachweisgrenze, ebenso wie die Konzentration von CH_3OH. Ein Non-Target-Screening mittels MS im Rohabgas ergibt, dass sowohl im kalten als auch heißen Fahrzyklus unverbrannte OME_n die höchsten Intensitäten im Spektrum aufweisen und keine weiteren Substanzen in vergleichbarem Maße auftreten. Dieses Ergebnis legitimiert für zukünftige Untersuchungen den Fokus auf die aus der Literatur bekannten, bei der OME-Verbrennung auftretenden Emissionen wie CH_2O, CH_2O_2, CH_4 und OME_n. Elektrisches Beheizen der AGN verkürzt aufgrund früherer Anspringzeitpunkt der Katalysatoren den NO_x-Ausstoß im gesamten Prüflauf um 47,7 %, bestehend aus kaltem und heißem WHTC. In Kombination mit möglichst früh einsetzendem Fuel Dosing ergibt sich eine NO_x-Reduktion um 64,9 %, allerdings auf Kosten einer durch das Fuel Dosing induzierten höheren CH_2O-Emission [189] um 90,5 %. Ein Kompromiss mit späterem Start von Fuel Dosing ergibt eine NO_x-Reduktion von 61,8 % bei einem um weniger als 0,1 % erhöhten CH_2O-Ausstoß.

Eigener Beitrag zur Publikation:

Mein Beitrag zur Publikation liegt in der Idee der Untersuchung, Konzeptionierung der Methodik für die Emissionsuntersuchungen und für die Aufheizmaßnahmen. Darüber hinaus führte ich die Datenerhebung am Versuchsträger durch. Ich wertete die Ergebnisse der Fahrzyklen aus und unterstützte bei der Auswertung der Massenspektren. Ich erstellte die Abbildungen für die Publikation. Das Manuskript der Publikation wurde von mir geschrieben und gemäß den Anmerkungen der Co-Autoren und Reviewer angepasst.

5. Diskussion der Ergebnisse mit Reflexion zur Literatur

Die vorgestellte, über 0D-/1D-Simulation erarbeitete Betriebsstrategie für OME-Motoren und die Demonstration der stationären und transienten Fahrzyklen am Nutzfahrzeugvollmotor mit AGN zeigen, dass ein Einsatz von OME im Serienmotor möglich ist. Konstruktive und applikative Anpassungen erhöhen den Wirkungsgrad und senken das NO_x-Rohemissionsniveau. Inwiefern die von *Barro et al.* vorgeschlagene Umrüstung der Injektoren zu größeren hydraulischen Düsendurchflüssen [18] notwendig ist, hängt vom Drehzahl-Last-Bereich der Serienanwendung und den konstruktiven Parametern des betrachteten Dieselmotors ab. Die in dieser Dissertation eingebundene Publikation [176] und die Arbeit von *Peter et al.* [174] zeigen, dass sich das Öffnungs- und Schließverhalten des Injektors aufgrund der im Vergleich zu Diesel veränderten physikalischen Eigenschaften von OME unterscheidet. Für den Einsatz von OME als Pilotkraftstoff im Dual-Fuel-Dieselmotor ergibt sich aus der Untersuchung von *Röll et al.* daraus keine Notwendigkeit der Umrüstung [175]. Der OME-Sprayaufbruch und das Penetrationsverhalten im Brennraum sind Gegenstand der Untersuchungen von *Li et al.* [199], *Pastor et al.* [153] und *Liu et al.* [200]. Aus diesen Ergebnissen leitet sich bei gleicher Einspritzmenge ebenfalls kein Umrüstungsbedarf ab. Entspricht das Drehzahl-Last-Kennfeld dem des Dieselbetriebs, ergibt sich aufgrund des reduzierten Heizwerts von OME die Notwendigkeit längerer Bestromungsdauern im Volllastbereich [176]. Insbesondere bei hohen Drehzahlen kommt es dabei zu Interaktionen des Kraftstoffs mit dem Schmierölfilm, welcher sich bei der Abwärtsbewegung in der Expansionsphase nicht mehr im Kolbenschatten befindet. Je nach chemischer Wechselwirkung des Schmieröls mit OME kommt es zur Ölverdünnung oder Abwaschung des Ölfilms [201]. Dies und direktes Auftreffen des flüssigen Kraftstoffstrahls auf den Kolben über eine lange Einspritzdauer führt langfristig zu Motorschäden durch Kolbenfresser [25]. Der Einsatz von Injektoren mit erhöhtem Düsendurchfluss reduziert dieses Risiko und geht mit einem höheren Wirkungsgrad einher [176]. Die pareto-optimale Betriebsstrategie bezüglich Wirkungsgrad und NO_x-Emissionen setzt hohe Raildrücke voraus. Nach den Ergebnissen von *Pöllmann et al.* ist die Eindringtiefe der Flüssigphase im OME-Betrieb primär vom Zylinderdruck abhängig [24], weshalb die Raildruckerhöhung das Risiko eines Motorschadens nicht erhöht, sondern aufgrund der dadurch verringerten Bestromungsdauer reduziert. Die höhere Zündwilligkeit von OME, welche sowohl die Arbeit von *Cai et al.* [202] als auch die von *Pélerin et al.* [20] bestätigen, ermöglicht die Vereinfachung der Einspritzstrategie in Form des Verzichts auf die Voreinspritzung.

Die Untersuchung der Nanopartikelemissionen im OME-Betrieb unterstreicht das geringe Emissionsniveau durch die rußfreie OME-Verbrennung. Die Ergebnisse zeigen, dass die von *Richter & Zellbeck* [15], *Omari et al.* [19] und *Barro et al.* [17] beobachtete Nukleationsmode mit einem Peak bei einer Partikelgröße von etwa 10 nm volatiler Natur ist. Der Anteil an festen Partikeln ist dabei geringer als im Dieselbetrieb, der Anteil dort ist analog zu den Ergebnissen von *Giechaskiel et al.* [203] um drei Größenordnungen geringer als der volatile Anteil. Dieses Ergebnis widerlegt die von *Barro et al.* aufgrund von Messungen mittels TEM abgeleiteter Hypothese, der Großteil dieser Mode sei auf feste Partikel zurückzuführen [17]. Es ist davon auszugehen, dass das im Mikroskop herrschende Vakuum zur Verdampfung volatiler Bestandteile führt und eine Bestimmung der Zusammensetzung der Partikel in den entnommenen Abgasproben über TEM irreführend ist. Das eingesetzte AGN-System entfernt sowohl volatile als auch nichtvolatile Partikel fast vollständig aus dem Rohabgas. Der aufgezeigte Einfluss der Reduktionsmitteldosierung für die SCR auf die Partikelemission ist näher zu untersuchen, insbesondere hinsichtlich der Beschaffenheit der auftretenden Partikel. *Amanatidis et al.* führen derartige Partikel auf die Entstehung von Ammonium(bi)sulfaten zurück [204]. Dieser Erklärungsansatz ist jedoch aufgrund der schwefelfreien Herstellung von OME unzureichend. Die Ergebnisse von *Schaber et al.* deuten auf die Bildung von Ammeliden, Ammelinen und Melaninen durch Harnstoffhydrolyse hin [205], während *Börnhorst & Deutschmann* die Partikelbildung auf unzureichende Sprayverdampfung zurückführen [206]. Die rußfreie Verbrennung von OME führt zu einer derart geringen Partikelkonzentration, dass der verwendete Versuchsträger den Grenzwert der diskutierten Euro VII-Stufe mit Berücksichtigung von PN_{10} [65] selbst ohne DPF unterschreitet. Die vorgestellte Publikation zur Untersuchung der Nanopartikelemission im OME-Betrieb zeigt, dass ein DPF entgegen der Hypothese von *Omari et al.* [19] auch bei kleinen Partikeldurchmessern eine hohe Filtrationseffizienz aufweist [180]. Daher unterschreitet der Versuchsträger sowohl im WHSC als auch im WHTC die durchschnittliche Hintergrundkonzentration städtischer und ländlicher Gebiete in Deutschland. Da jedoch die Beschaffenheit der emittierten Partikel bisher ungeklärt ist, ist ein Einfluss auf die menschliche Gesundheit trotz der geringen Konzentration schwer abzuschätzen. Ein positiver Effekt auf die Ziele der Luftreinhaltung über Reduktion des Feinstaubaufkommens ist jedoch zu erwarten. Die Untersuchung der Rußneigung von OME-Diesel-Blends zeigt auf, dass sich mit zunehmendem OME-Anteil die Rußneigung des Kraftstoffgemischs reduziert. Aus der Berechnung leitet sich ab, dass die in dieser Dissertation vorgestellten niedrigen Partikelniveaus allerdings einen Betrieb mit reinem OME voraussetzen. Neben der Reduktion des Feinstaubaufkommens hat der Einsatz von OME zur Substitution von fossilem Diesel zusätzlich zwei positive Effekte auf den Klimawandel: Zum einen ist regenerativ hergestelltes OME ebenso CO_2-neutral, wie es Dieselkraftstoffe aus biogenen

Quellen oder dem Fischer-Tropsch-Prozess sind [11]. Zum anderen gilt Ruß neben Treibhausgasemissionen als zweitstärkster Treiber der Erderwärmung [64], weshalb OME bezüglich des Klimaeinflusses gegenüber anderen e-Fuels und Biokraftstoffen einen zusätzlichen Vorteil aufweist. *Rohde et al.* [207] und *Ramanathan & Carmichael [208]* beziffern die durchschnittliche Verweildauer von Ruß in der Atmosphäre auf etwa zwei Wochen. Den Einsatz von OME als Kraftstoff für bestehende Dieselmotoren ergibt somit einen schnellwirkenden Hebel zur Verbesserung der Luftqualität und zur Reduktion des Treibhauseffekts. Dieser Hebel fällt in Schwellenländern und Entwicklungsländern aufgrund des höheren Anteils an Fahrzeugen älterer Emissionsstufen größer aus, insbesondere bei Fahrzeugen ohne DPF. Die in der vorgestellten Demonstration der Fahrzyklen aufgezeigten Emissionen von CH_4 und N_2O [187] sind in der Bewertung der Klimaneutralität zu berücksichtigen. Die Konzentrationsniveaus unter Berücksichtigung des jeweiligen Klimaeinflusses nach *Pachauri et al*. [2] und *Etminan et al.* [209] fallen im Vergleich zum CO_2-Ausstoß durch den Betrieb mit fossilem Diesel [148] marginal aus. Für einen klimaneutralen Motorbetrieb ist die Vermeidung dieser Sekundäremissionen dennoch Voraussetzung. Zielführend ist hier die Beschränkung der AGR-Rate/-Dynamik zur Vermeidung von CH_4-Emission und die Verbesserung der Effizienz und Selektivität des SCR-Systems. Bei der in dieser Arbeit verwendeten AGN handelt es um ein modulares Prototypensystem, welches aufgrund von Nachteilen im Wärmemanagement und Abgasführung über eine geringere Effizienz gegenüber einem Seriensystem nach Euro VI-Standard aufweist. Trotz dieser Nachteile unterschreitet das NO_x-Emissionsniveau im OME-Betrieb die Detektionsgrenze der Abgasmesstechnik [187]. Aus diesem Grund ist bei der Verwendung eines Euro VI-Seriensystems mit NO_x-Vollumsatz zu rechnen, selbst bei einem durch eine CH_4-Vermeidungsstrategie erhöhten Roh-NO_x-Niveau [210]. Da aufgrund der rußfreien Verbrennung kein NO_2 für die passive Regeneration des DPF notwendig ist, ergibt sich in der Dosierstrategie eines zweistufigen SCR-Systems ein Freiheitsgrad in der Reduktionsmitteldosiermenge an der ersten Stufe. Unter Berücksichtigung der demonstrierten Emissionsniveaus in den Fahrzyklen WHSC und WHTC in der in dieser Dissertation vorgestellten Publikation [187] ergibt sich damit das Potenzial eines sowohl schadstofffreien als auch klimaneutralen Motorbetriebs mit einem derzeitigen Euro VI-System. Die im Hinblick auf Euro 7/VII erforderlichen Verbesserungen in der AGN hinsichtlich Effizienz und Selektivität [109] bestärken dieses Potenzial. Für einen Motorbetrieb unter einfacheren Betriebsbedingungen, wie etwa in der stationären Anwendung als Range Extender in hybriden Anwendungen, sind potenziell vereinfachte AGN-Systeme ausreichend. *Pöllmann et al.* demonstrieren beispielsweise den stöchiometrischen OME-Betrieb in Kombination mit DOC und TWC mit ebenfalls geringsten Schadstoffkonzentrationen [30]. Dennoch setzt ein

schadstofffreier Motorbetrieb eine betriebswarme AGN voraus. Aufheizmaßnahmen des AGN-Systems sind im Hinblick auf die im Kaltstart ausgestoßenen Schadstoffe zu berücksichtigen. Die im Rahmen dieser Dissertation vorgestellte Publikation präsentiert Fuel Dosing als effiziente Methode [189]. Auch hier bietet die rußfreie Verbrennung von OME Vorteile, da eine Limitierung dieser Maßnahme durch Face Plugging [128] nicht auftritt. Die Implementierung erfolgt über den DPF-Regenerationsmodus oder einen bereits vorhandenen HC-Doser im Abgastrakt ohne Notwendigkeit der Integration eines zusätzlichen Bauteils, wie es bei dem von *Szolak et al.* vorgestellten System der Fall ist [211]. Das reziproke Verhalten zwischen Einspritzmenge und CH_2O-Emission ist auf Erhöhung der Reaktivität des DOC durch die exotherme Oxidation unverbrannter OME-Fragmente zurückzuführen [189]. *Bertole* beobachtete ein analoges Phänomen bei der CH_4-Oxidation am DOC während der Eindüsung von CO [212]. Die in der vorgestellten Publikation präsentierten Ergebnisse bilden die Grundlage für darauf aufbauende, von *Elsener et al.* durchgeführte Untersuchungen der Oxidations- und Hydrolyseaktivität von OME auf unterschiedlicher Katalysatoren [213]. Die in diesen Untersuchungen festgestellte hohe Aktivität bestätigt die vorgestellte, mittels Massenspektrometer beobachtete vollständige Konvertierung von OME_n im AGN-System selbst im Kaltstart [198]. Das Non-Target-Screening legitimiert den Fokus auf die aus der Literatur bekannten, im OME-Betrieb auftretenden Emissionen CH_2O und CH_2O_2, welche neben NO_x den Großteil der Schadstoffkonzentrationen ausmachen. Die von *Zengel et al.* [185] und *Elsener et al.* [186] beobachtete HCN-Bildung im SCR-System tritt in den eingebundenen Publikationen nicht auf [187, 198]. Dies bestätigt die Effektivität des gewählten AGN-Designs. Bezüglich der Werte der maximalen Arbeitsplatzkonzentration ist es zielführend, den Schwerpunkt auf die CH_2O-Reduktion im Gegensatz zur HCN-Reduktion zu legen [214]. Für eine schnelle Oxidation von CH_2O und eine schnelle Reduktion von NO_x ist die Kombination aus elektrisch beheiztem DOC und Fuel Dosing effektiv, wie die präsentierte Publikation darlegt [198].

6. Zusammenfassung und Ausblick

Diese Dissertation stellt folgende Untersuchungen ausführlich dar:

- Den Entwurf einer Betriebsstrategie eines mit OME betriebenen Motors,
- die Wechselwirkungen von OME mit den Komponenten des AGN-Systems,
- die Charakterisierung der im OME-Betrieb auftretenden Nanopartikelemissionen,
- die Demonstration homologationsrelevanter Fahrzyklen mit dem Ziel des schadstofffreien Motorbetriebs, auch im Hinblick auf bisher nicht reglementierte Emissionen,
- den Schadstoffausstoß im Kaltstart und Aufheizmaßnahmen für das AGN-System.

Die Untersuchung des Injektorverhaltens am Einspritzverlaufsindikator ergab, dass

- der hydraulische Einspritzverzug im OME-Betrieb größer als im Dieselbetrieb ist,
- der Injektor aufgrund der veränderten Dichte und Viskosität von OME im Vergleich zu Diesel langsamer schließt,
- diese Effekte bei Betrachtung des Energiestroms nicht ausreichen, um den geringeren Heizwert von OME zu kompensieren und daher eine Anpassung der Einspritzstrategie oder eine Erhöhung des Düsendurchflusses notwendig ist.

Die Variation der Betriebsparameter mittels 0D-/1D-Simulation zeigte, dass

- die Voreinspritzung aufgrund der höheren Zündwilligkeit von OME obsolet wird und ein Verzicht darauf sich weder negativ auf den Verbrauch, die NO_x-Entstehung oder das Geräuschverhalten auswirkt,
- ein pareto-optimaler Betrieb hinsichtlich Wirkungsgrad und NO_x-Entstehung hohe Raildrücke voraussetzt,
- die Erhöhung des Düsendurchflusses die Wirkungsgrad-NO_x-Paretofront verbessert,
- AGR als Stellhebel für die Bewegung auf der Paretofront je nach Entwicklungsziel hin zu höherem Wirkungsgrad oder geringeren NO_x-Emissionen dient.

Die Charakterisierung der Nanopartikelemissionen zeigte, dass

- die Akkumulationsmode im OME-Betrieb um drei Größenordnungen geringere Konzentrationen als im Dieselbetrieb aufweist,
- die Nukleationsmode mit einem Konzentrationspeak bei etwa 10 nm sowohl im Diesel- als auch im OME-Betrieb vorwiegend aus volatilen Partikeln besteht,
- die Konzentration fester Partikel im Sub-23-nm-Bereich im OME-Betrieb unter der im Dieselbetrieb liegt,
- das eingesetzte AGN-System sowohl volatile als auch feste Partikel mit einer Effizienz von bis zu 99,99 % entfernt,
- die Harnstoffdosierung zur NO_x-Reduktion über SCR zu einem Anstieg der Partikelkonzentration führt, insbesondere im Sub-23-nm-Bereich,
- der Versuchsträger im OME-Betrieb sowohl mit als auch ohne DPF in den Fahrzyklen WHSC und WHTC den Grenzwert der aktuellen Emissionsstufe Euro VI und den derzeit diskutierten Grenzwert der zukünftigen Stufe Euro VII unterschreitet,
- mit DPF die Partikelkonzentration in beiden Fahrzyklen unterhalb des aktuellen durchschnittlichen Hintergrundniveaus in städtischen und ländlichen Gebieten in Deutschland liegt.

Der Vergleich der Effizienz und Selektivität des SCR-System zwischen OME- und Dieselbetrieb hat ergeben, dass

- der NO_x-Umsatz im SCR-System im OME-Betrieb im Teillastbereich aufgrund geringerer Abgastemperaturen und dem Umsatz von CH_2O, welcher aktive Zentren auf dem Katalysator und NH_3 belegt, geringer ausfällt,
- die unselektive Reduktion von NO_x zu N_2O und der Schlupf von NH_3 in gleichem Maße wie im Dieselbetrieb auftritt.

Die Demonstration der Fahrzyklen WHSC und WHTC im OME-Betrieb haben ergeben, dass

- die durch die rußfreie Verbrennung von OME ermöglichte Aufhebung des Rauchkennfelds durch ein geringeres Roh-NO_x-Niveau die geringere SCR-Effizienz überkompensiert; die höhere mögliche Dosiermenge an der ersten SCR-Stufe kompensiert die geringere SCR-Effizienz ebenso, da kein NO_2 für den CRT-Effekt im DPF notwendig ist,

- die Konzentrationen der reglementierten Schadstoffe unter der Nachweisgrenze der verwendeten Abgasmesstechnik liegen – mit Ausnahme der Partikelanzahl, welche unterhalb des derzeitigen durchschnittlichen Hintergrundniveaus in städtischen und ländlichen Gebieten in Deutschland liegt –,

- auch für die beobachteten nicht reglementierten Spezies HNCO und $OME_{0\text{-}4}$ die Konzentrationen unterhalb der Nachweisgrenze der Abgasmesstechnik liegen,

- sich für die Treibhausgase CH_4 und N_2O Zielkonflikte mit den Maßnahmen der NO_x-Reduktion ergeben: Im Falle von CH_4 innermotorisch über eine Begrenzung der AGR-Rate und -Klappendynamik; im Falle von N_2O über die unselektive Reduktion von NO_x. Ausreichende Effizienz und Selektivität des SCR-Systems durch eine Verbesserung der Beschichtungstechnologie löst diese beiden Zielkonflikte auf.

Die Untersuchung des DOC-Verhaltens am Beispiel Fuel Dosing hat gezeigt, dass

- das Verhalten zwischen Einspritzmenge und Schlupf unverbrannter Kraftstofffragmente über den DOC an den untersuchten Betriebspunkten im Dieselbetrieb proportional und im OME-Betrieb reziprok ist,

- die CH_2O- und CH_4-Konzentrationen durch Fuel Dosing vor dem DOC höher als hinter dem DOC ausfallen und somit kein Produkt von OME-Zerfall auf dem Katalysator sind,

- Fuel Dosing die CO- und NO-Oxidation auf dem DOC im OME-Betrieb beschleunigt und im Dieselbetrieb ausbremst.

Der Emissionsvergleich zwischen kaltem und heißem WHTC mittels FT-IR und das Non-Target-Screening mittels Massenspektrometer haben ergeben, dass

- am Endrohr aufgrund der Kombination ausreichender Adsorptions- sowie Oxidations- und Hydrolysevorgängen im AGN-System die OME_n-Konzentration sowohl im kalten als auch heißen Fahrzyklus im Bereich weniger ppb liegt,
- OME_n im Rohabgas den Großteil der Kohlenwasserstoffemissionen ausmacht,
- CH_2O und CH_2O_2 neben NO_x den Großteil der am Endrohr emittierten Schadstoffe im Kaltstart ausmachen,
- im heißen WHTC lediglich CH_4-Konzentrationspeaks aufgrund des vorgestellten Zielkonflikts über die AGR auftreten,
- die HCN-Vermeidungsstrategie mit oxidativen Komponenten vor und nach der ersten SCR-Stufe sich als wirksam erweist.

Die Untersuchung der Kombination von elektrisch beheiztem DOC und Fuel Dosing als Aufheizmaßnahme des AGN-Systems hat ergeben, dass

- der e-DOC den beobachteten CH_2O-Konzentrationspeak als Sprungantwort beim Start von Fuel Dosing bei ausreichender Trägertemperatur abfängt
- der durch die Aufheizmaßnahme ermöglichte frühere Start der NO_x-Reduktion über SCR den NO_x-Ausstoß um 61,8 % in der WHTC-Prozedur, bestehend aus einem kalten und einem heißen WHTC-Fahrzyklus, ohne Mehrausstoß an CH_2O reduziert,
- alleiniges elektrisches Beheizen des DOC den NO_x-Ausstoß in der WHTC-Prozedur um 47,7 % reduziert.

OME als Dieselersatzkraftstoff bietet in Form einer höheren Zündwilligkeit und einer rußfreien Verbrennung günstigere Eigenschaften als vergleichbare e-Fuels. Diese Eigenschaften ermöglichen Vereinfachungen im Motorensystem und der Abgasnachbehandlung oder reduzieren den Schadstoffausstoß bestehender Dieselmotoren. Darüber hinaus schafft OME die Voraussetzung für einen klimaneutralen und schadstofffreien Motorbetrieb sofern die Herstellung und die Verteilung des Kraftstoffs klimaneutral ablaufen und das eingesetzte AGN-System über eine ausreichende Effizienz und Selektivität verfügt. Um die AGN möglichst schnell in einen Betriebsbereich für den Vollumsatz emittierter Schadstoffe zu überführen, sind Aufheizmaßnahmen notwendig. OME bietet als Energieträger für Fuel Dosing durch den Vorteil der rußfreien Verbrennung das Potenzial, den Aufheizvorgang im Vergleich mit fossilem oder paraffinischem Diesel zu verkürzen, ohne dabei die Deaktivierung der Katalysatoren zu riskieren. Sowohl die Erhöhung der Katalysatoreffizienz und -selektivität, als auch die Verkürzung der Kaltlaufphase sind gegenwärtig Entwicklungsziele zur Erreichung zukünftiger Abgasgesetzgebungen. Die aktuellen Fortschritte in der Motoren- und AGN-Technik verstärken somit das Potenzial zum schadstofffreien OME-Motorbetrieb.

Die Ergebnisse dieser Dissertation fokussieren sich auf die Betriebsstrategie von Motor und AGN sowie auf den Emissionsausstoß im OME-Betrieb. Um die Zukunftsfähigkeit von OME zur Substitution von Diesel in bestehenden und zukünftigen Motoren ganzheitlich zu bewerten, sind aufbauende Untersuchungen weiterer Aspekte notwendig. Insbesondere Langzeiterprobungen geben Aufschluss darüber, inwieweit konstruktive und applikative Anpassungen notwendig sind, um einen langfristig sicheren und schadensfreien Motorbetrieb mit OME zu gewährleisten. *Pélerin* erwähnt, dass durch die rußfreie Verbrennung die sonst übliche Rußschicht im Abgastrakt fehlt [148], welche korrosionsschützende und im Falle der Auslassventilsitzringe schmierende Eigenschaften hat. Neben Gewährleistung der mechanischen Beständigkeit der Bauteile ist auch eine Berücksichtigung der chemischen Eigenschaften von OME notwendig. Die veränderte Polarität im Vergleich zu Diesel führt zu veränderten Wechselwirkungen mit dem Schmieröl [201], weshalb mit Unterschieden in der Ölverdünnung zu rechnen ist. Da die Dichte von OME höher als die der meisten eingesetzten Schmieröle ist, ist bei einer Phasentrennung mit dem Absetzen von OME am Tankboden zu rechnen. Ein Einsatz von Polyalkylenglykolölen, welche derzeit in Klimakompressoren Anwendung finden, sind mögliche Alternativen zu bisher eingesetzten Motorölen. Analog dazu ist auch das Mischungsverhalten mit Wasser gegenüber Diesel verändert, was hinsichtlich der Speicherung und Verteilung zu berücksichtigen ist, ebenso wie die höhere Dichte von OME. Chemische Wechselwirkungen mit Polymeren in kraftstoffführenden Bauteilen in Form von Dichtungen oder Kraftstoffschläuchen sind ebenfalls aufgrund der veränderten Polarität zu untersuchen. OME führt über ein stärkeres Quellverhalten von Polymeren in für Diesel

konzipierten Systemen [20, 215]. Neben kraftstoffführenden Bauteilen sind auch die Komponenten Kolben, Zylinderköpfe und Injektoren hinsichtlich ihrer Geometrie für die Verbrennung von Diesel optimiert. Inwiefern eine Anpassung für die Verbrennung von OME Verbesserungspotenziale hinsichtlich Kraftstoffverbrauch und Emissionsentstehung bietet und ob diese die notwendigen Entwicklungskosten sowie den -aufwand kompensieren, ist zukünftig zu bewerten. Darüber hinaus ist weiteres Verständnis über die Mechanismen Emissionsentstehung bei der OME-Verbrennung notwendig, insbesondere hinsichtlich Formaldehyd, um Gegenmaßnahmen daraus abzuleiten. Sofern nicht der Anspruch eines schadstofffreien Motorbetriebs besteht, ermöglicht der Einsatz von OME die Vereinfachung der AGN-Komplexität und -Kosten durch die Reduktion zweistufiger SCR-Systeme oder den Verzicht auf den DPF bei fortwährender Einhaltung der Emissionsgrenzwerte. Eine breite Substitution von fossilem Diesel ist neben der Nutzfahrzeugbranche in stationären Verbrennungskraftmaschinen zur Energieerzeugung, in Range Extendern und in der Schifffahrt denkbar. Darüber hinaus besteht die Einsatzmöglichkeit in Feuerungsanlagen zur Wärmeerzeugung, welche neben dem Transportsektor als erhebliche Feinstaubemittenten gelten [216]. Der Umstieg von Heizöl auf OME bietet somit denselben Effekt hinsichtlich Luftqualität und Klimawandel wie im Verbrennungsmotor. Voraussetzung für die Substitution der fossilen Energieträger ist die wirtschaftliche Produktion in ausreichenden Mengen. Die Produktionskosten der Edukte CO_2 und H_2 tragen dabei substanziell zum Gesamtpreis von regenerativ hergestelltem OME bei, weshalb insbesondere in der Gewinnung dieser beiden Rohstoffe Forschungsbedarf zur Kostenreduktion besteht [217, 218]. Im Gegenzug dazu stehen die steigenden Kosten für fossile Energieträger [219]. Sind nur geringe Mengen an OME verfügbar, ist stets der Einsatz als Pilotkraftstoff in Dual-Fuel-Motoren in der Schifffahrt oder Energieerzeugung denkbar [75, 220]. Da der Pilotkraftstoff einen Großteil der Rußemissionen verursacht [221], bietet OME trotz der im Verhältnis zum Primärkraftstoff geringeren Einspritzmenge ein hohes Potenzial zur Emissionsreduktion.

7. Publikationsliste

7.1 In diese Dissertation eingebundene Publikationen

Gelner, A. D.; Höß, R. Zepf, A.; Härtl, M.; Wachtmeister, G.: *Engine Operation Strategies with the Alternative Diesel Fuel Oxymethylene Ether (OME): Evaluation Using Injection Rate Analyzer and 0D-/1D-Simulation*; SAE Technical Paper 2021-0050; 2021 [176]

Gelner, A. D.; Rothe, D.; Kykal, C.; Irwin, M.; Sommer, A.; Pastoetter, C.; Härtl, M.; Jaensch, M.; Wachtmeister, G.: *Particle Emissions of a Heavy-Duty Engine Fueled with Polyoxymethylene Dimethyl Ethers (OME)*; Environmental Science: Atmospheres (2), 2022, pp. 291-304. [180]

Gelner, A. D.; Beck, H. A.; Pastötter, C.; Härtl, M.; Wachtmeister, G.: *Ultra-Low Emissions of a Heavy-Duty Engine Powered with Oxymethylene Ether in Stationary and Transient Driving Conditions;* International Journal of Engine Research Vol. 23 (5), 2022, pp. 738-753. [187]

Gelner, A. D.; Pastötter, C.; Beck, H. A.; Härtl, M.; Wachtmeister, G.: *Fuel Dosing on a Diesel Oxidation Catalyst for After-Treatment System Heating on a Heavy-Duty Engine Powered by Polyoxymethylene Dimethyl Ethers*; SAE Technical Paper 2020-0050; 2020. [189]

Gelner, A. D.; Pang, G. A.; Weber, M.; Haisch, C.; Beck, H. A.; Härtl, M.; Jaensch, M.; Wachtmeister, G.: *Gaseous Emissions in Transient Cold-Start Operation of a Heavy-Duty Engine Fueled with Polyoxymethylene Dimethyl Ethers and Methods for After-Treatment System Heating*; Environmental Science: Advances (1), 2022, pp. 470-482. [198]

7.2 Weitere im Rahmen der Promotion entstandene Publikationen

Frankl, S. G.; Gelner, A. D.; Gleis, S.; Härtl, M.; Wachtmeister, G.: *Numerical Study on Renewable and Sustainable Fuels for HPDF Engines*; ASME 2020 Power Conference Proceedings, 2020. [75]

7.3 Konferenzbeiträge

Gelner, A. D.; Pöllmann, S.; Härtl, M.; Wachtmeister, G.: *OME - a Diesel E-Fuel with Potential to Sub-Zero Emissions*; präsentiert von Gelner A. D. beim Excellence, Diversity, and Mobility 2019 UTokyo – TUM Workshop am 11.03.2019.

Willems, W.; Weber, J.; Herrmann, O.; Pannwitz, M.; Lautrich, G.; Tietze, T.; Gaukel, K.; Gelner, A.; Pélerin, D.; Zubel, M.; Ottenwälder, T.; Lehrheuer, B.: *DME/OME1 - Nachhaltige Kraftstoffe für den selbstzündenden Verbrennungsmotor für Pkw und Nutzfahrzeuganwendungen*; präsentiert von Willems W. beim 40. Internationalen Wiener Motorensymposium am 17.05.2019.

Frankl, S. G.; Gelner, A. D.; Gleis, S.; Härtl, M.; Wachtmeister, G.: *Numerical Study on Renewable and Sustainable Fuels for HPDF Engines* [75]; präsentiert von Frankl S. G. bei der ASME 2020 POWER Conference am 04.08.2020.

Gelner, A. D.; Pastoetter, C. Beck, H. A.; Härtl, M.; Wachtmeister, G.: *Fuel Dosing on a Diesel Oxidation Catalyst for After-Treatment System Heating on a Heavy-Duty Engine Powered by Polyoxymethylene Dimethyl Ethers* [189]; präsentiert von Gelner A. D. beim SAE International Powertrains, Fuels & Lubricants Meeting 2020 am 22.09.2020.

Gelner, A. D.; Höß, R. Zepf, A.; Härtl, M.; Wachtmeister, G.: *Engine Operation Strategies with the Alternative Diesel Fuel Oxymethylene Ether (OME): Evaluation Using Injection Rate Analyzer and 0D-/1D-Simulation* [176]; präsentiert von Gelner A. D. beim SAE International Powertrains, Fuels & Lubricants Meeting 2021 am 28.09.2021.

Literaturverzeichnis

Literatur

[1] C. A. Horowitz, „Paris Agreement“, *Int. leg. mater.*, Jg. 55, Nr. 4, S. 740–755, 2016, doi: 10.1017/S0020782900004253.

[2] R. K. Pachauri und L. Meyer, Hg., *Climate change 2014: Synthesis report*. Geneva: Intergovernmental panel on climate change, 2015.

[3] D. H. König, M. Freiberg, R.-U. Dietrich und A. Wörner, „Techno-economic study of the storage of fluctuating renewable energy in liquid hydrocarbons“, *Fuel*, Jg. 159, S. 289–297, 2015, doi: 10.1016/j.fuel.2015.06.085.

[4] S. C. Trümper, S. Gerhard, S. Saatmann und O. Weinmann, „Qualitative Analysis of Strategies for the Integration of Renewable Energies in the Electricity Grid“, *Energy Procedia*, Jg. 46, S. 161–170, 2014, doi: 10.1016/j.egypro.2014.01.169.

[5] A. Tremel, P. Wasserscheid, M. Baldauf und T. Hammer, „Techno-economic analysis for the synthesis of liquid and gaseous fuels based on hydrogen production via electrolysis“, *International Journal of Hydrogen Energy*, Jg. 40, Nr. 35, S. 11457–11464, 2015, doi: 10.1016/j.ijhydene.2015.01.097.

[6] G. Centi und S. Perathoner, „Opportunities and prospects in the chemical recycling of carbon dioxide to fuels“, *Catalysis Today*, Jg. 148, 3-4, S. 191–205, 2009, doi: 10.1016/j.cattod.2009.07.075.

[7] R. Schlögl, „Chemical energy storage enables the transformation of fossil energy systems to sustainability“, *Green Chem.*, Jg. 23, Nr. 4, S. 1584–1593, 2021, doi: 10.1039/d0gc03171b.

[8] Iea, *Greenhouse Gas Emissions from Energy: Overview.* [Online]. Verfügbar unter: https://www.iea.org/reports/greenhouse-gas-emissions-from-energy-overview/emissions-by-sector (Zugriff am: 15. April 2022).

[9] H. Blanco und A. Faaij, „A review at the role of storage in energy systems with a focus on Power to Gas and long-term storage“, *Renewable and Sustainable Energy Reviews*, Jg. 81, S. 1049–1086, 2018, doi: 10.1016/j.rser.2017.07.062.

[10] N. Gray, S. McDonagh, R. O'Shea, B. Smyth und J. D. Murphy, „Decarbonising ships, planes and trucks: An analysis of suitable low-carbon fuels for the maritime, aviation and haulage sectors“, *Advances in Applied Energy*, Jg. 1, S. 100008, 2021, doi: 10.1016/j.adapen.2021.100008.

[11] S. Schemme, R. C. Samsun, R. Peters und D. Stolten, „Power-to-fuel as a key to sustainable transport systems – An analysis of diesel fuels produced from CO 2 and renewable electricity“, *Fuel*, Jg. 205, S. 198–221, 2017, doi: 10.1016/j.fuel.2017.05.061.

[12] L. Pellegrini, M. Marchionna, R. Patrini, C. Beatrice, N. Del Giacomo und C. Guido, „Combustion Behaviour and Emission Performance of Neat and Blended Polyoxymethylene Dimethyl Ethers in a Light-Duty Diesel Engine“ in *SAE 2012 World Congress & Exhibition*, 2012, doi: 10.4271/2012-01-1053.

[13] L. Pellegrini, M. Marchionna, R. Patrini und S. Florio, „Emission Performance of Neat and Blended Polyoxymethylene Dimethyl Ethers in an Old Light-Duty Diesel Car“ in *SAE 2013 World Congress & Exhibition*, 2013, doi: 10.4271/2013-01-1035.

[14] B. Lumpp, D. Rothe, C. Pastötter, R. Lämmermann und E. Jacob, „Oxymethylenether als Kraftstoffzusätze der Zukunft“, *Motortechnische Zeitschrift*, Jg. 72, Nr. 3, S. 198–203, 2011.

[15] G. Richter und H. Zellbeck, „OME als Kraftstoffersatz im Pkw-Dieselmotor“, *Motortechnische Zeitschrift*, Jg. 78, Nr. 12, S. 66–73, 2017.

[16] A. Damyanov, P. Hofmann, B. Geringer, N. Schwaiger, T. Pichler und M. Siebenhofer, „Biogenous ethers: production and operation in a diesel engine“, *Automot. Engine Technol.*, Jg. 3, 1-2, S. 69–82, 2018, doi: 10.1007/s41104-018-0028-x.

[17] C. Barro, M. Parravicini, K. Boulouchos und A. Liati, „Neat polyoxymethylene dimethyl ether in a diesel engine; part 2: Exhaust emission analysis“, *Fuel*, Jg. 234, S. 1414–1421, 2018, doi: 10.1016/j.fuel.2018.07.108.

[18] C. Barro, M. Parravicini und K. Boulouchos, „Neat polyoxymethylene dimethyl ether in a diesel engine; part 1: Detailed combustion analysis“, *Fuel*, Jg. 256, S. 115892, 2019, doi: 10.1016/j.fuel.2019.115892.

[19] A. Omari, B. Heuser, S. Pischinger und C. Rüdinger, „Potential of long-chain oxymethylene ether and oxymethylene ether-diesel blends for ultra-low emission

engines“, *Applied Energy*, Jg. 239, S. 1242–1249, 2019, doi: 10.1016/j.apenergy.2019.02.035.

[20] D. Pélerin, K. Gaukel, M. Härtl, E. Jacob und G. Wachtmeister, „Potentials to simplify the engine system using the alternative diesel fuels oxymethylene ether OME1 and OME3−6 on a heavy-duty engine“, *Fuel*, Jg. 259, S. 116231, 2020, doi: 10.1016/j.fuel.2019.116231.

[21] D. Pélerin, K. Gaukel, M. Härtl und G. Wachtmeister, „Nitrogen Oxide Reduction Potentials Using Dimethyl Ether and Oxymethylene Ether in a Heavy-Duty Diesel Engine“ in *Automotive Technical Papers*, 2020, doi: 10.4271/2020-01-5084.

[22] P. Dworschak, V. Berger, M. Härtl und G. Wachtmeister, „Neat Oxymethylene Ethers: Combustion Performance and Emissions of OME 2 OME 3 OME 4 and OME 5 in a Single-Cylinder Diesel Engine“ in *WCX SAE World Congress Experience*, 2020, doi: 10.4271/2020-01-0805.

[23] P. Dworschak, V. Berger, M. Härtl und G. Wachtmeister, „Particle Size Distribution Measurements of Neat and Water-Emulsified Oxymethylene Ethers in a Heavy-Duty Diesel Engine“, *SAE Int. J. Fuels Lubr.*, Jg. 13, Nr. 2, 2020, doi: 10.4271/04-13-02-0012.

[24] S. Pöllmann, M. Härtl und G. Wachtmeister, „Injection Process of the Synthetic Fuel Oxymethylene Ether: Optical Analysis in a Heavy-Duty Engine“ in *SAE Powertrains, Fuels & Lubricants Meeting*, 2020, doi: 10.4271/2020-01-2144.

[25] G. Richter, *Oxymethylendimethylether: Ein CO2-neutraler Kraftstoff zur Auflösung des Ruß-NOx-Zielkonflikts*. München: Verlag Dr. Hut, 2019.

[26] T. Steinhaus, A. Mokros, M. Thiem, M. Münz und C. Beidl, „Ultra-low emissions with OME at the CI engine – Implementation and potential for reduction of the immission level“, 2020.

[27] S. Pöllmann, M. Härtl und G. Wachtmeister, „Potential of miller timing with synthetic diesel fuels on a single cylinder heavy-duty engine“, *International Journal of Engine Research*, Jg. 23, Nr. 5, S. 769–780, 2022, doi: 10.1177/14680874211043649.

[28] P. Dworschak, M. Härtl und G. Wachtmeister, „Oxymethylene Ethers: Quantifying the Effect of Fuel Chain Length and Water Emulsification on Emissions and Combustion in

a Heavy-Duty Diesel Engine via Linear Regression Analysis“, *SAE Int. J. Fuels Lubr.*, Jg. 14, Nr. 3, 2021, doi: 10.4271/04-14-03-0009.

[29] P. Dworschak, V. Berger, M. Härtl und G. Wachtmeister, „Oxymethylene Ethers: Evaluating the Optimum Fuel Composition from an Engine Standpoint with Respect to Emissions and Combustion Performance“, *SAE Int. J. Fuels Lubr.*, Jg. 15, Nr. 2, 2022, doi: 10.4271/04-15-02-0008.

[30] S. Pöllmann, M. Härtl, M. JAensch und G. Wachtmeister, „Potentials of the Synthetic Diesel Fuel Oxymethylene Ether under Stoichiometric Conditions with Exhaust Aftertreatment: Manuskript in Bearbeitung“, 2022.

[31] W. Maus, „Zukünftige Mobilität: Die Physik entscheidet!“, *ATZ Extra*, Jg. 21, S11, S. 62, 2016, doi: 10.1007/s35778-016-0004-x.

[32] E. Jacob und W. Maus, „Oxymethylenether als potenziell CO2-neutraler Kraftstoff für saubere Dieselmotoren Teil 2: Erfüllung des Nachhaltigkeitsanspruchs“, *MTZ Motortech Z*, Jg. 78, Nr. 3, S. 54–61, 2017, doi: 10.1007/s35146-017-0017-z.

[33] R. Ellensohn und A. Link, „Gibt es in der Industrie in 20 Jahren noch Verbrennungsmotoren?“ in *Zukünftige Kraftstoffe*, W. Maus, Hg., Berlin, Heidelberg: Springer Berlin Heidelberg, 2019, S. 676–694, doi: 10.1007/978-3-662-58006-6_25.

[34] E. Jacob, „C-1 Oxygenate als nachhaltige Kraftstoffe und deren günstige Eigenschaften“ in *Zukünftige Kraftstoffe*, W. Maus, Hg., Berlin, Heidelberg: Springer Berlin Heidelberg, 2019, S. 155–180, doi: 10.1007/978-3-662-58006-6_9.

[35] U. Kramer, „Defossilizing the Transportation Sector“ in *Zukünftige Kraftstoffe*, W. Maus, Hg., Berlin, Heidelberg: Springer Berlin Heidelberg, 2019, S. 565–663, doi: 10.1007/978-3-662-58006-6_23.

[36] R. Schlögl, „Synthetic Fuels“ in *Zukünftige Kraftstoffe*, W. Maus, Hg., Berlin, Heidelberg: Springer Berlin Heidelberg, 2019, S. 191–223, doi: 10.1007/978-3-662-58006-6_11.

[37] W. Willems *et al.,* „DME/OMEi - Nachhaltige Kraftstoffe fur den selbstzündenden Verbrennungsmotor für Pkw und Nutzfahrzeuganwendungen /DME/OME1 - Sustainable Fuels for Compression Ignition Engines for Passenger Car and He“ in *40. Internationales Wiener Motorensymposium 15.-17. Mai 2019*, B. Geringer und H.-P. Lenz, Hg., VDI Verlag, 2019, II-103-II-142, doi: 10.51202/9783186811127-II-103.

[38] M. Münz, A. Mokros, D. Töpfer und C. Beidl, „OME - Assessment of Particle Emissions in Real Driving Conditions“, *MTZ Worldw*, Jg. 79, Nr. 3, S. 16–21, 2018, doi: 10.1007/s38313-017-0185-8.

[39] P. Giacomo, „Equation for the Determination of the Density of Moist Air (1981)“, *Metrologia*, Jg. 18, Nr. 1, S. 33–40, 1982, doi: 10.1088/0026-1394/18/1/006.

[40] C. T. Bowman, „Kinetics of pollutant formation and destruction in combustion“, *Progress in Energy and Combustion Science*, Jg. 1, Nr. 1, S. 33–45, 1975, doi: 10.1016/0360-1285(75)90005-2.

[41] V. I. Goldanskii, F. P. Schäfer, J. P. Toennies, H. K. V. Lotsch und H. Bockhorn, *Soot Formation in Combustion*. Berlin, Heidelberg: Springer Berlin Heidelberg, 1994.

[42] D. B. Kittelson, „Engines and nanoparticles“, *Journal of Aerosol Science*, Jg. 29, 5-6, S. 575–588, 1998, doi: 10.1016/S0021-8502(97)10037-4.

[43] C.-B. Kweon, D. E. Foster, J. J. Schauer und S. Okada, „Detailed Chemical Composition and Particle Size Assessment of Diesel Engine Exhaust“ in *SAE Powertrain & Fluid Systems Conference & Exhibition*, 2002, doi: 10.4271/2002-01-2670.

[44] G. A. Lavoie, J. B. Heywood und J. C. Keck, „Experimental and Theoretical Study of Nitric Oxide Formation in Internal Combustion Engines“, *Combustion Science and Technology*, Jg. 1, Nr. 4, S. 313–326, 1970, doi: 10.1080/00102206908952211.

[45] *Regelung Nr. 49 der Wirtschaftskommission der Vereinten Nationen für Europa (UN/ECE) — Einheitliche Bestimmungen hinsichtlich der Maßnahmen, die gegen die Emission von gas- und partikelförmigen Schadstoffen aus Selbstzündungs- und aus Fremdzündungsmotoren zum Antrieb von Fahrzeugen zu treffen sind: R49*, 2013.

[46] A. Rabl, „An estimate of regional and global O3 damage from precursor NOx and VOC emissions“, *Environment International*, Jg. 24, Nr. 8, S. 835–850, 1998, doi: 10.1016/S0160-4120(98)00053-1.

[47] D. T. Silverman *et al.,* „The Diesel Exhaust in Miners study: a nested case-control study of lung cancer and diesel exhaust“ (eng), *Journal of the National Cancer Institute*, Jg. 104, Nr. 11, S. 855–868, 2012, doi: 10.1093/jnci/djs034.

[48] M. D. Attfield *et al.,* „The Diesel Exhaust in Miners study: a cohort mortality study with emphasis on lung cancer“ (eng), *Journal of the National Cancer Institute*, Jg. 104, Nr. 11, S. 869–883, 2012, doi: 10.1093/jnci/djs035.

[49] *VERORDNUNG (EG) Nr. 595/2009 DES EUROPÄISCHEN PARLAMENTS UND DES RATES über die Typgenehmigung von Kraftfahrzeugen und Motoren hinsichtlich der Emissionen von schweren Nutzfahrzeugen (Euro VI) und über den Zugang zu Fahrzeugreparatur- und -wartungsinformationen, zur Änderung der Verordnung (EG) Nr. 715/2007 und der Richtlinie 2007/46/EG sowie zur Aufhebung der Richtlinien 80/1269/EWG, 2005/55/EG und 2005/78/EG*, 2009.

[50] Z. Samaras, S. Hausberger und G. Mellios, *Preliminary findings on possible Euro 7 emission limits for LD and HD vehicles* (Zugriff am: 15. April 2022).

[51] Q. Shi, Y. Zheng, R. Wang und Y. Li, „The study of a new method of driving cycles construction“, *Procedia Engineering*, Jg. 16, S. 79–87, 2011, doi: 10.1016/j.proeng.2011.08.1055.

[52] C. K. Westbrook und F. L. Dryer, „Chemical kinetic modeling of hydrocarbon combustion“, *Progress in Energy and Combustion Science*, Jg. 10, Nr. 1, S. 1–57, 1984, doi: 10.1016/0360-1285(84)90118-7.

[53] R. D. Stewart, „The effect of carbon monoxide on humans“ (eng), *Annual review of pharmacology*, Jg. 15, S. 409–423, 1975, doi: 10.1146/annurev.pa.15.040175.002205.

[54] G. P. Merker und R. Teichmann, *Grundlagen Verbrennungsmotoren*. Wiesbaden: Springer Fachmedien Wiesbaden, 2014.

[55] P. Carlier, H. Hannachi und G. Mouvier, „The chemistry of carbonyl compounds in the atmosphere—A review“, *Atmospheric Environment (1967)*, Jg. 20, Nr. 11, S. 2079–2099, 1986, doi: 10.1016/0004-6981(86)90304-5.

[56] S. E. Manahan, *Fundamentals of environmental chemistry*. Boca Raton, FL, London: Lewis Publishers, 2001.

[57] S. Machado Corrêa und G. Arbilla, „Carbonyl emissions in diesel and biodiesel exhaust“, *Atmospheric Environment*, Jg. 42, Nr. 4, S. 769–775, 2008, doi: 10.1016/j.atmosenv.2007.09.073.

[58] M. H. Fischer, „THE TOXIC EFFECTS OF FORMALDEHYDE AND FORMALIN“ (eng), *The Journal of experimental medicine*, Jg. 6, 4-6, S. 487–518, 1905, doi: 10.1084/jem.6.4-6.487.

[59] International Agency For Research On Cancer, *IARC Monographs on the Evaluation of Carcinogenic Risks to Humans: VOLUME 88 Formaldehyde, 2-Butoxyethanol and 1-tert-Butoxypropan-2-ol*. Lyon.

[60] M. Frenklach, W. C. Gardiner, S. E. Stein, D. W. Clary und T. Yuan, „Mechanism of Soot Formation in Acetylene-Oxygen Mixtures“, *Combustion Science and Technology*, Jg. 50, 1-3, S. 79–115, 1986, doi: 10.1080/00102208608923927.

[61] H. A. Beck, *Anwendung der photoakustischen Spektroskopie in der Prozess- und Umweltanalytik: Dissertation*, 2003.

[62] C. S. McEnally, L. D. Pfefferle, B. Atakan und K. Kohse-Höinghaus, „Studies of aromatic hydrocarbon formation mechanisms in flames: Progress towards closing the fuel gap“, *Progress in Energy and Combustion Science*, Jg. 32, Nr. 3, S. 247–294, 2006, doi: 10.1016/j.pecs.2005.11.003.

[63] C. J. L. Murray und et al., „Global burden of 87 risk factors in 204 countries and territories, 1990–2019: a systematic analysis for the Global Burden of Disease Study 2019“, *The Lancet*, Jg. 396, Nr. 10258, S. 1223–1249, 2020, doi: 10.1016/S0140-6736(20)30752-2.

[64] T. C. Bond *et al.,* „Bounding the role of black carbon in the climate system: A scientific assessment“, *J. Geophys. Res. Atmos.*, Jg. 118, Nr. 11, S. 5380–5552, 2013, doi: 10.1002/jgrd.50171.

[65] B. Giechaskiel, J. Vanhanen, M. Väkevä und G. Martini, „Investigation of vehicle exhaust sub-23 nm particle emissions“, *Aerosol Science and Technology*, Jg. 51, Nr. 5, S. 626–641, 2017, doi: 10.1080/02786826.2017.1286291.

[66] B. Giechaskiel, T. Lähde und Y. Drossinos, „Regulating particle number measurements from the tailpipe of light-duty vehicles: The next step?“ (eng), *Environmental research*, Jg. 172, S. 1–9, 2019, doi: 10.1016/j.envres.2019.02.006.

[67] J. Andersson, A. Mamakos und B. Giechaskiel, *Particle Measurement Programme (PMP) Heavy-duty Inter-laboratory Correlation Exercise (ILCE_HD)*. Luxembourg: Publications Office, 2010.

[68] Y. B. Zeldovich, „The Oxidation of Nitrogen in Combustion and Explosions“ in *Selected Works of Yakov Borisovich Zeldovich, Volume I*, Y. B. Zeldovich und R. A. Sunyaev, Hg., Princeton University Press, 1992, S. 364–403, doi: 10.1515/9781400862979.364.

[69] J. B. Heywood, *Internal combustion engines*. New York: McGraw-Hill, 2018.

[70] J. A. Miller und C. T. Bowman, „Mechanism and modeling of nitrogen chemistry in combustion“, *Progress in Energy and Combustion Science*, Jg. 15, Nr. 4, S. 287–338, 1989, doi: 10.1016/0360-1285(89)90017-8.

[71] C. P. Fenimore, „Formation of nitric oxide in premixed hydrocarbon flames“, *Symposium (International) on Combustion*, Jg. 13, Nr. 1, S. 373–380, 1971, doi: 10.1016/S0082-0784(71)80040-1.

[72] L. Moskaleva, W. Xia und M. Lin, „The CH+N2 reaction over the ground electronic doublet potential energy surface: a detailed transition state search“, *Chemical Physics Letters*, Jg. 331, 2-4, S. 269–277, 2000, doi: 10.1016/S0009-2614(00)01160-X.

[73] P. Glarborg, M. U. Alzueta, K. Dam-Johansen und J. A. Miller, „Kinetic Modeling of Hydrocarbon/Nitric Oxide Interactions in a Flow Reactor“, *Combustion and Flame*, Jg. 115, 1-2, S. 1–27, 1998, doi: 10.1016/S0010-2180(97)00359-3.

[74] J. Wolfrum, „Bildung von Stickstoffoxiden bei der Verbrennung“, *Chemie Ing. Techn.*, Jg. 44, Nr. 10, S. 656–659, 1972, doi: 10.1002/cite.330441004.

[75] S. G. Frankl, A. D. Gelner, S. Gleis, M. Härtl und G. Wachtmeister, „Numerical Study on Renewable and Sustainable Fuels for HPDF Engines“ in *ASME 2020 Power Conference collocated with the 2020 International Conference on Nuclear Engineering*, Virtual, Online, 2020, doi: 10.1115/POWER2020-16438.

[76] M. Rößler, A. Velji, C. Janzer, T. Koch und M. Olzmann, „Formation of Engine Internal NO 2 : Measures to Control the NO 2 /NO X Ratio for Enhanced Exhaust After Treatment“, *SAE Int. J. Engines*, Jg. 10, Nr. 4, S. 1880–1893, 2017, doi: 10.4271/2017-01-1017.

[77] B. Gaston, J. M. Drazen, J. Loscalzo und J. S. Stamler, „The biology of nitrogen oxides in the airways“ (eng), *American journal of respiratory and critical care medicine*, Jg. 149, 2 Pt 1, S. 538–551, 1994, doi: 10.1164/ajrccm.149.2.7508323.

[78] G. E. Likens, F. H. Bormann und N. M. Johnson, „Acid Rain“, *Environment: Science and Policy for Sustainable Development*, Jg. 14, Nr. 2, S. 33–40, 1972, doi: 10.1080/00139157.1972.9933001.

[79] P. J. Crutzen, „The influence of nitrogen oxides on the atmospheric ozone content“, *Q.J Royal Met. Soc.*, Jg. 96, Nr. 408, S. 320–325, 1970, doi: 10.1002/qj.49709640815.

[80] H. Johnston, „Reduction of stratospheric ozone by nitrogen oxide catalysts from supersonic transport exhaust“ (eng), *Science (New York, N.Y.)*, Jg. 173, Nr. 3996, S. 517–522, 1971, doi: 10.1126/science.173.3996.517.

[81] J. Schommers *et al.,* „Potential of Common Rail Injection System for Passenger Car DI Diesel Engines“ in *SAE 2000 World Congress*, 2000, doi: 10.4271/2000-01-0944.

[82] R. C. Yu, T.-W. Kuo, S. M. Shahed und T. W. Chang, „The Effect of Mixing Rate, End of Injection, and Sac Volume on Hydrocarbon Emissions from a D.I. Diesel Engine“ in *1983 SAE International Off-Highway and Powerplant Congress and Exposition*, 1983, doi: 10.4271/831294.

[83] H. Hiroyasu und M. Arai, „Structures of Fuel Sprays in Diesel Engines“ in *International Congress & Exposition*, 1990, doi: 10.4271/900475.

[84] A. Kilic, L. Schulze und H. Tschöke, „Influence of Nozzle Parameters on Single Jet Flow Quantities of Multi-Hole Diesel Injection Nozzles“ in *Non-Conference Specific Technical Papers - 2006*, 2006, doi: 10.4271/2006-01-1983.

[85] N.-H. Chung, B.-G. Oh und M.-H. Sunwoo, „Modelling and injection rate estimation of common-rail injectors for direct-injection diesel engines“, *Proceedings of the Institution of Mechanical Engineers, Part D: Journal of Automobile Engineering*, Jg. 222, Nr. 6, S. 1089–1101, 2008, doi: 10.1243/09544070JAUTO647.

[86] W. F. Colban, P. C. Miles und S. Oh, „Effect of Intake Pressure on Performance and Emissions in an Automotive Diesel Engine Operating in Low Temperature Combustion Regimes“ in *Powertrain & Fluid Systems Conference and Exhibition*, 2007, doi: 10.4271/2007-01-4063.

[87] M. Ehleskog, S. Gjirja und I. Denbratt, „Effects of Variable Inlet Valve Timing and Swirl Ratio on Combustion and Emissions in a Heavy Duty Diesel Engine“ in *SAE 2012 International Powertrains, Fuels & Lubricants Meeting*, 2012, doi: 10.4271/2012-01-1719.

[88] R. Şener, M. R. Özdemir und M. U. Yangaz, „Influence of piston bowl geometry on combustion and emission characteristics“, *Proceedings of the Institution of Mechanical Engineers, Part A: Journal of Power and Energy*, Jg. 233, Nr. 5, S. 576–587, 2019, doi: 10.1177/0957650919854637.

[89] N. Ladommatos, S. M. Abdelhalim, H. Zhao und Z. Hu, „The Dilution, Chemical, and Thermal Effects of Exhaust Gas Recirculation on Diesel Engine Emissions - Part 1: Effect of Reducing Inlet Charge Oxygen“ in *International Fuels & Lubricants Meeting & Exposition*, 1996, doi: 10.4271/961165.

[90] N. Ladommatos, S. M. Abdelhalim, H. Zhao und Z. Hu, „The Dilution, Chemical, and Thermal Effects of Exhaust Gas Recirculation on Diesel Engine Emissions - Part 2: Effects of Carbon Dioxide“ in *International Fuels & Lubricants Meeting & Exposition*, 1996, doi: 10.4271/961167.

[91] N. Ladommatos, S. M. Abdelhalim, H. Zhao und Z. Hu, „The Dilution, Chemical, and Thermal Effects of Exhaust Gas Recirculation on Diesel Engine Emissions - Part 3: Effects of Water Vapour“ in *International Spring Fuels & Lubricants Meeting & Exposition*, 1997, doi: 10.4271/971659.

[92] N. Ladommatos, S. M. Abdelhalim, H. Zhao und Z. Hu, „The Dilution, Chemical, and Thermal Effects of Exhaust Gas Recirculation on Disesel Engine Emissions - Part 4: Effects of Carbon Dioxide and Water Vapour“ in *International Spring Fuels & Lubricants Meeting & Exposition*, 1997, doi: 10.4271/971660.

[93] T. Kamimoto und M. Bae, „High Combustion Temperature for the Reduction of Particulate in Diesel Engines“ in *SAE International Congress and Exposition*, 1988, doi: 10.4271/880423.

[94] K. Akihama, Y. Takatori, K. Inagaki, S. Sasaki und A. M. Dean, „Mechanism of the Smokeless Rich Diesel Combustion by Reducing Temperature“ in *SAE 2001 World Congress*, 2001, doi: 10.4271/2001-01-0655.

[95] S. Kook, C. Bae, P. C. Miles, D. Choi und L. M. Pickett, „The Influence of Charge Dilution and Injection Timing on Low-Temperature Diesel Combustion and Emissions“ in *Powertrain & Fluid Systems Conference & Exhibition*, 2005, doi: 10.4271/2005-01-3837.

[96] J. E. Dec, „Advanced compression-ignition engines—understanding the in-cylinder processes“, *Proceedings of the Combustion Institute*, Jg. 32, Nr. 2, S. 2727–2742, 2009, doi: 10.1016/j.proci.2008.08.008.

[97] T. Li und H. Ogawa, „Analysis of the Trade-off between Soot and Nitrogen Oxides in Diesel-Like Combustion by Chemical Kinetic Calculation“, *SAE Int. J. Engines*, Jg. 5, Nr. 2, S. 94–101, 2012, doi: 10.4271/2011-01-1847.

[98] G. D. Neely, S. Sasaki, Y. Huang, J. A. Leet und D. W. Stewart, „New Diesel Emission Control Strategy to Meet US Tier 2 Emissions Regulations“ in *SAE 2005 World Congress & Exhibition*, 2005, doi: 10.4271/2005-01-1091.

[99] S. B. Pflaum, *Entwicklung und Untersuchung eines Brennverfahrens für Niedrigstemissionen bei Dieselmotoren: Dissertation*, 2011.

[100] D. Rothe, *Physikalische und chemische Charakterisierung der Rußpartikelemission von Nutzfahrzeugdieselmotoren und Methoden zur Emissionsminderung: Disertation*, 2006.

[101] *Richtlinie des Rates zur Änderung der Richtlinie 88 / 77/EWG zur Angleichung der Rechtsvorschriften der Mitgliedstaaten über Maßnahmen gegen die Emission gasförmiger Schadstoffe aus Dieselmotoren zum Antrieb von Fahrzeugen (91 / 542 / EWG)*, 1991.

[102] *RICHTLINIE 1999/96/EG DES EUROPÄISCHEN PARLAMENTS UND DES RATES zur Angleichung der Rechtsvorschriften der Mitgliedsstaaten über Maßnahmen gegen die Emission gasförmiger Schadstoffe und luftverunreinigender Partikel aus Selbstzündungsmotoren zum Antrieb von Fahrzeugen und die Emission gasförmiger Schadstoffe aus mit Erdgas oder Flüssiggas betriebenen Fremdzündungsmotoren zum Antrieb von Fahrzeugen und zur Änderung der Richtlinie 88/77/EWG des Rates*, 1999.

[103] W. A. Majewski, J. L. Ambs und K. Bickel, „Nitrogen Oxides Reactions in Diesel Oxidation Catalyst“ in *International Congress & Exposition*, 1995, doi: 10.4271/950374.

[104] M. Chen, „Morphology and composition of Pt$z.sbnd;Pd alloy crystallites on SiO2 in reactive atmospheres*1“, *Journal of Catalysis*, Jg. 56, Nr. 2, S. 198–218, 1979, doi: 10.1016/0021-9517(79)90107-6.

[105] F. C. Galisteo, R. Mariscal, M. L. Granados, J. Fierro, R. A. Daley und J. A. Anderson, „Reactivation of sintered Pt/Al2O3 oxidation catalysts“, *Applied Catalysis B: Environmental*, Jg. 59, 3-4, S. 227–233, 2005, doi: 10.1016/j.apcatb.2005.02.004.

[106] A. Russell und W. S. Epling, „Diesel Oxidation Catalysts“, *Catalysis Reviews*, Jg. 53, Nr. 4, S. 337–423, 2011, doi: 10.1080/01614940.2011.596429.

[107] W. S. Epling, L. E. Campbell, A. Yezerets, N. W. Currier und J. E. Parks, „Overview of the Fundamental Reactions and Degradation Mechanisms of NOx Storage/Reduction Catalysts“, *Catalysis Reviews*, Jg. 46, Nr. 2, S. 163–245, 2004, doi: 10.1081/CR-200031932.

[108] M. Argyle und C. Bartholomew, „Heterogeneous Catalyst Deactivation and Regeneration: A Review“, *Catalysts*, Jg. 5, Nr. 1, S. 145–269, 2015, doi: 10.3390/catal5010145.

[109] T. Selleri, A. D. Melas, A. Joshi, D. Manara, A. Perujo und R. Suarez-Bertoa, „An Overview of Lean Exhaust deNOx Aftertreatment Technologies and NOx Emission Regulations in the European Union“, *Catalysts*, Jg. 11, Nr. 3, S. 404, 2021, doi: 10.3390/catal11030404.

[110] M. Koebel, M. Elsener und T. Marti, „NOx -Reduction in Diesel Exhaust Gas with Urea and Selective Catalytic Reduction“, *Combustion Science and Technology*, Jg. 121, 1-6, S. 85–102, 1996, doi: 10.1080/00102209608935588.

[111] *ISO 22241-1:2019(en) Diesel engines — NOx reduction agent AUS 32: Part 1: Quality requirements*, 22241, International Organization for Standardization.

[112] S. D. Yim *et al.,* „Decomposition of Urea into NH 3 for the SCR Process“, *Ind. Eng. Chem. Res.*, Jg. 43, Nr. 16, S. 4856–4863, 2004, doi: 10.1021/ie034052j.

[113] F. Birkhold, U. Meingast, P. Wassermann und O. Deutschmann, „Modeling and simulation of the injection of urea-water-solution for automotive SCR DeNOx-systems“, *Applied Catalysis B: Environmental*, Jg. 70, 1-4, S. 119–127, 2007, doi: 10.1016/j.apcatb.2005.12.035.

[114] M. Koebel, G. Madia und M. Elsener, „Selective catalytic reduction of NO and NO2 at low temperatures“, *Catalysis Today*, Jg. 73, 3-4, S. 239–247, 2002, doi: 10.1016/S0920-5861(02)00006-8.

[115] J. W. Girard, C. Montreuil, J. Kim, G. Cavataio und C. Lambert, „Technical Advantages of Vanadium SCR Systems for Diesel NOx Control in Emerging Markets“, *SAE Int. J. Fuels Lubr.*, Jg. 1, Nr. 1, S. 488–494, 2009, doi: 10.4271/2008-01-1029.

[116] P. Forzatti, L. Lietti und E. Tronconi, „Nitrogen Oxides Removal-Industrial“ in *Encyclopedia of Catalysis*, I. Horváth, Hg., Hoboken, NJ, USA: John Wiley & Sons, Inc, 2002, doi: 10.1002/0471227617.eoc155.pub2.

[117] F. Willems *et al.,* „Is Closed-Loop SCR Control Required to Meet Future Emission Targets?“ in *SAE World Congress & Exhibition*, 2007, doi: 10.4271/2007-01-1574.

[118] K. Kamasamudram, C. Henry, N. Currier und A. Yezerets, „N 2 O Formation and Mitigation in Diesel Aftertreatment Systems“, *SAE Int. J. Engines*, Jg. 5, Nr. 2, S. 688–698, 2012, doi: 10.4271/2012-01-1085.

[119] I. Nova, M. Colombo, E. Tronconi, V. Schmeißer, B. Bandl-Konrad und L. Zimmermann, „Dual-Layer Ammonia Slip Catalysts for Automotive SCR Exhaust Gas Aftertreatment: An Experimental and Modeling Study“ in *Fundamental and Applied Catalysis, Urea-SCR Technology for deNOx After Treatment of Diesel Exhausts*, I. Nova und E. Tronconi, Hg., New York, NY: Springer New York, 2014, S. 553–586, doi: 10.1007/978-1-4899-8071-7_18.

[120] M. Tatur *et al.,* „Lean NOx Trap for Heavy-Duty On-Road Applications - A Feasible Alternative?“ in *SAE 2007 Commercial Vehicle Engineering Congress & Exhibition*, 2007, doi: 10.4271/2007-01-4179.

[121] S. K. Friedlander, „Theory of Aerosol Filtration“, *Ind. Eng. Chem.*, Jg. 50, Nr. 8, S. 1161–1164, 1958, doi: 10.1021/ie50584a036.

[122] J. Yang, M. Stewart, G. Maupin, D. Herling und A. Zelenyuk, „Single wall diesel particulate filter (DPF) filtration efficiency studies using laboratory generated particles“, *Chemical Engineering Science*, Jg. 64, Nr. 8, S. 1625–1634, 2009, doi: 10.1016/j.ces.2008.12.011.

[123] R. Brück, P. Hirth und R. Konieczny, „Der PM-Metalit™; Erfahrungen mit dem Nebenstrom Partikelfiltersystem hinsichtlich Reduzierung von Partikelanzahl und –Masse bei PKW- und LKW-Anwendungen“ in *4. Internationales AVL Abgas- und Partikelforum*, S. 92–107.

[124] W. Maus, R. Brück, J. Hodgson und C. Vorsmann, „Elektrostatischer Partikelfilter zur Reduktion der Nanopartikel“, *MTZ Motortech Z*, Jg. 72, Nr. 2, S. 116–121, 2011, doi: 10.1365/s35146-011-0029-z.

[125] A. G. Konstandopoulos, M. Kostoglou, E. Skaperdas, E. Papaioannou, D. Zarvalis und E. Kladopoulou, „Fundamental Studies of Diesel Particulate Filters: Transient Loading, Regeneration and Aging“ in *SAE 2000 World Congress*, 2000, doi: 10.4271/2000-01-1016.

[126] Wu, Zhang, Yao und Yang, „Modeling and Order Reduction for the Thermodynamics of a Diesel Oxidation Catalyst with Hydrocarbon Dosing“, *Catalysts*, Jg. 9, Nr. 4, S. 369, 2019, doi: 10.3390/catal9040369.

[127] W. Maus, R. Brück, R. Konieczny und A. Scheeder, „Electrically heated catalyst for thermal management in modern vehicle applications“, *MTZ Worldw*, Jg. 71, Nr. 5, S. 34–39, 2010, doi: 10.1007/BF03227013.

[128] K. Nakano, H. Okano, K. Inoue und A. Obuchi, „Study on the Prevention of Face-Plugging of Diesel Oxidation Catalyst (DOC)“ in *SAE/JSAE Small Engine Technology Conference*, 2018, doi: 10.4271/2018-32-0069.

[129] F. Hoppe *et al.,* „Tailor-made fuels for future engine concepts“, *International Journal of Engine Research*, Jg. 17, Nr. 1, S. 16–27, 2016, doi: 10.1177/1468087415603005.

[130] Z. Azizi, M. Rezaeimanesh, T. Tohidian und M. R. Rahimpour, „Dimethyl ether: A review of technologies and production challenges“, *Chemical Engineering and Processing: Process Intensification*, Jg. 82, S. 150–172, 2014, doi: 10.1016/j.cep.2014.06.007.

[131] R. Sun, I. Delidovich und R. Palkovits, „Dimethoxymethane as a Cleaner Synthetic Fuel: Synthetic Methods, Catalysts, and Reaction Mechanism“, *ACS Catal.*, Jg. 9, Nr. 2, S. 1298–1318, 2019, doi: 10.1021/acscatal.8b04441.

[132] S. Lüftl, V. P.M. und S. Chandran, *Polyoxymethylene Handbook*. Hoboken, NJ, USA: John Wiley & Sons, Inc, 2014.

[133] H. Ogawa, N. Miyamoto und M. Yagi, „Chemical-Kinetic Analysis on PAH Formation Mechanisms of Oxygenated Fuels“ in *SAE Powertrain & Fluid Systems Conference & Exhibition*, 2003, doi: 10.4271/2003-01-3190.

[134] M. Härtl, P. Seidenspinner, E. Jacob und G. Wachtmeister, „Oxygenate screening on a heavy-duty diesel engine and emission characteristics of highly oxygenated oxymethylene ether fuel OME1“, *Fuel*, Jg. 153, S. 328–335, 2015, doi: 10.1016/j.fuel.2015.03.012.

[135] W. Maus, Hg., *Zukünftige Kraftstoffe*. Berlin, Heidelberg: Springer Berlin Heidelberg, 2019.

[136] *Kraftstoffe – Dieselkraftstoff – Anforderungen und Prüfverfahren; Deutsche Fassung EN 590:2013+A1:2017*, 590, Deutsches Institut für Normung.

[137] *Fuels – Polyoxymethylene dimethylether (OME) – Requirements and Test Methods: M DIN/TS 51699*, 51699, Deutsches Institut für Normung.

[138] J. Burger, M. Siegert, E. Ströfer und H. Hasse, „Poly(oxymethylene) dimethyl ethers as components of tailored diesel fuel: Properties, synthesis and purification concepts“, *Fuel*, Jg. 89, Nr. 11, S. 3315–3319, 2010, doi: 10.1016/j.fuel.2010.05.014.

[139] J. Burger, E. Ströfer und H. Hasse, „Chemical Equilibrium and Reaction Kinetics of the Heterogeneously Catalyzed Formation of Poly(oxymethylene) Dimethyl Ethers from Methylal and Trioxane“, *Ind. Eng. Chem. Res.*, Jg. 51, Nr. 39, S. 12751–12761, 2012, doi: 10.1021/ie301490q.

[140] J. Burger, E. Ströfer und H. Hasse, „Production process for diesel fuel components poly(oxymethylene) dimethyl ethers from methane-based products by hierarchical optimization with varying model depth“, *Chemical Engineering Research and Design*, Jg. 91, Nr. 12, S. 2648–2662, 2013, doi: 10.1016/j.cherd.2013.05.023.

[141] N. Schmitz, E. Ströfer, J. Burger und H. Hasse, „Conceptual Design of a Novel Process for the Production of Poly(oxymethylene) Dimethyl Ethers from Formaldehyde and Methanol“, *Ind. Eng. Chem. Res.*, Jg. 56, Nr. 40, S. 11519–11530, 2017, doi: 10.1021/acs.iecr.7b02314.

[142] J. A. Wurzbacher, C. Gebald und A. Steinfeld, „Separation of CO2 from air by temperature-vacuum swing adsorption using diamine-functionalized silica gel“, *Energy Environ. Sci.*, Jg. 4, Nr. 9, S. 3584, 2011, doi: 10.1039/c1ee01681d.

[143] J. A. Wurzbacher, C. Gebald, N. Piatkowski und A. Steinfeld, „Concurrent separation of CO2 and H2O from air by a temperature-vacuum swing adsorption/desorption cycle“ (eng), *Environmental science & technology*, Jg. 46, Nr. 16, S. 9191–9198, 2012, doi: 10.1021/es301953k.

[144] M. Wang, A. Lawal, P. Stephenson, J. Sidders und C. Ramshaw, „Post-combustion CO2 capture with chemical absorption: A state-of-the-art review“, *Chemical Engineering*

Research and Design, Jg. 89, Nr. 9, S. 1609–1624, 2011, doi: 10.1016/j.cherd.2010.11.005.

[145] A. A. Olajire, „CO2 capture and separation technologies for end-of-pipe applications – A review“, *Energy*, Jg. 35, Nr. 6, S. 2610–2628, 2010, doi: 10.1016/j.energy.2010.02.030.

[146] G. Reuss, W. Disteldorf, A. O. Gamer und A. Hilt, „Formaldehyde“ in *Ullmann's Encyclopedia of Industrial Chemistry*, Weinheim, Germany: Wiley-VCH Verlag GmbH & Co. KGaA, 2000, doi: 10.1002/14356007.a11_619.

[147] M. Held, Y. Tönges, D. Pélerin, M. Härtl, G. Wachtmeister und J. Burger, „On the energetic efficiency of producing polyoxymethylene dimethyl ethers from CO 2 using electrical energy“, *Energy Environ. Sci.*, Jg. 12, Nr. 3, S. 1019–1034, 2019, doi: 10.1039/c8ee02849d.

[148] D. Pélerin, *Potentiale der synthetischen Kraftstoffe Oxymethylenether und Dimethylether zur Realisierung klimaneutraler, schadstoffarmer sowie vereinfachter Dieselmotoren: Dissertation*, 2021.

[149] Q. Lin *et al.,* „Polyoxymethylene dimethyl ether 3 (PODE3) as an alternative fuel to reduce aerosol pollution“, *Journal of Cleaner Production*, Jg. 285, S. 124857, 2021, doi: 10.1016/j.jclepro.2020.124857.

[150] M. Parravicini, C. Barro und K. Boulouchos, „Experimental characterization of GTL, HVO, and OME based alternative fuels for diesel engines“, *Fuel*, Jg. 292, S. 120177, 2021, doi: 10.1016/j.fuel.2021.120177.

[151] P. Dimopoulos Eggenschwiler, D. Schreiber, K. Schröter und C. Barro, „Oxidative Reactivity of Soot Particles Generated from the Combustion of Conventional Diesel, HVO and OME Collected in Particle Filter Structures“ in *15th International Conference on Engines & Vehicles*, 2021, doi: 10.4271/2021-24-0085.

[152] J. V. Pastor, J. M. Garcia-Oliver, C. Micó und F. J. Tejada, „Combustion Behaviour of Blends of Synthetic Fuels in an Optical Single Cylinder Engine“ in *15th International Conference on Engines & Vehicles*, 2021, doi: 10.4271/2021-24-0038.

[153] J. V. Pastor, A. García, C. Micó und F. Lewiski, „An optical investigation of Fischer-Tropsch diesel and Oxymethylene dimethyl ether impact on combustion process for CI engines“, *Applied Energy*, Jg. 260, S. 114238, 2020, doi: 10.1016/j.apenergy.2019.114238.

[154] J. Preuß, K. Munch und I. Denbratt, „Performance and emissions of renewable blends with OME3-5 and HVO in heavy duty and light duty compression ignition engines“, *Fuel*, Jg. 303, S. 121275, 2021, doi: 10.1016/j.fuel.2021.121275.

[155] I. P. Venugopal, D. Balasubramanian und A. Rajarajan, „Potential improvement in conventional diesel combustion mode on a common rail direct injection diesel engine with PODE/WCO blend as a high reactive fuel to achieve effective Soot-NOx trade-off“, *Journal of Cleaner Production*, Jg. 327, S. 129495, 2021, doi: 10.1016/j.jclepro.2021.129495.

[156] Q. Zhu, Y. Zong, W. Yu, W. Yang und M. Kraft, „Understanding the blending effect of polyoxymethylene dimethyl ethers as additive in a common-rail diesel engine“, *Applied Energy*, Jg. 300, S. 117380, 2021, doi: 10.1016/j.apenergy.2021.117380.

[157] H. Chen, X. Su, J. Li und X. Zhong, „Effects of gasoline and polyoxymethylene dimethyl ethers blending in diesel on the combustion and emission of a common rail diesel engine“, *Energy*, Jg. 171, S. 981–999, 2019, doi: 10.1016/j.energy.2019.01.089.

[158] T. Popp, R. Lechner, M. Becker, M. Hebauer, N. O'Connell und M. Brautsch, „Potentials of OME/diesel blends for stationary power production – Improving emission characteristics of a diesel CHP unit“, *Applied Thermal Engineering*, Jg. 153, S. 483–492, 2019, doi: 10.1016/j.applthermaleng.2019.03.015.

[159] H. Huang *et al.,* „Influence of n-butanol-diesel-PODE3-4 fuels coupled pilot injection strategy on combustion and emission characteristics of diesel engine“, *Fuel*, Jg. 236, S. 313–324, 2019, doi: 10.1016/j.fuel.2018.09.051.

[160] A. García, A. Gil, J. Monsalve-Serrano und R. Lago Sari, „OMEx-diesel blends as high reactivity fuel for ultra-low NOx and soot emissions in the dual-mode dual-fuel combustion strategy“, *Fuel*, Jg. 275, S. 117898, 2020, doi: 10.1016/j.fuel.2020.117898.

[161] Y. Zhao, Y. Xie, X. Wang, Z. Li, T. Niu und S. Liu, „Energy balance analysis, combustion characteristics, and particulate number concentration-NO trade-off of a heavy-duty diesel engine fueled with various PODEn/diesel blends“, *Energy Conversion and Management*, Jg. 225, S. 113489, 2020, doi: 10.1016/j.enconman.2020.113489.

[162] J. Liu *et al.,* „Effects of PODE/diesel blends on particulate matter emission and particle oxidation characteristics of a common-rail diesel engine“, *Fuel Processing Technology*, Jg. 212, S. 106634, 2021, doi: 10.1016/j.fuproc.2020.106634.

[163] H. Chen *et al.,* „Filtration Efficiency and Regeneration Behavior in a Catalytic Diesel Particulate Filter with the Use of Diesel/Polyoxymethylene Dimethyl Ether Mixture“, *Catalysts*, Jg. 11, Nr. 12, S. 1425, 2021, doi: 10.3390/catal11121425.

[164] Q. Wang, J. Ni und R. Huang, „The potential of oxygenated fuels (n-octanol, methylal, and dimethyl carbonate) as an alternative fuel for compression ignition engines with different load conditions“, *Fuel*, Jg. 309, S. 122129, 2022, doi: 10.1016/j.fuel.2021.122129.

[165] Y. Wei, Y. Zhang, Z. Zhu, X. Zhu, H. Gu und S. Liu, „Effect of PODE on Emission Characteristics of a China VI Heavy-Duty Diesel Engine“, *Applied Sciences*, Jg. 12, Nr. 3, S. 1108, 2022, doi: 10.3390/app12031108.

[166] A. García, J. Monsalve-Serrano, D. Villalta und Á. Fogué-Robles, „Evaluating OMEx combustion towards stoichiometric conditions in a compression ignition engine“, *Fuel*, Jg. 303, S. 121273, 2021, doi: 10.1016/j.fuel.2021.121273.

[167] W. Bosch, „The Fuel Rate Indicator: A New Measuring Instrument For Display of the Characteristics of Individual Injection“ in *National Powerplant and Transportation Meetings*, 1966, doi: 10.4271/660749.

[168] S. Schuckert, *Kompensation von Alterungserscheinungen von Common-Rail-Diesel-Einspritzdüsen: Dissertation im Promotionsverfahren*.

[169] H. Stein, *Bestimmungsmethoden und Stoffwerte von OME nach M DIN TS 51699*.

[170] M. E. Wieser und T. B. Coplen, „Atomic weights of the elements 2009 (IUPAC Technical Report)“, *Pure and Applied Chemistry*, Jg. 83, Nr. 2, S. 359–396, 2010, doi: 10.1351/PAC-REP-10-09-14.

[171] G. Audi und A. H. Wapstra, „The 1993 atomic mass evaluation“, *Nuclear Physics A*, Jg. 565, Nr. 1, S. 1–65, 1993, doi: 10.1016/0375-9474(93)90024-R.

[172] L. Lautenschütz, D. Oestreich, P. Seidenspinner, U. Arnold, E. Dinjus und J. Sauer, „Physico-chemical properties and fuel characteristics of oxymethylene dialkyl ethers“, *Fuel*, Jg. 173, S. 129–137, 2016, doi: 10.1016/j.fuel.2016.01.060.

[173] I. Bogatykh, T. Osterland, H. Stein und T. Wilharm, „Investigation of the Oxidative Degradation of the Synthetic Fuel Oxymethylene Dimethyl Ether“, *Energy Fuels*, Jg. 34, Nr. 3, S. 3357–3366, 2020, doi: 10.1021/acs.energyfuels.9b04464.

[174] A. Peter, B. Siewert, S. Riess, L. Strauss, C. Pastoetter und M. Wensing, „MIXTURE FORMATION ANALYSIS OF POLYOXYMETHYLENETHER INJECTION“, *Atomiz Spr*, Jg. 30, Nr. 11, S. 843–859, 2020, doi: 10.1615/AtomizSpr.2020035250.

[175] A. Röll, F. Luo, N. O'Connell, R. Lechner, C. Wang und M. Brautsch, „Hydraulic stability of micro injections using a two-layered 8-hole solenoid injector with PODE“, *Fuel*, Jg. 297, S. 120748, 2021, doi: 10.1016/j.fuel.2021.120748.

[176] A. D. Gelner, R. Höß, A. Zepf, M. Härtl und G. Wachtmeister, „Engine Operation Strategies for the Alternative Diesel Fuel Oxymethylene Ether (OME): Evaluation Based on Injection Rate Analyzer and 0D-/1D-Simulation“ in *SAE Powertrains, Fuels & Lubricants Digital Summit*, 2021, doi: 10.4271/2021-01-1190.

[177] S. Schuckert, M. Huthmacher und G. Wachtmeister, „Compensation Strategies for Aging Effects of Common-Rail Injector Nozzles“ in *WCX SAE World Congress Experience*, 2019, doi: 10.4271/2019-01-0944.

[178] Q. Lin, K. L. Tay, W. Yu, W. Yang und Z. Wang, „Effects of polyoxymethylene dimethyl ether 3 (PODE3) addition and injection pressure on combustion performance and particle size distributions in a diesel engine“, *Fuel*, Jg. 283, S. 119347, 2021, doi: 10.1016/j.fuel.2020.119347.

[179] F. Ferraro, C. Russo, R. Schmitz, C. Hasse und M. Sirignano, „Experimental and numerical study on the effect of oxymethylene ether-3 (OME3) on soot particle formation“, *Fuel*, Jg. 286, S. 119353, 2021, doi: 10.1016/j.fuel.2020.119353.

[180] A. D. Gelner *et al.,* „Particle emissions of a heavy-duty engine fueled with polyoxymethylene dimethyl ethers (OME)“, *Environ. Sci.: Atmos.*, Jg. 2, Nr. 2, S. 291–304, 2022, doi: 10.1039/d1ea00084e.

[181] C. S. McEnally *et al.,* „Sooting tendencies of co-optima test gasolines and their surrogates“, *Proceedings of the Combustion Institute*, Jg. 37, Nr. 1, S. 961–968, 2019, doi: 10.1016/j.proci.2018.05.071.

[182] Z. Xiang, K. Chen, C. McEnally und L. Pfefferle, *Sooting tendencies of diesel fuel component mixtures follow a linear mixing rule*, 2022.

[183] G. Fioroni *et al.,* „Screening of Potential Biomass-Derived Streams as Fuel Blendstocks for Mixing Controlled Compression Ignition Combustion“ in *WCX SAE World Congress Experience*, 2019, doi: 10.4271/2019-01-0570.

[184] M. Münz, D. Töpfer, A. Mokros und C. Beidl, „Oxygenate fuel in a Diesel engine – Is a CI engine capable of lambda 1?“ in *Proceedings, Internationaler Motorenkongress 2017*, J. Liebl und C. Beidl, Hg., Wiesbaden: Springer Fachmedien Wiesbaden, 2017, S. 457–472, doi: 10.1007/978-3-658-17109-4_29.

[185] D. Zengel, P. Koch, B. Torkashvand, J.-D. Grunwaldt, M. Casapu und O. Deutschmann, „Emission of Toxic HCN During NOx Removal by Ammonia SCR in the Exhaust of Lean-Burn Natural Gas Engines“ (eng), *Angewandte Chemie (International ed. in English)*, Jg. 59, Nr. 34, S. 14423–14428, 2020, doi: 10.1002/anie.202003670.

[186] M. Elsener, R. J. G. Nuguid, O. Kröcher und D. Ferri, „HCN production from formaldehyde during the selective catalytic reduction of NOx with NH3 over V2O5/WO3-TiO2“, *Applied Catalysis B: Environmental*, Jg. 281, S. 119462, 2021, doi: 10.1016/j.apcatb.2020.119462.

[187] A. D. Gelner, H. A. Beck, C. Pastoetter, M. Härtl und G. Wachtmeister, „Ultra-low emissions of a heavy-duty engine powered with oxymethylene ethers (OME) under stationary and transient driving conditions“, *International Journal of Engine Research*, Jg. 23, Nr. 5, S. 738–753, 2022, doi: 10.1177/14680874211047922.

[188] J. Gao, G. Tian, A. Sorniotti, A. E. Karci und R. Di Palo, „Review of thermal management of catalytic converters to decrease engine emissions during cold start and warm up“, *Applied Thermal Engineering*, Jg. 147, S. 177–187, 2019, doi: 10.1016/j.applthermaleng.2018.10.037.

[189] A. D. Gelner, C. Pastoetter, H. A. Beck, M. Härtl und G. Wachtmeister, „Fuel Dosing on a Diesel Oxidation Catalyst for After-Treatment System Heating on a Heavy-Duty Engine Powered by Polyoxymethylene Dimethyl Ethers“ in *SAE Powertrains, Fuels & Lubricants Meeting*, 2020, doi: 10.4271/2020-01-2157.

[190] L. Yang *et al.,* „Experimental Assessment of NOx Emissions from 73 Euro 6 Diesel Passenger Cars“ (eng), *Environmental science & technology*, Jg. 49, Nr. 24, S. 14409–14415, 2015, doi: 10.1021/acs.est.5b04242.

[191] R. Williams *et al.,* „Impact of Demanding Low Temperature Urban Operation on the Real Driving Emissions Performance of Three European Diesel Passenger Cars“ in *International Powertrains, Fuels & Lubricants Meeting*, 2018, doi: 10.4271/2018-01-1819.

[192] C. Dardiotis, G. Martini, A. Marotta und U. Manfredi, „Low-temperature cold-start gaseous emissions of late technology passenger cars“, *Applied Energy*, Jg. 111, S. 468–478, 2013, doi: 10.1016/j.apenergy.2013.04.093.

[193] A. Broatch, B. Tormos, P. Olmeda und R. Novella, „Impact of biodiesel fuel on cold starting of automotive direct injection diesel engines“, *Energy*, Jg. 73, S. 653–660, 2014, doi: 10.1016/j.energy.2014.06.062.

[194] M. Weilenmann, P. Soltic, C. Saxer, A.-M. Forss und N. Heeb, „Regulated and nonregulated diesel and gasoline cold start emissions at different temperatures“, *Atmospheric Environment*, Jg. 39, Nr. 13, S. 2433–2441, 2005, doi: 10.1016/j.atmosenv.2004.03.081.

[195] A. S. Ramadhas und H. Xu, „Cold start particle number, size and mass emissions from a CRDI diesel engine running on biodiesel blends in a cold environment“, *Biofuels*, Jg. 7, Nr. 4, S. 353–363, 2016, doi: 10.1080/17597269.2015.1138037.

[196] R. Suarez-Bertoa und C. Astorga, „Impact of cold temperature on Euro 6 passenger car emissions“ (eng), *Environmental pollution (Barking, Essex : 1987)*, Jg. 234, S. 318–329, 2018, doi: 10.1016/j.envpol.2017.10.096.

[197] B. Giechaskiel und M. Clairotte, „Fourier Transform Infrared (FTIR) Spectroscopy for Measurements of Vehicle Exhaust Emissions: A Review“, *Applied Sciences*, Jg. 11, Nr. 16, S. 7416, 2021, doi: 10.3390/app11167416.

[198] A. D. Gelner *et al.,* „Gaseous emissions of a heavy-duty engine fueled with polyoxymethylene dimethyl ethers (OME) in transient cold-start operation and methods for after-treatment system heating“, *Environ. Sci.: Adv.*, Jg. 1, Nr. 4, S. 470–482, 2022, doi: 10.1039/D2VA00080F.

[199] D. Li, Y. Gao, S. Liu, Z. Ma und Y. Wei, „Effect of polyoxymethylene dimethyl ethers addition on spray and atomization characteristics using a common rail diesel injection system“, *Fuel*, Jg. 186, S. 235–247, 2016, doi: 10.1016/j.fuel.2016.08.082.

[200] Y. Liu, J. Tian, Z. Song, F. Li, W. Zhou und Q. Lin, „Spray characteristics of diesel, biodiesel, polyoxymethylene dimethyl ethers blends and prediction of spray tip penetration using artificial neural network“, *Physics of Fluids*, Jg. 34, Nr. 1, S. 15117, 2022, doi: 10.1063/5.0077405.

[201] L. Cosimbescu, K. B. Campbell, T. J. Baker, M. Swita und D. J. Gaspar, „The quest for efficient oxygenated fuels: Examining interactions between lubricant components and oxygenates“, *Fuel*, Jg. 288, S. 119728, 2021, doi: 10.1016/j.fuel.2020.119728.

[202] L. Cai, S. Jacobs, R. Langer, F. vom Lehn, K. A. Heufer und H. Pitsch, „Auto-ignition of oxymethylene ethers (OMEn, n = 2–4) as promising synthetic e-fuels from renewable electricity: shock tube experiments and automatic mechanism generation“, *Fuel*, Jg. 264, S. 116711, 2020, doi: 10.1016/j.fuel.2019.116711.

[203] B. Giechaskiel, A. Melas und T. Lähde, „Detailed Characterization of Solid and Volatile Particle Emissions of Two Euro 6 Diesel Vehicles“, *Applied Sciences*, Jg. 12, Nr. 7, S. 3321, 2022, doi: 10.3390/app12073321.

[204] S. Amanatidis, L. Ntziachristos, B. Giechaskiel, A. Bergmann und Z. Samaras, „Impact of selective catalytic reduction on exhaust particle formation over excess ammonia events“ (eng), *Environmental science & technology*, Jg. 48, Nr. 19, S. 11527–11534, 2014, doi: 10.1021/es502895v.

[205] P. M. Schaber, J. Colson, S. Higgins, D. Thielen, B. Anspach und J. Brauer, „Thermal decomposition (pyrolysis) of urea in an open reaction vessel“, *Thermochimica Acta*, Jg. 424, 1-2, S. 131–142, 2004, doi: 10.1016/j.tca.2004.05.018.

[206] M. Börnhorst und O. Deutschmann, „Advances and challenges of ammonia delivery by urea-water sprays in SCR systems“, *Progress in Energy and Combustion Science*, Jg. 87, S. 100949, 2021, doi: 10.1016/j.pecs.2021.100949.

[207] H. Rodhe, C. Persson und O. Åkesson, „An investigation into regional transport of soot and sulfate aerosols“, *Atmospheric Environment (1967)*, Jg. 6, Nr. 9, S. 675–693, 1972, doi: 10.1016/0004-6981(72)90025-x.

[208] V. Ramanathan und G. Carmichael, „Global and regional climate changes due to black carbon“, *Nature Geosci*, Jg. 1, Nr. 4, S. 221–227, 2008, doi: 10.1038/ngeo156.

[209] M. Etminan, G. Myhre, E. J. Highwood und K. P. Shine, „Radiative forcing of carbon dioxide, methane, and nitrous oxide: A significant revision of the methane radiative forcing“, *Geophys. Res. Lett.*, Jg. 43, Nr. 24, 2016, doi: 10.1002/2016GL071930.

[210] H.-O. Herrmann, P. Kožuch, H. Lettmann und R. Brünemann, „Die neueste Heavy-Duty-Motorengeneration von Mercedes-Benz Teil 2: Verbrennung und Emissionen“, *MTZ Motortech Z*, Jg. 77, 7-8, S. 60–65, 2016, doi: 10.1007/s35146-016-0061-0.

[211] R. Szolak *et al.,* „CatVap® – New Heating Measure for Exhaust Aftertreatment Systems to Fulfill the Strictest Future Emission Limits“ in *Proceedings, Heavy-Duty-, On- und Off-Highway-Motoren 2020*, J. Liebl, Hg., Wiesbaden: Springer Fachmedien Wiesbaden, 2021, S. 121–133, doi: 10.1007/978-3-658-34362-0_8.

[212] C. Bertole, „Formaldehyde Oxidation over Emission Control Catalysts“ in *WCX World Congress Experience*, 2018, doi: 10.4271/2018-01-1274.

[213] M. Elsener, D. Ferri, E. Jacob und O. Kröcher, „Stability and reactivity of a polyoxymethylene dimethyl ether over typical catalysts of Diesel emission control: Manuskript im Review“, *Topics in catalysis*, 2022.

[214] Ständige Senatskommission zur Prüfung gesundheitsschädlicher Stoffe, *MAK- und BAT-Werte-Liste 2021: Maximale Arbeitsplatzkonzentrationen und Biologische Arbeitsstofftoleranzwerte.* [Online]. Verfügbar unter: https://mak-dfg.publisso.de/ (Zugriff am: 16. April 2022).

[215] J. Schröder und K. Görsch, „Storage Stability and Material Compatibility of Poly(oxymethylene) Dimethyl Ether Diesel Fuel“, *Energy Fuels*, Jg. 34, Nr. 1, S. 450–459, 2020, doi: 10.1021/acs.energyfuels.9b03101.

[216] T. Kaivosoja *et al.,* „Comparison of emissions and toxicological properties of fine particles from wood and oil boilers in small (20–25 kW) and medium (5–10 MW) scale“, *Atmospheric Environment*, Jg. 77, S. 193–201, 2013, doi: 10.1016/j.atmosenv.2013.05.014.

[217] F. Mantei *et al.,* „Techno-economic assessment and carbon footprint of processes for the large-scale production of oxymethylene dimethyl ethers from carbon dioxide and hydrogen“, *Sustainable Energy Fuels*, Jg. 6, Nr. 3, S. 528–549, 2022, doi: 10.1039/d1se01270c.

[218] D. F. Rodríguez-Vallejo, A. Valente, G. Guillén-Gosálbez und B. Chachuat, „Economic and life-cycle assessment of OME 3–5 as transport fuel: a comparison of production pathways“, *Sustainable Energy Fuels*, Jg. 5, Nr. 9, S. 2504–2516, 2021, doi: 10.1039/d1se00335f.

[219] B. H. Kreps, „The Rising Costs of Fossil-Fuel Extraction: An Energy Crisis That Will Not Go Away“, *Am J Econ Sociol*, Jg. 79, Nr. 3, S. 695–717, 2020, doi: 10.1111/ajes.12336.

[220] A. Srna, C. Barro, K. Herrmann, F. Möri, R. Hutter und K. Boulouchos, „POMDME as an Alternative Pilot Fuel for Dual-Fuel Engines: Optical Study in a RCEM and Application in an Automotive Size Dual-Fuel Diesel Engine“ in *International Powertrains, Fuels & Lubricants Meeting*, 2018, doi: 10.4271/2018-01-1734.

[221] H. L. Jones, G. P. Mctaggart-Cowan, S. N. Rogak, W. K. Bushe, S. R. Munshi und B. A. Buchholz, „Source Apportionment of Particulate Matter from a Diesel Pilot-Ignited Natural Gas Fuelled Heavy Duty DI Engine“ in *2005 SAE Brasil Fuels & Lubricants Meeting*, 2005, doi: 10.4271/2005-01-2149.

Anhang: Eingebundene Publikationen in Originalform

Gelner, A. D.; Höß, R.; Zepf, A.; Härtl, M.; Wachtmeister, G.: *Engine Operation Strategies with the Alternative Diesel Fuel Oxymethylene Ether (OME): Evaluation Using Injection Rate Analyzer and 0D-/1D-Simulation*; SAE Technical Paper 2021-0050; 2021. [176]

Order Date	18-Oct-2022	Type of Use	Republish in a thesis/dissertation
Order License ID	1280572-2		
ISSN	0148-7191	Publisher	SOCIETY OF AUTOMOTIVE ENGINEERS,
		Portion	Chapter/article

LICENSED CONTENT

Publication Title	SAE technical paper series	Language	English
Article Title	Engine Operation Strategies for the Alternative Diesel Fuel Oxymethylene Ether (OME): Evaluation based on Injection Rate Analyzer and 0D-/1D-Simulation	Country	United States of America
		Rightsholder	SAE International
		Publication Type	Monographic Series
Author/Editor	SOCIETY OF AUTOMOTIVE ENGINEERS.		
Date	01/01/1970		

REQUEST DETAILS

Portion Type	Chapter/article	Rights Requested	Main product
Page Range(s)	1-14	Distribution	Worldwide
Total Number of Pages	14	Translation	Original language of publication
Format (select all that apply)	Electronic	Copies for the Disabled?	No
Who Will Republish the Content?	Academic institution	Minor Editing Privileges?	No
		Incidental Promotional Use?	No
Duration of Use	Life of current edition		
Lifetime Unit Quantity	More than 2,000,000	Currency	EUR

NEW WORK DETAILS

Title	OME as enabler of climate-neutral and pollutant-free diesel engines	Institution Name	Technical University of Munich
		Expected Presentation Date	2022-11-08
Instructor Name	Alexander Daniel Gelner		

ADDITIONAL DETAILS

Order Reference Number	N/A

The Requesting Person/Organization to Appear on the License	Alexander Daniel Gelner

REUSE CONTENT DETAILS

Title, Description or Numeric Reference of the Portion(s)	https://doi.org/10.4271/2021-01-1190	Title of the Article/Chapter the Portion Is From	Engine Operation Strategies for the Alternative Diesel Fuel Oxymethylene Ether (OME): Evaluation based on Injection Rate Analyzer and 0D-/1D-Simulation
Editor of Portion(s)	Gelner, Alexander D.; Höß, Rudolf; Zepf, Andreas; Härtl, Martin; Wachtmeister, Georg	Author of Portion(s)	Gelner, Alexander D.; Höß, Rudolf; Zepf, Andreas; Härtl, Martin; Wachtmeister, Georg
Volume of Serial or Monograph	N/A	Issue, if Republishing an Article From a Serial	N/A
Page or Page Range of Portion	1-14	Publication Date of Portion	2021-09-21

Marketplace Order General Terms and Conditions

The following terms and conditions ("General Terms"), together with any applicable Publisher Terms and Conditions, govern User's use of Works pursuant to the Licenses granted by Copyright Clearance Center, Inc. ("CCC") on behalf of the applicable Rightsholders of such Works through CCC's applicable Marketplace transactional licensing services (each, a "Service").

1) Definitions. For purposes of these General Terms, the following definitions apply:

"License" is the licensed use the User obtains via the Marketplace platform in a particular licensing transaction, as set forth in the Order Confirmation.

"Order Confirmation" is the confirmation CCC provides to the User at the conclusion of each Marketplace transaction. "Order Confirmation Terms" are additional terms set forth on specific Order Confirmations not set forth in the General Terms that can include terms applicable to a particular CCC transactional licensing service and/or any Rightsholder-specific terms.

"Rightsholder(s)" are the holders of copyright rights in the Works for which a User obtains licenses via the Marketplace platform, which are displayed on specific Order Confirmations.

"Terms" means the terms and conditions set forth in these General Terms and any additional Order Confirmation Terms collectively.

"User" or "you" is the person or entity making the use granted under the relevant License. Where the person accepting the Terms on behalf of a User is a freelancer or other third party who the User authorized to accept the General Terms on the User's behalf, such person shall be deemed jointly a User for purposes of such Terms.

"Work(s)" are the copyright protected works described in relevant Order Confirmations.

2) Description of Service. CCC's Marketplace enables Users to obtain Licenses to use one or more Works in accordance with all relevant Terms. CCC grants Licenses as an agent on behalf of the copyright rightsholder identified in the relevant Order Confirmation.

3) Applicability of Terms. The Terms govern User's use of Works in connection with the relevant License. In the event of any conflict between General Terms and Order Confirmation Terms, the latter shall govern. User acknowledges that Rightsholders have complete discretion whether to grant any permission, and whether to place any limitations on any grant, and that CCC has no right to supersede or to modify any such discretionary act by a Rightsholder.

4) Representations; Acceptance. By using the Service, User represents and warrants that User has been duly authorized by the User to accept, and hereby does accept, all Terms.

5) Scope of License; Limitations and Obligations. All Works and all rights therein, including copyright rights, remain the sole and exclusive property of the Rightsholder. The License provides only those rights expressly set forth in the terms and conveys no other rights in any Works

6) General Payment Terms. User may pay at time of checkout by credit card or choose to be invoiced. If the User chooses to be invoiced, the User shall: (i) remit payments in the manner identified on specific invoices, (ii) unless otherwise specifically stated in an Order Confirmation or separate written agreement, Users shall remit payments upon receipt of the relevant invoice from CCC, either by delivery or notification of availability of the invoice via the Marketplace platform, and (iii) if the User does not pay the invoice within 30 days of receipt, the User may incur a service charge of 1.5% per month or the maximum rate allowed by applicable law, whichever is less. While User may exercise the rights in the License immediately upon receiving the Order Confirmation, the License is automatically revoked and is null and void, as if it had never been issued, if CCC does not receive complete payment on a timely basis.

7) General Limits on Use. Unless otherwise provided in the Order Confirmation, any grant of rights to User (i) involves only the rights set forth in the Terms and does not include subsequent or additional uses, (ii) is non-exclusive and non-transferable, and (iii) is subject to any and all limitations and restrictions (such as, but not limited to, limitations on duration of use or circulation) included in the Terms. Upon completion of the licensed use as set forth in the Order Confirmation, User shall either secure a new permission for further use of the Work(s) or immediately cease any new use of the Work(s) and shall render inaccessible (such as by deleting or by removing or severing links or other locators) any further copies of the Work. User may only make alterations to the Work if and as expressly set forth in the Order Confirmation. No Work may be used in any way that is defamatory, violates the rights of third parties (including such third parties' rights of copyright, privacy, publicity, or other tangible or intangible property), or is otherwise illegal, sexually explicit, or obscene. In addition, User may not conjoin a Work with any other material that may result in damage to the reputation of the Rightsholder. User agrees to inform CCC if it becomes aware of any infringement of any rights in a Work and to cooperate with any reasonable request of CCC or the Rightsholder in connection therewith.

8) Third Party Materials. In the event that the material for which a License is sought includes third party materials (such as photographs, illustrations, graphs, inserts and similar materials) that are identified in such material as having been used by permission (or a similar indicator), User is responsible for identifying, and seeking separate licenses (under this Service, if available, or otherwise) for any of such third party materials; without a separate license, User may not use such third party materials via the License.

9) Copyright Notice. Use of proper copyright notice for a Work is required as a condition of any License granted under the Service. Unless otherwise provided in the Order Confirmation, a proper copyright notice will read substantially as follows: "Used with permission of [Rightsholder's name], from [Work's title, author, volume, edition number and year of copyright]; permission conveyed through Copyright Clearance Center, Inc." Such notice must be provided in a reasonably legible font size and must be placed either on a cover page or in another location that any person, upon gaining access to the material which is the subject of a permission, shall see, or in the case of republication Licenses, immediately adjacent to the Work as used (for example, as part of a by-line or footnote) or in the place where substantially all other credits or notices for the new work containing the republished Work are located. Failure to include the required notice results in loss to the Rightsholder and CCC, and the User shall be liable to pay liquidated damages for each such failure equal to twice the use fee specified in the Order Confirmation, in addition to the use fee itself and any other fees and charges specified.

10) Indemnity. User hereby indemnifies and agrees to defend the Rightsholder and CCC, and their respective employees and directors, against all claims, liability, damages, costs, and expenses, including legal fees and expenses, arising out of any use of a Work beyond the scope of the rights granted herein and in the Order Confirmation, or any use of a Work which has been altered in any unauthorized way by User, including claims of defamation or infringement of rights of copyright, publicity, privacy, or other tangible or intangible property.

11) Limitation of Liability. UNDER NO CIRCUMSTANCES WILL CCC OR THE RIGHTSHOLDER BE LIABLE FOR ANY DIRECT, INDIRECT, CONSEQUENTIAL, OR INCIDENTAL DAMAGES (INCLUDING WITHOUT LIMITATION DAMAGES FOR LOSS OF BUSINESS PROFITS OR INFORMATION, OR FOR BUSINESS INTERRUPTION) ARISING OUT OF THE USE OR INABILITY TO USE A WORK, EVEN IF ONE OR BOTH OF THEM HAS BEEN ADVISED OF THE POSSIBILITY OF SUCH DAMAGES. In any event, the total liability of the Rightsholder and CCC (including their respective employees and directors) shall not exceed the total amount actually paid by User for the relevant License. User assumes full liability for the actions and omissions of its principals, employees, agents, affiliates, successors, and assigns.

12) Limited Warranties. THE WORK(S) AND RIGHT(S) ARE PROVIDED "AS IS." CCC HAS THE RIGHT TO GRANT TO USER THE

RIGHTS GRANTED IN THE ORDER CONFIRMATION DOCUMENT. CCC AND THE RIGHTSHOLDER DISCLAIM ALL OTHER WARRANTIES RELATING TO THE WORK(S) AND RIGHT(S), EITHER EXPRESS OR IMPLIED, INCLUDING WITHOUT LIMITATION IMPLIED WARRANTIES OF MERCHANTABILITY OR FITNESS FOR A PARTICULAR PURPOSE. ADDITIONAL RIGHTS MAY BE REQUIRED TO USE ILLUSTRATIONS, GRAPHS, PHOTOGRAPHS, ABSTRACTS, INSERTS, OR OTHER PORTIONS OF THE WORK (AS OPPOSED TO THE ENTIRE WORK) IN A MANNER CONTEMPLATED BY USER; USER UNDERSTANDS AND AGREES THAT NEITHER CCC NOR THE RIGHTSHOLDER MAY HAVE SUCH ADDITIONAL RIGHTS TO GRANT.

13) Effect of Breach. Any failure by User to pay any amount when due, or any use by User of a Work beyond the scope of the License set forth in the Order Confirmation and/or the Terms, shall be a material breach of such License. Any breach not cured within 10 days of written notice thereof shall result in immediate termination of such License without further notice. Any unauthorized (but licensable) use of a Work that is terminated immediately upon notice thereof may be liquidated by payment of the Rightsholder's ordinary license price therefor; any unauthorized (and unlicensable) use that is not terminated immediately for any reason (including, for example, because materials containing the Work cannot reasonably be recalled) will be subject to all remedies available at law or in equity, but in no event to a payment of less than three times the Rightsholder's ordinary license price for the most closely analogous licensable use plus Rightsholder's and/or CCC's costs and expenses incurred in collecting such payment.

14) Additional Terms for Specific Products and Services. If a User is making one of the uses described in this Section 14, the additional terms and conditions apply:

a) *Print Uses of Academic Course Content and Materials (photocopies for academic coursepacks or classroom handouts).* For photocopies for academic coursepacks or classroom handouts the following additional terms apply:

i) The copies and anthologies created under this License may be made and assembled by faculty members individually or at their request by on-campus bookstores or copy centers, or by off-campus copy shops and other similar entities.

ii) No License granted shall in any way: (i) include any right by User to create a substantively non-identical copy of the Work or to edit or in any other way modify the Work (except by means of deleting material immediately preceding or following the entire portion of the Work copied) (ii) permit "publishing ventures" where any particular anthology would be systematically marketed at multiple institutions.

iii) Subject to any Publisher Terms (and notwithstanding any apparent contradiction in the Order Confirmation arising from data provided by User), any use authorized under the academic pay-per-use service is limited as follows:

A) any License granted shall apply to only one class (bearing a unique identifier as assigned by the institution, and thereby including all sections or other subparts of the class) at one institution;

B) use is limited to not more than 25% of the text of a book or of the items in a published collection of essays, poems or articles;

C) use is limited to no more than the greater of (a) 25% of the text of an issue of a journal or other periodical or (b) two articles from such an issue;

D) no User may sell or distribute any particular anthology, whether photocopied or electronic, at more than one institution of learning;

E) in the case of a photocopy permission, no materials may be entered into electronic memory by User except in order to produce an identical copy of a Work before or during the academic term (or analogous period) as to which any particular permission is granted. In the event that User shall choose to retain materials that are the subject of a photocopy permission in electronic memory for purposes of producing identical copies more than one day after such retention (but still within the scope of any permission granted), User must notify CCC of such fact in the applicable permission request and such retention shall constitute one copy actually sold for purposes of calculating permission fees due; and

F) any permission granted shall expire at the end of the class. No permission granted shall in any way include any right by User to create a substantively non-identical copy of the Work or to edit or in any other way modify the Work (except by means of deleting material immediately preceding or following the entire portion of the Work copied).

iv) Books and Records; Right to Audit. As to each permission granted under the academic pay-per-use Service, User

shall maintain for at least four full calendar years books and records sufficient for CCC to determine the numbers of copies made by User under such permission. CCC and any representatives it may designate shall have the right to audit such books and records at any time during User's ordinary business hours, upon two days' prior notice. If any such audit shall determine that User shall have underpaid for, or underreported, any photocopies sold or by three percent (3%) or more, then User shall bear all the costs of any such audit; otherwise, CCC shall bear the costs of any such audit. Any amount determined by such audit to have been underpaid by User shall immediately be paid to CCC by User, together with interest thereon at the rate of 10% per annum from the date such amount was originally due. The provisions of this paragraph shall survive the termination of this License for any reason.

b) *Digital Pay-Per-Uses of Academic Course Content and Materials (e-coursepacks, electronic reserves, learning management systems, academic institution intranets).* For uses in e-coursepacks, posts in electronic reserves, posts in learning management systems, or posts on academic institution intranets, the following additional terms apply:

i) The pay-per-uses subject to this Section 14(b) include:

A) Posting e-reserves, course management systems, e-coursepacks for text-based content, which grants authorizations to import requested material in electronic format, and allows electronic access to this material to members of a designated college or university class, under the direction of an instructor designated by the college or university, accessible only under appropriate electronic controls (e.g., password);

B) Posting e-reserves, course management systems, e-coursepacks for material consisting of photographs or other still images not embedded in text, which grants not only the authorizations described in Section 14(b)(i)(A) above, but also the following authorization: to include the requested material in course materials for use consistent with Section 14(b)(i)(A) above, including any necessary resizing, reformatting or modification of the resolution of such requested material (provided that such modification does not alter the underlying editorial content or meaning of the requested material, and provided that the resulting modified content is used solely within the scope of, and in a manner consistent with, the particular authorization described in the Order Confirmation and the Terms), but not including any other form of manipulation, alteration or editing of the requested material;

C) Posting e-reserves, course management systems, e-coursepacks or other academic distribution for audiovisual content, which grants not only the authorizations described in Section 14(b)(i)(A) above, but also the following authorizations: (i) to include the requested material in course materials for use consistent with Section 14(b)(i)(A) above; (ii) to display and perform the requested material to such members of such class in the physical classroom or remotely by means of streaming media or other video formats; and (iii) to "clip" or reformat the requested material for purposes of time or content management or ease of delivery, provided that such “clipping” or reformatting does not alter the underlying editorial content or meaning of the requested material and that the resulting material is used solely within the scope of, and in a manner consistent with, the particular authorization described in the Order Confirmation and the Terms. Unless expressly set forth in the relevant Order Conformation, the License does not authorize any other form of manipulation, alteration or editing of the requested material.

ii) Unless expressly set forth in the relevant Order Confirmation, no License granted shall in any way: (i) include any right by User to create a substantively non-identical copy of the Work or to edit or in any other way modify the Work (except by means of deleting material immediately preceding or following the entire portion of the Work copied or, in the case of Works subject to Sections 14(b)(1)(B) or (C) above, as described in such Sections) (ii) permit "publishing ventures" where any particular course materials would be systematically marketed at multiple institutions.

iii) Subject to any further limitations determined in the Rightsholder Terms (and notwithstanding any apparent contradiction in the Order Confirmation arising from data provided by User), any use authorized under the electronic course content pay-per-use service is limited as follows:

A) any License granted shall apply to only one class (bearing a unique identifier as assigned by the institution, and thereby including all sections or other subparts of the class) at one institution;

B) use is limited to not more than 25% of the text of a book or of the items in a published collection of essays, poems or articles;

C) use is limited to not more than the greater of (a) 25% of the text of an issue of a journal or other periodical or (b) two articles from such an issue;

D) no User may sell or distribute any particular materials, whether photocopied or electronic, at more than one institution of learning;

E) electronic access to material which is the subject of an electronic-use permission must be limited by means of electronic password, student identification or other control permitting access solely to students and instructors in the class;

F) User must ensure (through use of an electronic cover page or other appropriate means) that any person, upon gaining electronic access to the material, which is the subject of a permission, shall see:

- a proper copyright notice, identifying the Rightsholder in whose name CCC has granted permission,
- a statement to the effect that such copy was made pursuant to permission,
- a statement identifying the class to which the material applies and notifying the reader that the material has been made available electronically solely for use in the class, and
- a statement to the effect that the material may not be further distributed to any person outside the class, whether by copying or by transmission and whether electronically or in paper form, and User must also ensure that such cover page or other means will print out in the event that the person accessing the material chooses to print out the material or any part thereof.

G) any permission granted shall expire at the end of the class and, absent some other form of authorization, User is thereupon required to delete the applicable material from any electronic storage or to block electronic access to the applicable material.

iv) Uses of separate portions of a Work, even if they are to be included in the same course material or the same university or college class, require separate permissions under the electronic course content pay-per-use Service. Unless otherwise provided in the Order Confirmation, any grant of rights to User is limited to use completed no later than the end of the academic term (or analogous period) as to which any particular permission is granted.

v) Books and Records; Right to Audit. As to each permission granted under the electronic course content Service, User shall maintain for at least four full calendar years books and records sufficient for CCC to determine the numbers of copies made by User under such permission. CCC and any representatives it may designate shall have the right to audit such books and records at any time during User's ordinary business hours, upon two days' prior notice. If any such audit shall determine that User shall have underpaid for, or underreported, any electronic copies used by three percent (3%) or more, then User shall bear all the costs of any such audit; otherwise, CCC shall bear the costs of any such audit. Any amount determined by such audit to have been underpaid by User shall immediately be paid to CCC by User, together with interest thereon at the rate of 10% per annum from the date such amount was originally due. The provisions of this paragraph shall survive the termination of this license for any reason.

c) *Pay-Per-Use Permissions for Certain Reproductions (Academic photocopies for library reserves and interlibrary loan reporting) (Non-academic internal/external business uses and commercial document delivery).* The License expressly excludes the uses listed in Section (c)(i)-(v) below (which must be subject to separate license from the applicable Rightsholder) for: academic photocopies for library reserves and interlibrary loan reporting; and non-academic internal/external business uses and commercial document delivery.

i) electronic storage of any reproduction (whether in plain-text, PDF, or any other format) other than on a transitory basis;

ii) the input of Works or reproductions thereof into any computerized database;

iii) reproduction of an entire Work (cover-to-cover copying) except where the Work is a single article;

iv) reproduction for resale to anyone other than a specific customer of User;

v) republication in any different form. Please obtain authorizations for these uses through other CCC services or directly from the rightsholder.

Any license granted is further limited as set forth in any restrictions included in the Order Confirmation and/or in these Terms.

d) *Electronic Reproductions in Online Environments (Non-Academic-email, intranet, internet and extranet).* For "electronic reproductions", which generally includes e-mail use (including instant messaging or other electronic transmission to a defined group of recipients) or posting on an intranet, extranet or Intranet site (including any display or performance incidental thereto), the following additional terms apply:

i) Unless otherwise set forth in the Order Confirmation, the License is limited to use completed within 30 days for any use on the Internet, 60 days for any use on an intranet or extranet and one year for any other use, all as measured from the "republication date" as identified in the Order Confirmation, if any, and otherwise from the date of the Order Confirmation.

ii) User may not make or permit any alterations to the Work, unless expressly set forth in the Order Confirmation (after request by User and approval by Rightsholder); provided, however, that a Work consisting of photographs or other still images not embedded in text may, if necessary, be resized, reformatted or have its resolution modified without additional express permission, and a Work consisting of audiovisual content may, if necessary, be "clipped" or reformatted for purposes of time or content management or ease of delivery (provided that any such resizing, reformatting, resolution modification or “clipping” does not alter the underlying editorial content or meaning of the Work used, and that the resulting material is used solely within the scope of, and in a manner consistent with, the particular License described in the Order Confirmation and the Terms.

15) Miscellaneous.

a) User acknowledges that CCC may, from time to time, make changes or additions to the Service or to the Terms, and that Rightsholder may make changes or additions to the Rightsholder Terms. Such updated Terms will replace the prior terms and conditions in the order workflow and shall be effective as to any subsequent Licenses but shall not apply to Licenses already granted and paid for under a prior set of terms.

b) Use of User-related information collected through the Service is governed by CCC's privacy policy, available online at www.copyright.com/about/privacy-policy/.

c) The License is personal to User. Therefore, User may not assign or transfer to any other person (whether a natural person or an organization of any kind) the License or any rights granted thereunder; provided, however, that, where applicable, User may assign such License in its entirety on written notice to CCC in the event of a transfer of all or substantially all of User's rights in any new material which includes the Work(s) licensed under this Service.

d) No amendment or waiver of any Terms is binding unless set forth in writing and signed by the appropriate parties, including, where applicable, the Rightsholder. The Rightsholder and CCC hereby object to any terms contained in any writing prepared by or on behalf of the User or its principals, employees, agents or affiliates and purporting to govern or otherwise relate to the License described in the Order Confirmation, which terms are in any way inconsistent with any Terms set forth in the Order Confirmation, and/or in CCC's standard operating procedures, whether such writing is prepared prior to, simultaneously with or subsequent to the Order Confirmation, and whether such writing appears on a copy of the Order Confirmation or in a separate instrument.

e) The License described in the Order Confirmation shall be governed by and construed under the law of the State of New York, USA, without regard to the principles thereof of conflicts of law. Any case, controversy, suit, action, or proceeding arising out of, in connection with, or related to such License shall be brought, at CCC's sole discretion, in any federal or state court located in the County of New York, State of New York, USA, or in any federal or state court whose geographical jurisdiction covers the location of the Rightsholder set forth in the Order Confirmation. The parties expressly submit to the personal jurisdiction and venue of each such federal or state court.

2021-01-1190 Published 21 Sep 2021

Engine Operation Strategies for the Alternative Diesel Fuel Oxymethylene Ether (OME): Evaluation Based on Injection Rate Analyzer and 0D-/1D-Simulation

Alexander D. Gelner, Rudolf Höß, Andreas Zepf, Martin Härtl, and Georg Wachtmeister
Technical University of Munich (TUM)

Citation: Gelner, A.D., Höß, R., Zepf, A., Härtl, M. et al., "Engine Operation Strategies for the Alternative Diesel Fuel Oxymethylene Ether (OME): Evaluation Based on Injection Rate Analyzer and 0D-/1D-Simulation," SAE Technical Paper 2021-01-1190, 2021, doi:10.4271/2021-01-1190.

Abstract

Polyoxymethylene dimethyl ethers (OME) are promising alternative diesel fuels with a biogenic or electricity-based production, which offer carbon neutral mobility with internal combustion engines. Among other e-fuels, they stand out because of soot-free combustion, which resolves the trade-off between nitrogen oxide (NO_x) and soot emissions. Additionally, long-chain OME have a high ignitability, indicated by a cetane number (CN) greater than 70. This opens up degrees of freedom in the injection strategy and enables simplifications compared to the operation with fossil diesel. This study investigates the hydraulic behavior of two solenoid injectors with different injector geometry for heavy-duty applications on an Injection Rate Analyzer (IRA) in diesel and OME operation. For OME, both injectors show longer injection delays in all injection pressure ranges investigated, increasing with rail pressure. However, these delays are less than two degrees of crank angle in the speed range of heavy-duty engines. Moreover, due to the slower motion of the needle, closing lasts longer in OME operation. The maximum mass flow rate is higher than in diesel operation. A purpose-built 0D-/1D-simulation model of a single-cylinder research engine in OME operation allows an evaluation of different injection strategies: A full-factorial simulation of several operating points shows that the high ignitability of OME enables the omission of pilot injection without disadvantages in NO_x emission or fuel consumption. Furthermore, the maximum pressure gradient of combustion remains approximately the same with and without pilot injection. Therefore, this measure does not provide advantages in acoustics in OME operation. This effect is also due to the lower energy flow gradient, caused by the decreased lower heating value, which reduces the so-called premixed-peak. The results indicate that for a Pareto-optimal operation with OME regarding NO_x emission and fuel consumption around a relative air-fuel ratio of 1.2, high rail pressures are necessary with the EGR rate and the start of injection serving as Pareto control parameters for moving on the Pareto front.

Introduction

The aim of the Paris Agreement, to restrict global warming [1], requires efforts to reduce greenhouse gases, especially carbon dioxide (CO_2) [2]. Besides electrification, synthetic fuels, carbon neutrally produced with renewable power and CO_2 (so-called e-fuels) serve as a promising bridge technology and help to reduce the carbon footprint of internal combustion engines. Moreover, they enable the storage and distribution of the renewable energies such as solar and wind energy, which fluctuate locally and temporally [3]. Long-chain polyoxymethylene dimethyl ethers (OME) as a highly oxygenated fuel are promising candidates for the substitution of fossil diesel fuel [4], as they offer the possibility of carbon neutral production [5] and of a soot-free combustion [6, 7, 8, 9, 10]. Therefore, OME fuel supports both climate change mitigation and air pollution control efforts. With physico-chemical properties similar to fossil diesel and an excellent ignitability [11, 12], which exceeds the requirements of the standard EN 590 for a cetane number (CN) greater than 51 [13], OME is very suitable for a combustion process with compression ignition. The lack of intermolecular C-C bonds results in the absence of soot precursors such as polycyclic aromatic hydrocarbons [14], which suppresses soot formation. This resolves the typical trade-off between soot and nitrogen oxide (NO_x) emissions in diesel engines [15]. For this reason, OME fuel shows a high compatibility with exhaust gas recirculation (EGR) for NO_x reduction, which even allows a combustion process under stoichiometric conditions [16, 17, 18] and enables operation in combination with a three-way-catalyst [19]. However, Härtl et al. discovered an increasing emission of methane (CH_4) and unburned fuel fragments such as formaldehyde (CH_2O) on a single-cylinder

research engine during the use of dimethoxymethane, abbreviated as OME_1, when the air-fuel ratio λ falls below 1.1 [17]. They assumed long-chain OME to produce lower methane emissions, as the ratio of oxygen to hydrogen increases compared to short-chain OME such as dimethoxymethane and dimethyl ether (DME). Pélerin et al. tested this hypothesis on the same single-cylinder engine and compared OME_1 to a mix of OME_{3-6}, but did not confirm this theory. The observed CH_4 emissions below a λ of 1.1 appeared in the same range for both investigated fuels [18]. Therefore, they suggested avoiding operation with $\lambda < 1.1$, because the diesel oxidation catalyst (DOC) used did not reduce CH_4 emission sufficiently.

The results in that study and in [20] highlight the potential of OME for simplifications of the injection system, because they demonstrated NO_x reduction by decreasing rail pressure without increasing particulate emission and suggest operation without pilot injection because of the higher CN. However, the reduction of rail pressure in OME operation requires injectors with a higher nozzle flow rate, in order to compensate the lower heating value of OME compared to fossil diesel. The higher nozzle flow rate is necessary to avoid long and inefficient combustion durations [21]. Li et al. investigated the effect of OME on the injection behavior of a diesel solenoid injector in an optical injection chamber [22]. They showed that the tip penetration, the spray cone angle and the Sauter mean diameter were smaller in OME operation than in diesel operation with the same hole diameter. However, these effects did not compensate the increasing tip penetration because of the necessity of increasing the nozzle flow rate for OME injection by increasing hole diameters. Honecker et al. confirmed the shorter liquid penetration length (LPL) of OME compared to diesel [23]. Pöllmann et al. investigated the effects of pilot injection, rail pressure and boost pressure on different nozzle geometries in OME operation on an optically accessible research engine [24]. Peter et al. provided information about the differences in the hydraulic behavior of injectors using fossil diesel fuel and OME. They assume needle movement to be slower in OME operation, due to the higher density of the fuel [25]. Furthermore, their results indicate differences due to the various sizes of the injectors, showing reverse effects on the mass flow rates with passenger car and heavy-duty engine injectors. Röll et al. judged the differences in the injection delay and injection rate to be negligible for the usage of OME as pilot fuel and therefore propose operation without changing the injector setting [26]. However, since Barro et al. suggest an increase in the nozzle flow rate in order to compensate the lower-level heating value of OME compared to fossil diesel during operation as the main fuel [21], the focus on the injection behavior resulting from this measure becomes important. Therefore, this study is an investigation of the hydraulic behavior with an IRA according to the Bosch principle [27] and compares the injection delay and the injection rate of two solenoid injectors for heavy-duty engines operated with an OME_{3-5} mix and a fossil diesel fuel. Further, a 0D-/1D-simulation of the single-cylinder research engine used in [17,18] clarifies the potential for omitting pilot injection in OME operation and shows a Pareto-optimal injection strategy for lowest NO_x emissions and lowest fuel consumption.

Tested Fuels

Polyoxymethylene dimethyl ethers are oligomers with the structure $CH_3\text{-}O\text{-}(CH_2O)_n\text{-}CH_3$. The fuel used for the experiments in this study contains various OME_n with major percentages of n = 3 - 6 (OME_3: 47 %, OME_4: 29 %, OME_5: 17 %, OME_6: 6 %) and 300 mg/kg each of butylated hydroxytoluene and a flow improver as additives. In this work, the abbreviation OME refers to this explicit mixture, which also fulfills the standard DIN SPEC 51699 [28]. Diesel describes fossil fuel according to the EN 590 standard with a maximum content of 7 % (v/v) fatty acid methyl esters (FAME) [13]. Table 1 shows the properties of the investigated fuels. ASG Analytik-Service AG provided the OME fuel used and determined the values of the physical properties. The appendix contains the respective standard of the measurement method used for providing the substance value. Values for diesel come from the fuel EN 590 standard, unless indicated otherwise. The oxygen content of OME is around 46 %, which reduces the lower heating value (LHV) of the fuel to one about 2.2 times lower compared to fossil diesel. The higher density of OME compensates for this partially, resulting in a volumetric diesel equivalent ratio of

$$\frac{LHV_{Diesel}}{LHV_{OME}} \cdot \frac{\rho_{Diesel}}{\rho_{OME}} \cong 1.7 \tag{1}$$

The flash point of the investigated OME mixture exceeds the requirement of the EN 590 standard, which allows for storage and distribution systems similar to those for fossil diesel. Since there is no standardization of the boiling range, the values for diesel are from Lautenschütz et al. [11], where the characteristic values of diesel fuel according to EN 590 were determined. The calculation of the volumetric equivalent ratio also uses the LHV of diesel from this publication.

TABLE 1 Properties of the investigated fuels. ASG Analytik-Service AG determined the values for OME; the values for diesel are from Lautenschütz et al. [11] unless specified in the standard EN 590 [13]. The gravimetric oxygen content of diesel was calculated according to the values from Hoekman et al. [31] with the assumption that the FAME proportion is made of oleic acid.

	OME	Diesel (EN 590)
Cetane number	70	≥ 51
Diesel equivalent in m^3/m^3	1.7	1
Oxygen content in % (w/w)	46	0 - 0.8[31] with max. 7 % (v/v) FAME
Lower heating value in MJ/kg	19.2	42.6[11]
Density (15 °C at 1 bar) in kg/dm^3	1067	820 - 845
Boiling range at 1 bar in °C	153 - 260	170 - 390[11]
Flash point at 1 bar in °C	68	> 55.0
Kinematic viscosity in mm^2/s	1.183	2.0 - 4.5
Lubricity - HFRR at 60 °C in µm	435	≤ 460

FIGURE 1 Measured and calculated physical properties of the OME mix used. Left side: liquid phase. Right side: vapor phase. μ describes dynamic viscosity; κ, thermal conductivity; and c_p, specific heat capacity at constant pressure.

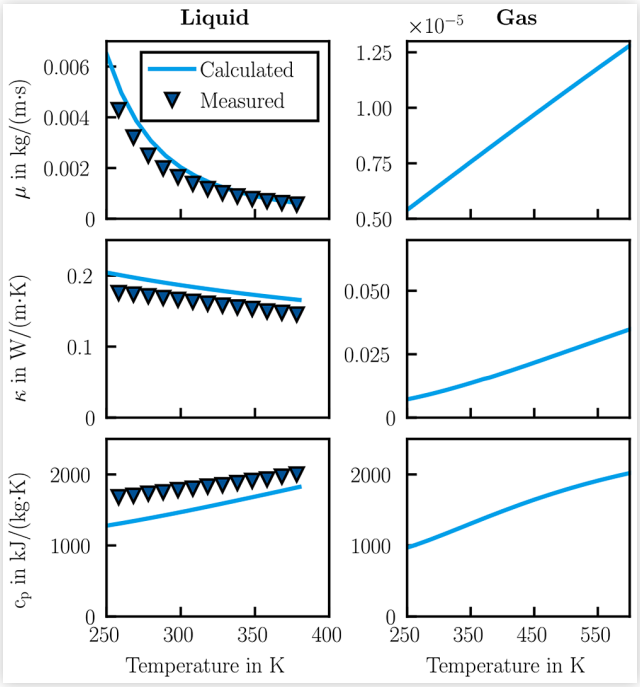

The lubricity of OME surpasses the requirement of the standard, while the kinematic viscosity is lower than the interval specified in the standard.

The creation of a fuel object in the simulation environment used in this work, GT SUITE, which reflects the physical properties of the used OME fuel, requires additional values, which the standard DIN SPEC 51699 does not indicate. Therefore, a calculation according to Burger [29, 30] provides the necessary substance data. In this calculation, the proportions of the respective OME_n in the mixture are normalized with the assumption that the OME mix contains only OME_n. In order to validate the models used for substance data calculation, measurements of the substance values in the liquid phase of the fuel provide supporting points. The appendix shows the respective standard of the measurement method for providing the substance value used by ASG Analytik-Service AG. Figure 1 contains the calculated substance values of the used OME mix in the liquid and the gas phase, as well as measured values of the liquid phase.

Methodology

Injection Rate Analyzer (IRA)

An IRA enables the determination of the injected fuel mass flow rates of an injector, using several approaches such as Coriolis Flow measurement [32] or signal processing of pressure sensors [27]. In this work, the experiments to measure

FIGURE 2 Schematic of the Injection Rate Analyzer, according to Schuckert [33], using the technical principle of Bosch [27].

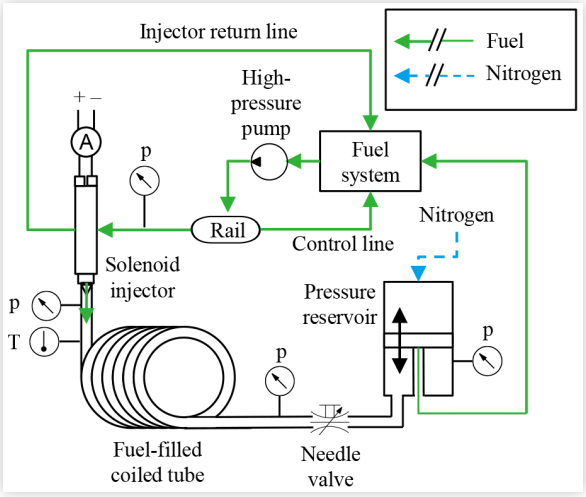

the injection rate were performed on a purpose-built IRA [33] similar to the concept published in [34] and according to the technical principle first developed by Bosch [27]. Figure 2 shows a schematic of the experimental IRA setup.

A fuel system with a commercial high-pressure pump provides the injection pressure for the injector via a common rail. A piezo-resistive pressure sensor (Kistler Type 4067A3000) allows high-frequency measurement of fuel pressure. The solenoid injector discharges into a fuel-filled coiled tube, with a pressure measured close to the injection point by a piezo-electric Kistler Type 601A pressure sensor and a temperature measured with a resistance thermometer (WIKA Type TR33). This generates a pressure wave, which propagates with the speed of sound in the pipe. This hydraulic shock has a linear relation to the injected fuel mass flow rate. Another pressure sensor (also Kistler Type 4065A) enables the calculation of the prevailing speed of sound inside the pipe, in combination with the temperature value of the resistance thermometer at the beginning of the pipe. A piston accumulator, filled with nitrogen, serves as a pressure reservoir. The adjusted nitrogen pressure closes the fuel return line with the piston membrane and therefore generates a backpressure in the measuring pipe, verifiable by a static pressure sensor (WIKA Type S-10). This allows a representation of the pressure inside the combustion chamber of a diesel engine. The needle valve simulates an open pipe end in order to avoid reflection waves in the liquid. The cross-section opening is adjusted depending on injection frequency, and therefore depending on simulated engine speed. The appendix contains a detailed list of the sensors used and their respective accuracies.

The fuel injection process was investigated on two different solenoid common rail injectors for heavy-duty applications, manufactured by Bosch. Table 2 displays the technical data of these injectors. Injector 1 represents the used reference of a diesel application, while Injector 2 has a larger flow rate in order to compensate the difference in lower heating value of OME. However, the investigation is based on both injectors

TABLE 2 Technical data of the used injectors.

	Injector 1	Injector 2
Injector body	Bosch CRIN3	Bosch CRIN2
Number of nozzle holes	10	8
Layout of nozzle holes	one-row	two-row (zig-zag)
Nozzle hole diameter in µm	210	335
Hydraulic nozzle flow rate in cm^3 / 30 s at 100 bar	1400	2200

with both fuels in order to compare the hydraulic behavior during the injection process.

The injector current of the IRA measurements corresponds to the current during operation on the engine test bench: The current of the boost phase is 25 A at 48 V for 110 µs, while the current of the hold phase is 15 A at 24 V. The set backpressure in the pressure reservoir is 50 bar. The pressure sensors' sampling rate is 250 kHz. The evaluation logic averages 50 consecutive injection events after post-processing by a Butterworth filter. A multiple gravimetric control measurement accomplished by determining the injected fuel mass during a period of five minutes using a measuring cup and a scale enables additional correction of the injection rates. This is necessary because the IRA may not map the exact flow rates in absolute values, but only follow the shape of the injection process [35]. For these test runs, the fuel return line of the pressure reservoir runs into the cup instead of into back to the fuel system. All test cycles with the IRA ran without applied backpressure in the injector return line.

Test Engine

The single-cylinder research engine used derives from a MAN D2066 heavy-duty six-cylinder diesel engine. Except for the seals in contact with the fuel, the engine components and test bench periphery are not specially adapted to OME operation. Table 3 displays the attributes of the test engine and Figure 3 depicts a scheme of the test bench setup.

An external compressor screw provides boost pressure in the test bench air supply. The compressed air passes through an air filter and refrigeration dryer. An Aerzen ZE 039.0 rotary displacement meter determines the volumetric airflow upstream of the plenum. An Ahlborn FHAD 46-C7 humidity

TABLE 3 Attributes of the single-cylinder research engine.

Number of cylinders	1
Displaced volume	1753 cm^3
Stroke	120 mm
Bore	155 mm
Compression ratio	17:1
Number of valves per cylinder	4 (2 inlet / 2 exhaust)
Charge	External via compressor
Exhaust gas recirculation	High-pressure & cooled
Injection system	Common Rail (max. 3000 bar)

FIGURE 3 Test bench schematic of the single-cylinder research engine.

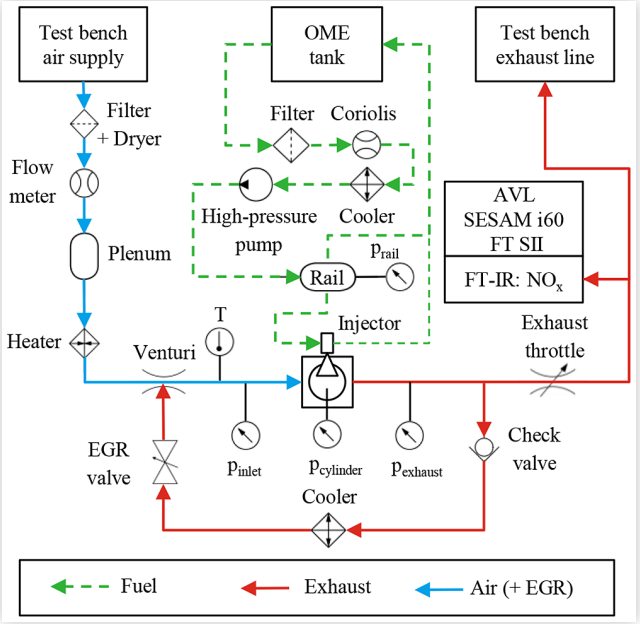

sensor enables the calculation of the gravimetric air flow rate. A heater connected downstream heats the air depending on the set EGR rate, so the intake temperature of the gas is at a constant 40 °C. A Type K thermocouple downstream of the venturi mixing point for EGR enables this temperature conditioning. The test engine has a pressure indication system with a Kistler Type 4045A10 piezo-resistive pressure sensor for high-frequency measurement of the intake pressure, a Kistler Type 7061B piezo-electric sensor for measurement of cylinder pressure and a Kistler Type 4045A10 piezo-resistive sensor for measurement of exhaust pressure. Kistler Type 5011 and Kistler Type 5025 transducers convert the signals from the pressure sensors. An ASM POSIROT PMIS4 magneto-resistive encoder enables the accurate allocation of these pressure values to crank angle with a resolution of 0.1°. The exhaust gas flows through a variable exhaust throttle, in order to simulate the backpressure of a turbocharger. The cross-section depends on engine behavior and is set to the specific backpressure, which results in a theoretical turbocharger efficiency of 0.6. Upstream of the throttle, a check valve designed as a flutter valve, provides exhaust gas recirculation at an adjustable rate by an EGR valve downstream of an EGR cooler. Downstream of the exhaust throttle, an AVL SESAM i60 FT SII Fourier-transform infrared-spectrometer (FT-IR) determines the NO_x concentration in the exhaust gas. The fuel system on the test bench includes a fuel filter and an Emerson CMF010M Coriolis flow meter for fuel consumption indication. A water-rinsed cooler ensures a constant fuel temperature of 15 °C upstream of the Bosch CP3 high-pressure pump. Similar to the IRA, the injection system is a common rail system equipped with a Kistler Type 4067E3000 piezo-resistive sensor for the determination of the rail pressure. The appendix contains a detailed list of the sensors used and their respective accuracies.

0D-/1D-Simulation Model

The single-cylinder research engine is modeled in the GT SUITE 2019 simulation environment from Gamma Technologies, LLC. While the fuel object is created using the measured values of the physical properties in the liquid phase, the gas phase object relies on the calculations with the empirical models from [29, 30], both displayed in Figure 1. According to the respective manual, a polynomial formed over the course of the specific heat capacity over temperature provides the needed values for enthalpy. The thermal conductivity and dynamic viscosity values, the latter adapted across density, go directly into the fuel object. For density, a linear polynomial depending on temperature transfers the value to the simulation environment. The parameters of the combustion chamber model derive largely from Table 3. The measurements with the IRA provide the needed injection rates for injector model data entry. Together with curves for intake and cylinder and exhaust pressure on the test engine, a so-called Three Pressure Analysis (TPA) enables the calculation of the heat release and therefore the combustion process. With these values, a calibration of a combustion model becomes possible. The mass flow rates determined for the respective injector at the IRA form a look-up table in the simulation model and replace a modeling of the injector. The incremental steps between the parameters of measured injection rates are 400 bar of rail pressure and 0.4 ms energizing duration with additional support points in between. The injector object in GT SUITE interpolates between these specified injection rates. In this work, the predictive combustion model DI PULSE simulates the combustion process on several operating points. Figure 4 depicts the simulated cylinder pressure (p_{Cyl}) curve of the

FIGURE 4 Comparison of the simulated and measured cylinder pressure curve of the operation point with n = 1200 rpm and IMEP = 13 bar with EGR.

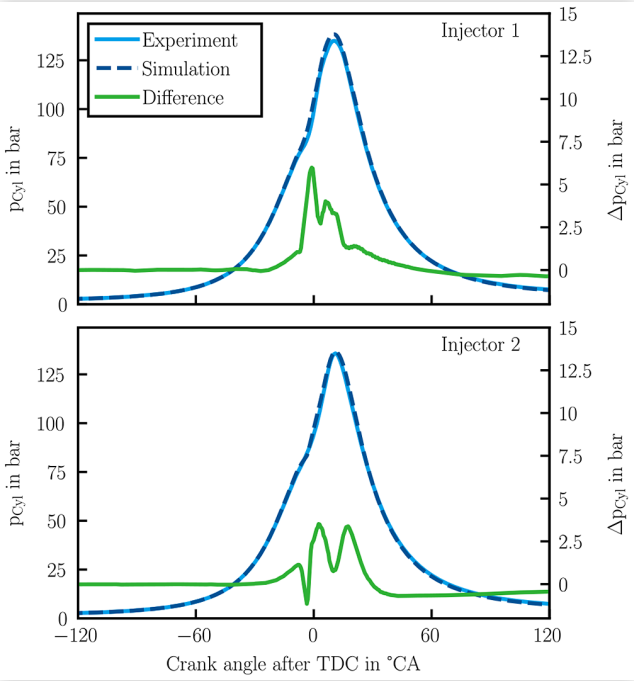

FIGURE 5 Comparison of the simulated and measured heat release rate of the operation point with n = 1200 rpm and IMEP = 13 bar with EGR.

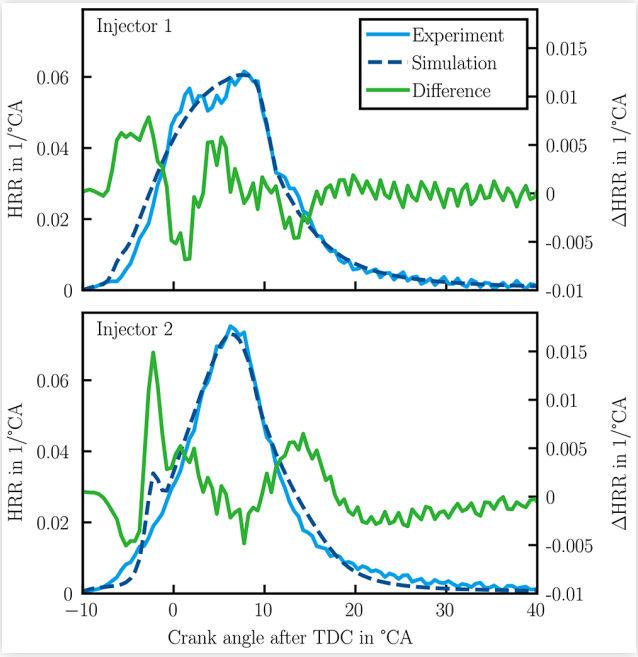

operation point with an engine speed (n) of 1200 revolutions per minute (rpm) and an indicated mean effective pressure (IMEP) of 13 bar, as well as the measured pressure and the deviation between simulation and measurement. The maximum difference in the simulation model of Injector 1 is less than 7 bar, which is located at the start of the combustion, while the maximum difference of Injector 2 is less than 5 bar.

Figure 5 compares the heat release rate (HRR) of this operation point. The maximum deviation for Injector 1 is less than 1 % absolute, about 5 degrees of crank angle (°CA) after the beginning of combustion. For Injector 2, the maximum difference between simulation and measurement is at the same point, but reaches a value of approximately 1.5 %. This is mainly due to the deteriorated vaporization of the fuel in the simulation, because the injector hole diameters of Injector 2 are bigger than the diameters of Injector 1. This leads to a higher ignition delay in the simulation, since the modeled evaporation behavior deviates from the evaporation behavior during the experiment. Figure 6 depicts a characteristic map of the deviation between the simulation and the experiment using the value of the root-mean-square error (RMSE) according to the following formula:

$$RMSE = \frac{\sqrt{\int_{t_0}^{t_f} \left(LHV_{pred} \cdot HRR_{pred} - HRR_{meas} \right)^2 dt}}{t_f - t_0} \qquad (2)$$

The fuel rate multiplier (LHV_{pred}) compensates for the cumulative error of the model calibration using measured cylinder pressure values. This multiplier is automatically determined by GT SUITE. HRR_{pred} describes the simulated HRR by the DI PULSE model, HRR_{meas} is determined using

FIGURE 6 Interpolated characteristic map of the RMSE of the simulation regarding the HRR with EGR and λ = 1.2.

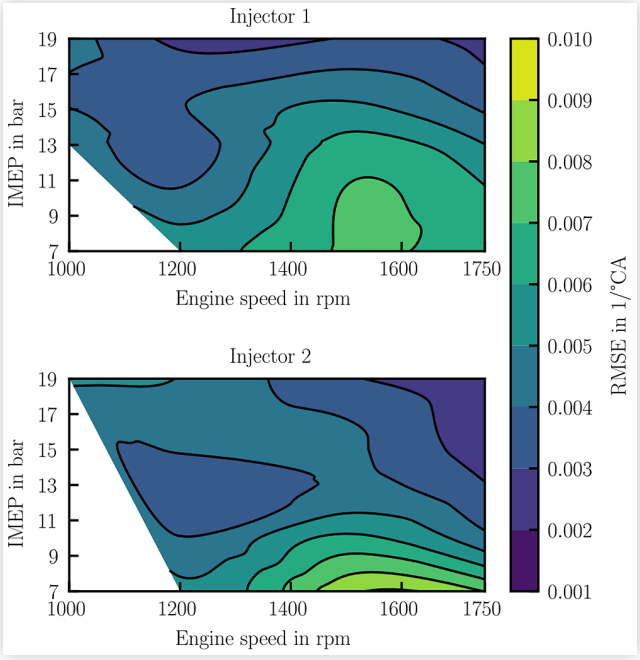

a TPA. t_0 is the beginning of the combustion and t_f is the point, where 90 % of the injected fuel is burned, abbreviated as MFB90.

The values of NO_x emissions, measured by the FT-IR, enable an additional calibration of a NO_x model. With this configuration, a simulation-based evaluation of different injection strategies for an OME engine, considering fuel consumption, NO_x emission and pressure gradient, becomes possible. The modeling of soot emission becomes unnecessary due to the soot-free combustion of OME. As this research involves two different injectors, the 0D-/1D-simulation model is created separately with each injector. Both models fulfill the quality criteria set by Gamma Technologies suggested in the manual. The appendix contains a list of the operating points of the test engine used for calibration and validation of the simulation models.

Figure 7 represents a variation of EGR rate and rail pressure (p_{Rail}) at the operating point with n = 1200 rpm and IMEP = 13 bar and Injector 1. The start of injection (SOI) is set to the respective value leading to a center of combustion at 8 °CA after top dead center (TDC). The values simulated and on the test bench determined by the FT-IR show the same qualitative progression for both variations, indicating an increase in NO_x emissions with an increase in rail pressure, a decrease in NO_x emissions with an increase in EGR rate and vice versa. Therefore, the emission model represents the impact of these operation parameters. Figure 8 shows a detailed comparison of NO_x emissions of the simulation and the experiment for the operating map marked out by the validation points with an overall λ of 1.2. The maximum deviation for Injector 1 is less than 400 parts per million (ppm); for Injector 2 it is 500 ppm. Both injectors show these maximum differences at the high-load point at 1200 rpm and an IMEP of 19 bar. However, the model forms the qualitative tendencies

FIGURE 7 EGR rate and rail pressure variation and comparison between simulated and measured NO_x emissions at the operation point with n = 1200 rpm and IMEP = 13 bar with Injector 1. The SOI is set to enable a center of the combustion at 8 °CA after TDC. The standard deviation for each average is indicated but invisible, because the marker size exceeds the range of the error bars.

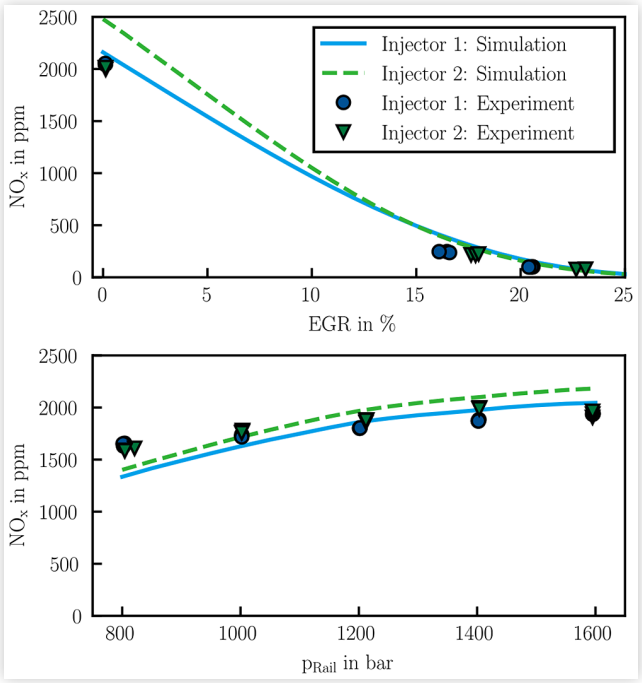

FIGURE 8 Interpolated difference maps for both injectors for the whole validation indicator field, comparing NO_x emissions of simulation and experiment with EGR and λ = 1.2.

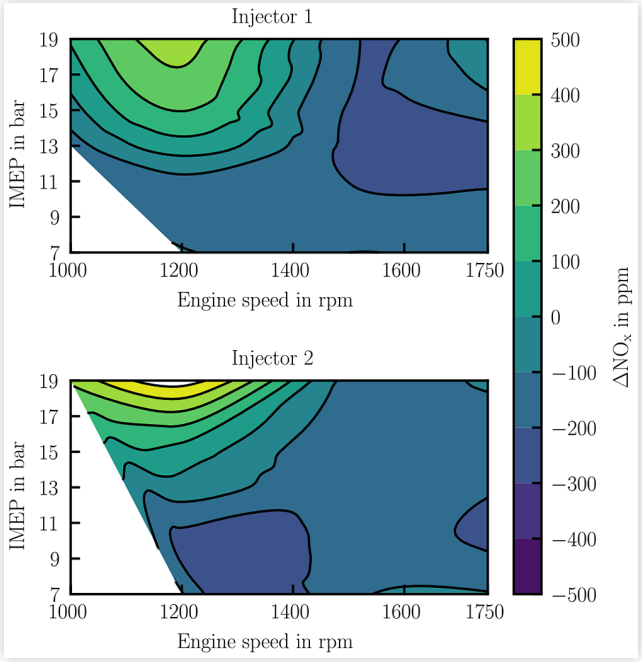

of NO_x emission behavior and is therefore suitable for the evaluation of operation strategies regarding efficiency and NO_x emission.

Results and Discussion

Injection Delay

In order to compare the hydraulic behavior of the solenoid injectors, the first investigation focuses on the injection delay between start of energizing (SOE) of the injector and the start of injection (SOI). Figure 9 displays a scatter plot of these delays for both injectors and both fuels in dependence of the rail pressure. The delay is higher in OME operation, as Peter et al. already showed [25]. The results indicate that there is a dependency between rail pressure and the difference in injection delay, which increases with a higher rail pressure between OME and diesel. Injector 1 shows higher injection delays in general than Injector 2 for both fuels, but the difference between OME and diesel operation is larger for Injector 2. Since the injector bodies come from different product ranges, the differences between them are not primarily due to the different fuel properties. However, the difference between both fuels for each injector is clear. The maximum difference for Injector 2 at 1400 bar of approximately 0.12 ms equals 0.9 °CA at an engine speed of 1200 rpm, while the minimum injection delay of diesel at this point with 0.36 ms results in a delay of 2.7 °CA. This effect must be taken into account during a comparison of the heat release rates of OME and diesel combustion with the same injector and same energizing timing. However, the high CN of OME overcompensates this delay, leading to faster ignition [18, 21]. If the injection delay is mainly due to density, this observation explains the phenomena presented in [36]: in that study, the ignition delay of palm oil biodiesel (PD) is higher than with fossil diesel, although the CN of PD is higher [31]. In order to validate this hypothesis and investigate the influence of the lower viscosity of a fuel on the injection delay, further studies, including hydraulic simulations and a variation of several fuels, are necessary.

FIGURE 9 Injection delays of diesel and OME operation for different rail pressures. Scattering of the average of 50 shots for each duration of energizing. The standard deviation for each average is indicated but invisible, because the marker size exceeds the range of the error bars.

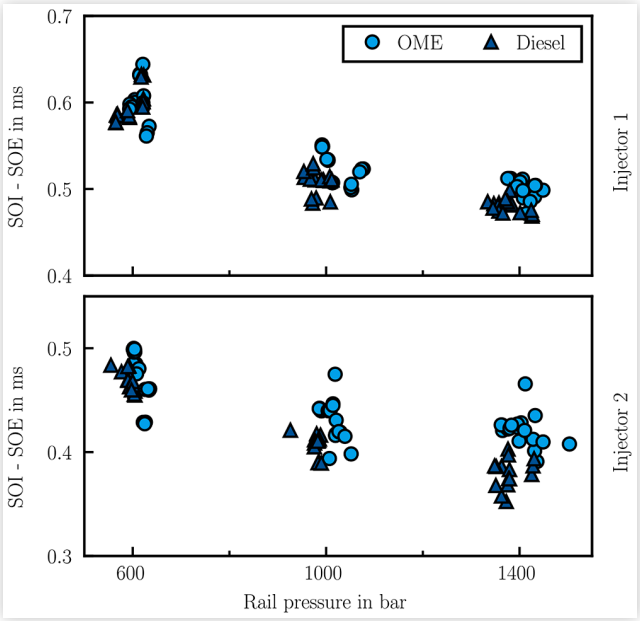

Injection Rate

Figure 10 contrasts the injection rates of both injectors in OME and diesel operation. A measurement point for Injector 2 with diesel at 1400 bar with an energizing duration of 2.5 ms is missing, since this parameter setting exceeds the load range of the single-cylinder engine used. At most of the investigated operation points, the injector closes more slowly in OME operation, leading to longer injection. Peter et al. [25] assume that this is due to the higher density of OME, which slows needle movement. They observed this behavior also during the opening process of the injector. The injection rates in Figure 10 do not show a clear trend in differences in opening movement. However, the results indicate that the effect of slower closing movement increases for longer injection durations and higher rail pressures, because in these cases, the injector is open completely and therefore the needle lift becomes higher. This becomes clearer for Injector 1, which opens faster due to the smaller nozzle flow rate,

FIGURE 10 Comparison of the injection rates in diesel and OME operation. Left side: Injector 1. Right side: Injector 2 (enlarged nozzle flow rate). The lines show the averaged injection rates of 150 shots; the shaded areas indicate the respective standard deviations. Energizing durations are 0.5 ms, 1 ms, 1.6 ms, 2 ms, and 2.5 ms.

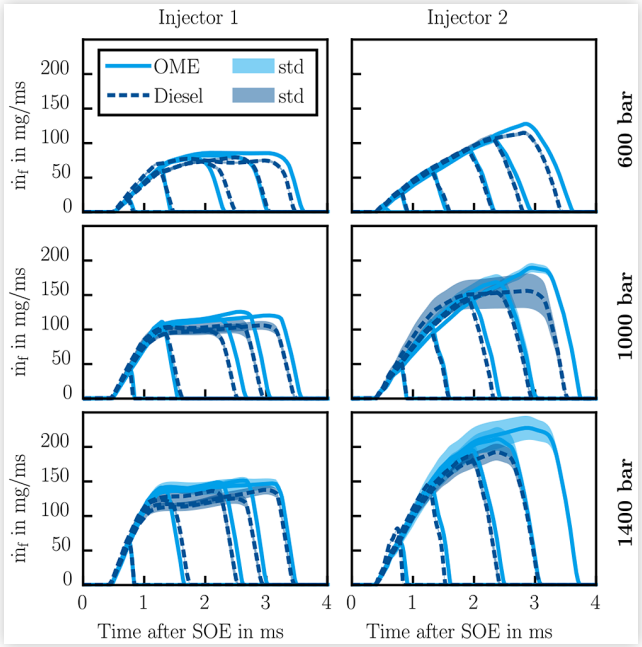

FIGURE 11 Comparison of the energy flow rate ($\dot{E}_f$) for both injectors in diesel and OME operation. The used LHVs derive from Table 1. Left side: Injector 1. Right side: Injector 2 (enlarged nozzle flow rate). The lines show the averaged energy flow rates of 150 shots; the shaded areas indicate the respective standard deviations. Energizing durations are 0.5 ms, 1 ms, 1.6 ms, 2 ms, and 2.5 ms.

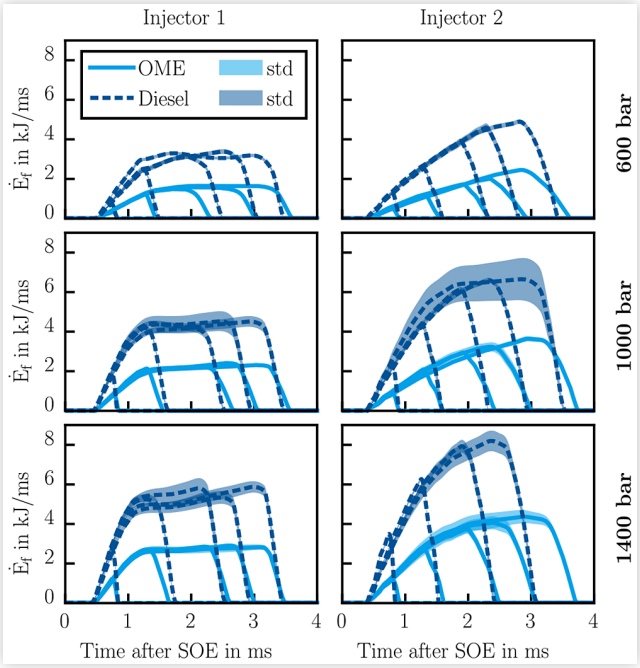

compared to Injector 2. The observations of the slower closing behavior of the injector operated with OME become important when it comes to penetration behavior in the combustion chamber, especially for interactions with the liner. In general, the progression of the injection rates show the same tendency as mentioned in [25]: the maximum mass flow rate is higher in OME operation, if the injector is fully open. This and the slower needle movement during the closing of the injector partially compensates the lower LHV of OME. Nevertheless, OME showed shorter combustion duration in several studies [18, 21, 37] at low-load points. The authors of these studies attributed this to the inner-molecular oxygen content, which increases oxygen availability during late-phase-combustion.

However, in order to avoid long combustion durations at medium- and high-load points as mentioned in [21] and to enable NO_x reduction through a rail pressure decrease as mentioned in [20], the conversion of a diesel engine to an OME engine requires an increase in the nozzle flow rate. Figure 11 clarifies this by a comparison of the energy flow rates derived from the injection rates of Figure 10 with multiplication of the LHVs of Table 1. Although the nozzle flow rate of Injector 2 is larger than the flow rate of Injector 1, it cannot compensate the difference in lower heating value during the same energizing time. Additionally, the gradient of energy flow at the SOI is smaller in OME operation, which is - next to the higher CN resulting in a reduced premixed peak [38] - an explanation for the flatter rise of the heat release curve [18, 21].

FIGURE 12 Mass fractions and heat release rate of OME combustion on the operation point at 1200 rpm and an IMEP of 13 bar.

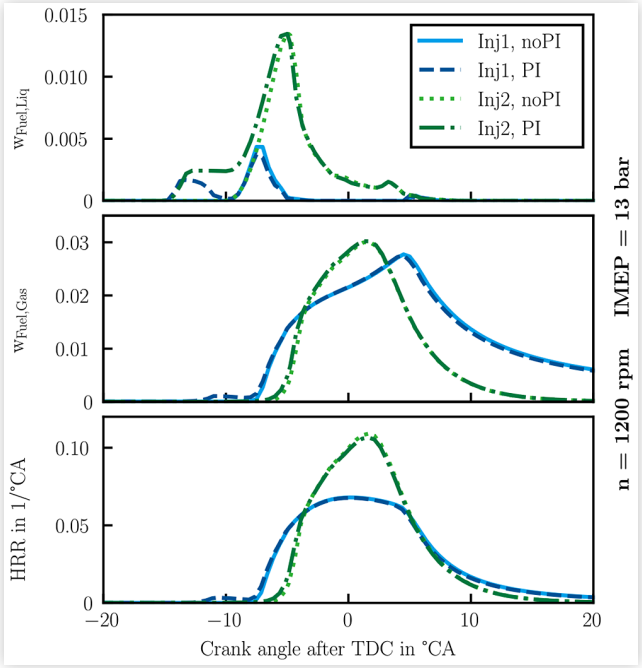

0D-/1D-Simulation of OME Combustion

In order to investigate the effect of pilot injection (PI) and increase in nozzle flow rate on the combustion of OME, a comparison of both parameter settings is necessary. Figure 12 depicts the injected mass fraction of liquid and gas phase of the fuel ($w_{Fuel,Liq}$ and $w_{Fuel,Gas}$) as well as heat release rate (HRR) at the operation point with an engine speed of 1200 rpm and an engine load of 13 bar IMEP. Due to the larger injection hole diameters of Injector 2, the liquid phase fraction of the injected OME is higher compared to Injector 1, and results in a slower fuel vaporization analogous to the behavior in Figure 5. However, the simulation results are based on the estimation of the physical properties of OME and modeling of the droplet decomposition in GT SUITE and may deviate from the exact vaporization behavior inside the combustion chamber. More detailed studies on this topic providing information about the effect of injector geometry on the vaporization of OME, are therefore necessary. Nevertheless, the 0D-/1D-simulation enables a relative comparison of the two injector configurations. The operation parameters are as follows for both injectors: the rail pressure is 1950 bar, the SOI is at 10 °CA before TDC, the EGR rate is 15 % (w/w).

Due to the increase in nozzle flow rate, the heat release rate of the OME combustion with Injector 2 is higher than with Injector 1. The influence of the PI regarding the HRR at this operation point is marginal for both injectors, due to the high CN. This leads to almost identical premixed and diffusive combustion. Although the injection delay of Injector 2 is higher according to the behavior observed in Figure 9, the combustion starts later than with Injector 1. This is due to

FIGURE 13 Pareto-optima and results of the full-factorial variation of rail pressure, SOI and EGR rate for four operation points with the specified engine speed n and the specified indicated mean effective pressure (IMEP).

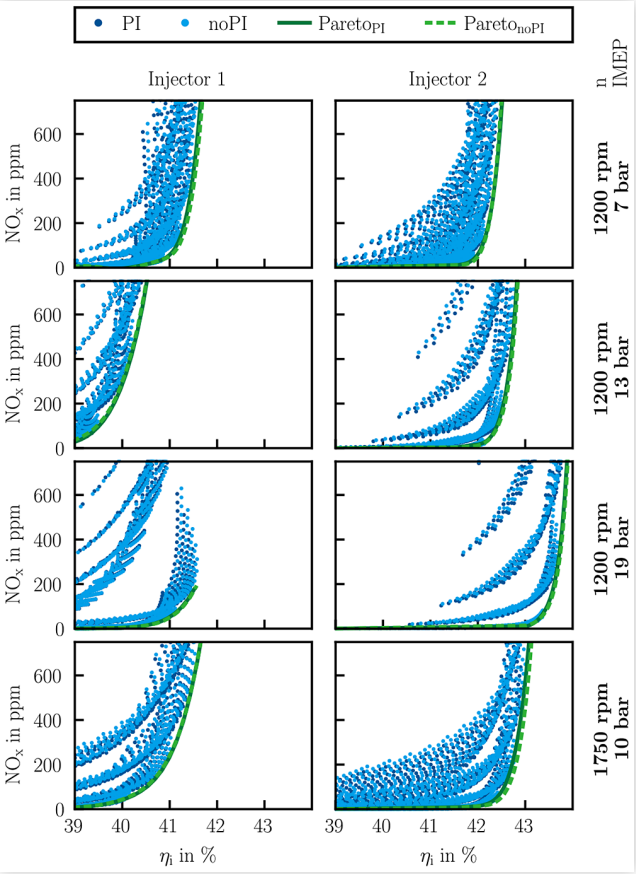

the longer vaporization time. Nevertheless, the combustion duration with Injector 2 is shorter.

A full-factorial simulation of the operation parameters rail pressure, SOI, EGR rate and pilot injection on four operation points reveals the Pareto-optimal settings of these parameters, regarding NO_x emissions and indicated efficiency (η_i). The step sizes are 50 bar of rail pressure, 1 °CA of SOI and 5 % of EGR rate. Figure 13 presents these Pareto fronts with distinction between set PI and no set PI. This comparison enables an evaluation of the effect of PI on NO_x emissions and η_i. The results indicate that this effect is marginal at the observed operation points. With Injector 1 at 1200 rpm and an IMEP of 7 bar, the operation points without PI show a Pareto front at higher efficiencies than the ones with PI for indicated efficiencies higher than 41 %. Injector 2 shows the same tendency at 1750 rpm and an IMEP of 10 bar for η_i higher than 42 %. A consideration of the effect of an omission of the PI on the acoustic behavior due to the maximum pressure gradient results in the following: For every investigated point, the maximum difference is 0.2 bar per °CA, with every maximum pressure gradient smaller than 10 bar per °CA, except for the high load point with 19 bar of IMEP, with maximum pressure gradients smaller than 13 bar per °CA. On this point, combustion reaches the maximum pressure gradient value predominantly during diffusive combustion.

In general, the points on the Pareto optima of Injector 2 have higher efficiency at the same NO_x level than Injector 1. For this reason, the presented results in Figure 12 and Figure 13 confirm the suggestion of Barro et al. [21] to enlarge the nozzle flow rate in OME operation. Moreover, they also confirm the proposal of Pélerin et al. [18] to dispense with pilot injection in order to simplify the injection system.

In order to suggest a Pareto-optimal operation strategy with OME, an investigation of the parameter settings of the points on the Pareto front provides information for a NO_x and η_i optimal operation. Figure 14 depicts varying parameter settings at the operation point with n = 1200 rpm and IMEP = 13 bar with Injector 2. The illustrated Pareto front indicates the Pareto optimal setting values of EGR rate, rail pressure and start of injection. Every point in Figure 14 has a global λ greater than 1.1, which avoids CH_4 formation by considering the limit of λ suggested by Pélerin et al. [18]. The parameter settings show the following tendencies: although a reduction in rail pressure in OME operation results in a decrease of NO_x emissions [20], a Pareto-optimal strategy regarding NO_x emissions and η_i requires higher rail pressures even with the bigger nozzle. The results indicate that a slightly higher rate of EGR compensates the higher NO_x emissions of increased rail pressure at higher efficiency. Since the simulation does not consider the mechanical efficiency of the engine and losses for high-pressure generation, the results have to

FIGURE 14 Selected points for illustration of the effect of parameter settings at the operation point with n = 1200 rpm and IMEP = 13 bar and the respective Pareto front.

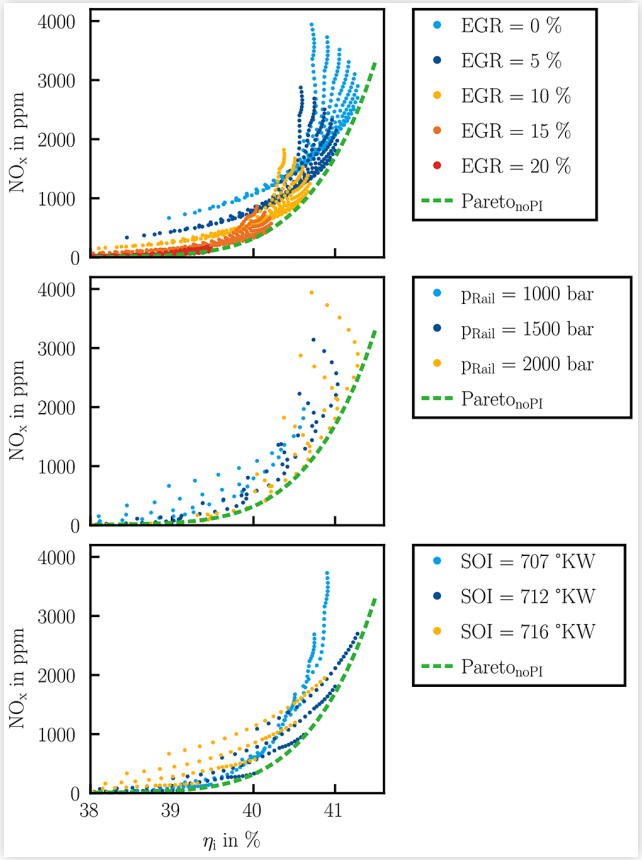

be verified on a test bench using a state-of-the-art heavy-duty engine. However, the simulation results provide an indication of an optimal operation strategy with OME. The results show that the variation of the EGR rate is a suitable control factor for moving on the Pareto front. Higher rail pressures result in a higher efficiency at every EGR rate but with higher NO_x emissions, and vice versa. The SOI additionally shows up as a Pareto-optimal control factor. Nevertheless, the operation strategy depends on the objective of the application. Therefore, these suggestions are not universal for every operation mode of an OME engine.

Conclusions and Outlook

The present work presents an evaluation of different operating strategies for a heavy-duty diesel engine fueled with OME as substitution to fossil diesel based on observations on the IRA and results of 0D-/1D-simulation of a single-cylinder research engine. The investigated effects of the operation parameters rail pressure, start of injection, exhaust gas recirculation rate and the injector configuration regarding nozzle flow rate result in the following conclusions:

- In OME operation, both solenoid injectors show higher injection delays than in diesel operation, increasing with higher rail pressure. This effect counteracts the higher ignitability of the fuel. Nevertheless, in terms of the absolute value of the injection delay in diesel operation, this difference is negligible. This is also due to overcompensation by the higher cetane number, which leads to a faster ignition.
- The observation of the injection rates indicates that the needle of the injector moves more slowly in OME operation and that OME shows higher mass flow rates when the injector is fully open. However, this and a slower closing motion cannot compensate the decreased LHV compared to diesel.

Pilot injection becomes obsolete in OME operation, as the high cetane number and lower energy flow rate due to the oxygen content reduce the premixed combustion peak. The slower motion of the injector needle enhances this effect.

- The impact on the acoustic behavior from the omission of the pilot injection is negligible, with a maximum difference of less than 0.2 bar per °CA of the maximum pressure gradient for all investigated points. Since these observations do not refer to operation under extreme conditions or cold start, further investigations regarding this and varying PI quantities are necessary.
- Increasing the nozzle flow rate enables more efficient operation. This is primarily due to shorter combustion durations. Further studies on the effect of this modification considering fluid mechanical behavior, vaporization in the combustion chamber and the impact on pollutant emissions are necessary. Since incomplete combustion of OME leads to formaldehyde [18, 39], the injector geometry may also influence this aspect.
- In order to operate the OME engine on a Pareto-optimal setting regarding NO_x emissions and efficiency, the EGR rate and the start of injection are the Pareto control parameters. They enable motion on the Pareto front towards higher efficiency at the cost of higher NO_x emissions and vice versa. The Pareto front contains only parameter settings with higher rail pressure, leading to higher efficiency.

These conclusions are based on the results of this work and are therefore limited to stationary operation of the single-cylinder research engine used for it. Further studies are planned in order to confirm their validity regarding operation on a state-of-the-art heavy-duty engine in test cycles, considering cold start and dynamic operation.

Declaration of Competing Interest

The authors declare that they have no known competing financial interests or personal relationship that could have appeared to influence the work reported in this paper.

CRediT authorship contribution statement

Alexander D. Gelner: conceptualization, data curation, formal analysis, investigation, methodology, project administration, validation, visualization, writing - original draft, writing - review & editing

Rudolf Höß: data curation, methodology, software, formal analysis, investigation, software, writing - review & editing

Andreas Zepf: data curation, methodology, software, validation, visualization, writing - review & editing

Martin Härtl: funding acquisition, project administration, supervision, writing - review & editing

Georg Wachtmeister: funding acquisition, resources, project administration, supervision, writing - review & editing

Contact Information

Alexander D. Gelner
ORCID iD: 0000-0001-9628-798X
gelner@lvk.mw.tum.de

Acknowledgments

This study formed part of the "Sub-Zero-Emissions Dieselmotor" project, which was funded by the Bavarian Research Foundation. The project was carried out in collaboration with MAN Truck & Bus SE, VT Vitesco Technologies Emitec GmbH, Chair of Analytical Chemistry of TUM and ASG Analytik-Service AG. Their support is gratefully

acknowledged. The authors also want to thank Ms. Elena Filipovic, B.Sc. and Mr. Paul Hopf, M.Sc., who supported the experiments and evaluation of the IRA during a thesis project and as a student assistant. They also want to thank Mr. Théotime Asselin (ISAE-ENSMA), who supported the experiments of the IRA during his ERASMUS semester at TUM and Mr. Markus Mühlthaler, M.Sc. (TUM) for consultation in this study regarding the IRA.

Definitions/Abbreviations

°CA - Degree of crank angle
CH_4 - Methane
CH_2O - Formaldehyde (IUPAC: Methanal)
CN - Cetane number
CO_2 - Carbon dioxide
c_p - Specific heat capacity at constant pressure
DME - Dimethyl ether
DOC - Diesel oxidation catalyst
$\dot{E}_f$ - Energy flow rate
EGR - Exhaust gas recirculation
FAME - Fatty acid methyl esters
FT-IR - Fourier-transform infrared spectrometer
HFRR - High frequency reciprocating rig
$HRR_{(x)}$ - Heat release rate
(determined by x)
IMEP - Indicated mean effective pressure
IRA - Injection Rate Analyzer
$LHV_{(n)}$ - Lower heating value (of the component n)
LPL - Liquid penetration length
MFB50 / MFB90 - 50 % / 90 % Mass fraction burned
n - Engine speed
NO_x - Nitrogen oxides
$OME_{(n)}$ - Polyoxymethylene dimethyl ethers (of the chain-length n)
p_{Cyl} - Cylinder pressure
PD - Palm oil biodiesel
PI - Pilot injection
ppm - Parts per million
p_{Rail} - Rail pressure
RMSE - Root-mean-square error
rpm - Revolutions per minute
SOE - Start of energizing
SOI - Start of injection
t_0 - Start of the combustion
t_f - Point of MFB90
TDC - Top dead center
TPA - Three pressure analysis
$w_{Fuel,Gas.}$ - Mass fraction of gaseous fuel
$w_{Fuel,Liq}$ - Mass fraction of liquid fuel
η_i - Indicated efficiency
κ - Thermal conductivity
λ - Air-fuel ratio
μ - Dynamic viscosity
$\rho_{(n)}$ - Density (of the component n)

References

1. Horowitz, C.A., "Paris Agreement," *Int. Leg. Mater.* 55, no. 4 (2016): 740-755, doi:10.1017/S0020782900004253.
2. Pachauri, R.K. and Mayer, L. (Eds), *Climate Change 2014: Synthesis Report* (Geneva, Switzerland: Intergovernmental Panel on Climate Change, 2015), ISBN:978-92-9169-143-2
3. König, D.H., Freiberg, M., Dietrich, R.-U., and Wörner, A., "Techno-Economic Study of the Storage of Fluctuating Renewable Energy in Liquid Hydrocarbons," *Fuel* 159 (2015): 289-297, doi:10.1016/j.fuel.2015.06.085.
4. Schemme, S., Samsun, R.C., Peters, R., and Stolten, D., "Power-to-Fuel as a Key to Sustainable Transport Systems - An Analysis of Diesel Fuels Produced from CO 2 and Renewable Electricity," *Fuel* 205 (2017): 198-221, doi:10.1016/j.fuel.2017.05.061.
5. Held, M., Tönges, Y., Pélerin, D., Härtl, M. et al., "On the Energetic Efficiency of Producing Polyoxymethylene Dimethyl Ethers from CO 2 Using Electrical Energy," *Energy Environ. Sci.* 12, no. 3 (2019): 1019-1034, doi:10.1039/c8ee02849d.
6. Pellegrini, L., Marchionna, M., Patrini, R., and Florio, S., "Emission Performance of Neat and Blended Polyoxymethylene Dimethyl Ethers in an Old Light-Duty Diesel Car," in *SAE Technical Paper Series, SAE Technical Paper Series, SAE 2013 World Congress & Exhibition, APR. 16, 2013, SAE International400 Commonwealth Drive*, Warrendale, PA, United States, 2013.
7. Iannuzzi, S.E., Barro, C., Boulouchos, K., and Burger, J., "Combustion Behavior and Soot Formation/Oxidation of Oxygenated Fuels in a Cylindrical Constant Volume Chamber," *Fuel* 167 (2016): 49-59, doi:10.1016/j.fuel.2015.11.060.
8. Barro, C., Parravicini, M., Boulouchos, K., and Liati, A., "Neat Polyoxymethylene Dimethyl Ether in a Diesel Engine; Part 2: Exhaust emission analysis," *Fuel* 234 (2018): 1414-1421, doi:10.1016/j.fuel.2018.07.108.
9. Damyanov, A., Hofmann, P., Geringer, B., Schwaiger, N. et al., "Biogenous Ethers: Production and Operation in a Diesel Engine," *Automot. Engine Technol.* 3, no. 1-2 (2018): 69-82, doi:10.1007/s41104-018-0028-x.
10. Omari, A., Heuser, B., Pischinger, S., and Rüdinger, C., "Potential of Long-Chain Oxymethylene Ether and Oxymethylene Ether-Diesel Blends for Ultra-Low Emission Engines," *Applied Energy* 239 (2019): 1242-1249, doi:10.1016/j.apenergy.2019.02.035.
11. Lautenschütz, L., Oestreich, D., Seidenspinner, P., Arnold, U. et al., "Physico-Chemical Properties and Fuel Characteristics

of Oxymethylene Dialkyl Ethers," *Fuel* 173 (2016): 129-137, doi:10.1016/j.fuel.2016.01.060.

12. Lautenschütz, L., Oestreich, D., Seidenspinner, P., Arnold, U. et al., "Corrigendum to "Physico-Chemical Properties and Fuel Characteristics of Oxymethylene Dialkyl Ethers" [Fuel 173 (2016) 129-137]," *Fuel* 209 (2017): 812, doi:10.1016/j.fuel.2017.07.083.
13. DIN EN 590:2017-10, *Kraftstoffe - Dieselkraftstoff* (Beuth Verlag GmbH)
14. Ogawa, H., Miyamoto, N., and Yagi, M., "Chemical-Kinetic Analysis on PAH Formation Mechanisms of Oxygenated Fuels," in *SAE Technical Paper Series, SAE Technical Paper Series, SAE Powertrain & Fluid Systems Conference & Exhibition, OCT. 27, 2003, SAE International400 Commonwealth Drive*, Warrendale, PA, United States, 2003.
15. Pellegrini, L., Marchionna, M., Patrini, R., Beatrice, C. et al., "Combustion Behaviour and Emission Performance of Neat and Blended Polyoxymethylene Dimethyl Ethers in a Light-Duty Diesel Engine," in *SAE Technical Paper Series, SAE Technical Paper Series, SAE 2012 World Congress & Exhibition, APR. 24, 2012, SAE International400 Commonwealth Drive*, Warrendale, PA, United States, 2012.
16. Ogawa, H., Nabi, N., Minami, M., Miyamoto, N. et al., "Ultra Low Emissions and High Performance Diesel Combustion with a Combination of High EGR, Three-Way Catalyst, and a Highly Oxygenated Fuel, Dimethoxy Methane (DMM)," in *SAE Technical Paper Series, SAE Technical Paper Series, CEC/SAE Spring Fuels & Lubricants Meeting & Exposition, JUN. 19, 2000, SAE International400 Commonwealth Drive*, Warrendale, PA, United States, 2000.
17. Härtl, M., Seidenspinner, P., Jacob, E., and Wachtmeister, G., "Oxygenate Screening on a Heavy-Duty Diesel Engine and Emission Characteristics of Highly Oxygenated Oxymethylene Ether Fuel OME1," *Fuel* 153 (2015): 328-335, doi:10.1016/j.fuel.2015.03.012.
18. Pélerin, D., Gaukel, K., Härtl, M., Jacob, E. et al., "Potentials to Simplify the Engine System Using the Alternative Diesel Fuels Oxymethylene Ether OME1 and OME3−6 on a Heavy-Duty Engine," *Fuel* 259 (2020): 116231, doi:10.1016/j.fuel.2019.116231.
19. Münz, M., Töpfer, D., Mokros, A., and Beidl, C., "Oxygenate Fuel in a Diesel Engine - Is a CI Engine Capable of Lambda 1?" in: Liebl, J. and Beidl, C. (Eds), *Internationaler Motorenkongress 2017, Proceedings*, (Wiesbaden: Springer Fachmedien Wiesbaden, 2017), 457-472, ISBN:978-3-658-17108-7.
20. Pélerin, D., Gaukel, K., Härtl, M., and Wachtmeister, G., "Nitrogen Oxide Reduction Potentials Using Dimethyl Ether and Oxymethylene Ether in a Heavy-Duty Diesel Engine," in *SAE Technical Paper Series, SAE Technical Paper Series, Automotive Technical Papers, JAN. 01, 2020, SAE International400 Commonwealth Drive*, Warrendale, PA, United States, 2020.
21. Barro, C., Parravicini, M., and Boulouchos, K., "Neat Polyoxymethylene Dimethyl Ether in a Diesel Engine; Part 1: Detailed Combustion Analysis," *Fuel* 256 (2019): 115892, doi:10.1016/j.fuel.2019.115892.
22. Li, D., Gao, Y., Liu, S., Ma, Z. et al., "Effect of Polyoxymethylene Dimethyl Ethers Addition on Spray and Atomization Characteristics Using a Common Rail Diesel Injection System," *Fuel* 186 (2016): 235-247, doi:10.1016/j.fuel.2016.08.082.
23. Honecker, C., Neumann, M., Glueck, S., Schoenen, M. et al., "Optical Spray Investigations on OME3-5 in a Constant Volume High Pressure Chamber," in *SAE Technical Paper Series, SAE Technical Paper Series, Conference on Sustainable Mobility, OCT. 14, 2019, SAE International400 Commonwealth Drive*, Warrendale, PA, United States, 2019.
24. Pöllmann, S., Härtl, M., and Wachtmeister, G., "Injection Process of the Synthetic Fuel Oxymethylene Ether: Optical Analysis in a Heavy-Duty Engine," in *SAE Technical Paper Series, SAE Technical Paper Series, SAE Powertrains, Fuels & Lubricants Meeting, SEP. 22, 2020, SAE International400 Commonwealth Drive*, Warrendale, PA, United States, 2020.
25. Peter, A., Siewert, B., Riess, S., Strauss, L. et al., "Mixture Formation Analysis of Polyoxymethylenether Injection," *Atomiz Spr* 30, no. 11 (2020): 843-859, doi:10.1615/AtomizSpr.2020035250.
26. Röll, A., Luo, F., O'Connell, N., Lechner, R. et al., "Hydraulic Stability of Micro Injections Using a Two-Layered 8-Hole Solenoid Injector with Pode," *Fuel* 297 (2021): 120748, doi:10.1016/j.fuel.2021.120748.
27. Bosch, W., "The Fuel Rate Indicator: A New Measuring Instrument For Display of the Characteristics of Individual Injection," in *SAE Technical Paper Series, SAE Technical Paper Series, National Powerplant and Transportation Meetings, OCT. 17, 1966, SAE International400 Commonwealth Drive*, Warrendale, PA, United States, 1966.
28. DIN/TS 51699, "Fuels - Polyoxymethylene Dimethyl Ether (OME),"
29. Burger, J., Siegert, M., Ströfer, E., and Hasse, H., "Poly(oxymethylene) Dimethyl Ethers as Components of Tailored Diesel Fuel: Properties, Synthesis and Purification Concepts," *Fuel* 89, no. 11 (2010): 3315-3319, doi:10.1016/j.fuel.2010.05.014.
30. Burger, J., *A Novel Process for the Production of Diesel Fuel Additives by Hierarchical Design, Zugl.: Kaiserslautern, Techn. Univ., Diss., 2012, Scientific report series / Laboratory of Engineering Thermodynamics*. Vol. 3 (Kaiserslautern: Techn. Univ, 2012), ISBN:978-3-944433-02-8
31. Hoekman, S.K., Broch, A., Robbins, C., Ceniceros, E. et al., "Review of Biodiesel Composition, Properties, and Specifications," *Renewable and Sustainable Energy Reviews* 16, no. 1 (2012): 143-169, doi:10.1016/j.rser.2011.07.143.
32. Leach, F., Davy, M., Henry, M., Tombs, M. et al., "A New Method for Measuring Fuel Flow in an Individual Injection in Real Time," *SAE Int. J. Engines* 11, no. 6 (2018): 687-695. https://doi.org/10.4271/2018-01-0285.
33. Schuckert, S., "A Purpose-Built Injection Rate Analyzer according to the Bosch Principle," interview by Gelner, A.D., April 4, 2021.
34. Schuckert, S. and Wachtmeister, G., "Characteristics of Control Piston Motion and Pressure Inside of a Common Rail Diesel Injector," in *Proceedings ILASS-Europe 2017. 28th Conference on Liquid Atomization and Spray Systems, ILASS2017 - 28th European Conference on Liquid Atomization and Spray Systems*, Universitat Politècnica València, València, 2017, ISBN 9788490485804.

35. Vass, S. and Németh, H., "Sensitivity Analysis of Instantaneous Fuel Injection Rate Determination for Detailed Diesel Combustion Models," *Per. Pol. Transp. Eng.* 41, no. 1 (2013): 77, doi:10.3311/PPtr.7106.

36. Kim, H.Y., Ge, J.C., and Choi, N.J., "Effects of Fuel Injection Pressure on Combustion and Emission Characteristics under Low Speed Conditions in a Diesel Engine Fueled with Palm Oil Biodiesel," *Energies* 12, no. 17 (2019): 3264, doi:10.3390/en12173264.

37. Pastor, J.V., García, A., Micó, C., and Lewiski, F., "An Optical Investigation of Fischer-Tropsch diesel and Oxymethylene Dimethyl Ether Impact on Combustion Process for CI Engines," *Applied Energy* 260 (2020): 114238, doi:10.1016/j.apenergy.2019.114238.

38. Szybist, J.P. and Bunting, B.G., "Cetane Number and Engine Speed Effects on Diesel HCCI Performance and Emissions," in *SAE Technical Paper Series, SAE Technical Paper Series, Powertrain & Fluid Systems Conference & Exhibition, OCT. 24, 2005, SAE International400 Commonwealth Drive*, Warrendale, PA, United States, 2005.

39. Gelner, A.D., Pastoetter, C., Beck, H.A., Härtl, M. et al., "Fuel Dosing on a Diesel Oxidation Catalyst for After-Treatment System Heating on a Heavy-Duty Engine Powered by Polyoxymethylene Dimethyl Ethers," in *SAE Technical Paper Series, SAE Technical Paper Series, SAE Powertrains, Fuels & Lubricants Meeting, SEP. 22, 2020, SAE International400 Commonwealth Drive*, Warrendale, PA, United States, 2020.

Appendix

TABLE 4 Determined values of OME and the respective measurement method

	Value	Method
Cetane number	74.1	IP 617
Oxygen content in % (w/w)	46.3	DIN 51732 mod.
Sulfur content in mg/kg	< 5	DIN EN ISO 20884
Lower heating value in MJ/kg	19.2	DIN 51900-2 mod.
Density (15 °C at 1 bar) in kg/dm^3	1067.0	DIN EN ISO 12185
Boiling range at 1 bar in °C	153,4 - 260,2	DIN EN ISO 3405
Flash point at 1 bar in °C	68.0	DIN EN ISO 2719
Cold Filter Plugging Point in °C	-23	DIN EN 116
Cloud Point in °C	-21	DIN EN 23015
Kinematic viscosity at 40 °C in mm^2/s	1.183	DIN EN ISO 3104
Lubricity - HFRR at 60 °C in µm	350	DIN EN ISO 12156-1

TABLE 5 Measurement methods of additionally determined values of OME for creation of a fuel object in the simulation environment.

Fuel property	Method
Density at 1 bar	DIN EN ISO 12185:1997
Kinematic viscosity at 1 bar	DIN EN 16896:2017
Thermal conductivity at 1 bar	ASTM D 2717:2009
Specific heat capacity at 1 bar	ASG 2023

TABLE 6 Measurement equipment of the IRA setup with the respective method and accuracy.

Variable	Measuring method	Measuring device	Accuracy / Linearity
Temperature	Resistive	WIKA Type TR33	± 1.2 K
Pressure (high frequency)	Piezo-resistive	Kistler Type 4067A3000	≤ ± 0.5 % FSO (in this work: ≤ ± 15 bar)
	Piezo-electric	Kistler Type 601A	≤ ± 0.5 % FSO (in this work: ≤ ± 1.25 bar)
	Piezo-resistive	Kistler Type 4065A	≤ ± 0.5 % FSO (in this work: ≤ ± 1 bar)
Pressure (low frequency)	Capacitive	WIKA Type S-10	≤ ± 0.5 % FSO (in this work: ≤ ± 1 bar)

TABLE 7 Measurement equipment of the test bench setup with the respective method and accuracy.

Variable	Measuring method	Measuring device	Accuracy / Linearity
Temperature	Thermoelectric	Thermocouple Type K	2.2 °C
Pressure (high frequency)	Piezo-resistive	Kistler Type 4067E3000	≤ ± 0.8 % FSO (in this work: = ± 24 bar)
	Piezo-resistive	Kistler Type 4045A10	≤ ± 0.3 % FSO (in this work: = ± 0.03 bar)
	Piezo-electric	Kistler Type 7061B	≤ ± 0.5 % FSO (in this work: = ± 1.25 bar)
Crank Angle	Magneto-resistive	ASM POSIROT PMIS4	± 0.1°
Volumetric air flow rate	Rotary piston	Aerzen Ze 039.0	± 0.1 %
Gravimetric fuel flow rate	Coriolis	Emerson CMF010M	± 0.1 %
Humidity	Capacitive	Ahlborn FHAD 46-C7	± 2.0 % rel. hum.
NO_x concentration	Fourier-transform infrared spectroscopy	AVL SESAM i60 FT SII	≤ ± 2 %

TABLE 8 Operation points of the single-cylinder research engine used for calibration and validation of the simulation model. Every point is recorded with and without the specified EGR rate. If the operation point uses pilot injection, the duration of energizing is 0.35 ms, with a SOE at 5 °CA before the SOE of the main injection both with and without EGR. (*) Boost pressure indicated for operation without EGR; in EGR mode, boost pressure is reduced about 0.2 bar in order to simulate enthalpy loss in the turbine of the turbocharger due to EGR. (**) λ equals 1.2 in EGR mode in order to avoid CH_4 emissions. (***) These points were not used for calibration, because the set rail pressure on the test bench exceeded the measured pressure range on the IRA.

Engine speed in rpm	IMEP in bar	Rail pressure in bar		SOE in °CA after TDC without EGR (and in EGR mode)		Boost pressure in bar (*)	EGR rate in % (w/w)			Air-fuel ratio λ (**) (according to Coriolis and air flow meter)	Pilot injection	
		Injector 1	Injector 2	Injector 1	Injector 2			Injector 1	Injector 2		Injector 1	Injector 2
1000	13	800	(***)	711 (710)	(***)	1.9	0	14.8	(***)	1.8	Yes	(***)
1000	15	850	(***)	711 (708)	(***)	2.2	0	16.0	(***)	1.7	Yes	(***)
1000	19	1200	950	712 (710)	711 (709)	2.9	0	19.5	20.2	1.8	Yes	Yes
1200	7	1000	800	714 (712)	711 (708)	1.2	0	21.1	21.4	2.0	Yes	Yes
1200	10	1000	800	711 (710)	710 (707)	1.6	0	12.3	13.3	1.8	Yes	Yes
1200	13	1100	850	710 (708)	709 (706)	2.0	0	11.7	14.6	1.8	No	No
1200	15	1300	1000	711 (708)	710 (707)	2.3	0	15.2	16.9	1.8	No	No
1200	19	1800	1400	712 (710)	711 (710)	2.9	0	17.1	17.8	1.8	No	No
1500	7	1400	1100	713 (711)	709 (707)	1.2	0	25.5	22.8	1.9	Yes	No
1500	13	1600	1250	710 (707)	708 (705)	2.1	0	21.7	24.0	1.9	No	No
1500	15	1750	1350	710 (708)	708 (706)	2.4	0	23.1	25.1	1.8	No	No
1500	19	1800	1400	708 (706)	707 (705)	3.0	0	23.1	25.0	1.8	No	No
1750	7	1600	1250	710 (710)	707 (704)	1.2	0	20.0	23.7	2.0	Yes	No
1750	10	1600	1250	708 (705)	706 (704)	1.6	0	19.8	20.2	1.9	No	No
1750	13	1800	1400	707 (705)	705 (703)	2.0	0	18.9	20.9	1.8	No	No
1750	15	1800	1400	706 (704)	705 (702)	2.3	0	19.5	21.3	1.8	No	No
1750	19	1800	1400	704 (701)	703 (700)	2.9	0	22.5	22.0	1.9	No	No

ISSN 0148-7191

Gelner, A. D.; Rothe, D.; Kykal, C.; Irwin, M.; Sommer, A.; Pastoetter, C.; Härtl, M.; Jaensch, M.; Wachtmeister, G.: *Particle Emissions of a Heavy-Duty Engine Fueled with Polyoxymethylene Dimethyl Ethers (OME)*; Environmental Science: Atmospheres (2), 2022, pp. 291-304. [180]

Particle emissions of a heavy-duty engine fueled with polyoxymethylene dimethyl ethers (OME)

A. D. Gelner, D. Rothe, C. Kykal, M. Irwin, A. Sommer, C. Pastoetter, M. Härtl, M. Jaensch and G. Wachtmeister,
Environ. Sci.: Atmos., 2022, **2**, 291 **DOI:** 10.1039/D1EA00084E

Environmental Science: Atmospheres

ROYAL SOCIETY OF CHEMISTRY

PAPER

Cite this: *Environ. Sci.: Atmos.*, 2022, **2**, 291

Particle emissions of a heavy-duty engine fueled with polyoxymethylene dimethyl ethers (OME)†

Alexander D. Gelner, *[a] Dieter Rothe,[b] Carsten Kykal,[c] Martin Irwin,[d] Alessandro Sommer,[a] Christian Pastoetter,[b] Martin Härtl,[a] Malte Jaensch[a] and Georg Wachtmeister[a]

Received 19th October 2021
Accepted 3rd January 2022

DOI: 10.1039/d1ea00084e

rsc.li/esatmospheres

Polyoxymethylene dimethyl ethers (OME) are promising substitutes for fossil diesel fuel. Besides the possibility of closing the carbon cycle, OME also feature soot-free combustion. Although this has been demonstrated sufficiently, nanoparticle emission in OME exhaust is mainly unknown. Many studies provide information about the particle size distribution (PSD) in the exhaust of OME-fueled diesel engines, but lack a distinction between solid particles and particles of a volatile nature. This distinction is necessary in order to evaluate the potential of OME regarding Euro VI and the Euro VII exhaust gas legislation being discussed. This study investigates the PSD of fossil diesel and the OME exhaust of a heavy-duty engine with and without removal of the volatile fraction *via* a catalytic stripper, by means of a purpose-built sampling system based on proposals from the Particle Measurement Programme (PMP). The experiments showed that most of the nuclei mode investigated in OME operation is of a volatile nature and that the solid particle number (PN) emission is below that of Euro VI diesel operation. Moreover, the results indicate that a state-of-the-art aftertreatment system removes most of the particle emission, regardless of whether it is volatile or solid. Selective catalytic reduction using aqueous urea dosing increases solid particle emission, especially in the sub-23 nm range. However, a PMP-conformant measurement of PN_{23} and PN_{10} during WHSC and WHTC runs demonstrated that the PN emission of an OME-fueled engine falls below the average immission level of urban and regional background in Germany.

Environmental significance

OME as sustainable e-fuel helps to reduce the impact of diesel engines on the environment regarding climate change and air pollution due to black carbon emission. Although the soot-free combustion of OME is well demonstrated, the emission of nanoparticles in the exhaust of an OME-fueled engine has been poorly characterized. This study investigates the particle size distribution of OME exhaust with respect to good practices in aerosol measurement technology. The results help to evaluate the environmental impact of OME-fueled compression ignition engines and demonstrate the importance of exhaust measurement standards regarding sampling systems for particle measurement.

Introduction

It is widely accepted that in order to better mitigate climate change, anthropogenic greenhouse gas emissions must be reduced, primarily carbon dioxide (CO_2).[1] Although there has been a push for mobile applications used to migrate to battery-electric vehicles operated with renewable power, substituting fossil fuels with renewable, synthetic, electricity-based fuels is a beneficial short-term and target-oriented approach that can be performed with relative ease alongside the move towards electrification. These so-called e-fuels offer the possibility of diminishing the CO_2 impact of existing and future internal combustion engines; the present fuel distribution infrastructure can mostly be used.[2] In the case of diesel engines, long-chain polyoxymethylene dimethyl ethers (OME) have physico-chemical properties similar to that of fossil diesel and are among the most promising of e-fuels.[3] The synthesis process of renewable OME-fuel over formaldehyde and methanol starts with hydrogen and CO_2,[4] hence offering the potential for a closed carbon cycle. The prerequisite for this process is hydrogen from renewable sources, such as electrolysis by solar or wind power. Furthermore, CO_2 must be obtained by post-combustion capture or direct air capture,[5] and the synthesis process must not lead to additional CO_2 emissions. In addition to the possibility of renewable production, OME also provides

[a]*Technical University of Munich (TUM), Schragenhofstraße 31, 80992 Munich, Germany. E-mail: gelner@tum.de*

[b]*MAN Truck & Bus SE, Vogelweiherstraße 33, Nuremberg, Germany*

[c]*TSI GmbH, Neuköllner Straße 4, 52068 Aachen, Germany*

[d]*Catalytic Instruments GmbH & Co. KG, Zellerhornstraße 7, 83026 Rosenheim, Germany*

† Electronic supplementary information (ESI) available. See DOI: 10.1039/d1ea00084e

the advantage of soot-free combustion.[6–10] The reason for this is the intramolecular lack of C–C-bonds, which suppresses the formation of soot precursors such as polyaromatic hydrocarbons.[11] This resolves the trade-off between soot and nitrogen oxide (NO_x) emissions from diesel engines[6] and opens up the opportunity for massive NO_x reduction in the raw exhaust by measures such as high exhaust gas recirculation (EGR) rates or decreased injection pressure.[12,13] Soot and nitrogen oxide emissions are both harmful to the human body[14,15] and the environment.[16,17] Therefore, the resolution of this trade-off supports the efforts for air pollution control being implemented by governmental regulations of emission legislation.

However, although many studies have demonstrated the soot-free combustion of OMEs, the extent of nanoparticle emissions in the exhaust has been poorly characterized. According to Kittelson, particles form a trimodal size distribution in the exhaust of a diesel engine.[18] The nuclei mode with particles of electrical mobility diameter from typically 5 to 50 nm consists of mostly volatile organic and sulfur compounds formed during exhaust dilution and cooling, as well as solid carbon and metal compounds. The accumulation mode with particles between 100 nm and 300 nm contains carbonaceous agglomerates and associated adsorbed materials and makes up most of the particle mass. The coarse mode consists of accumulation mode particles, which re-entrain to the exhaust after growth during deposition on surfaces in the exhaust system. The current legislation considers only solid particles with a diameter of 23 nm and larger, although future legislative proposals are pushing this to <23 nm with a 10 nm-cut-point.[19,20] The Particle Measurement Programme (PMP) by UN/ECE recommends the removal of volatile particles by means of evaporation or catalytic conversion.[21] Although many studies have examined this topic, the composition of the particle size distribution (PSD) in OME exhaust remains unknown. Lin *et al.* and Liu *et al.* studied the PSD of diesel exhaust and blends with OME up to a volumetric mixing ratio of 30% and varying different effects on the accumulation mode, depending on the injection pressure[22] and the operating point.[23] Ferraro *et al.* investigated the effect of OME_3 on soot particle formation in a premixed ethylene burner and observed a shift of the maxima towards smaller particle diameters.[24] Popp *et al.* also observed this effect with OME-diesel-blends on a heavy-duty engine.[25] Investigations with an OME_{3-5} mix in a single-cylinder research engine demonstrated particle emissions in the so-called sub-23 nm range with a peak around a size of 10 nm.[26,27] Neither study included a description of the sampling system, so it is unknown whether or not the results contained volatile particles. Preuß *et al.* observed an increase of this sub-23 nm mode with increasing mixing ratios of OME_{3-5} in blends with hydrogenated vegetable oil (HVO) and rapeseed methyl ester used as diesel reference fuels, but also without specifying the sampling system.[28] Barro *et al.* observed a similar peak in OME exhaust, located at the nuclei mode of diesel exhaust.[29] An additional investigation in that study using transmission electron microscopy (TEM) indicated that some of the observed particles below 20 nm consisted of soot and metal particles. They therefore assumed that the measured particles in this range were solid in nature, although the particle measurement device did not include a volatile particle remover. Dworschak *et al.* compared the PSD of neat OME_3, OME_4 and OME_5 [30] as well as a mix of OME_{2-6} [31] to the PSD of HVO as a diesel reference fuel. The sampling system used in these studies contained an evaporation tube for volatile particle removal. Neither of these studies had results demonstrating a particle emission peak around 10 nm. In order to distinguish between volatile and solid particles in the PSD of OME, a systematic observation within the scope of the present work investigated the exhaust of a state-of-the-art heavy-duty engine with a modular exhaust aftertreatment system (ATS), by means of several sampling systems, which differ in dilution. The systems for solid particle measurement only, contain a catalytic stripper for the removal of volatile particles according to Abdul-Khalek & Kittelson[32] and Swanson & Kittelson.[33] A two-stage dilution sampling system enables a comparison of the PSD in raw exhaust in diesel and OME operation. Removing the second dilution stage makes the investigation of the volatile and nonvolatile PSD of OME more accurate and enables an investigation of the difference between raw exhaust and tailpipe particle emissions. Moreover, this work contains an investigation on the effect of urea dosing on the particle emissions of an OME engine with a twin-dosing system for selective catalytic reduction (SCR). Another series of experiments indicates the effect of a diesel particulate filter (DPF) and urea dosing on the solid particle number (PN) emission in the legislative test cycles "World harmonised steady-state cycle" (WHSC) and "World harmonised transient cycle" (WHTC) with a PMP-conform exhaust measurement and an additional sampling of sub-23 nm particles. An outlook evaluates the potential of OME as a carbon-neutral and low-emission alternative diesel fuel.

Materials and methods

Tested fuels

Polyoxymethylene dimethyl ethers (OME) are oligomers from the group of C_1 oxygenates. They have the chemical structure of $CH_3–O–(CH_2O)_n–CH_3$, while n as the number of oxymethylene groups is often used as an index to specify the respective OME_n. In this work, the abbreviation OME refers to a mixture with major percentages of $n = 3–6$ (OME_3: 58%, OME_4: 29%, OME_5: 10%, OME_6: 2%), which fulfills the M DIN TS 51699 standard for OME-fuel.[34] The mixture also contains 300 mg kg^{-1} each of butylated hydroxytoluene (BHT) for oxidation stabilization, and a flow improver as additives. Fossil diesel according to the EN 590 standard with a maximum content of 7% (v/v) fatty acid methyl esters (FAME) sets the reference fuel for comparing the particle emission behavior. ASG Analytik-Service AG provided the OME-fuel and determined the values of the physical properties. The ESI† contains the respective standard of the measurement method used for providing the substance values. Table 1 compares these values with the EN 590 standard. The oxygen content of OME is around 45% (w/w). This reduces the lower heating value (LHV) of the fuel to about 2.2 times lower than that of fossil diesel. The higher density of OME compensates this marginally, resulting in a volumetric diesel equivalent

Table 1 Properties of the tested fuels. ASG Analytik-Service AG determined the values of OME; the values of diesel come from Lautenschütz *et al.*[36] if not specified in the standard EN 590.[35] The calculation of the gravimetric oxygen content of diesel is based on the values from Hoekman *et al.*,[37] with the assumption that the FAME proportion is made of oleic acid

	Diesel	OME
Cetane number	>51	69
Lower heating value in MJ kg^{-1}	42.6 [36]	19.2
Oxygen content in % (w/w)	0–1 [37] (with max. 7% (v/v) FAME)	45
Density in kg m^{-3}	820–845	1057
Boiling range in °C	170–390 [36]	145–242
Flash point in °C	>55	65
Sulfur content in ppm	<10	<5

ratio of around 1.7 liters of OME for 1 liter of diesel. The flash point of the OME mixture investigated exceeds the requirements of the EN 590 standard,[35] which enables storage and distribution systems similar to fossil diesel. Values of the boiling range of diesel come from Lautenschütz *et al.*,[36] who have determined characteristic values of diesel according to EN 590. The calculation of the volumetric diesel equivalent ratio also uses the LHV of diesel from this publication. The sulfur content of OME is lower than 5 ppm according to DIN EN ISO 20884:2011, so it reaches the lower limit of the determination standard for this value. Because of the sulfur-free educts and synthesis of OME, the sulfur content is furthermore assumed to be less than 1 ppm.

Test engine and operating points

The test engine used was a MAN D2676LF51 six-cylinder heavy-duty diesel. Apart from the high-pressure fuel pump seals, the engine was not specially adapted for OME operation. Therefore, the engine components, such as the piston geometry and cylinder head, were optimized for operation with conventional fossil diesel. In order to avoid long and inefficient combustion durations due to the lower-level heating value,[38] the solenoid injectors for OME operation had higher nozzle flow rates. Besides the effect of decreasing efficiency during longer combustion durations, interactions of the fuel jet with the lubricant oil film are undesirable. Therefore, higher nozzle flow rates enabled a shorter injection process which stops before the piston reveals the liner during the downward movement. The ESI† displays the properties of the test engine.

The test engine had a modular aftertreatment system provided by VT Vitesco Technologies Emitec GmbH, which enabled removal or exchange of the components. The system had a twin-dosing design, which means that there were two positions, in which urea dosers provide the reducing agent for the selective catalytic reduction in the form of aqueous urea solution according to ISO 22241-1:2019, abbreviated as AdBlue®.[39] The injection and conversion of the aqueous urea solution to ammonia (NH_3) happens in a so-called Universal Decomposition Pipe (UDP) equipped with a titanium dioxide (TiO_2)-coated hydrolysis catalyst (Hyd).[40] The copper-zeolite (CuZe) SCR catalysts reduce NO_x with the reducing agent NH_3.[41] An ammonia slip catalyst (ASC) oxidizes excess ammonia after the SCR system selectively in order to avoid an unselective oxidation to nitrous oxide (N_2O) in the diesel oxidation catalyst (DOC) placed downstream.[42] The DPF was an uncoated Cordierite wall flow filter. A second SCR stage ideally converted any remaining NO_x emissions. The second stage had no ASC installed. The ESI† displays the properties of the ATS components.

The investigation of the PSD focused on two stationary operating points: L1 represents a high-load point with comparatively high exhaust gas temperatures; L2 represents a low-load point with high engine speed, resulting in lower exhaust gas temperatures and higher space velocities than L1. Table 2 describes the parameter settings of the operating points in diesel and OME operation.

Measuring setup

The Scanning Mobility Particle Sizer (SMPS, TSI Model 3938) ascertained the PSD in the exhaust gas and contained the following components: the model 3082 classifier selected the exhaust gas by electrical mobility classification into a monodisperse aerosol *via* the following steps: a Model 3088 soft X-ray neutralizer ionized the aerosol carrier gas, leading to a bipolar charge distribution.[43] The model 3081A differential mobility analyzer (abbreviated as "longDMA") selected particles in the aerosol according to their electrical mobility diameter. The ultrafine condensation particle counter (TSI Model 3776, with a 50% cut-off at 2.5 nm) determined the particle number of the respective particle size range. Upstream of the aerosol inlet of the classifier, an impactor separated large particles above the set SMPS measurement range in order to minimize the deviation of the multiple charge correction[44] in the TSI "Aerosol Instrument Manager" evaluation software. The measurement range of the SMPS in this work was set to 6.38 nm to 224.7 nm. The sampling duration of every run was 72 seconds, including the automatic purging process of the SMPS.

The equipment for particle number measurements during the test cycles consisted of an AVL Advanced Particle Counter 489, standard equipped with a condensation particle counter (CPC) with a 50% cut-off at 23 nm. This measurement device fulfilled the specifications of PMP.[21] It contained a PN_{23}-compliant volatile particle remover (VPR), consisting of three elements according to the PMP in this chronological order: a hot dilution with a minimum dilution ratio of one to ten stabilized the aerosol and reduced the particle concentration;

Table 2 Operating points for measurement of the PSD. The pressure indication system AVL Indimodul 621 and an optical encoder determined the respective point in time with 50% mass fraction burnt (MFB50) in degrees of crank angle (CA) after the top dead center (TDC). The engine's lambda probe determined the air–fuel-ratio (λ)

	Diesel		OME	
Load point	L1	L2	L1	L2
Engine speed in RPM	1100	2000	1100	2000
Brake mean effective pressure in bar	18	6	18	6
Rail pressure in bar	1200	1800	1000	1600
MFB50 in °C after TDC	9	6	15	6
EGR rate in % (w/w)	20	33	18	43
Air-fuel ratio λ	1.35	2.30	1.45	1.90
Exhaust temperature downstream of the second turbocharger in °C	410	260	370	250

an evaporation tube heated to 350 ± 50 °C vaporized volatile material like the condensed fuel drops mentioned by Kittelson;[18] a cool dilution with a minimum dilution ratio of one to ten decreased the temperature of the aerosol and reduced the particle concentration and avoided re-nucleation of the evaporated substances. Furthermore, an additional CPC with a 50% cut-off at 10 nm (TSI Model 3772, calibrated by the Federal Institute of Metrology METAS), connected with the secondary outlet of the APC, enabled a synchronous PN measurement, including the sub-23 nm range. In this additional measurement setup, an auxiliary pump enabled a flow rate of 1.0 l min^{-1} through the CPC, controlled by an internal critical orifice.

While the APC had an integrated sampling system which was connectable to the respective location at the exhaust pipe, the measurement setup for PSD determination with the SMPS required a purpose-built sampling system. In this work, this sampling system contained the following elements, which were based on the PMP proposals: the exhaust gas flowed through an ejector diluter (DEKATI diluter with a dilution ratio of one to ten). A heating cover with a set temperature of 200 °C reduced the cooling of the aerosol. In addition, the filtered and dried dilution air flowed through a heater set to 150 °C. A "Catalytic Stripper CS10" (hereinafter abbreviated as CS) according to Abdul-Khalek & Kittelson[32] and Swanson & Kittelson,[33] provided by Catalytic Instruments GmbH & Co. KG enabled removal of volatile particles with an operational set temperature of 350 °C. The operational performance of the CS is well documented in the literature.[45–52] A diluted aerosol flow enters the device whose temperature is elevated to the operational setpoint of 350 °C. The aerosol flow then enters the catalyst monolith, where, in the presence of oxygen, hydrocarbon (HC) particles evaporate and HC vapors are converted into the gaseous water (H_2O) and CO_2. The residence time within the monolith is a function of the flow rate and the design value chosen to balance between HC conversion efficiency and particle penetration. The CS is optimized for this balance, ensuring that even the most stringent legislative tests pose no problem for the performance of this device. Some sulfur present in the aerosol is adsorbed to the catalyst itself, which directly acts as a sulfur trap, minimizing artifacts caused by sulfuric acid.[33] If high-sulfur fuels are used, then the CS requires servicing, but this was not the case for these experiments. The CS also oxidizes organic substances adhering to solid particle cores, which suppresses an increase in the size of the particles due to this phenomenon.[18] It is possible to directly compare solid and non-solid fractions of aerosol in the sampling system by alternating the use of the CS. Sampling without the CS results in a "total particle" concentration, and with the CS the "solid particle concentration". Subtracting the solid from the total gives an approximation of the volatile fraction. An integrated cooler inside the CS resulted in an outlet temperature of approximately 30 °C. In order to avoid overwhelming the measurement equipment by exceedingly high particle concentrations, a second ejector diluter (DEKATI Diluter with a dilution ratio of one to eight) reduced the particle concentration downstream of the CS. Due to the integrated cooler inside the CS, the cooling function of this dilution was obsolete in the setup with the CS. The removal of this second dilution stage enabled a higher measurement accuracy due to a higher particle concentration upstream of the measurement device in an operation with a lower level of particle emission. The CPC connected to the SMPS system had a flow rate of 1.5 l min^{-1}. The "Catalytic Stripper CS10" is designed for a nominal aerosol flow of 10 standard liter per minute (SLPM). In order to use the device at this flow, an auxiliary vacuum pump connected with a tee at the inlet of the SMPS increased the total flow in the sampling system to the respective nominal flow of the CS. The tubing to the auxiliary pump used the specific connection to the tee, which had an offset of 90° to the aerosol flow from the sampling system towards the impactor of the SMPS. Fig. 1 depicts a scheme of the sampling systems for the determination of the PSD using the SMPS and the PN emission in the test cycles using the AVL APC.

The purpose-built sampling system requires calculating the respective particle concentration reduction factor (PCRF) due to transport losses depending on the particle size. Von der Weiden *et al.* developed a "Particle Loss Calculator"[53] according to mechanisms described by Hinds[54] and Willeke & Baron.[55] Although the estimation of the transport losses in this work did not use this specific calculator, it was based on the mechanisms mentioned in ref. 53. The calculation of losses due to gravitational settling in the inlet, sedimentation, bent tubing and coagulation[55] resulted in a transportation efficiency of more than 99.9% for a minimal particle diameter of 6 nm and a maximal particle diameter of 0.23 μm. They are therefore

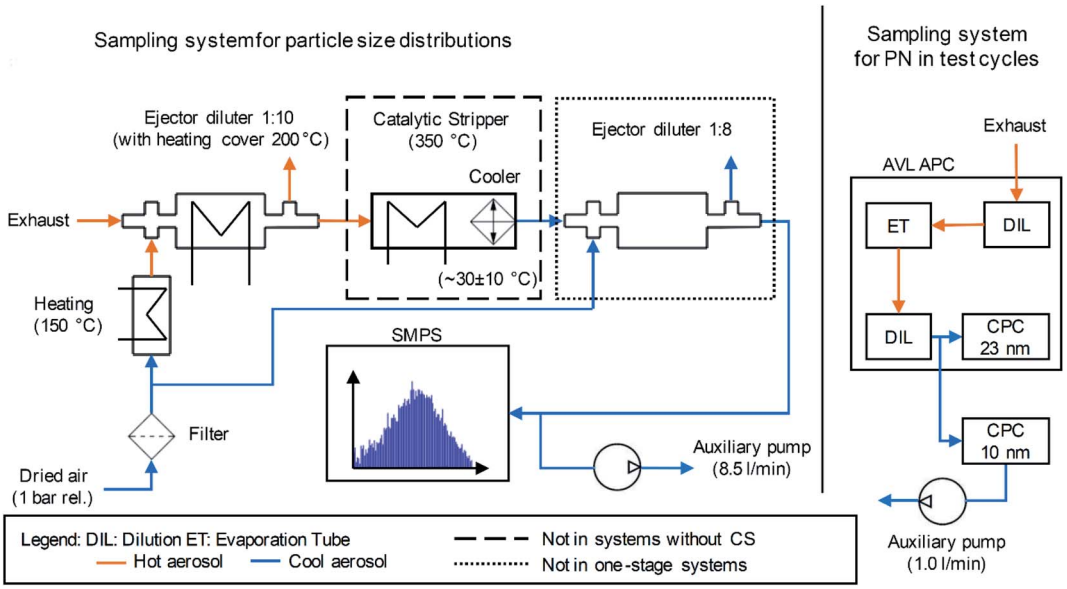

Fig. 1 Scheme of the sampling systems.

neglected in the following. This is due to the isokinetic sampling, the tube inner diameter of 6 mm and the mean flow velocity of approximately 5.9 m s^{-1}. The Reynolds number inside the tubing was about 2350, which allows an estimation of a laminar flow. Thermophoretic losses according to ref. 54–56 were neglected except for the CS, because the calculation of the thermophoretic velocity results in less than 0.001 m s^{-1} for the sampling system in this work. Moreover, transport losses due to electrostatic fields were neglected due to the usage of stainless steel wherever possible and an intermediate connection using Tygon tubing. This polymer is known as a tubing material having lower electrostatic losses than other kinds of tubing.[57–59] However, the manufacturer of the catalytic stripper (Catalytic Instruments GmbH & Co. KG) provides in the manual, penetration efficiency data at nominal flow (10 l min^{-1}) due to diffusional and thermophoretic losses. The loss calculation uses this penetration efficiency, supplemented by a calculation of the transportation losses due to Brownian diffusion according to Hinds.[54] Additionally, the transportation losses of the ejector diluters were assumed to be 5% for each diluter and for any particle diameter, according to the measurements of Giechaskiel *et al.*[60] Fig. 2 shows the calculated penetration efficiencies of the purpose-built sampling systems with and without the CS or the second dilution stage. The ESI† shows a detailed calculation of the mentioned losses. The results of the PSD in this work use the PCRF of these calculations. Furthermore, the TSI "Aerosol Instrument Manager" software includes the option of considering the diffusion losses inside the SMPS and a multiple charge correction. The evaluations in this study include these considerations.

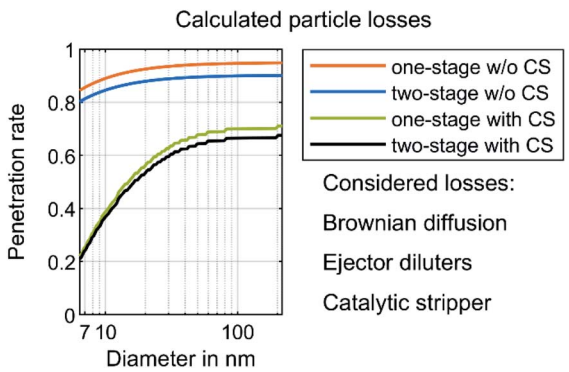

Fig. 2 Calculated particle losses. The losses due to Brownian diffusion are based on calculations according to Hinds[54] with the assumption of a laminar flow inside the tubing. The losses of each ejector diluter were assumed to be 5% according to Giechaskiel *et al.*[60] The manufacturer of the catalytic stripper determined the respective penetration efficiency at a nominal flow rate of 10 l min^{-1}.

Since the setup for PN measurement contained a commercial device in the form of the AVL APC 489, the manufacturer specifies a respective value of the PCRF in this setup. The evaluation in this study uses this PCRF for the correction of the particle number emission determined by the CPCs during the test cycles. Particle losses in the Tygon tubing from the secondary outlet to the CPC with a 50% cut-off at 10 nm were disregarded due to a tubing length of 300 mm, resulting in an overall penetration rate of more than 95% for particles with a diameter larger than 10 nm regarding the losses considered in the purpose-built sampling system.

Test procedure

The ESI† shows the chronological order of the experiments for measuring the PSD on the stationary operating points presented in Table 2. In order to avoid artifacts in the form of adsorbed organic substances during the operation without the CS, the test run with the consideration of volatile particles took place after the test run using the CS. After the operation without the CS, a cleaning procedure using the CS and the auxiliary pump with a duration of 60 minutes for the removal of adhering

particles inside the sampling system was performed. Furthermore, a cleaning of the impactor of the SMPS in an ultrasonic bath enabled the same for this element before the first run and after the change from diesel to OME. After the fuel change, the engine ran several test cycles to remove remaining diesel residues in the fuel system or adhering soot in the engine or exhaust system. During this cleaning process, the sampling system ran with two-stage dilution and the CS with a set temperature of 350 °C and operated auxiliary pump.

Since the test runs could not take place on the same day under identical ambient conditions, a monitoring of the air temperature, ambient pressure, and humidity enabled an assumption regarding the comparability of the volatile particle measurement results. Nevertheless, the respective test runs with and without the CS happened on the same day, while the change of the fuel or the sampling position prevented a same-day-measurement. However, the ambient conditions for the test runs without removal of volatile particles differ by 1 °C in ambient temperature, 5% in humidity, and 6 mbar in ambient pressure. Three measurement recordings mapped the PSD in the exhaust gas at every stationary operation point.

For the tailpipe PN measurement of OME operation during the WHSC and WHTC based on the regulation No. 49 of the UN/ECE,[61] the chronological order of the test runs was as follows. Before every test cycle, the engine was pre-conditioned to the respective operating point of the WHSC according to the regulation. This study does not consider cold start operation in WHTC. This is due to the modular aftertreatment system, which has a poorer thermal behavior than a state-of-the art system. The first run consisted of a WHSC without DPF but with urea dosing, followed by WHTC with the same setup. Since the DPF was able to build up a soot layer in diesel operation, a regeneration of the DPF in an oven at 500 °C for six hours took place before reinstallation of the DPF in the ATS. The experiment continued with a run of a WHSC with DPF and urea dosing, followed by a run without urea dosing. Between these two runs, the engine ran in a regeneration mode without dosing, providing a cleaning of the SCR catalysts. A WHTC followed with the same order, beginning with urea dosing.

Results and discussion

The following chapter compares the PSD of diesel and OME at two engine operation points with different sampling points and different sampling systems. In order to compare the respective size distributions, the scale of the figures is the same in diesel and OME operation. The figures plot the data using normalized concentration according to the following formula:

$$\frac{\mathrm{d}N}{\mathrm{d}\log_{10} D_p} = \frac{\mathrm{d}N}{\log_{10} D_{\mathrm{p,u}} - \log_{10} D_{\mathrm{p,l}}} \quad (1)$$

dN describes the number of particles in the total concentration and $D_{\mathrm{p,u}}$ and $D_{\mathrm{p,l}}$ are the upper and lower bin boundaries, respectively. Therefore, the particle concentration is divided by the bin width. This gives a normalization which is independent of the specific bin width. This normalization enables comparison of particle concentrations between different measurement devices with different resolutions. The figures contain the average (arithmetic mean, abbreviated as avg) of three samples and the respective standard deviation (std). The average was filtered using a Savitzky–Golay filter of polynomial order 3 and frame length 21.

Fig. 3 shows the raw exhaust PSD for diesel and OME operation at the load points L1 and L2 without the catalytic stripper. Therefore, the PSD contains both volatile and solid particles.

The PSD in diesel operation showed a clear nucleation mode around 10 nm for both points, which originates mainly from volatile organic and sulfur compounds.[18] This mode also appeared in OME operation, with a similar level at L2 and with lower amplitude at L1. For both fuels, a significant part of the nucleation mode might be derived from the lube oil, since several studies demonstrated sub-23 nm particles even during engine motoring.[62–65] Diesel operation shows a bimodal distribution similar to the results of Abdul-Khalek *et al.*,[66] with a separate accumulation mode that describes its maximum at 40 nm in the same order of magnitude as the nucleation mode at L2. According to the relevant literature, this mode contains predominantly solid soot particles.[18] This accumulation mode also appeared at L1, but to a lesser degree than the respective nucleation mode. The exhaust in OME operation showed no accumulation mode on the same scale as in diesel operation.

In order to distinguish between volatile and solid particles in the exhaust, Fig. 4 shows the raw exhaust PSD for diesel and OME operation with the CS.

In diesel operation, both operating points show a broad accumulation mode of solid particles that is assumed to consist of soot particles. In contrast to the presentation of Fig. 3, this

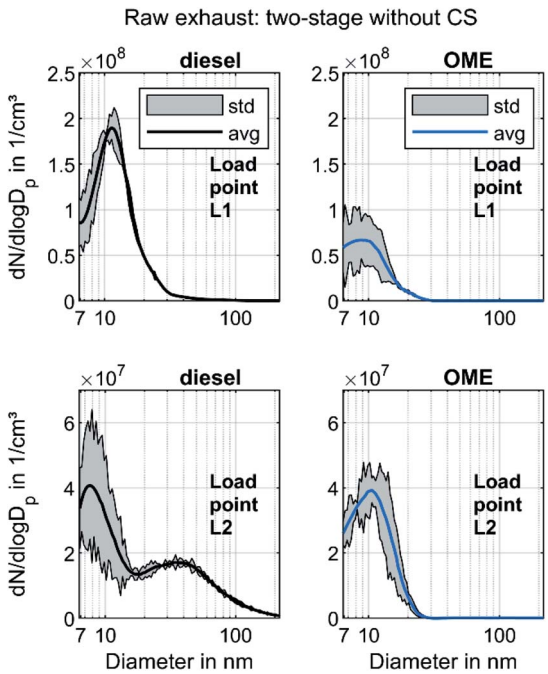

Fig. 3 Particle size distribution of OME and diesel raw exhaust without volatile particle remover and two-stage dilution: filtered average (arithmetic mean) of three recordings and indication of the standard deviation.

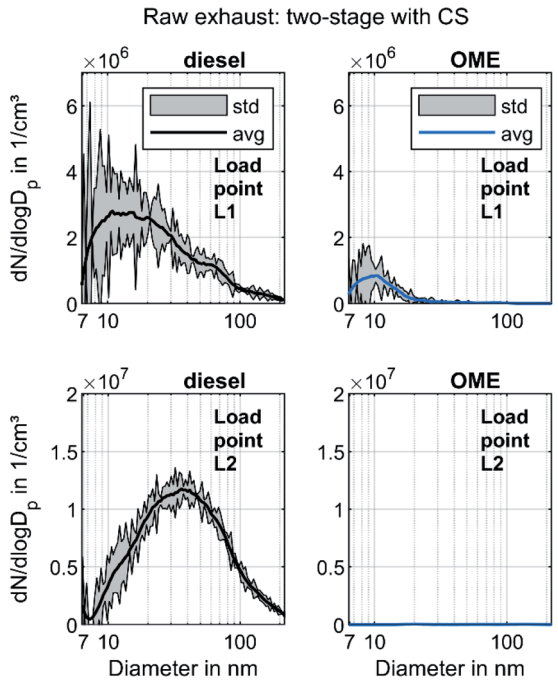

Fig. 4 Particle size distributions of OME and diesel raw exhaust with volatile particle remover and two-stage dilution: filtered average (arithmetic mean) of three recordings and indication of the standard deviation.

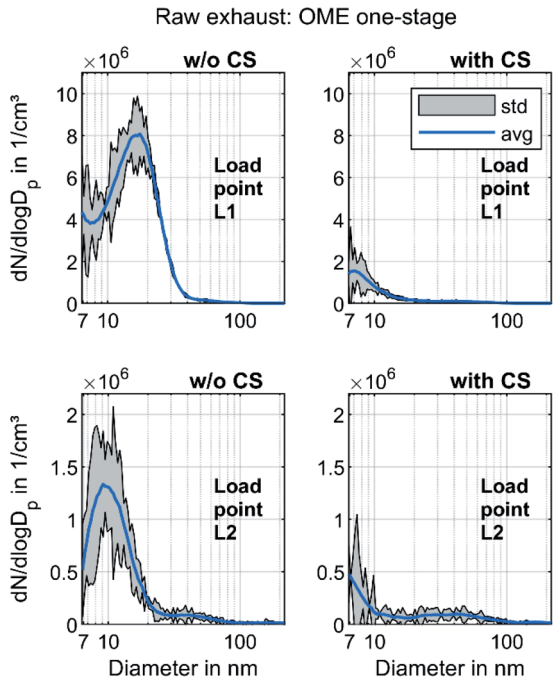

Fig. 5 Particle size distributions of OME raw exhaust with and without volatile particle remover and one-stage dilution: filtered average (arithmetic mean) of three recordings and indication of the standard deviation.

mode is clearly visible at L1, since the removal of the dominant mode of volatile particles by the CS enables the adjustment of the axis scale maximum to a lower value. At L2, the mode with a maximum at 40 nm remains unchanged and shows the same order of magnitude as without CS, which confirms the hypothesis that the observed mode in Fig. 3 consists of solid particles and builds the typical accumulation mode in diesel exhaust. In OME operation, the nucleation mode at L1 observed in Fig. 3 decreases in the same ratio as in diesel operation with usage of the CS. From this observation it follows that the majority of the nucleation mode around 10 nm is of a volatile nature. Since several studies confirm the soot-free combustion of OME, the remaining solid particles might consist mainly of engine oil ash or metallic abrasion.[18] At L2, no particle mode is visible with the same scaling of particulate emissions as in diesel operation. The comparison of the two fuels regarding solid particle size distributions shows lower particulate emission in OME operation, irrespective of the particle size range.

In order to investigate the size distribution in OME operation in more detail, the measurements are carried out with a one-stage dilution system as well. Fig. 5 depicts the PSD of OME using this sampling system with and without CS for the two operating points.

Without CS, the exhaust contained a strong nucleation mode similar to that observed in Fig. 3 at both operating points. While the maximum of this mode was at 10 nm at L2, the maximum moved in the direction of a larger diameter at L1. This might have been due to an increase in the particle growth rate due to the lower dilution ratio and subsequent cooling upstream of the SMPS.[67,68] With CS, the nucleation mode decreased, corresponding well to Fig. 4. The maximum was at less than 10 nm, in contrast to the curve without CS. This led to the assumption that these nonvolatile particle cores consisting of ash or metallic abrasion[29] form a shell with condensed hydrocarbons during cooling, leading to particle growth. Rönkkö *et al.* discovered this phenomenon in the exhaust of a heavy-duty diesel engine.[69] Furthermore, the nucleation mode observed without CS may have also contained condensed water droplets, since the concentration of water in the exhaust in OME operation was higher than 10% for the operating points investigated. Another possibility is the binary homogeneous nucleation of sulfuric acid and water.[70] Since OME is assumed to have a sulfur content of less than 1 ppm, this phenomenon is limited to sulfur originating from the engine oil, but it might still be present.[71] The PSD of Fig. 5 with CS did not contain these particle cores consisting of sulfuric acid, as sulfur is adsorbed in the Catalytic Stripper. Given the lower dilution ratio than in Fig. 5, an accumulation mode became visible at L2. This mode may consist of a small amount of soot particles. However, the observations in Fig. 5 refute the assumption of Barro *et al.*,[29] *i.e.*, that the particles forming the nucleation mode in OME exhaust are mostly of a solid nature. Based on the observations in Fig. 3–5, the authors propose that, in the case of a comparison with pollutant emission legislation such as Euro VI or upcoming regulations, the volatile fraction in OME exhaust must be removed, as it is the case for diesel exhaust according to the PMP.[21] The effect of an evaporation tube on OME exhaust will have to be studied in further investigations.

Modern commercial heavy-duty engines that comply with today's emissions legislation, *e.g.* Euro VI, are equipped with a complex exhaust gas aftertreatment system. This system usually contains a diesel oxidation catalyst, a system for selective catalytic reduction and a diesel particulate filter. In order to evaluate the effectivity of these components regarding the particle removal efficiency, Fig. 6 presents the PSD at the tailpipe sampling point. The filtration efficiency (FE) was calculated according to the following formula and the values depicted in Fig. 4 and 5 were used:

$$\mathrm{FE} = \frac{\mathrm{PN_{raw}} - \mathrm{PN_{tailpipe}}}{\mathrm{PN_{raw}}} \quad (2)$$

The particle concentration at the tailpipe sampling position was near the detection limit of the SMPS, since it was in the range of 1–5 particles per cm^3 in every step interval of the classifier at both operating points. No clear difference between the PSD with and w/o CS was visible, so the volatile material that was detected in Fig. 5 might be oxidized in the aftertreatment system, predominantly in the DOC, as observed by Gren *et al.*[65] The particle concentrations at load point L2 were lower than those at L1. Rothe *et al.* discovered that some ash particles can penetrate the DPF at elevated temperatures.[72] Since L1 had higher exhaust gas temperatures than L2, this might be one reason. In addition, the friction between the piston and the liner is higher at L1 due to a higher load, with an associated higher piston side force and the lower engine speed resulting in higher proportions of solid and mixed friction.[73] Therefore, metallic abrasion might have been another reason for the higher particle concentrations at L1. Nevertheless, the FE curves in Fig. 6 confirmed that the aftertreatment system also ensured a reduction in solid particles even with a nearly empty DPF, which is assumed not to build up a soot layer in OME operation. This observation refutes the assumption by Omari *et al.*[27] They assumed that OME exhaust might become challenging for conventional particulate filters. The well-known filtration gap around 100 nm, which marks the transition between diffusive and impactive deposition,[54] also appeared in OME operation. Moreover, the results showed that the tailpipe level of total PN emissions in OME operation was significantly lower than the level in the raw exhaust, irrespective of sampling conditions.

Fig. 7 depicts the results of the investigation on the effect of urea dosing on nanoparticle emission. During the operation with urea dosing, both dosers provided AdBlue for SCR, with a reduction target of 100% for the nitrogen oxide emissions.

The operating points with active urea dosing formed a distinct nucleation mode. The particles survive the CS, which indicates that they were non-volatile. Several studies have observed increasing particle number emissions due to pure ammonia or urea solution dosing.[74,75] Mamakos *et al.* observed a formation of non-volatile particles due to urea injection, which spans from less than 10 nm to above 200 nm but with mode peaks below 20 nm.[76] Amanatidis *et al.* suggested that these particles consist of ammonium sulphate and ammonium bisulphate particles.[77] Since they observed the particle emissions even with pure ammonia, they ruled out impurities in the urea solution as the main reason. Schaber *et al.* observed the

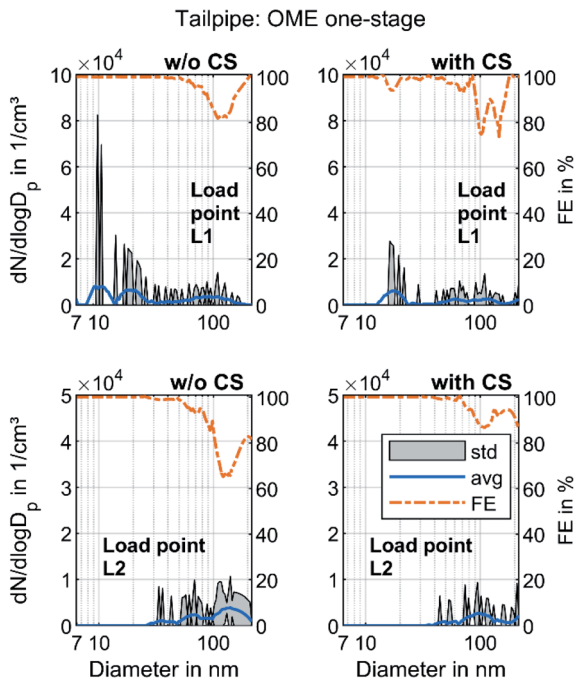

Fig. 6 Filtration efficiency FE of the aftertreatment system and particle size distributions of OME tailpipe exhaust with and without volatile particle remover and one-stage dilution: filtered average (arithmetic mean) of three recordings and indication of the standard deviation.

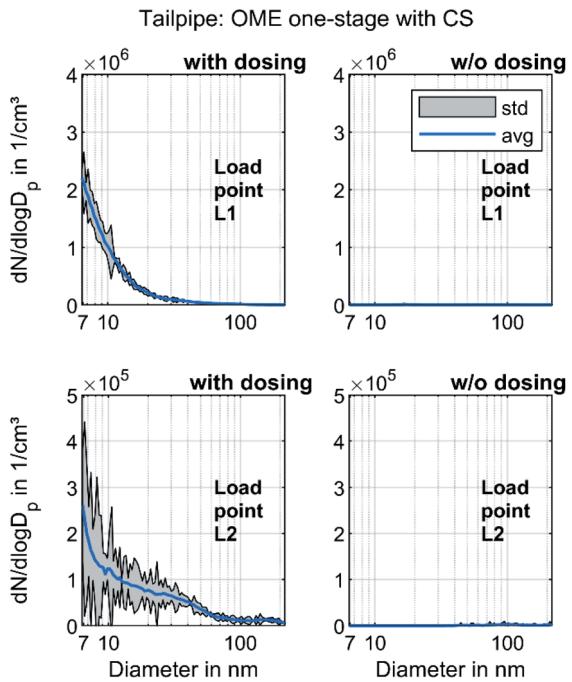

Fig. 7 Particle size distribution of OME tailpipe exhaust with and without urea dosing and one-stage dilution with volatile particle remover: filtered average (arithmetic mean) of three recordings and indication of the standard deviation.

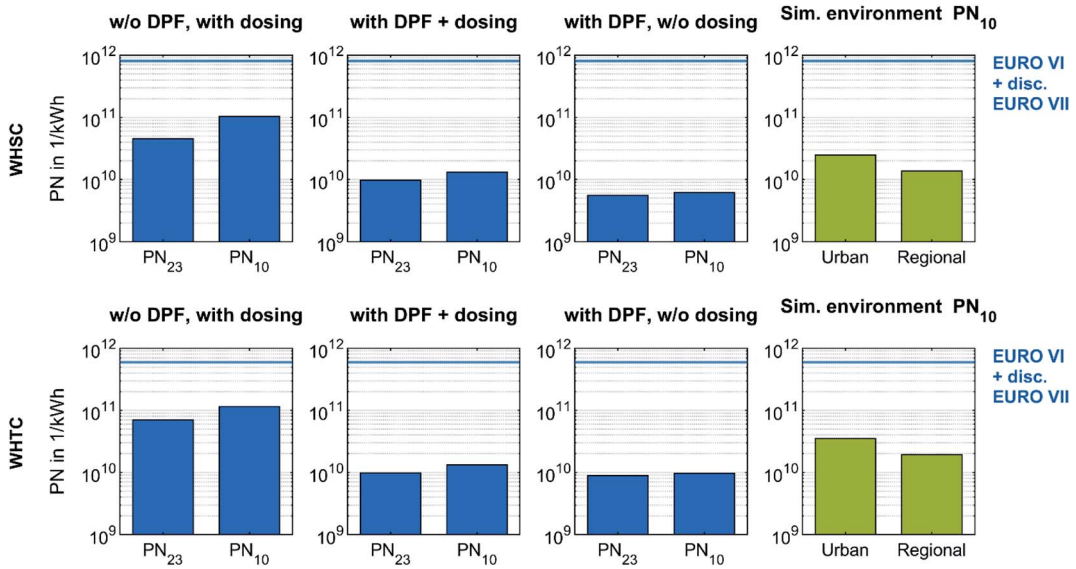

Fig. 8 Effect of DPF and urea dosing on particle number emissions during a stationary and transient test cycle fueled with OME. All test cycles result in PN emissions below the Euro VI legislation limit and furthermore below the discussed limit for Euro VII with a switch of the CPC setup towards a 50% cut-off at 10 nm. The simulated background evaluations of the test cycles use particle concentrations of Sun *et al.*,[80] who measured environmental particle concentrations from 10 to 800 nm Germany-wide.

formation of ammelides, ammelines and melamines *via* pyrolysis of urea in an open reaction vessel.[78] Börnhorst & Deutschmann attribute the formation of solid urea deposits to incomplete spray evaporation.[79] Regardless of what the solid particles are made of, Fig. 7 clarifies that they originated from the urea dosage and not from OME combustion. However, further research regarding their formation mechanisms and impact on human health and environment will be necessary.

Pre-conditioned WHSC and WHTC runs enabled an evaluation of the efficiency of the DPF in OME operation and the impact of urea dosing on particle number emission under stationary and transient driving conditions. The investigation on solid particle number (PN) emission in these test cycles used the PMP-conformant PN measurement system. In order to compare the PN emission with the Euro VII regulations discussed and in consideration of sub-23 nm particles,[19,20] a CPC with a 50% cut-off at 10 nm complemented the system. Fig. 8 depicts the PN emissions of the test cycles with different configurations on a logarithmic scale. PN_{23} describes the emission determined by the CPC inside the AVL APC 489, and PN_{10} describes the emission determined by the additional CPC.

In every configuration, the value of PN_{10} was higher than that of PN_{23}. Therefore, the solid particles in the form of ash originating from engine lube oil or in form of metallic abrasion originating from engine wear observed in Fig. 5 contributed more to the value of PN_{10} than to PN_{23}. The effect of the DPF is clear: the difference between PN_{10} and PN_{23} decreased during WHSC and WHTC, while the overall level of PN emission decreased as well. The filtration efficiency was similar to that shown in Fig. 6, confirming that the DPF was able to significantly reduce particle emissions in OME operation, regardless of whether the scope is for PN_{23} or PN_{10}. The PN increase due to urea dosing appears again in Fig. 8 comparison. In both test cycles, the reduction factor of PN by DPF was higher than the impact of urea dosing. Since the observed nucleation modes of urea-originated particles have their maxima below 10 nm in Fig. 7, this source of PN emissions may have been underestimated in Fig. 8. However, the PN emissions in the stationary and transient test cycle in OME operation were far below the limit values of Euro VI and the Euro VII values discussed, even without DPF and with urea dosing.

The bars on the right side of Fig. 8 represent the simulated cycle evaluation using the particle concentration of representative urban and regional backgrounds in Germany. These values of 6381 1 cm^{-3} and 3519 1 cm^{-3}, respectively, were derived from an estimation using the arithmetic mean of the medians of the measurements of Sun *et al.*,[80] who considered solid nanoparticles from 10 to 800 nm Germany-wide in 2018. This comparison demonstrates the ultra-low level of PN emissions of an OME heavy-duty engine equipped with an exhaust aftertreatment system. Nevertheless, the particles in the OME exhaust are assumed to consist of ash, metallic abrasion and soot, so their impact on human health and environment might be more serious than the urban background level.

Conclusions and outlook

The present work contains a comparison of particle size distributions in the raw exhaust of a heavy-duty engine in diesel and OME operations at two stationary operating points. Two sampling systems with a two-stage dilution were used in order to distinguish between PSD containing volatile material and PSD after removing volatile material *via* a catalytic stripper in general accordance with PMP specifications. In order to investigate the PSD in OME operation, a second dilution stage was removed in additional measurements. With this sampling

system, the comparison between raw exhaust and tailpipe sampling showed the particle reduction efficiency of a modern aftertreatment system, containing oxidizing catalysts, a twin-dosing SCR system and a DPF. The effect of urea dosing on the PSD was investigated at the tailpipe sampling position. Test runs of the regulated test cycles WHSC and WHTC with and without DPF and with and without urea dosing demonstrated the ultra-low level of PN emissions in OME operation.

The results are summed up by the following conclusions:

The nucleation mode with a maximum at 10 nm in OME raw exhaust mainly consisted of volatile material. This is in contrast to assumptions made in previous studies.[27,29]

Because of the mostly soot-free combustion, OME exhaust shows smaller solid PN emissions than diesel, even in the sub-23 nm range. In this range, the solid particles are assumed to mainly consist of ash from engine lube oil and metallic abrasion. However, it cannot be ruled out that small soot particles also occur, because Barro *et al.* observed them in OME exhaust using TEM.[29]

The aftertreatment system reduced the particle concentration in OME exhaust. No difference between the PSD with and without removing volatile particles was visible at the tailpipe sampling position. The observed volatile material in the raw exhaust was therefore oxidized in the DOC and ASC.

An uncoated DPF showed a significant filtration efficiency in OME operation, in contrast to the assumption by Omari *et al.*[27]

Even given PN10 legislation with the current limit values, the OME still falls below the limits whether in stationary or transient operation, with and without DPF. However, the direct comparison with the limit value is only valid for the WHSC because this study used a pre-conditioned WHTC without cold start operation.

During these test cycles, the particle concentration in OME exhaust was lower than the concentration in a representative background of urban and regional areas in Germany. Nevertheless, the environmental impact of particles from OME exhaust is not clear.

Urea dosing leads to an increase of solid PN emissions, especially in the sub-23 nm range. Therefore, improvement of the SCR system is a target-oriented way of reducing PN emissions in an OME engine.

The conclusions are based on the observations in this study and are therefore limited to the methodology used.

Nevertheless, the following research will be necessary in the future:

The necessity of regenerating a DPF in OME combustion must be investigated. Similar effects to those observed by Rothe *et al.*[72] and Dimopoulos Eggenschwiler *et al.*[81] may occur, since they observed that the soot oxidation velocity decreases with a higher proportion of organic material on the particle surface.

Furthermore, an open channel filter may be a good approach for OME engines, since this offers a compromise between filtration efficiency and exhaust backpressure, leading to higher thermodynamic efficiency.[82]

A validation of the observed behavior using different sampling systems will be necessary. For example, Su *et al.* demonstrated a difference of on average 20% using a catalytic stripper and a dilution tunnel with an evaporation tube.[83]

In the context of future exhaust gas legislation, the impact of cold start operation on pollutant emissions may increase in importance. Therefore, further investigation in this area is essential.

In order to evaluate the sooting tendency of OME regardless of the parameters effecting soot formation in an engine, *e.g.* injection, exhaust gas recirculation and oxygen availability, investigations using a laminar burner as in Palazzo *et al.*[84] or McEnally *et al.*[85] will be necessary.

Furthermore, Bartholet *et al.* demonstrated that different molecular structures of OME and derivatives affect the nanoparticle behavior during combustion in a laminar burner.[86] This must be investigated in the inner-engine combustion environment.

Definitions and abbreviations

ASC	Ammonia slip catalyst
ATS	Aftertreatment system
avg	Average (arithmetic mean)
BHT	Butylated hydroxytoluene
CPC	Condensation particle counter
CS	Catalytic stripper CS10
DIL	Dilution
DOC	Diesel oxidation catalyst
$D_{p,l}$	Lower bin boundary
$D_{p,u}$	Upper bin boundary
dN	Number of particles
DPF	Diesel particulate filter
EGR	Exhaust gas recirculation
ET	Evaporation tube
FAME	Fatty acid methyl esters
FE	Filtration efficiency
HC	Hydrocarbon
HVO	Hydrogenated vegetable oil
Hyd	Hydrolysis catalyst
LHV	Lower heating value
MFB50	50% mass fraction burnt
OFA	Open frontal area
OME	Polyoxymethylene dimethyl ethers (with the specific mixture fractions used in this study)
$OME_{(n)}$	Polyoxymethylene dimethyl ethers (of the chain-length n)
PCRF	Particle concentration reduction factor
PGM	Platinum group metals
PMP	Particle measurement programme
PN	Particle number
PN_{23}	Particle number emission, determined *via* CPC with a 50% cut-off at 23 nm
PN_{10}	Particle number emission, determined *via* CPC with a 50% cut-off at 10 nm
PN_{raw}	Particle number, determined at raw exhaust sampling position
$PN_{tailpipe}$	Particle number, determined at tailpipe exhaust sampling position

PSD	Particle size distribution
SCR	Selective catalytic reduction
SLPM	Standard liter per minute
SMPS	Scanning mobility particle sizer
std	Standard deviation
TDC	Top dead center
TEM	Transmission electron microscopy
UDP	Universal decomposition pipe
VPR	Volatile particle remover
WHSC	World harmonised steady-state cycle
WHTC	World harmonised transient cycle
λ	Air–fuel ratio

Author contributions

Alexander D. Gelner: conceptualization, data curation, formal analysis, investigation, methodology, project administration, software, validation, visualization, writing – original draft, writing – review & editing. Dieter Rothe: methodology, resources, supervision, validation, writing – original draft, writing – review & editing Carsten Kykal: methodology, validation, writing – review & editing. Martin Irwin: methodology, resources, validation, writing – original draft, writing – review & editing. Alessandro Sommer: conceptualization, validation, writing – review & editing. Christian Pastoetter: conceptualization, supervision, funding acquisition, project administration, writing – review & editing. Martin Härtl: funding acquisition, project administration, supervision, writing – review & editing. Malte Jaensch: writing – review & editing. Georg Wachtmeister: funding acquisition, project administration, supervision, writing – review & editing.

Conflicts of interest

The authors declare that they have no known competing financial interests or personal relationship that could have appeared to influence the work reports in this paper. The Catalytic Stripper was provided by Catalytic Instruments GmbH & Co. KG and their involvement with this study was on an advisory basis only and had no bearing on the outcomes achieved.

Acknowledgements

The project “Sub-Zero-Emissions Dieselmotor” (grant number AZ-1266-17) was funded by the Bavarian Research Foundation (BFS) and was carried out in collaboration with MAN Truck & Bus SE, VT Vitesco Technologies Emitec GmbH, Chair of Analytical Chemistry of TUM and ASG Analytik-Service AG. Their support is gratefully acknowledged. The authors also want to thank Catalytic Instruments GmbH & Co. KG for providing a Catalytic Stripper. Furthermore, the authors want to thank Mr Florian Lindner (MAN Truck & Bus SE) for his support in commissioning urea dosage and Mr Patrick Swarovsky (MAN Truck & Bus SE) for providing a 10 nm-CPC and consultation in this study.

References

1 *Climate Change 2014: Synthesis Report : [longer Report]*, ed. R. K. Pachauri and L. Meyer, Intergovernmental Panel on Climate Change, Geneva, Switzerland, 2015.
2 N. Gray, S. McDonagh, R. O'Shea, B. Smyth and J. D. Murphy, Decarbonising ships, planes and trucks: An analysis of suitable low-carbon fuels for the maritime, aviation and haulage sectors, *Advances in Applied Energy*, 2021, **1**, 100008.
3 S. Schemme, R. C. Samsun, R. Peters and D. Stolten, Power-to-fuel as a key to sustainable transport systems – An analysis of diesel fuels produced from CO_2 and renewable electricity, *Fuel*, 2017, **205**, 198–221.
4 J. Burger, M. Siegert, E. Ströfer and H. Hasse, Poly(oxymethylene) dimethyl ethers as components of tailored diesel fuel: Properties, synthesis and purification concepts, *Fuel*, 2010, **89**(11), 3315–3319.
5 M. Held, Y. Tönges, D. Pélerin, M. Härtl, G. Wachtmeister and J. Burger, On the energetic efficiency of producing polyoxymethylene dimethyl ethers from CO_2 using electrical energy, *Energy Environ. Sci.*, 2019, **12**(3), 1019–1034.
6 L. Pellegrini, M. Marchionna, R. Patrini, C. Beatrice, N. Del Giacomo and C. Guido, Combustion Behaviour and Emission Performance of Neat and Blended Polyoxymethylene Dimethyl Ethers in a Light-Duty Diesel Engine, in *SAE Technical Paper Series. SAE International400 Commonwealth Drive*, SAE Technical Paper Series, Warrendale, PA, United States, 2012.
7 L. Pellegrini, M. Marchionna, R. Patrini and S. Florio, Emission Performance of Neat and Blended Polyoxymethylene Dimethyl Ethers in an Old Light-Duty Diesel Car, in *SAE Technical Paper Series. SAE International400 Commonwealth Drive*, SAE Technical Paper Series, Warrendale, PA, United States, 2013.
8 M. Härtl, P. Seidenspinner, E. Jacob and G. Wachtmeister, Oxygenate screening on a heavy-duty diesel engine and emission characteristics of highly oxygenated oxymethylene ether fuel OME1, *Fuel*, 2015, **153**, 328–335.
9 S. E. Iannuzzi, C. Barro, K. Boulouchos and J. Burger, Combustion behavior and soot formation/oxidation of oxygenated fuels in a cylindrical constant volume chamber, *Fuel*, 2016, **167**, 49–59.
10 A. Damyanov, P. Hofmann, B. Geringer, N. Schwaiger, T. Pichler and M. Siebenhofer, Biogenous ethers: production and operation in a diesel engine, *Automot. Engine Technol.*, 2018, **3**(1–2), 69–82.
11 H. Ogawa, N. Miyamoto and M. Yagi, Chemical-Kinetic Analysis on PAH Formation Mechanisms of Oxygenated Fuels, in *SAE Technical Paper Series. SAE International400 Commonwealth Drive*, SAE Technical Paper Series, Warrendale, PA, United States, 2003.
12 D. Pélerin, K. Gaukel, M. Härtl, E. Jacob and G. Wachtmeister, Potentials to simplify the engine system using the alternative diesel fuels oxymethylene ether OME1 and OME3−6 on a heavy-duty engine, *Fuel*, 2020, **259**, 116231.

13 D. Pélerin, K. Gaukel, M. Härtl and G. Wachtmeister, Nitrogen Oxide Reduction Potentials Using Dimethyl Ether and Oxymethylene Ether in a Heavy-Duty Diesel Engine, in *SAE Technical Paper Series. SAE International400 Commonwealth Drive*, SAE Technical Paper Series, Warrendale, PA, United States, 2020.

14 B. Gaston, J. M. Drazen, J. Loscalzo and J. S. Stamler, The biology of nitrogen oxides in the airways, *Am. J. Respir. Crit. Care Med.*, 1994, **149**(2 Pt 1), 538–551.

15 C. J. L. Murray, A. Y. Aravkin, P. Zheng, C. Abbafati, K. M. Abbas, M. Abbasi-Kangevari, *et al.*, Global burden of 87 risk factors in 204 countries and territories, 1990–2019: a systematic analysis for the Global Burden of Disease Study 2019, *The Lancet*, 2020, **396**(10258), 1223–1249.

16 K. Li, L. Chen, S. J. White, K. Han, B. Lv, K. Bao, *et al.*, Effect of nitrogen oxides (NO and NO_2) and toluene on SO 2 photooxidation, nucleation and growth: A smog chamber study, *Atmos. Res.*, 2017, **192**, 38–47.

17 T. C. Bond, S. J. Doherty, D. W. Fahey, P. M. Forster, T. Berntsen, B. J. DeAngelo, *et al.*, Bounding the role of black carbon in the climate system: A scientific assessment, *J. Geophys. Res.: Atmos.*, 2013, **118**(11), 5380–5552.

18 D. B. Kittelson, Engines and nanoparticles, *J. Aerosol Sci.*, 1998, **29**(5–6), 575–588.

19 B. Giechaskiel, J. Vanhanen, M. Väkevä and G. Martini, Investigation of vehicle exhaust sub-23 nm particle emissions, *Aerosol Sci. Technol.*, 2017, **51**(5), 626–641.

20 B. Giechaskiel, T. Lähde and Y. Drossinos, Regulating particle number measurements from the tailpipe of light-duty vehicles: The next step?, *Environ. Res.*, 2019, **172**, 1–9.

21 J. Andersson, A. Mamakos and B. Giechaskiel. *Particle Measurement Programme (PMP) Heavy-Duty Inter-laboratory Correlation Exercise (ILCE_HD)*, Publications Office, Luxembourg, 2010, EUR (Luxembourg), vol. 24561.

22 Q. Lin, K. L. Tay, W. Yu, W. Yang and Z. Wang, Effects of polyoxymethylene dimethyl ether 3 (PODE3) addition and injection pressure on combustion performance and particle size distributions in a diesel engine, *Fuel*, 2021, **283**, 119347.

23 J. Liu, Z. Liu, L. Wang, P. Wang, P. Sun, H. Ma, *et al.*, Effects of PODE/diesel blends on particulate matter emission and particle oxidation characteristics of a common-rail diesel engine, *Fuel Process. Technol.*, 2021, **212**, 106634.

24 F. Ferraro, C. Russo, R. Schmitz, C. Hasse and M. Sirignano, Experimental and numerical study on the effect of oxymethylene ether-3 (OME3) on soot particle formation, *Fuel*, 2021, **286**, 119353.

25 T. Popp, R. Lechner, M. Becker, M. Hebauer, N. O'Connell and M. Brautsch, Potentials of OME/diesel blends for stationary power production – Improving emission characteristics of a diesel CHP unit, *Appl. Therm. Eng.*, 2019, **153**, 483–492.

26 G. Richter and H. Zellbeck, Oxymethylene Ethers as an Alternative for Passenger Car Diesel Engines, *MTZ Worldw.*, 2017, **78**(12), 60–67.

27 A. Omari, B. Heuser, S. Pischinger and C. Rüdinger, Potential of long-chain oxymethylene ether and oxymethylene ether-diesel blends for ultra-low emission engines, *Appl. Energy*, 2019, **239**, 1242–1249.

28 J. Preuß, K. Munch and I. Denbratt, Performance and emissions of renewable blends with OME3-5 and HVO in heavy duty and light duty compression ignition engines, *Fuel*, 2021, **303**, 121275.

29 C. Barro, M. Parravicini, K. Boulouchos and A. Liati, Neat polyoxymethylene dimethyl ether in a diesel engine; part 2: Exhaust emission analysis, *Fuel*, 2018, **234**, 1414–1421.

30 P. Dworschak, V. Berger, M. Härtl and G. Wachtmeister, Neat Oxymethylene Ethers: Combustion Performance and Emissions of OME 2 OME 3 OME 4 and OME 5 in a Single-Cylinder Diesel Engine, in *SAE Technical Paper Series. SAE International400 Commonwealth Drive*, SAE Technical Paper Series, Warrendale, PA, United States, 2020.

31 P. Dworschak, V. Berger, M. Härtl and G. Wachtmeister, Particle Size Distribution Measurements of Neat and Water-Emulsified Oxymethylene Ethers in a Heavy-Duty Diesel Engine, *SAE Int. J. Fuels Lubr.*, 2020, **13**(2), 187–203.

32 I. S. Abdul-Khalek and D. B. Kittelson, Real Time Measurement of Volatile and Solid Exhaust Particles Using a Catalytic Stripper, in *SAE Technical Paper Series. SAE International400 Commonwealth Drive*, SAE Technical Paper Series, Warrendale, PA, United States, 1995.

33 J. Swanson and D. Kittelson, Evaluation of thermal denuder and catalytic stripper methods for solid particle measurements, *J. Aerosol Sci.*, 2010, **41**(12), 1113–1122.

34 DIN/TS 51699, Fuels - polyoxymethylene dimethyl ether (OME): Draft German Standard.

35 *DIN EN 590:2017-10 - Automotive Fuels - Diesel: Requirements and Test Methods; EN 590*, Beuth Verlag GmbH, Berlin, 2017, 2013+A1.

36 L. Lautenschütz, D. Oestreich, P. Seidenspinner, U. Arnold, E. Dinjus and J. Sauer, Physico-chemical properties and fuel characteristics of oxymethylene dialkyl ethers, *Fuel*, 2016, **173**, 129–137.

37 S. K. Hoekman, A. Broch, C. Robbins, E. Ceniceros and M. Natarajan, Review of biodiesel composition, properties, and specifications, *Renewable Sustainable Energy Rev.*, 2012, **16**(1), 143–169.

38 C. Barro, M. Parravicini and K. Boulouchos, Neat polyoxymethylene dimethyl ether in a diesel engine; part 1: Detailed combustion analysis, *Fuel*, 2019, **256**, 115892.

39 *ISO 22241-1:2019 - Diesel engines - NOx reduction agent AUS 32: Part 1*, Quality requirements, 2019, (43.060.40 Fuel Systems) 2019-02.

40 S. D. Yim, S. J. Kim, J. H. Baik, I. Nam, Y. S. Mok, J.-H. Lee, *et al.*, Decomposition of Urea into NH_3 for the SCR Process, *Ind. Eng. Chem. Res.*, 2004, **43**(16), 4856–4863.

41 M. Koebel, M. Elsener and T. Marti, NO_x-Reduction in Diesel Exhaust Gas with Urea and Selective Catalytic Reduction, *Combust. Sci. Technol.*, 1996, **121**(1–6), 85–102.

42 K. Kamasamudram, C. Henry, N. Currier and A. Yezerets, N_2O Formation and Mitigation in Diesel Aftertreatment Systems, *SAE Int. J. Engines*, 2012, **5**(2), 688–698.

43 L. Tigges, A. Wiedensohler, K. Weinhold, J. Gandhi and H.-J. Schmid, Bipolar charge distribution of a soft X-ray diffusion charger, *J. Aerosol Sci.*, 2015, **90**, 77–86.

44 T. J. Johnson, R. T. Nishida, X. Zhang, J. P. Symonds, J. S. Olfert and A. M. Boies, Generating an aerosol of homogeneous, non-spherical particles and measuring their bipolar charge distribution, *J. Aerosol Sci.*, 2021, **153**, 105705.

45 D. B. Kittelson, W. F. Watts, J. C. Savstrom and J. P. Johnson, Influence of a catalytic stripper on the response of real time aerosol instruments to diesel exhaust aerosol, *J. Aerosol Sci.*, 2005, **36**(9), 1089–1107.

46 I. A. Khalek, Sampling System for Solid and Volatile Exhaust Particle Size, Number, and Mass Emissions, in *SAE Technical Paper Series. SAE International400 Commonwealth Drive*, SAE Technical Paper Series, Warrendale, PA, United States, 2007.

47 J. Swanson, D. Kittelson, B. Giechaskiel, A. Bergmann and M. Twigg, A Miniature Catalytic Stripper for Particles Less Than 23 Nanometers, *SAE Int. J. Fuels Lubr.*, 2013, **6**(2), 542–551.

48 S. Amanatidis, L. Ntziachristos, B. Giechaskiel, D. Katsaounis, Z. Samaras and A. Bergmann, Evaluation of an oxidation catalyst ("catalytic stripper") in eliminating volatile material from combustion aerosol, *J. Aerosol Sci.*, 2013, **57**, 144–155.

49 L. Ntziachristos, S. Amanatidis, Z. Samaras, B. Giechaskiel and A. Bergmann, Use of a Catalytic Stripper as an Alternative to the Original PMP Measurement Protocol, *SAE Int. J. Fuels Lubr.*, 2013, **6**(2), 532–541.

50 Y. Otsuki, K. Takeda, K. Haruta and N. Mori, A Solid Particle Number Measurement System Including Nanoparticles Smaller than 23 Nanometers, in *SAE Technical Paper Series. SAE International400 Commonwealth Drive*, SAE Technical Paper Series, Warrendale, PA, United States, 2014.

51 S. Amanatidis, L. Ntziachristos, P. Karjalainen, E. Saukko, P. Simonen, N. Kuittinen, *et al.*, Comparative performance of a thermal denuder and a catalytic stripper in sampling laboratory and marine exhaust aerosols, *Aerosol Sci. Technol.*, 2018, **52**(4), 420–432.

52 B. Giechaskiel, A. D. Melas, T. Lähde and G. Martini, Non-Volatile Particle Number Emission Measurements with Catalytic Strippers: A Review, *Vehicles*, 2020, **2**(2), 342–364.

53 S.-L. von de Weiden, F. Drewnick and S. Borrmann, Particle Loss Calculator – a new software tool for the assessment of the performance of aerosol inlet systems, *Atmos. Meas. Tech.*, 2009, **2**(2), 479–494.

54 W. C. Hinds, *Aerosol Technology: Properties, Behavior, and Measurement of Airborne Particles*, Wiley, 1999.

55 P. Kulkarni, P. A. Baron and K. Willeke, *Aerosol Measurement*, John Wiley & Sons, Inc, Hoboken, NJ, USA, 2011.

56 L. Talbot, R. K. Cheng, R. W. Schefer and D. R. Willis, Thermophoresis of particles in a heated boundary layer, *J. Fluid Mech.*, 1980, **101**(4), 737–758.

57 B. Y. Liu, D. Y. Pui, K. L. Rubow and W. W. Szymanski, Electrostatic effects in aerosol sampling and filtration, *Ann. Occup. Hyg.*, 1985, **29**(2), 251–269.

58 C. S.-J. Tsai, Characterization of Airborne Nanoparticle Loss in Sampling Tubing, *J. Occup. Environ. Hyg.*, 2015, **12**(8), D161–D167.

59 C. Asbach, H. Kaminski, Y. Lamboy, U. Schneiderwind, M. Fierz and A. M. Todea, Silicone sampling tubes can cause drastic artifacts in measurements with aerosol instrumentation based on unipolar diffusion charging, *Aerosol Sci. Technol.*, 2016, **50**(12), 1375–1384.

60 B. Giechaskiel, L. Ntziachristos and Z. Samaras, Effect of ejector dilutors on measurements of automotive exhaust gas aerosol size distributions, *Meas. Sci. Technol.*, 2009, **20**(4), 45703.

61 Office P, *Regulation No 49 of the Economic Commission for Europe of the United Nations (UN/ECE) — Uniform Provisions Concerning the Measures to Be Taken against the Emission of Gaseous and Particulate Pollutants from Compression-Ignition Engines and Positive Ignition Engines for Use in Vehicles*, 2013.

62 T. Rönkkö, L. Pirjola, L. Ntziachristos, J. Heikkilä, P. Karjalainen, R. Hillamo, *et al.*, Vehicle engines produce exhaust nanoparticles even when not fueled, *Environ. Sci. Technol.*, 2014, **48**(3), 2043–2050.

63 P. Karjalainen, L. Ntziachristos, T. Murtonen, H. Wihersaari, P. Simonen, F. Mylläri, *et al.*, Heavy Duty Diesel Exhaust Particles during Engine Motoring Formed by Lube Oil Consumption, *Environ. Sci. Technol.*, 2016, **50**(22), 12504–12511.

64 S. Blochum, F. H. Ruch, T. Bastuck, M. Härtl, R. Mittler and G. Wachtmeister, Identification of In-Cylinder Aerosol Flow Induced Emissions due to Piston Ring Design in a DISI Single Cylinder LV Engine Using Oxygenated Synthetic Fuels, in *SAE Technical Paper Series. SAE International400 Commonwealth Drive*, SAE Technical Paper Series, Warrendale, PA, United States, 2021.

65 L. Gren, V. B. Malmborg, J. Falk, L. Markula, M. Novakovic, S. Shamun, *et al.*, Effects of renewable fuel and exhaust aftertreatment on primary and secondary emissions from a modern heavy-duty diesel engine, *J. Aerosol Sci.*, 2021, **156**, 105781.

66 I. S. Abdul-Khalek, D. B. Kittelson, B. R. Graskow, Q. Wei and F. Bear, Diesel Exhaust Particle Size: Measurement Issues and Trends, in *SAE Technical Paper Series. SAE International400 Commonwealth Drive*, SAE Technical Paper Series, Warrendale, PA, United States, 1998.

67 I. A. Khalek, D. B. Kittelson and F. Brear, Nanoparticle Growth During Dilution and Cooling of Diesel Exhaust: Experimental Investigation and Theoretical Assessment, in *SAE Technical Paper Series. SAE International400 Commonwealth Drive*, SAE Technical Paper Series, Warrendale, PA, United States, 2000.

68 U. Mathis, J. Ristimäki, M. Mohr, J. Keskinen, L. Ntziachristos, Z. Samaras, *et al.*, Sampling Conditions for the Measurement of Nucleation Mode Particles in the Exhaust of a Diesel Vehicle, *Aerosol Sci. Technol.*, 2004, **38**(12), 1149–1160.

69 T. Rönkkö, A. Virtanen, J. Kannosto, J. Keskinen, M. Lappi and L. Pirjola, Nucleation mode particles with

a nonvolatile core in the exhaust of a heavy duty diesel vehicle, *Environ. Sci. Technol.*, 2007, **41**(18), 6384–6389.

70 J. I. Steinfeld, Atmospheric Chemistry and Physics: From Air Pollution to Climate Change, *Environment*, 1998, **40**(7), 26.

71 P. Karjalainen, T. Rönkkö, L. Pirjola, J. Heikkilä, M. Happonen, F. Arnold, *et al.*, Sulfur driven nucleation mode formation in diesel exhaust under transient driving conditions, *Environ. Sci. Technol.*, 2014, **48**(4), 2336–2343.

72 D. Rothe, M. Knauer, G. Emmerling, D. Deyerling and R. Niessner, Emissions during active regeneration of a diesel particulate filter on a heavy duty diesel engine: Stationary tests, *J. Aerosol Sci.*, 2015, **90**, 14–25.

73 A. Merkle, S. Kunkel and G. Wachtmeister, Analysis of the Mixed Friction in the Piston Assembly of a SI Engine, *SAE Int. J. Engines*, 2012, **5**(3), 1487–1497.

74 K. Arun Prasath, H. Bernemyr and A. Erlandsson, On the Effects of Urea and Water Injection on Particles across the SCR Catalyst in a Heavy - Duty Euro VI Diesel Engine, in *SAE Technical Paper Series. SAE International400 Commonwealth Drive*, SAE Technical Paper Series, Warrendale, PA, United States, 2020.

75 M. A. Robinson, J. Backhaus, R. Foley and Z. G. Liu, The Effect of Diesel Exhaust Fluid Dosing on Tailpipe Particle Number Emissions, in, *SAE Technical Paper Series. SAE International400 Commonwealth Drive*, SAE Technical Paper Series, Warrendale, PA, United States, 2016.

76 A. Mamakos, M. Schwelberger, M. Fierz and B. Giechaskiel, Effect of selective catalytic reduction on exhaust nonvolatile particle emissions of Euro VI heavy-duty compression ignition vehicles, *Aerosol Sci. Technol.*, 2019, **53**(8), 898–910.

77 S. Amanatidis, L. Ntziachristos, B. Giechaskiel, A. Bergmann and Z. Samaras, Impact of selective catalytic reduction on exhaust particle formation over excess ammonia events, *Environ. Sci. Technol.*, 2014, **48**(19), 11527–11534.

78 P. M. Schaber, J. Colson, S. Higgins, D. Thielen, B. Anspach and J. Brauer, Thermal decomposition (pyrolysis) of urea in an open reaction vessel, *Thermochim. Acta*, 2004, **424**(1–2), 131–142.

79 M. Börnhorst and O. Deutschmann, Advances and challenges of ammonia delivery by urea-water sprays in SCR systems, *Prog. Energy Combust. Sci.*, 2021, **87**, 100949.

80 J. Sun, W. Birmili, M. Hermann, T. Tuch, K. Weinhold, G. Spindler, *et al.*, Variability of black carbon mass concentrations, sub-micrometer particle number concentrations and size distributions: results of the German Ultrafine Aerosol Network ranging from city street to High Alpine locations, *Atmos. Environ.*, 2019, **202**, 256–268.

81 P. Dimopoulos Eggenschwiler and D. Schreiber, Investigation of the Oxidation Behavior of Soot in Diesel Particle Filter structures, in *SAE Technical Paper Series. SAE International400 Commonwealth Drive*, SAE Technical Paper Series, Warrendale, PA, United States, 2015.

82 J. Heikkilä, T. Rönkkö, T. Lähde, M. Lemmetty, A. Arffman, A. Virtanen, *et al.*, Effect of open channel filter on particle emissions of modern diesel engine, *J. Air Waste Manage. Assoc.*, 2009, **59**(10), 1148–1154.

83 S. Su, T. Lv, Y. Lai, J. Mu, Y. Ge and B. Giechaskiel, Particulate emissions of heavy duty diesel engines measured from the tailpipe and the dilution tunnel, *J. Aerosol Sci.*, 2021, **156**, 105799.

84 N. Palazzo, M. Kögl, P. Bauer, M. N. Mannazhi, L. Zigan, F. J. T. Huber, *et al.*, Investigation of Soot Formation in a Novel Diesel Fuel Burner, *Energies*, 2019, **12**(10), 1993.

85 C. Mcenally and L. Pfefferle, Improved sooting tendency measurements for aromatic hydrocarbons and their implications for naphthalene formation pathways, *Combust. Flame*, 2007, **148**(4), 210–222.

86 D. L. Bartholet, M. A. Arellano-Treviño, F. L. Chan, S. Lucas, J. Zhu, P. C. St. John, *et al.*, Property predictions demonstrate that structural diversity can improve the performance of polyoxymethylene ethers as potential bio-based diesel fuels, *Fuel*, 2021, **295**, 120509.

Gelner, A. D.; Beck, H. A.; Pastötter, C.; Härtl, M.; Wachtmeister, G.: *Ultra-Low Emissions of a Heavy-Duty Engine Powered with Oxymethylene Ether in Stationary and Transient Driving Conditions*; International Journal of Engine Research Vol. 23 (5), 2022, pp. 738-753. [187]

Ultra-low emissions of a heavy-duty engine powered with oxymethylene ethers (OME) under stationary and transient driving conditions

Author:
Alexander D Gelner, Harald A Beck, Christian Pastoetter, Martin Härtl, et al.

Publication: International Journal of Engine Research

Publisher: SAGE Publications

Date: 2021-09-23

Gratis Reuse

If you are a SAGE journal author requesting permission to reuse material from your journal article, please note you may be able to reuse your content without requiring permission from SAGE. Please review SAGE's author re-use and archiving policies at https://us.sagepub.com/en-us/nam/journal-author-archiving-policies-and-re-use for more information.

If your request does not fall within SAGE's reuse guidelines, please proceed with submitting your request by selecting one of the other reuse categories that describes your use. Please note, a fee may be charged for reuse of content requiring permission. Please submit a ticket through the SAGE Permissions Portal if you have questions.

BACK CLOSE WINDOW

International journal of engine research

Article: Ultra-low emissions of a heavy-duty engine powered with oxymethylene ethers (OME) under st...

GENERAL INFORMATION

Request ID	Request Date
600083707	13 Jun 2022
Request Status	Deny Reason
Denied	Permission may not be needed for this request

ALL DETAILS

COMMENTS

Add Comment / Attachment

18 Jun 2022 12:06:00 AM, by Publisher Representative

Thank you for your order. This use is covered under SAGE's journal author reuse policy (https://us.sagepub.com/en-us/nam/journal-author-archiving-policies-and-re-use) which allows you to include the published version of your article (version 3) in your dissertation or thesis, which may be posted in an Institutional Repository or database. Please note that this permission does not cover any 3rd party material that may be found within the work. You must properly credit the original source, SAGE Publications, Inc., referencing the original publication and linking to the appropriate DOI where possible. As permission is pre-approved, we will cancel this order. If you require formal written permission, please place an order via our Customer Permission Portal (https://jira.sagepub.com/servicedesk/customer/portal/9)

Kind regards,
The SAGE Permission Team

View Less

International Journal of ENGINE RESEARCH

Special Issue Article

International J of Engine Research
2022, Vol. 23(5) 738–753

DOI: 10.1177/14680874211047922
journals.sagepub.com/home/jer
SAGE

Ultra-low emissions of a heavy-duty engine powered with oxymethylene ethers (OME) under stationary and transient driving conditions

Alexander D Gelner[1], Harald A Beck[2], Christian Pastoetter[2], Martin Härtl[1] and Georg Wachtmeister[1]

Abstract

Polyoxymethylene dimethyl ethers (OME) are promising candidates as substitutes for fossil diesel fuel. A regenerative electricity-based production, using captured airborne carbon dioxide (CO_2) and hydrogen (H_2) from water electrolysis as reactants, provides a valuable contribution to the energy transition in mobile applications. Besides the possibility of carbon-neutral production, OME offer the advantage of a sootless combustion, which resolves the trade-off between soot and nitrogen oxides (NO_x) emissions, and supports the efforts of air pollution control. While the emission behaviour of OME-powered diesel engines in raw exhaust has been studied extensively, interactions between this exhaust and components of the after-treatment system are mainly unknown. This study contains investigations conducted using a urea dosing variation (alpha titration) on a heavy-duty engine in combination with a system for selective catalytic reduction (SCR). These investigations showed a lower NO_x reduction efficiency in OME operation in partial load operation compared with the one in fossil diesel operation. This can be attributed, among other reasons, to lower exhaust temperatures in OME operation. However, the high tolerance of OME to exhaust gas recirculation (EGR) compensates for this disadvantage because of the reduction of the raw NO_x emission level. The difference in SCR efficiency disappeared at a high load operation point. Additionally, the alpha titration revealed, that urea dosing decreases formaldehyde emission in the SCR system. A pre-conditioned WHSC and WHTC cycle demonstrated the potential of an OME engine with after-treatment in the form of a twin-dosing SCR system for ultra-low emissions. For the specific evaluation of the emissions during these test cycles, this study contains the detailed calculation of the required factors – so-called '*u*-values' – for OME exhaust according to the technical standard UN/ECE R49.

Keywords

OME, POMDME, internal combustion engine, exhaust after-treatment, SCR, alternative fuels, emissions, test cycles, WHSC, WHTC

Date received: 30 May 2021; accepted: 1 September 2021

Introduction

Climate change creates the need for reduction of anthropogenic carbon dioxide (CO_2) emissions.[1] In the transportation sector, alternative fuels based on biomass or an electricity-based synthesis (so-called e-fuels) may play an important role in the transition towards sustainable mobility solutions.[2] Starting with CO_2, the successive hydrogenation via hydrogen (H_2) from water electrolysis enables the formation of several hydrocarbon compounds with different oxidation stages. Among others, these include oxygenates such as aldehydes, ketones, alcohols, esters and ethers, as well as paraffinic fuels in general. These ideally carbon-neutrally produced fuels even enable a decrease in the greenhouse gas emissions of existing internal combustion engines. In addition, it is possible to use current storage and distribution infrastructure.[3] While some e-fuels show a similar combustion behaviour to their fossil counterpart, other alternatives provide advantages such as a

[1]Technical University of Munich (TUM), Munich, Germany
[2]MAN Truck & Bus SE, Nuremberg, Germany

Corresponding author:
Alexander D Gelner, Technical University of Munich, Schragenhofstraße 31, 80992 Munich, Germany.
Email: gelner@lvk.mw.tum.de

lower emission of pollutants. For diesel engines, many studies focus on long-chain polyoxymethylene dimethyl ethers (OME) as a blend candidate or even a substitute for fossil diesel.[4] They meet the requirements of both a carbon-neutral production,[5,6] and of air pollution control because the combustion in a diesel engine is soot-free.[7–12] The lack of intramolecular C–C bonds suppresses the formation of soot precursors like acetylene and polycyclic aromatic hydrocarbons[13] and therefore resolves the trade-off between soot and nitrogen oxide (NO_x) emissions. For this reason, OME show a high tolerance against exhaust gas recirculation (EGR) for an inner-engine NO_x reduction.[14] Even a stoichiometric operation without an increase of soot emission is possible.[12] While the emission behaviour of a diesel engine powered by short chain[15–17] and long-chain[9,11,12] OME has been studied sufficiently, interactions with after-treatment systems (ATS) are still somewhat unknown. Münz et al.[18] investigated the potential of a three-way-catalyst (TWC) on a single-cylinder research engine, powered with short-chain OME_1. Pöllmann et al.[19] studied the combination of a DOC and a TWC with long-chain OME in stoichiometric operation on a single-cylinder research engine. Studies on long-chain OME on complete systems, consisting of a full engine in combination with state-of-the-art ATS including a diesel oxidation catalyst (DOC), a diesel particulate filter (DPF) and a system for selective catalytic reduction (SCR) of NO_x emissions, are limited to passenger car systems.[20,21] They focus on regulated emissions in real driving cycles, but not on different effectivities of ATS components. Gelner et al.[22] demonstrated the contrary behaviour of fuel oxidation between OME and fossil diesel on a DOC of a heavy-duty engine, but focused on fuel dosing for after-treatment system heating. An additional study will evaluate the filtration activity of a DPF on a heavy-duty engine with ATS powered by OME, as well as the volatile and non-volatile particle size distribution and the effect of urea dosing on particle emissions.[23] The NO_x reduction effectivity of a SCR system on a lean-operated OME engine is still unknown. An incomplete combustion of OME produces formaldehyde (CH_2O),[12] which is toxic to the human body.[24] CH_2O also occurs in the exhaust gas composition of lean biogas engines[25] and several research studies provide information about the interactions of CH_2O in the ATS of these engines,[26,27] or in general.[28] Besides the oxidation on a DOC,[17,22] OME-powered diesel engines have not been studied sufficiently in this field. For this reason, this study observes the connection between urea dosing and a decrease in CH_2O in the SCR system of a heavy-duty engine, using a urea dosing variation, the so-called alpha titration. Moreover, a parallel investigation points out the NO_x reduction efficiency of the SCR system in OME and fossil diesel operation. Pre-conditioned stationary and transient test cycles demonstrate the potential of a heavy-duty OME engine with a twin-dosing SCR after-treatment system with a focus also on unregulated pollutant emissions.

Table 1. Physico-chemical properties of the tested fuels.

	Diesel	OME
Cetane number	> 51	69
Lower heating value in MJ/kg	42.6[30]	19.2
Boiling range in °C	170–390[30]	145–242
Flash point in °C	> 55	65
Density in kg/m^3	820–845	1,057
Oxygen content in % (w/w)	0–1[31] (with max. 7% (v/v) FAME)	45
Volumetric diesel equivalent ratio	1	1.75
Sulphur content in ppm	< 10	< 5
Kinematic viscosity in mm^2/s	2.0–4.5	1.082
Lubricity – HFRR at 60°C in μm	⩽460	320
Formaldehyde content in mg/kg	–	233

ASG Analytik-Service AG measured the values of OME. The values of diesel are from the standard EN 590,[32] except for the LHV and boiling range, which are from Lautenschütz et al.[30] and the oxygen content, with the calculation using values from Hoekman et al.[31] This calculation assumes that the FAME content consists of oleic acid.

Methodology

Tested fuels

Polyoxymethylene dimethyl ethers (OME) are oligomers with the structure $CH_3–O–(CH_2O)_n–CH_3$. n as the amount of oxymethylene groups is often used to abbreviate the respective molecule or a mixture of different OME. For example, $OME_{3–6}$ refers to a mixture of OME with three, four, five and six oxymethylene groups. In this study, the fuel used for the experiments contains various OME_n with major percentages of $n = 3–6$ (OME_3: 58%, OME_4: 29%, OME_5: 10%, OME_6: 2%). Additionally, the fuel contains 300 mg/kg each of butylated hydroxytoluene (BHT) as an antioxidant and a flow improver as additives. The mixture fulfils the standard M DIN TS 51699 for OME fuel[29] and will be simply abbreviated to OME in the following. For reference, diesel describes fossil fuel with a maximum content of 7% (v/v) fatty acid methyl esters (FAME) according to the standard EN 590[32]. Table 1 compares the physico-chemical properties of the fuels investigated. ASG Analytik-Service AG provided the OME fuel used and measured the values of the properties. Appendix Table A1 contains the respective standard of the measurement method used to determine each value. The values for diesel are largely from the fuel EN 590 standard. Where the standard does not provide information about a specific property, this value is taken from Lautenschütz et al.[30] The calculation of the oxygen content is based on the assumption that the FAME content consists of oleic acid, with the respective values from Hoekman et al.[31]

The OME mixture used contains about 45% (w/w) oxygen. This reduces the lower heating value (LHV) of

the fuel by a factor of 2.2 compared to fossil diesel. However, the higher density of OME compensates this in part, at a volumetric diesel equivalent ratio of

$$\frac{LHV_{Diesel}}{LHV_{OME}} \cdot \frac{\rho_{Diesel}}{\rho_{OME}} \cong 1.75. \quad (1)$$

The Cetane number of OME exceeds the requirements of the EN 590 standard, which is noticeable from an excellent ignitability, proven in previous studies.[12,33] The boiling range is similar to diesel, but with an initial boiling start and end at lower temperatures. The flash point of the OME mixture surpasses the value of EN 590. This allows the mixture to be stored and distributed in a similar way to fossil diesel. The lubricity of OME exceeds the requirement of the standard. However, the kinematic viscosity of OME is below the specification interval of the EN 590 standard. The sulphur content of OME is lower than 5 parts per million (ppm) and therefore reaches the lower limit of the determination standard for this value. Since formaldehyde is a reactant in the synthesis process of OME,[6] the fuel tested contains an amount of 233 mg/kg. The additivation with BHT prevents OME from decomposing, which results in increasing amounts of CH_2O in the fuel.

Test engine and after-treatment system

The characterisation of the behaviour of an SCR system in OME operation takes place on an MAN D2676LF51 heavy-duty six-cylinder engine. The engine has two modifications in OME operation: On the one hand, the high-pressure pump has adapted seals, in order to avoid incomparability of the sealing material in diesel operation, because both fuels differ in chemical polarity. On the other hand, the injectors in OME operation have higher nozzle flow rates in order to compensate for the reduced LHV. This is necessary to avoid longer injection durations on high-load points, which cause reduced efficiency due to an increase in the combustion duration.[33,34] Longer injection durations may also result in interactions between the fuel jet and the lubricating film when the piston reveals the liner during downward movement. Furthermore, the higher nozzle flow rate enables rail pressure to be reduced at low- and medium-load points, which results in lower NO_x emissions.[12,17] Table 2 shows the properties of the test engine used.

VT Vitesco Technologies Emitec GmbH provided the after-treatment system in this study. The system is modular, which allows several components to be removed or added. Table 3 contains the properties of the ATS components in downstream order of the construction. The so-called e-DOC contains a heating disc in front of the coated structure of the DOC for electrical heating. However, the experiments in this paper do not make use of this option since they focus on the behaviour of the SCR system and emissions in pre-conditioned test cycles. The system has two positions at which a doser injects the reducing agent for the SCR reaction in form of aqueous urea solution, which leads to the designation 'twin-dosing design'. This injection happens in a so-called Universal Decomposition Pipe (UDP). The conversion of urea to ammonia (NH_3) takes place in the downstream component, a titanium dioxide (TiO_2) coated hydrolysis catalyst.[35] Downstream, a copper-zeolite (CuZe) SCR catalyst reduces NO_x with the reducing agent NH_3.[36] For the demonstration using the test cycles, this SCR stage contains three discs of the catalytic monoliths, resulting in a volume of 21.5 dm^3. To characterise the behaviour in diesel and OME operation, this stage contains only two monolithic discs, resulting in a volume of 14.3 dm^3. The ammonia slip catalyst (ASC) oxidises excess ammonia after the SCR system selectively. This avoids the unselective oxidation to nitrous oxide (N_2O) in the DOC placed downstream.[37] This DOC does not contain any heating discs. The DPF is an uncoated Cordierite wall flow filter. The second UDP is followed by a mixer for the homogenisation of the ammonia in the exhaust. This supports the hydrolysis catalyst in the decomposition of the injected urea,[38] since the exhaust gas temperature is lower at the second stage. The second SCR stage ideally converts remaining NO_x emissions. For the demonstration using the test cycles, this SCR stage contains four discs of the catalytic monoliths, resulting in a volume of 28.8 dm^3. For the characterisation of the behaviour in diesel and OME operation, this stage contains only two monolithic discs, resulting in a volume of 14.3 dm^3. This stage does not have an ASC installed. The reduction of the SCR stages to two discs each allows the catalyst behaviour to be compared between the first and second stage during the characterisation.

Table 2. Properties of the test engine MAN D2676LF51.

Number of cylinders	6 (inline)
Bore	126 mm
Stroke	166 mm
Displacement	12,419 cm^3
Compression ratio	18:1
Power	294 kW
Number of valves per cylinder	4 (2 inlet/2 exhaust)
Charge	Two-stage waste-gate turbocharger
Exhaust gas recirculation	High-pressure and cooled
Injection system	Common rail (max. 1,800 bar)
Hydraulic nozzle flow rate	Diesel: 1,300 cm^3/30 s (at 100 bar) OME: 1,835 cm^3/30 s (at 100 bar)

The injectors in OME operation have a higher nozzle flow rate to reduce the combustion duration at high load points.

Test bench setup

Figure 1 shows a diagram of the test bench setup. The air from the test bench air supply passes through an

Table 3. Properties of the ATS components provided by VT Vitesco Technologies Emitec GmbH in downstream order.

Component	Catalytic coating	PGM in g/ft^3	cpsi	Diameter in mm	Length in mm	Volume in dm^3	Carrier material	Carrier structure	OFA* in %
e-DOC	Pt, Pd (1:1)	35	N/A	285.8	101.5	6.51	Metal	300/600 LS	82
Hyd	TiO_2	–	N/A	174.6	60	1.43	Metal	300/600 LSPE	89
SCR	CuZe	–	N/A	300	3 × 101.5	21.5	Metal	600 CS	79
ASC	Pt	3	300	300	90	6.4	Metal	E300	78
DOC	Pt, Pd (1:1)	35	300	300	150	10.6	Metal	300/600 LS	82
DPF	Uncoated	None	300	305	381	27.8	Cordierite	Symmetrical	83
Hyd	TiO_2	–	N/A	174.6	60	1.43	Metal	300 PE	89
SCR	CuZe	–	400	300	4 × 101.5	28.8	Metal	E400	77

The value of the Platinum Group Metals (PGM) density represents the total quantity of the precious metal content. Before the experiments in this study, the ATS had a mileage of about 400 km in diesel operation.*The value of the open frontal area (OFA) is based on the following assumptions: coating of the DOC is 150 g/dm^3, coating of the UDP is 60 g/dm^3 and coating of the SCR is 200 g/dm^3, with a wash-coat density of 1.35 g/cm^3.

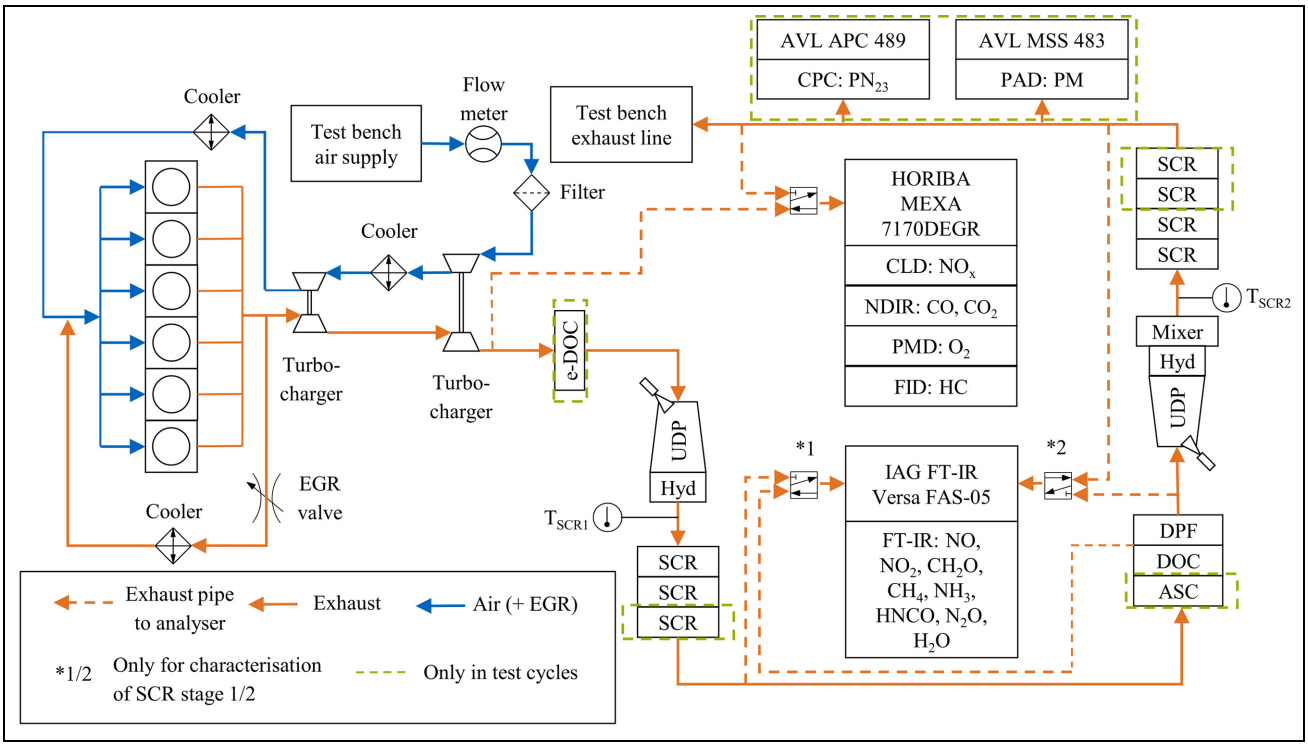

Figure 1. Test bench setup. For the characterisation of the SCR system via alpha titration, the e-DOC and ASC are removed and the SCR stages are reduced to two monolithic discs each. During the experiment with the alpha titration at the first stage, the FT-IR switches between the two sampling points marked with *1, at the second stage, it switches between the sampling points marked with *2. During the test cycles, both exhaust gas analysers extract from the tailpipe sampling position.

ABB MDM DN150 thermal dispersion mass flow meter, which determines the volumetric airflow to calculate the exhaust mass flow. Downstream, a filter avoids the contamination of the turbocharger. An intercooler reduces the temperature of the compressed air. A second turbocharger with another intercooler increases the boost pressure. The six-cylinder engine has a high-pressure EGR with intercooling, controlled by an EGR valve. Downstream of the second turbocharger, an electrically heatable DOC oxidises species in the exhaust. In this study, the heating function via electricity remains unused. Furthermore, for the characterisation of the SCR system, this e-DOC is removed in order to generate different CH_2O emission levels in the SCR stages. The UDP contains an EMITEC 'JC-2' urea doser and the hydrolysis catalyst. This component provides the reducing agent NH_3 for the SCR of NO_x on the catalytic surface of the following SCR stage. During the test cycles, this stage contains three monolithic discs, while during the alpha titration, the stage is reduced to two discs. The ASC downstream of this stage also is not equipped during the alpha titration. A

second DOC also oxidises species in the exhaust, while the DPF filters particles. The second UDP is equipped with an EMITEC 'A^2-8' urea doser. An EMITEC 'GEN V' urea dosing pump provides the delivery pressure for both dosers simultaneously. The second SCR stage contains four monolithic discs during the test cycles and two discs during the alpha titration. Two thermocouples of Type K, each downstream of the hydrolysis catalyst, enable the monitoring of the specific exhaust temperature upstream of the SCR catalysts. The HORIBA MEXA-7170DEGR exhaust gas analyser allows pollutants to be determined using the following components. A chemiluminescence detector (CLD) measures NO_x emissions; a nondispersive infrared sensor (NDIR) determines the concentration of carbon monoxide (CO). This analyser also measures the CO_2 concentration at the air intake of the cylinder head and downstream of the engine in order to determine the EGR rate. A paramagnetic detector (PMD) is used for the determination of the oxygen content and a flame ionisation detector (FID) displays the concentration of hydrocarbon emissions (HC) in the exhaust. The specific term of HC emissions is used for the emissions displayed by the FID in this study according to the technical standard UN/ECE Regulation No. 49.[39] When a comparison of this respective value takes place between diesel and OME operation, it is important to consider that the specific response factor of the partially oxidised fuel fragments in OME operation may be lower than in diesel operation because they are assumed to contain mostly oxygen.[40–43] The measurement device has two sampling points, located downstream of the second turbocharger and tailpipe, which means downstream of the second SCR stage. A 3/2-directional control solenoid valve makes it possible to switch between these sampling points. An IAG Versa FAS-05 Fourier-transform infrared spectrometer (FT-IR) is calibrated to determine specific emissions monitored in previous studies.[12,16] These are methane (CH_4) and formaldehyde (CH_2O). Additionally, the device measures NH_3, NO and nitrogen dioxide (NO_2), as well as isocyanic acid (HNCO) because of its health effects[44,45] and its function as pre-cursor of deposits due to the incomplete hydrolysis of urea in the SCR system. The device also determines nitrous oxide (N_2O) because of its climate relevance.[1] Moreover, the FT-IR enables the measurement of the water (H_2O) content in the exhaust gas. The method implemented does not include the determination of the species hydrogen cyanide (HCN), which Zengel et al.[27] and Elsener et al.[28] observed during the NO_x removal via SCR with NH_3 in the presence of CH_2O. Nevertheless, during the test cycles a recording of the specific FT-IR spectra enabled a retrospective evaluation. Therefore, the test runs of the test cycles include this respective emission value and additionally values of OME_n emissions. The sampling points of the FT-IR differ between the test runs for characterisation of the first and second SCR stage. For the first stage, the points are located downstream of the first SCR stage and downstream of the DOC, while for the second stage, they are located downstream of the DPF and tailpipe. For both setups, another 3/2-way solenoid valve enables switching during the experiment. During the test cycles, an AVL Advanced Particle Counter 489 (APC) determines the particle number (PN) emission with a condensation particle counter (CPC) and a sampling system according to the requirements of the Particle Measurement Programme.[46] An AVL Microsoot Sensor 483 (MSS) determines the soot mass, using a photoacoustic detector (PAD).[47] This value is representatively referred to as Particulate Matter (PM) in the following, since the aim is to highlight the soot reduction potential of OME. However, it is important to take into account that this value contains only black carbon in this study.

In order to determine the fuel mass flow, the fuel supply system has a DFM DR 50.02 impeller counter. The value of this device and the flow meter in the air path of the test bench add up to the value of the exhaust mass flow according to the following formula:

$$\dot{m}_{Exh} = \dot{V}_{Fuel} \cdot \rho_{Fuel} + \dot{m}_{Air}. \quad (2)$$

While the mass flow meter in the air path provides this value directly, the impeller counter provides only a volumetric flow. Therefore, this figure must be multiplied by the density of the respective fuel. In OME operation, the value from Table 1 is used. In diesel operation, the reference value of the density is 835 kg/m^3.

Alpha titration and operating points

The characterisation of the SCR system in OME and diesel operation uses an alpha titration. α describes the ratio of the injected amount of urea and the required amount for the total removal of the present NO_x concentration in the exhaust. Alpha titration investigates the conversion efficiency of the system by a successive increase of α. The main reactions inside the SCR system are as follows:

$$4NO + 4NH_3 + O_2 \rightarrow 4N_2 + 6H_2O^{36}, \quad (3)$$

$$6NO_2 + 8NH_3 \rightarrow 7N_2 + 12H_2O^{48}, \quad (4)$$

$$NO + NO_2 + 2NH_3 \rightarrow 2N_2 + 3H_2O^{48}. \quad (5)$$

Reaction (3) is designated as Standard-SCR, reaction (4) is designated as NO_2-SCR and reaction (5) is designated as Fast-SCR. However, since the NO_2/NO_x ratio rarely surpasses 50% even after the NO has been oxidised inside the DOC, Standard-SCR and Fast-SCR are assumed to account for the majority of the reactions. In that case, the stoichiometric ratio of NH_3 to NO_x is assumed to be 1 to 1 in this work. Besides these main reactions, further chemical processes happen as side reactions inside the SCR system, leading to the formation of ammonium nitrate at temperatures below 180°C[48] and N_2O.[49] These are neglected in the

Table 4. Operating points for the alpha titration.

Fuel	Diesel			OME		
Load point	*L*1	*L*2	*L*3	*L*1	*L*2	*L*3
Engine speed in rpm	1,200	1,100	2,000	1,200	1,100	2,000
Break mean effective pressure in bar	8	18	8	8	18	8
Rail pressure in bar	1,330	1,190	1,800	1,150	990	1,640
λ	1.6	1.4	2.3	1.8	1.5	1.9
EGR rate in % (w/w)	32	20	33	32	18	43
T_{SCR1} in °C	320	400	290	280	365	260
T_{SCR2} in °C	290	370	275	260	345	250
$\dot{m}_{Exh}$ in kg/h	465	800	1,070	525	870	1,040
sv in 1/h	25,200	43,270	57,870	28,390	47,050	56,245
$NO_{x,Engine,out}$ in ppm (CLD)	380	1,075	460	240	660	235
NO_2/NO_x upstream of SCR_2	0.51	0.42	0.30	0.30	0.35	0.24
CH_2O upstream of SCR_1 in ppm	0	0	0	25	17	22
CH_2O upstream of SCR_2 in ppm	0	0	0	12	1	11

The engine lambda probe determines the air-fuel ratio λ. The gravimetric EGR rate is calculated via the CO_2 concentration upstream and downstream of the engine, determined by the NDIR. The calculation of the space velocity (sv) uses the exhaust mass flow according to formula (2), the volume of the SCR catalyst with two monolithic discs according to Table 3 and the density of exhaust gas of 1.293 kg/m^3 according UN/ECE R49.[39] The CLD determines the value of the engine-out NO_x emissions. The NO_2/NO_x ratio upstream of SCR_1 is lower than 1% at every operating point.

calculation of the amount of urea required during the alpha titration. Depending on the desired α, the urea mass flow is calculated as follows:

$$\dot{m}_{Urea} = \frac{\phi_{NO_x} \cdot \dot{m}_{Exh} \cdot M_{Urea}}{w_{Urea,\,AdBlue} \cdot \rho_{Exhaust} \cdot V_m \cdot r_{NH_3,\,Urea}} \cdot \alpha. \quad (6)$$

ϕ_{NO_x} describes the respective value of the volumetric NO_x concentration determined by the CLD in ppm. $\dot{m}_{Exh}$ is the exhaust mass flow according to formula (2). M_{Urea} is the molar mass of urea, assumed to be 60.06 g/mol.[50] $w_{Urea,\,AdBlue}$ describes the mass fraction of urea within the solution used, marked as AdBlue®, which is 32.5%.[51] $\rho_{Exhaust}$ is the density of the exhaust gas, estimated as 1.293 kg/m^3 according to UN/ECE R49.[39] V_m describes the molar volume of an ideal gas with a value of 22.414 l/mol and $r_{NH_3,\,Urea}$ is the molar ratio of NH_3 in urea, with a value of 2.

The alpha titration starts with an α of 0.8. Before the test procedure starts, the SCR system is purged at operating point *L*2. The successive increase of α happens without the SCR system being cleared out. After a stationary operating status with fluctuations less than 5 ppm of NO_x emission value has been reached at both sampling points, the recording is taken three times at 1 Hz over 30 s. On the other hand, a switch to another operating point includes the cleaning process. If the value of the NH_3 concentration downstream of the SCR exceeds 10 ppm, the titration ends for this operating point. The experiments start with the characterisation of the system in diesel operation. First, the alpha titration takes place at the first SCR stage with the FT-IR sampling points switched to the specific location pointed out in Figure 1. During titration, the urea doser of the second stage is switched off. The characterisation uses three stationary operating points in the respective order of their enumeration, as Table 4 shows. The alpha titration in diesel operation happens twice in order to evaluate on reproducibility.

The space velocity sv results from

$$sv = \frac{\dot{m}_{Exh}}{\rho_{Exh} \cdot V_{SCR}}. \quad (7)$$

After the characterisation of the first SCR stage, the experiment continues with the second stage, combined with the change of the sampling positions of the FT-IR. During these test runs, the first urea doser remains unused. For the switch from diesel to OME operation, a flush of the fuel system and several test cycles remove diesel residues. Moreover, the injector configuration changes to a setup with higher nozzle flow rates in OME operation. Additionally, the DPF is regenerated in an oven at 500°C for 6 h, as the DPF built up a soot layer in diesel operation. The SCR system is characterised in OME operation in the same chronological order as in diesel operation, starting with the first stage after a purge run. Table 4 provides the parameters of the operating points in diesel and OME operation. *L*1 represents an operating point with an effective power of 100 kW, *L*2 is a high-load point at moderate engine speed and *L*3 represents an operating point with a high space velocity due to high engine speed in combination with a low exhaust temperature. The exhaust temperatures upstream of the SCR stages are lower in OME operation for every operating point, while the space velocity is higher, except for *L*3. However, the exhaust temperatures exceed the light-off temperature of CuZe-catalysts.[52] The higher space velocity in OME operation is due to the higher fuel mass flow, which is necessary to compensate for the lower LHV. This, in turn, ensures a higher intake air mass flow rate due to a higher enthalpy flow rate through the turbine of the turbochargers. The engine's

lambda probe determines the air-fuel-ratio λ. The adjustment of λ happens via EGR rate, which influences the intake air flow. The NO_2/NO_x ratio in the raw exhaust is $< 1\%$ for every operating point with both fuels. For this reason, the Fast-SCR reaction plays no role in the NO_x reduction at the first SCR stage.

Test cycles

The test cycles used to demonstrate the potential of the system presented for low pollutant emissions are the World Harmonized Stationary Cycle (WHSC) and the World Harmonized Transient Cycle (WHTC), in accordance with UN/ECE Regulation No. 49 (R49).[39] Contrary to the requirements of this regulation, the test cycles in this study start after pre-conditioning at the operating point *L*2. This measure replaces the preconditioning before the WHSC according to R49 and the cold run of the WHTC. Since the modular aftertreatment system consists of the monolithic discs, connected via flanges and pipes, the heat losses are higher than with standard integration in a thermally insulated silencer. Therefore, an evaluation of the emission potential in this study is limited to the pre-conditioned after-treatment system. The effects of OME on the behaviour in cold-start operation will be presented in a later publication.[53]

Contrary to the experiments of the alpha titration, the urea dosing is active at both SCR stages during the test cycles. The dosing strategy is based on an ideal distribution between the two stages, in consideration of the temperature, the ammonia storage capacity and the determined NO_x concentrations in the exhaust.

Calculation of u-values in OME operation

The comparison of emissions during the test cycles with the limit value stipulated by the Euro VI legislation requires the emissions to be specifically evaluated. According to UN/ECE R49, this evaluation is based on the multiplication of the integrated values over the cycle with specific factors, so-called '*u*-values', depending on the density of the exhaust. The R49 provides *u*-values for several fuels, but not for OME. Therefore, the *u*-values must be calculated in OME operation. This calculation can be used in future work for OME according to DIN SPEC 51699. The *u*-value $u_{gas,i}$ of the specific emission i is calculated as follows, using the density of the specific gas component $\rho_{gas,i}$ in kg/m^3 and the density of the exhaust gas ρ_e in kg/m^3:

$$u_{gas,i} = \frac{\rho_{gas,i}}{\rho_e \cdot 1000}. \tag{8}$$

While the standard R49 provides the densities of NO_x and CO, the density of HC depends on the respective fuel. It is defined as the ratio of the molar mass $M_{\text{gas, i}}$ of the component i in g/mol and the molar volume of an ideal gas of 22.414 l/mol according to Avogadro's law:

$$\rho_{gas,i} = \frac{M_{gas,i}}{22.414 \frac{l}{mol}}. \tag{9}$$

The values according to the fuel certificate of the OME fuel used result in a substitute molecule of $C_xH_yO_z$ with $x = 5.53$, $y = 13.45$ and $z = 4.43$. The conversion of the substitute molecule into a carbon-normalised molecule with the formula $CH_\upsilon O_\zeta$ gives rise to the molecule $CH_{2.432}O_{0.801}$. Using the atomic masses of C, H and O according to R49, the calculation of the molar mass of the normalised substitute molecule results in:

$$\begin{aligned} M_{OME} = 12.011 \frac{g}{mol} + \upsilon \cdot 1.00794 \frac{g}{mol} \\ + \zeta \cdot 15.9994 \frac{g}{mol} = 27.2778 \frac{g}{mol}. \end{aligned} \tag{10}$$

According to formula (9), this results in a density of HC of 1.2170 kg/m^3 in OME operation.

The calculation of the density of the exhaust gas $\rho_{e,i}$ again requires the substitute molecule being converted into a carbon-normalised molecule with the formula $CH_{2.432}O_{0.801}$. Furthermore, the stoichiometric air to fuel ratio A/F_{st} in OME operation must also be determined. This value is calculated according from formula (11) according to R49, assuming that the fuel does not contain sulphur or nitrogen:

$$\begin{aligned} \frac{A}{F_{st}} = \frac{138 \cdot \left(1 + \frac{\upsilon}{4} - \frac{\zeta}{2}\right)}{12.011 + 1.00794 \cdot \upsilon + 15.9994 \cdot \zeta}. \\ = 6.1088 \frac{kg}{kg} \end{aligned} \tag{11}$$

The depicted *u*-values of the emissions refer to the conditions with λ = 2 and dry air at a temperature of 273 K and a pressure of 101.3 kPa. The calculation of the exhaust gas density ρ_e for these specific conditions according to the formula

$$\rho_e = \frac{1000 + 1000 \cdot \frac{q_{mf}}{q_{mad}}}{773.4 + k_{f,w} \cdot 1000 \cdot \frac{q_{mf}}{q_{mad}}}; [\rho_e] = \frac{kg}{m^3}. \tag{12}$$

requires the ratio of the fuel mass flow rate q_{mf} in kg/h to the intake air mass flow rate on a dry basis q_{mad} in kg/h. Under the condition of λ = 2, this ratio equals $\frac{1}{2 \cdot A/F_{st}}$. Furthermore, the calculation requires the fuel-specific factor of wet exhaust $k_{\text{f,w}}$, which is calculated according to the formula given:

$$k_{f,w} = 0.055594 \cdot w_\upsilon + 0.0070046 \cdot w_\zeta. \tag{13}$$

w_υ is the mass fraction of hydrogen in %, which is 8.99 for the OME used. w_ζ is the mass fraction of oxygen in %; for the OME used this equals 46.98 according to the atomic weights given, and the substitute molecule. Inserted in formula (13), this results in a factor of $k_{\text{f,w}} = 0.8287$.

Inserted in formula (13), the density of the exhaust in OME operation equals 1.2860 kg/m^3 with λ = 2, dry air at a temperature of 273 K and a pressure of 101.3 kPa.

Table 5. Calculated *u*-values of OME exhaust according to the formulas given in R49 and the respective *u*-values in diesel operation.

Fuel	ρ_e in kg/m^3	Gas		
		NO_x	CO	HC
			$\rho_{gas,i}$ in kg/m^3	
		2.053	1.250	1.217**
			$u_{gas,i}$***	
Diesel (B7)*	1.2943	0.001586	0.000966	0.000482
OME	1.2860	0.001596	0.000972	0.000946

*Diesel (B7) indicates that the fuel contains up to 7% (v/v) FAME.
**For the carbon-normalised substitution molecule of OME with the molecular structure $CH_{2.432}O_{0.801}$.
***At $\lambda = 2$, dry air at a temperature of 273 K and a pressure of 101.3 kPa.

Table 6. Calculated *u*-values of OME exhaust according to the formulas given in R49.

Fuel	ρ_e in kg/m^3	Gas		
		NH_3	N_2O	CH_2O
			$\rho_{gas,i}$ in kg/m^3	
		0.7598	1.9636	1.3396
			$u_{gas,i}$**	
OME	1.2860	0.000591	0.001527	0.001042

**At $\lambda = 2$, dry air at a temperature of 273 K and a pressure of 101.3 kPa.

Using formula (8), the calculated values result in the *u*-values for OME operation, given in Table 5.

Furthermore, this study contains a specific evaluation of the unregulated emissions NH_3, N_2O and CH_2O. Table 6 contains the *u*-values for these emissions in OME operation according to this calculation using formula (8) to (13).

Results and discussion

SCR efficiency

The NO_x conversion rate of an SCR system depends on several factors. A higher conversion rate is mainly caused by higher exhaust temperatures, predominant reactions according to the Fast-SCR mechanism, higher residence times on the catalytic surface and lower raw emission levels. Figure 2 contains the results of the alpha titration at both SCR stages. The procedure stops after the NH_3 slip exceeds the termination criterion of 10 ppm. The reproducibility run in diesel operation shows a maximum deviation of 5% in NO_x conversion for load point *L*1, 1% for *L*2 and 5% for *L*3.

At the load points *L*1 and *L*3, the SCR shows lower NO_x conversion rates in OME operation, although the engine-out NO_x level is lower. This is mainly due to lower exhaust temperatures in OME operation at both stages. The space velocity is also higher in OME operation at *L*1, which results in lower retention times. It is slightly lower at *L*3 than in diesel operation, but at the second SCR stage, the NO_2/NO_x ratio is lower, which reduces the amount of NO_2 available for the Fast-SCR reaction. Although the exhaust temperature upstream of the SCR stages is lower in OME operation, it exceeds

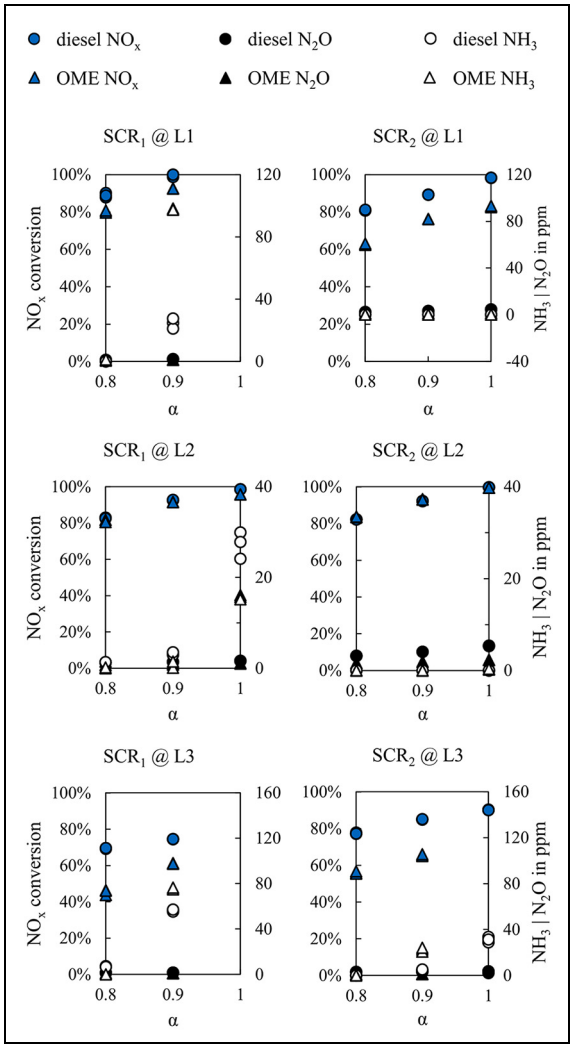

Figure 2. NO_x conversion, ammonia slip and nitrous oxide emission of the alpha titration in diesel and OME operation for both SCR stages at the operating points. The standard deviation for each point is less than 1% in NO_x conversion and 1 ppm for NH_3 and N_2O.

the light-off temperature for NO_x conversion of CuZe-catalysts.[52,54] However, the connection between the lower exhaust temperature in OME operation and the reduced NO_x conversion is evident at both operating points. The difference is 25°C–40°C between OME and diesel operation for both SCR stages. At the high-load

point *L*2, the temperature difference does not result in a lower NO_x conversion efficiency in OME operation, nor does the higher space velocity and the lower NO_2/NO_x ratio at the second SCR stage.

Elsener et al.[28] revealed the reduction of NO_x conversion efficiency in the presence of 300 ppm CH_2O at a vanadium oxide SCR catalyst. Table 4 shows that the CH_2O concentration in OME operation upstream of the SCR stages is higher than 10 ppm for every operating point except *L*2, where the high exhaust temperature leads to a nearly total oxidation of CH_2O in the DOC. Therefore, the NO_x conversion rate may also be affected by the CH_2O concentration in OME operation. Because of the lower concentration levels in this work compared to in the study by Elsener et al.[28] this effect is assumed to be less pronounced in the presented results. Nevertheless, measures are necessary to reduce tailpipe NO_x emissions in OME operation with an SCR system according to the results presented in Figure 2. One effective method for this is a reduction of the raw NO_x emission by applying the injection[12,34] or increasing the EGR rate.

Furthermore, Figure 2 reveals the effect of a mixer on the ammonia slip over the SCR system: While the first SCR stage without a mixer reaches the termination condition of a NH_3 slip of 10 ppm before a conversion rate of 100% at every load point, the second SCR stage does not reach this limit except for *L*3. The emission of N_2O is lower than 10 ppm at both stages with both fuels. This is due to the set α lower than 1, resulting in low ammonia storage levels. However, since it is not possible to synchronise the boundary conditions temperature, space velocity, NO_2/NO_x ratio and NO_x concentration in the raw exhaust on a heavy-duty engine, further investigations are needed to characterise the exact behaviour of the SCR system in diesel and OME operation. Nevertheless, the observed ammonia slip requires an installation of an ASC before the DOC in order to avoid the unselective oxidation of NH_3 to N_2O. Since the aim of this study is to demonstrate the emission potential of OME operation, the system for the experiments using the test cycles contains an ASC upstream of the DOC. Moreover, the soot-free combustion of OME enables a higher α at the first SCR stage, since a lower NO_2 concentration is necessary for the passive regeneration of the DPF.[55] This and an increase in the EGR rate without a subsequent soot increase compensates for the lower activity of the SCR system. However, the first stage still has to provide a NO_x slip in order to prevent the removal of stored ammonia from the second stage in dynamic operation with increasing exhaust temperature due to a NO_x conversion of 100% at the first stage.

Avoidance of hydrogen cyanide emission

Figure 3 shows the decrease of formaldehyde in the SCR system during the alpha titration. These results confirm the conclusion drawn by Bertole[26] and Elsener et al.[28] that the injection of urea and therefore NH_3 leads to a reduction in CH_2O emission. The CH_2O concentrations upstream and downstream of the SCR systems without urea dosing differ by only 1 ppm, which means that the reduction by the catalysts without the SCR reaction is marginal. At operating point *L*2, the DOC between the two SCR stages oxidises formaldehyde completely.

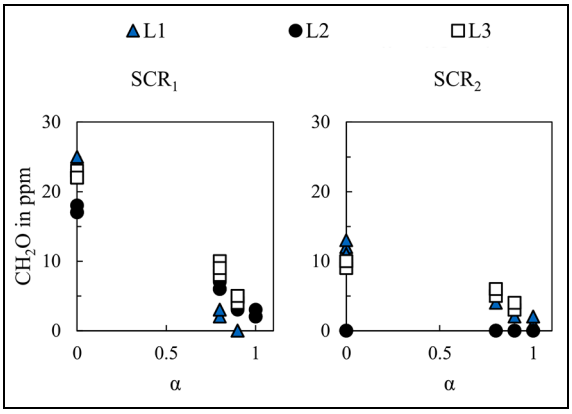

Figure 3. Reduction of formaldehyde during the alpha titration. The standard deviation for each point is less than 1 ppm.

Zengel et al.[27] and Elsener et al.[28] confirmed the formation of toxic[56] hydrogen cyanide in the presence of CH_2O in the SCR system. The highest yields of HCN occurred in the absence of water via formation over a formic acid pathway and at high temperatures via formation over a formaldehyde pathway at V_2O_5/WO_3-TiO_2-catalysts.[28] As the exhaust gas of the OME engine contains water concentrations around 10% (v/v), the formation via formic acid is negligible in the present study.

In order to avoid the emission of HCN, an oxidative catalyst downstream of the SCR system is necessary to prevent HCN from entering the environment.[57] Another possibility in order to avoid HCN formation is to install an oxidative catalyst upstream of the SCR system in order to oxidise CH_2O emission. As both options require exhaust temperatures above the light-off temperature of the oxidative catalysts, the emission of HCN during cold-start operation may occur. Although the formation of ammonium nitrate prevents urea dosing during cold start operation,[49] stored ammonia[58] may play a role in the formation of HCN. An investigation into the interactions of the components of the ATS during cold-start operation is necessary and therefore forms the scope of further investigations.[53] For the test runs using the preconditioned WHSC and WHTC cycle, the additional e-DOC upstream of the first SCR stage is installed in order to oxidise CH_2O emission and prevent HCN formation.

Emissions during pre-conditioned WHSC in OME operation

Since Figure 2 reveals the lower NO_x conversion efficiency of the SCR system in OME operation, it becomes necessary to reduce the raw emission level.

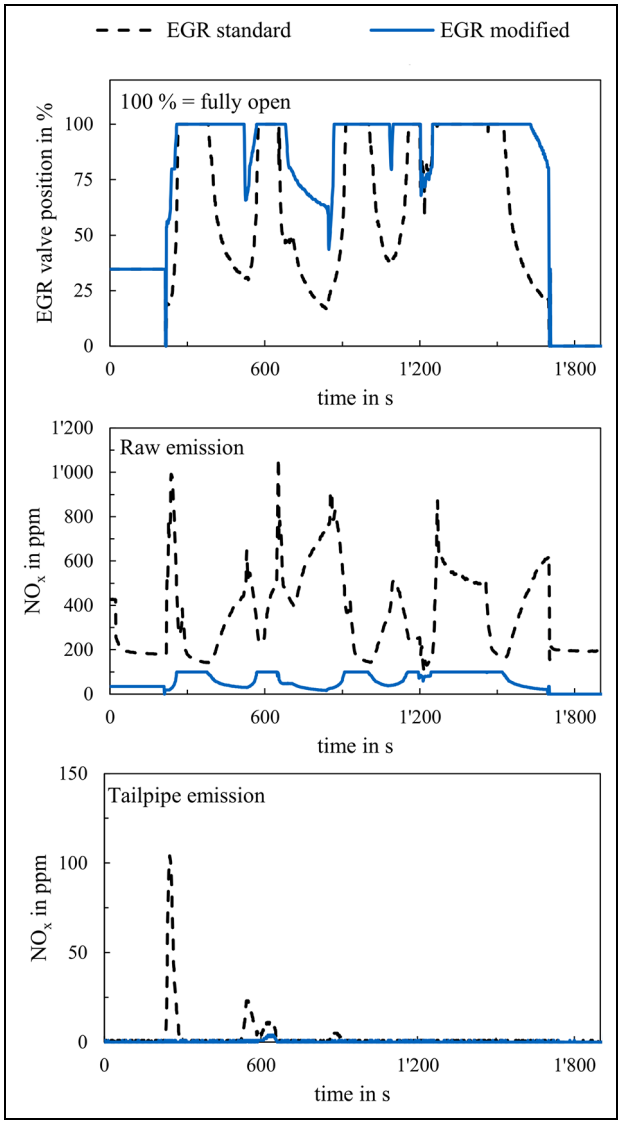

Figure 4. EGR valve position and NO_x emissions in the raw exhaust and tailpipe during the WHSC with the standard EGR application and a modified EGR application for OME operation. The engine NO_x sensor provides the raw emission values, and the CLD provides the tailpipe values.

Previous studies demonstrated the effect of high EGR rates for NO_x reduction in OME operation without an increase in soot emissions.[11,12,14] Therefore, the following investigation is dedicated to this approach. Figure 4 compares the NO_x emissions of two EGR applications in OME operation during the WHSC. The engine NO_x sensor provides the values of raw emission levels, and the CLD provides the values of the tailpipe emission levels. Since the deviation between NO_x sensor and CLD is less than 4% in diesel operation and less than 5% in OME operation during the experiments using the alpha titration, the comparison of these two values is valid. While the EGR standard application uses the λ map of the diesel application, including the limitation of the so-called smoke limit, the EGR modified application enables the EGR valve to open faster and further. The modified EGR application reduces the engine's raw NO_x emissions. This reduces the level of NO_x raw emissions by approximately 46% compared to diesel operation. This leads to a nearly total conversion of NO_x in the ATS, and therefore to lower-level tailpipe emissions.

Table 7. Emissions during pre-conditioned WHSC with modified EGR application.

	Result of test cycle	Euro VI limit
Emission		
CO (NDIR) in mg/kWh	0.23	4,000
NO_x (CLD) in mg/kWh	8.67	460
HC (FID) in mg/kWh	0.02	160
PM (PAD) in mg/kWh	0.027	10*
PN_{23} (CPC) in 1/kWh	9.75×10^9	8×10^{11}
NH_3 (FT-IR) in ppm	0.1	10
Unregulated emissions		
CH_4 (FT-IR) in ppm	0.0	–
CH_2O (FT-IR) in mg/kWh	0.97	–
N_2O (FT-IR) in mg/kWh	22.58	–
HNCO (FT-IR) in ppm	1.1	–
NH_3 (FT-IR) in mg/kWh	0.405	–
HCN (FT-IR) in ppm	0.1	–
$OME_{0,1,2,3,4}$ in ppm	< 1	–

*This value refers to a measurement using filter paper.

Table 7 gives the emissions of the WHSC test run using the modified EGR application. The list contains regulated emissions according to the Euro VI legislation, as well as several unregulated emissions. The Euro VI limits for heavy-duty diesel engines allow the order of magnitude of emissions in OME operation to be estimated. However, these values are not fully comparable. On the one hand, the operating point used for pre-conditioning has a higher exhaust temperature in order to compensate for the higher heat losses of the modular ATS system. On the other hand, the value of PM emission of the Euro VI legislation refers to a measurement using filter paper. In this study, a PAD determines the PM emission value, represented by the mass of soot emission.

The emission in OME operation during the WHSC is below the Euro VI limit value for every indicated species. The values are in the size range of the detection limit of the exhaust gas measurement devices used except for the PN emission. The manufacturers of the CLD, NDIR and FT-IR specify the detection limit as concentrations of around 1 ppm for every species. The unregulated emissions observed are also in this order of magnitude except for N_2O emission. Since N_2O is a greenhouse gas with massive effects on climate change,[1] further approaches to reduce this emission are necessary. Although the 100-year global warming potential of the N_2O emission during the test cycle equals less than 6 g/kWh of CO_2 equivalent with a factor of 265,[1] it is essential to avoid this emission for a climate-neutral

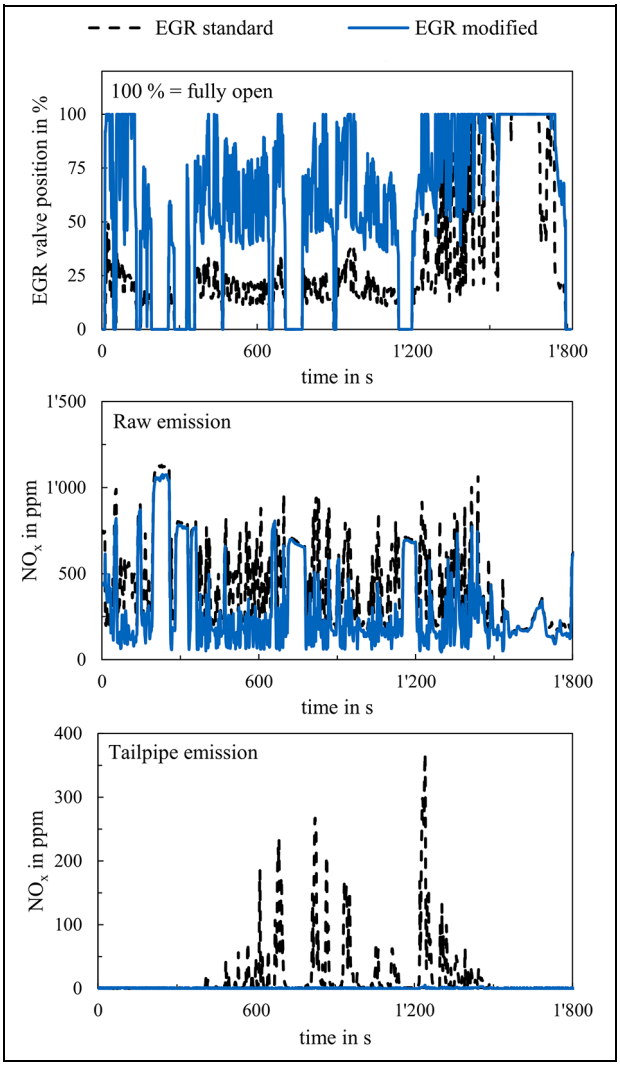

Figure 5. EGR valve position and NO_x emissions in the raw exhaust and tailpipe during the WHTC with the standard EGR application and a modified EGR application for OME operation. The engine NO_x sensor provides the raw emission values, and the CLD provides the tailpipe values.

engine operation in the case of carbon-neutrally produced OME fuel. An improvement in selectivity of the SCR catalyst is one effective means of reducing N_2O emission. The retrospective evaluation of the FT-IR spectra reveals that the emission of the test run for each OME_{0-4} is less than 1 ppm. With the ATS configuration used in this study, the emission of HCN during the test run was 0.1 ppm. The value of the HNCO emission is 1.1 ppm.

Emissions during pre-conditioned WHTC in OME operation

Figure 5 shows the NO_x emissions in raw and tailpipe exhaust using the same EGR applications as in the WHSC cycle. Similar to the results presented in Figure 4, modified EGR application for OME operation reduces the NO_x raw emissions level by approximately 62% compared to diesel operation. While there are several points with NO_x slip using the standard EGR application, the modified strategy enables nearly total conversion in the ATS.

Table 8. Emissions during pre-conditioned WHTC with modified EGR application.

	Result of test cycle	Euro VI limit
Emission		
CO (NDIR) in mg/kWh	14.5	4,000
NO_x (CLD) in mg/kWh	4.31	460
HC (FID) in mg/kWh	18.72	160
PM (MSS) in mg/kWh	0.068	10*
PN_{23} (CPC) in 1/kWh	1.56×10^{10}	6×10^{11}
NH_3 (FT-IR) in ppm	0.1	10
Unregulated emissions		
CH_4 (FT-IR) in ppm	2.3	–
CH_2O (FT-IR) in mg/kWh	1.56	–
N_2O (FT-IR) in mg/kWh	23.64	–
HNCO (FT-IR) in ppm	1.3	–
NH_3 (FT-IR) in mg/kWh	0.277	–
HCN (FT-IR) in ppm	0.0	–
$OME_{0,1,2,3,4}$ in ppm	< 1	–

*This value refers to a measurement using filter paper.

Table 8 shows the results of the WHTC test run with modified EGR application in OME operation. As in the WHSC evaluation, the table also gives the limits according to the Euro VI legislation. Just like in the WHSC, a direct comparison of the results and the limit values is limited, as the pre-conditioning differs from the mandatory test procedure in the technical standard R49. Moreover, the Euro VI limit refers to a test run including a cold-start cycle and a subsequent run of the WHTC. Nevertheless, a classification of the order of magnitude is possible.

The emission in OME operation during the pre-conditioned WHTC is below the Euro VI limit value for every species indicated. Again, the values are in the size range of the detection limit of the exhaust gas measurement devices used except for the PN emission, as with the WHSC results. The unregulated emissions observed are also in this magnitude of order except for N_2O emission. Moreover, the CH_4 emission is higher in dynamic operation. In a test run with the standard EGR application, the CH_4 emission is 0 ppm. As Barro et al.[9] and Pélerin et al.[12] previously revealed, high EGR rates, leading to a λ of lower than 1.1, result in the formation of CH_4. Therefore, a NO_x-CH_4 trade-off replaces the resolved NO_x-soot trade-off in OME operation, especially in transient operation. Since CH_4 is another greenhouse gas,[1,59] this has to be considered in the application of OME engines. The remaining emissions considered are in the range of the WHSC results. This demonstrates, that an OME engine with a twin-dosing ATS offers the potential of a stationary and transient operation with the lowest pollutant emissions. Due to the reduction in the level of NO_x emissions in

the raw exhaust presented, simplifications of the ATS are also considerable in order to improve the economic efficiency in the cost of tailpipe emissions. A one-stage SCR system may also be able to meet upcoming legislation standards. Furthermore, the sootless combustion enables the removal of the DPF. The effects of an OME-operated engine on the PN emission of the regulated nanoparticles with a minimum diameter of 23 nm and unregulated particle sizes form the scope of another study, in addition to the effect of the DPF and urea dosing on the tailpipe emission level of nanoparticles.[23]

Conclusions and outlook

The present work contains a comparison of the efficiency of a CuZe-SCR system in operation with fossil diesel and OME. Furthermore, the investigation reveals the diminishing effect of urea dosing on formaldehyde emission in OME operation. The demonstration of a pre-conditioned WHSC and WHTC run confirm the potential for lowest pollutant emissions of an OME engine in combination with a twin-dosing after-treatment system. Furthermore, this study contains the calculation of the specific *u*-values for OME operation according to UN/ECE R49 for the specific emission evaluation of the test cycles. The results are summarised in the following conclusions:

- In OME operation, the exhaust gas temperatures are lower than in diesel operation. This results in a lower relative NO_x conversion efficiency in the SCR system. This does not apply for the investigated high-load point, where the efficiency is approximately equal.
- The sootless combustion of OME enables a high-EGR strategy, leading to lower NO_x emissions in the raw exhaust. This compensates for the reduced conversion efficiency. Moreover, the sootless combustion reduces the required amount of NO_2 for the continuous regeneration of the DPF, enabling a higher α at the first SCR stage in twin-dosing operation. Nevertheless, removal of stored ammonia in the second SCR stage at increasing exhaust temperatures restricts the urea dosing at the first stage.
- Urea dosing in the SCR system reduces the level of formaldehyde emission in the exhaust of OME engines. Since the literature provides information about the formation of HCN in the presence of formaldehyde and ammonia, either the removal of formed HCN by oxidative catalysts downstream of the SCR system or the previous total oxidation of CH_2O upstream of the SCR system are necessary to avoid the emission of this toxic species into the environment. During the pre-conditioned runs of the test cycles WHSC and WHTC, no emission of HCN occurred.
- With the twin-dosing after-treatment system used, regulated pollutant emissions fall within the range of the detection limits of the exhaust gas measurement devices used during the pre-conditioned runs of the test cycles WHSC and WHTC, except for particle number emission. Nevertheless, the emission of PN with particles with a minimum diameter of 23 nm are each lower than the Euro VI limit by a double-digit factor. The ultra-low level of NO_x emission is due to the modified EGR application in OME operation, which features faster and further opening of the EGR valve. The unregulated pollutant emissions CH_2O, HNCO, HCN and OME_n are also in the range of the detection limit.
- The emission value of the greenhouse gas N_2O requires further reduction efforts, because of its massive impact on the climate change.
- While no CH_4 emission was detected in stationary operation, several emission peaks in dynamic operation result in a minimally increased cycle result of the WHTC compared to the WHSC. A test run with the standard EGR application reveals that this is due to a brief undershoot of the λ limit of CH_4 formation. For ultra-low emissions applications, an increase in SCR performance enables higher NO_x conversion efficiencies, so the EGR application may consider the NO_x-CH_4 trade-off in dynamic operation without the disadvantage of higher NO_x tailpipe emissions. However, the lower-level NO_x emission in the raw exhaust due to the modified EGR strategy also enables the after-treatment system to be simplified, leading to lower costs, while upcoming exhaust gas legislation still may be fulfilled.

Although this study demonstrates the potential of an OME engine in combination with after-treatment for ultra-low emissions, these observations refer to an operationally warm system. Therefore, an investigation into the emission behaviour of the system used in cold-start operation is necessary in order to evaluate the system holistically. In particular, emission of HCN in cold-start operation with a temperature level of the oxidative catalysts below their respective light-off temperature requires further observation. Another study is planned with a focus on this subject.[53] Furthermore, the emission of nanoparticles below the regulated particle size of minimum 23 nm in the system presented, as well as the effect of the DPF and urea dosing on PN emission will be discussed in another publication.[23]

Acknowledgements

The project 'Sub-Zero-Emissions Dieselmotor' was funded by the Bavarian Research Foundation (BFS) and was carried out in collaboration with MAN Truck & Bus SE, VT Vitesco Technologies Emitec GmbH, Chair of Analytical Chemistry of TUM and ASG Analytik-Service AG. Their support is gratefully acknowledged. The authors also want to thank Dr. Dieter Rothe and Dipl.-Ing. Florian Lindner (both MAN Truck & Bus SE) for their support and consultation in this study.

Author contributions

Alexander D Gelner: conceptualisation, data curation, formal analysis, investigation, methodology, project administration, validation, visualisation, writing – original draft and writing – review and editing. Harald A Beck: validation, formal analysis, data curation and writing – review and editing. Christian Pastoetter: funding acquisition, project administration and writing – review and editing. Martin Härtl: funding acquisition, project administration, supervision and writing – review and editing. Georg Wachtmeister: funding acquisition, project administration, supervision and writing – review and editing.

Declaration of conflicting interests

The authors declared no potential conflicts of interest with respect to the research, authorship, and/or publication of this article.

Funding

The authors disclosed receipt of the following financial support for the research, authorship, and/or publication of this article: The research was part of the project 'Sub-Zero-Emissions Dieselmotor', funded by the Bavarian Research Foundation (grant number AZ-1266-17).

ORCID iD

Alexander D Gelner https://orcid.org/0000-0001-9628-798X

References

1. Pachauri RK and Meyer L (eds.). *Climate change 2014: synthesis report [longer report]*. Geneva, Switzerland: Intergovernmental Panel on Climate Change, 2015.
2. Schemme S, Breuer JL, Köller M, et al. H_2-based synthetic fuels: a techno-economic comparison of alcohol, ether and hydrocarbon production. *Int J Hydrogen Energy* 2020; 45: 5395–5414.
3. Gray N, McDonagh S, O'Shea R, Smyth B and Murphy JD. Decarbonising ships, planes and trucks: an analysis of suitable low-carbon fuels for the maritime, aviation and haulage sectors. *Adv Appl Energy* 2021; 1: 100008.
4. Schemme S, Samsun RC, Peters R and Stolten D. Power-to-fuel as a key to sustainable transport systems – an analysis of diesel fuels produced from CO_2 and renewable electricity. *Fuel* 2017; 205: 198–221.
5. Centi G and Perathoner S. Opportunities and prospects in the chemical recycling of carbon dioxide to fuels. *Catal Today* 2009; 148: 191–205.
6. Held M, Tönges Y, Pélerin D, Härtl M, Wachtmeister G and Burger J. On the energetic efficiency of producing polyoxymethylene dimethyl ethers from CO_2 using electrical energy. *Energy Environ Sci* 2019; 12: 1019–1034.
7. Pellegrini L, Marchionna M, Patrini R, et al. Emission performance of neat and blended polyoxymethylene dimethyl ethers in an old light-duty diesel car. SAE technical paper 2013-01-1035, 2013.
8. Iannuzzi SE, Barro C, Boulouchos K and Burger J. Combustion behavior and soot formation/oxidation of oxygenated fuels in a cylindrical constant volume chamber. *Fuel* 2016; 167: 49–59.
9. Barro C, Parravicini M, Boulouchos K and Liati A. Neat polyoxymethylene dimethyl ether in a diesel engine; part 2: exhaust emission analysis. *Fuel* 2018; 234: 1414–1421.
10. Damyanov A, Hofmann P, Geringer B, Schwaiger N, Pichler T and Siebenhofer M. Biogenous ethers: production and operation in a diesel engine. *Automot Engine Technol* 2018; 3: 69–82.
11. Omari A, Heuser B, Pischinger S and Rüdinger C. Potential of long-chain oxymethylene ether and oxymethylene ether-diesel blends for ultra-low emission engines. *Appl Energy* 2019; 239: 1242–1249.
12. Pélerin D, Gaukel K, Härtl M, Jacob E and Wachtmeister G. Potentials to simplify the engine system using the alternative diesel fuels oxymethylene ether OME_1 and OME_{3-6} on a heavy-duty engine. *Fuel* 2020; 259: 116231.
13. Ogawa H, Miyamoto N and Yagi M. Chemical-kinetic analysis on PAH formation mechanisms of oxygenated fuels. SAE technical paper 2003-01-3190, 2003.
14. Pellegrini L, Marchionna M, Patrini R, et al. Combustion behaviour and emission performance of neat and blended polyoxymethylene dimethyl ethers in a light-duty diesel engine. SAE technical paper 2012-01-1053, 2012.
15. Ogawa H, Nabi N, Minami M, et al. Ultra low emissions and high performance diesel combustion with a combination of high EGR, three-way catalyst, and a highly oxygenated fuel, dimethoxy methane (DMM). SAE technical paper 2000-01-1819, 2000.
16. Härtl M, Seidenspinner P, Jacob E and Wachtmeister G. Oxygenate screening on a heavy-duty diesel engine and emission characteristics of highly oxygenated oxymethylene ether fuel OME_1. *Fuel* 2015; 153: 328–335.
17. Pélerin D, Gaukel K, Härtl M, et al. Nitrogen oxide reduction potentials using dimethyl ether and oxymethylene ether in a heavy-duty diesel engine. SAE technical paper series 2020-01-5084, 2020.
18. Münz M, Töpfer D, Mokros A, et al. Oxygenate fuel in a diesel engine – is a CI engine capable of lambda 1? In: Liebl J and Beidl C (eds) *Internationaler Motorenkongress 2017*. Wiesbaden, Germany: Springer Fachmedien Wiesbaden, 2017, pp.457–472.
19. Pöllmann S, Härtl M and Wachtmeister G. Potentials of the synthetic diesel fuel oxymethylene ether under stoichiometric conditions with aftertreatment. Manuscript in preparation.
20. Münz M, Mokros A, Töpfer D and Beidl C. OME – assessment of particle emissions in real driving conditions. *MTZ Worldw* 2018; 79: 16–21.
21. Münz M, Mokros A and Beidl C. Analysis of two engine configurations using OME as a potential CO_2-neutral and low emission diesel substitute. In: Liebl J, Beidl C and Maus W (eds) *Internationaler Motorenkongress 2019*. Wiesbaden, Germany: Springer Fachmedien Wiesbaden, 2019, pp.369–384.
22. Gelner AD, Pastoetter C, Beck HA, et al. Fuel dosing on a diesel oxidation catalyst for after-treatment system heating on a heavy-duty engine powered by polyoxymethylene dimethyl ethers. SAE technical paper 2020-01-2157, 2020.
23. Gelner AD, Rothe D, Irwin M, et al. Particle emissions of a heavy-duty engine powered by polyoxymethylene dimethyl ethers (OME): volatile and nonvolatile particle size distributions and PN-emissions in test cycles. 2021. Manuscript in preparation.
24. Fischer MH. The toxic effects of formaldehyde and formalin. *J Exp Med* 1905; 6: 487–518.

25. Bauer M and Wachtmeister G. Formation of formaldehyde in lean-burn gas engines. *MTZ Worldw* 2009; 70: 50–57.
26. Bertole C. Formaldehyde oxidation over emission control catalysts. SAE technical paper 2018-01-1274, 2018.
27. Zengel D, Koch P, Torkashvand B, Grunwaldt JD, Casapu M and Deutschmann O. Emission of toxic HCN during NO_x removal by ammonia SCR in the exhaust of lean-burn natural gas engines. *Angew Chem Int Ed Engl* 2020; 59: 14423–14428.
28. Elsener M, Nuguid RJG, Kröcher O and Ferri D. HCN production from formaldehyde during the selective catalytic reduction of NO_x with NH_3 over V_2O_5/WO_3-TiO_2. *Appl Catal B* 2021; 281: 119462.
29. DIN/TS 51699 – Fuels – Polyoxymethylene dimethyl ether (OME).
30. Lautenschütz L, Oestreich D, Seidenspinner P, Arnold U, Dinjus E and Sauer J. Physico-chemical properties and fuel characteristics of oxymethylene dialkyl ethers. *Fuel* 2016; 173: 129–137.
31. Hoekman SK, Broch A, Robbins C, Ceniceros E and Natarajan M. Review of biodiesel composition, properties, and specifications. *Renew Sustain Energ Rev* 2012; 16: 143–169.
32. DIN EN 590:2017-10 – Automotive fuels – diesel. CEN/TC 19 WG 24, 2017. https://www.din.de/en/getting-involved/standards-committees/nmp/publications/wdc-beuth:din21:278413784?
33. Barro C, Parravicini M and Boulouchos K. Neat polyoxymethylene dimethyl ether in a diesel engine; part 1: detailed combustion analysis. *Fuel* 2019; 256: 115892.
34. Gelner AD, Höß R, Zepf A, et al. Engine operation strategies with the alternative diesel fuel oxymethylene ether (OME): evaluation based on injection rate analyzer and 0D-/1D-simulation. *SAE technical paper 2021-01-1190*, 2021. Manuscript submitted for publication.
35. Yim SD, Kim SJ, Baik JH, et al. Decomposition of urea into NH_3 for the SCR process. *Ind Eng Chem Res* 2004; 43: 4856–4863.
36. Koebel M, Elsener M and Marti T. NO_x-reduction in diesel exhaust gas with urea and selective catalytic reduction. *Combust Sci Technol* 1996; 121: 85–102.
37. Kamasamudram K, Henry C, Currier N and Yezerets A. N_2O formation and mitigation in diesel aftertreatment systems. *SAE Int J Engines* 2012; 5: 688–698.
38. Birkhold F, Meingast U, Wassermann P and Deutschmann O. Modeling and simulation of the injection of urea-water-solution for automotive SCR $DeNO_x$-systems. *Appl Catal B* 2007; 70: 119–127.
39. Regulation No. 49 of the Economic Commission for Europe of the United Nations (UN/ECE)—uniform provisions concerning the measures to be taken against the emission of gaseous and particulate pollutants from compression-ignition engines and positive ignition engines for use in vehicles, 2013.Official Journal of the European Union; https://eur-lex.europa.eu/legal-content/EN/TXT/PDF/?uri = CELEX:42013X0624(01)&from = DE.
40. Scanlon JT and Willis DE. Calculation of flame ionization detector relative response factors using the effective carbon number concept. *J Chromatogr Sci* 1985; 23: 333–340.
41. Jorgensen AD, Picel KC and Stamoudis VC. Prediction of gas chromatography flame ionization detector response factors from molecular structures. *Anal Chem* 1990; 62: 683–689.
42. Huang Y, Ou Q and Yu W. Characteristics of flame ionization detection for the quantitative analysis of complex organic mixtures. *Anal Chem* 1990; 62: 2063–2064.
43. Wallner T. Correlation between speciated hydrocarbon emissions and flame ionization detector response for gasoline/alcohol blends. In: *ASME 2010 Internal Combustion Engine Division Fall Technical Conference*, San Antonio, TX, USA, 12–15 September 2010, pp. 119–128. ASMEDC.
44. Roberts JM, Veres PR, Cochran AK, et al. Isocyanic acid in the atmosphere and its possible link to smoke-related health effects. *Proc Natl Acad Sci U S A* 2011; 108: 8966–8971.
45. Leslie MD, Ridoli M, Murphy JG and Borduas-Dedekind N. Isocyanic acid (HNCO) and its fate in the atmosphere: a review. *Environ Sci Process Impacts* 2019; 21: 793–808.
46. Andersson J, Mamakos A and Giechaskiel B. *Particle measurement programme (PMP) heavy-duty inter-laboratory correlation exercise (ILCE_HD)*. Luxembourg: Publications Office of the European Union, 2010.
47. Beck HA, Niessner R and Haisch C. Development and characterization of a mobile photoacoustic sensor for online soot emission monitoring in diesel exhaust gas. *Anal Bioanal Chem* 2003; 375: 1136–1143.
48. Koebel M, Madia G and Elsener M. Selective catalytic reduction of NO and NO_2 at low temperatures. *Catal Today* 2002; 73: 239–247.
49. Forzatti P, Lietti L and Tronconi E. Nitrogen oxides removal-industrial. In: I Horváth (ed.) *Encyclopedia of Catalysis*. Hoboken, NJ: John Wiley & Sons, Inc, 2002, p.6.
50. National Center for Biotechnology Information. PubChem compound summary for CID 1176, Urea, https://pubchem.ncbi.nlm.nih.gov/compound/Urea. (2020 accessed 9 May 2021).
51. ISO 22241-1:2019. Diesel engines – NOx reduction agent AUS 32.
52. Kamasamudram K, Currier N, Szailer T and Yezerets A. Why Cu- and Fe-zeolite SCR catalysts behave differently at low temperatures. *SAE Int J Fuel Lubricants* 2010; 3: 664–672.
53. Gelner AD, Pang G, Haisch C, et al. Emissions of a heavy-duty diesel engine powered with polyoxymethylene dimethyl ethers during cold start operation. Manuscript in preparation.
54. Kröcher O. Chapter 9. Aspects of catalyst development for mobile urea-SCR systems — from Vanadia-Titania catalysts to metal-exchanged zeolites. In: Granger P and Pârvulescu VI (eds) *Past and present in $DeNO_x$ catalysis – from molecular modelling to chemical engineering*. Studies in Surface Science and Catalysis. Elsevier, 2007, pp.261–289.
55. Kandylas IP and Koltsakis GC. NO_2-assisted regeneration of diesel particulate filters: a modeling study. *Ind Eng Chem Res* 2002; 41: 2115–2123.
56. Higgins EA, Fiorca V, Thomas AA and Davis HV. Acute toxicity of brief exposures to HF, HCl, NO_2 and HCN with and without CO. *Fire Technol* 1972; 8: 120–130.
57. Kröcher O and Elsener M. Hydrolysis and oxidation of gaseous HCN over heterogeneous catalysts. *Appl Catal B* 2009; 92: 75–89.

58. Johnson TV. Review of selective catalytic reduction (SCR) and related technologies for mobile applications. In: Nova I and Tronconi E (eds) *Urea-SCR technology for deNO$_x$ after treatment of diesel exhausts*. New York, NY: Springer, 2014, pp.3–31.
59. Etminan M, Myhre G, Highwood EJ and Shine KP. Radiative forcing of carbon dioxide, methane, and nitrous oxide: a significant revision of the methane radiative forcing. *Geophys Res Lett* 2016; 43: 12,614–12,623.

Appendix

Definitions/Abbreviations

A/F_{st}	stoichiometric air to fuel ratio
ASC	ammonia slip catalyst
ATS	after-treatment system
BHT	butylated hydroxytoluene
CLD	chemiluminescence detector
cpsi	cells per square inch
CuZe	copper zeolite
DOC	diesel oxidation catalyst
DPF	diesel particulate filter
EGR	exhaust gas recirculation
FAME	fatty acid methyl esters
FID	flame ionisation detector
FT-IR	Fourier-transform infrared spectrometer
HC	hydrocarbon (determined by the flame ionisation detector)
HFRR	high-frequency reciprocating rig
$LHV_{(n)}$	lower heating value (of the component *n*)
$k_{f,w}$	fuel-specific factor of wet exhaust
$\dot{m}_{Air}$	air mass flow
$\dot{m}_{Exh}$	exhaust gas mass flow
$M_{gas,i}$	molar mass of the component i
M_{OME}	molar mass of OME
M_{Urea}	molar mass of urea
$\dot{m}_{Urea}$	urea mass flow
NDIR	nondispersive infrared sensor
OFA	open frontal area
$OME_{(n)}$	polyoxymethylene dimethyl ethers (of the chain-length *n*)
PAD	photoacoustic detector
PGM	platinum group metals
PM	particulate matter
$PN_{(23)}$	particle number (with a 50%-cut-off at 23 nm)
ppm	parts per million
q_{mad}	intake air mass flow rate on a dry basis
q_{mf}	fuel mass flow rate
$r_{NH3,Urea}$	molar fraction of NH_3 in urea
SCR	selective catalytic reduction
sv	space velocity
TiO_2	titanium dioxide
TWC	three-way catalyst
$u_{gas,i}$	*u*-value of the specific component i
UDP	Universal Decomposition Pipe
$\dot{V}_{Fuel}$	fuel volume flow
V_m	molar volume of an ideal gas
V_{SCR}	volume of the SCR catalysts
$w_{Urea,AdBlue.}$	mass fraction of urea in AdBlue®
w_υ	mass fraction of hydrogen in %
w_ζ	mass fraction of oxygen in %
WHSC	World Harmonized Stationary Cycle
WHTC	World Harmonized Transient Cylce
x	index of carbon atoms in the substitution molecule
y	index of hydrogen atoms in the substitution molecule
z	index of oxygen atoms in the substitution molecule
α	ratio of dosed amount of urea to the required amount of urea for total conversion of the NO_x emissions
λ	air-fuel ratio
φ_{NOx}	volume fraction of NO_x in the exhaust
$\rho_{(n)}$	density (of the component *n*)
ρ_e	exhaust gas density
$\rho_{gas,i}$	density of the specific gas component *i*
υ	index of hydrogen atoms in the substitution molecule, normalised to $x = 1$

Table A1 Determined values of OME and the respective measurement method.

	Value	Method
Cetane number	68.8	DIN EN 17155: 2018
Oxygen content in % (w/w)	45.0	DIN 51732: 2014 mod.
Sulphur content in mg/kg	< 5	DIN EN ISO 20884: 2011
Lower heating value in MJ/kg	19.21	DIN 51900-2: 2003 mod.
Density (15°C at 1 bar) in kg/dm^3	1,057.1	DIN EN ISO 12185: 1997
Boiling range at 1 bar in °C	144.9–242.4	DIN EN ISO 3405: 2011
Flash point at 1 bar in °C	65.0	DIN EN ISO 2719: 2016
Cold filter plugging point in °C	−40	DIN EN 116: 2018
Cloud point in °C	−38	DIN EN 23015: 1994
Kinematic viscosity at 40°C in mm^2/s	1.082	DIN EN ISO 3104: 1999
Lubricity – HFRR at 60°C in µm	320	DIN EN ISO 12156-1: 2016
Formaldehyde content in mg/kg	233	ASG 1855 Voltammetry

ζ	index of hydrogen atoms in the substitution molecule, normalised to $x = 1$

Chemical formula

CH_4	methane
CH_2O	formaldehyde (IUPAC: methanal)
CO	carbon monoxide
CO_2	carbon dioxide
CO_2	carbon dioxide
H_2	hydrogen
H_2O	water
HCN	hydrogen cyanide (IUPAC: formonitrile)
HNCO	isocyanic acid
N_2	nitrogen
N_2O	nitrous oxide
NH_3	ammonia
NO	nitric oxide
NO_2	nitrogen dioxide
NO_x	nitrogen oxides
TiO_2	titanium dioxide

Gelner, A. D.; Pastötter, C.; Beck, H. A.; Härtl, M.; Wachtmeister, G.: *Fuel Dosing on a Diesel Oxidation Catalyst for After-Treatment System Heating on a Heavy-Duty Engine Powered by Polyoxymethylene Dimethyl Ethers*; SAE Technical Paper 2020-0050; 2020. [189]

Order Date	18-Oct-2022	Type of Use	Republish in a thesis/dissertation
Order License ID	1280572-1		
ISSN	0148-7191	Publisher	SOCIETY OF AUTOMOTIVE ENGINEERS,
		Portion	Chapter/article

LICENSED CONTENT

Publication Title	SAE technical paper series	Language	English
Article Title	Fuel Dosing on a Diesel Oxidation Catalyst for After-Treatment System Heating on a Heavy-Duty Engine Powered by Polyoxymethylene Dimethyl Ethers	Country	United States of America
		Rightsholder	SAE International
		Publication Type	Monographic Series
Author/Editor	SOCIETY OF AUTOMOTIVE ENGINEERS.		
Date	01/01/1970		

REQUEST DETAILS

Portion Type	Chapter/article	Rights Requested	Main product
Page Range(s)	1-12	Distribution	Worldwide
Total Number of Pages	12	Translation	Original language of publication
Format (select all that apply)	Electronic	Copies for the Disabled?	No
Who Will Republish the Content?	Academic institution	Minor Editing Privileges?	No
		Incidental Promotional Use?	No
Duration of Use	Life of current edition		
Lifetime Unit Quantity	More than 2,000,000	Currency	EUR

NEW WORK DETAILS

Title	OME as enabler	Institution Name	Technical University of Munich (TUM)
Instructor Name	Alexander Daniel Gelner		
		Expected Presentation Date	2022-11-08

ADDITIONAL DETAILS

Order Reference Number	N/A

The Requesting Person/Organization to Appear on the License	Alexander Daniel Gelner

REUSE CONTENT DETAILS

Title, Description or Numeric Reference of the Portion(s)	https://doi.org/10.4271/2020-01-2157	Title of the Article/Chapter the Portion Is From	Fuel Dosing on a Diesel Oxidation Catalyst for After-Treatment System Heating on a Heavy-Duty Engine Powered by Polyoxymethylene Dimethyl Ethers
Editor of Portion(s)	Gelner, Alexander D.; Pastoetter, Christian; Beck, Harald A.; Härtl, Martin; Wachtmeister, Georg	Author of Portion(s)	Gelner, Alexander D.; Pastoetter, Christian; Beck, Harald A.; Härtl, Martin; Wachtmeister, Georg
Volume of Serial or Monograph	N/A	Issue, if Republishing an Article From a Serial	N/A
Page or Page Range of Portion	1-12	Publication Date of Portion	2020-09-15

Marketplace Order General Terms and Conditions

The following terms and conditions ("General Terms"), together with any applicable Publisher Terms and Conditions, govern User's use of Works pursuant to the Licenses granted by Copyright Clearance Center, Inc. ("CCC") on behalf of the applicable Rightsholders of such Works through CCC's applicable Marketplace transactional licensing services (each, a "Service").

1) Definitions. For purposes of these General Terms, the following definitions apply:

"License" is the licensed use the User obtains via the Marketplace platform in a particular licensing transaction, as set forth in the Order Confirmation.

"Order Confirmation" is the confirmation CCC provides to the User at the conclusion of each Marketplace transaction. "Order Confirmation Terms" are additional terms set forth on specific Order Confirmations not set forth in the General Terms that can include terms applicable to a particular CCC transactional licensing service and/or any Rightsholder-specific terms.

"Rightsholder(s)" are the holders of copyright rights in the Works for which a User obtains licenses via the Marketplace platform, which are displayed on specific Order Confirmations.

"Terms" means the terms and conditions set forth in these General Terms and any additional Order Confirmation Terms collectively.

"User" or "you" is the person or entity making the use granted under the relevant License. Where the person accepting the Terms on behalf of a User is a freelancer or other third party who the User authorized to accept the General Terms on the User's behalf, such person shall be deemed jointly a User for purposes of such Terms.

"Work(s)" are the copyright protected works described in relevant Order Confirmations.

2) Description of Service. CCC's Marketplace enables Users to obtain Licenses to use one or more Works in accordance with all relevant Terms. CCC grants Licenses as an agent on behalf of the copyright rightsholder identified in the relevant Order Confirmation.

3) Applicability of Terms. The Terms govern User's use of Works in connection with the relevant License. In the event of any conflict between General Terms and Order Confirmation Terms, the latter shall govern. User acknowledges that Rightsholders have complete discretion whether to grant any permission, and whether to place any limitations on any grant, and that CCC has no right to supersede or to modify any such discretionary act by a Rightsholder.

4) Representations; Acceptance. By using the Service, User represents and warrants that User has been duly authorized by the User to accept, and hereby does accept, all Terms.

5) Scope of License; Limitations and Obligations. All Works and all rights therein, including copyright rights, remain the sole and exclusive property of the Rightsholder. The License provides only those rights expressly set forth in the terms and conveys no other rights in any Works

6) General Payment Terms. User may pay at time of checkout by credit card or choose to be invoiced. If the User chooses to be invoiced, the User shall: (i) remit payments in the manner identified on specific invoices, (ii) unless otherwise specifically stated in an Order Confirmation or separate written agreement, Users shall remit payments upon receipt of the relevant invoice from CCC, either by delivery or notification of availability of the invoice via the Marketplace platform, and (iii) if the User does not pay the invoice within 30 days of receipt, the User may incur a service charge of 1.5% per month or the maximum rate allowed by applicable law, whichever is less. While User may exercise the rights in the License immediately upon receiving the Order Confirmation, the License is automatically revoked and is null and void, as if it had never been issued, if CCC does not receive complete payment on a timely basis.

7) General Limits on Use. Unless otherwise provided in the Order Confirmation, any grant of rights to User (i) involves only the rights set forth in the Terms and does not include subsequent or additional uses, (ii) is non-exclusive and non-transferable, and (iii) is subject to any and all limitations and restrictions (such as, but not limited to, limitations on duration of use or circulation) included in the Terms. Upon completion of the licensed use as set forth in the Order Confirmation, User shall either secure a new permission for further use of the Work(s) or immediately cease any new use of the Work(s) and shall render inaccessible (such as by deleting or by removing or severing links or other locators) any further copies of the Work. User may only make alterations to the Work if and as expressly set forth in the Order Confirmation. No Work may be used in any way that is defamatory, violates the rights of third parties (including such third parties' rights of copyright, privacy, publicity, or other tangible or intangible property), or is otherwise illegal, sexually explicit, or obscene. In addition, User may not conjoin a Work with any other material that may result in damage to the reputation of the Rightsholder. User agrees to inform CCC if it becomes aware of any infringement of any rights in a Work and to cooperate with any reasonable request of CCC or the Rightsholder in connection therewith.

8) Third Party Materials. In the event that the material for which a License is sought includes third party materials (such as photographs, illustrations, graphs, inserts and similar materials) that are identified in such material as having been used by permission (or a similar indicator), User is responsible for identifying, and seeking separate licenses (under this Service, if available, or otherwise) for any of such third party materials; without a separate license, User may not use such third party materials via the License.

9) Copyright Notice. Use of proper copyright notice for a Work is required as a condition of any License granted under the Service. Unless otherwise provided in the Order Confirmation, a proper copyright notice will read substantially as follows: "Used with permission of [Rightsholder's name], from [Work's title, author, volume, edition number and year of copyright]; permission conveyed through Copyright Clearance Center, Inc." Such notice must be provided in a reasonably legible font size and must be placed either on a cover page or in another location that any person, upon gaining access to the material which is the subject of a permission, shall see, or in the case of republication Licenses, immediately adjacent to the Work as used (for example, as part of a by-line or footnote) or in the place where substantially all other credits or notices for the new work containing the republished Work are located. Failure to include the required notice results in loss to the Rightsholder and CCC, and the User shall be liable to pay liquidated damages for each such failure equal to twice the use fee specified in the Order Confirmation, in addition to the use fee itself and any other fees and charges specified.

10) Indemnity. User hereby indemnifies and agrees to defend the Rightsholder and CCC, and their respective employees and directors, against all claims, liability, damages, costs, and expenses, including legal fees and expenses, arising out of any use of a Work beyond the scope of the rights granted herein and in the Order Confirmation, or any use of a Work which has been altered in any unauthorized way by User, including claims of defamation or infringement of rights of copyright, publicity, privacy, or other tangible or intangible property.

11) Limitation of Liability. UNDER NO CIRCUMSTANCES WILL CCC OR THE RIGHTSHOLDER BE LIABLE FOR ANY DIRECT, INDIRECT, CONSEQUENTIAL, OR INCIDENTAL DAMAGES (INCLUDING WITHOUT LIMITATION DAMAGES FOR LOSS OF BUSINESS PROFITS OR INFORMATION, OR FOR BUSINESS INTERRUPTION) ARISING OUT OF THE USE OR INABILITY TO USE A WORK, EVEN IF ONE OR BOTH OF THEM HAS BEEN ADVISED OF THE POSSIBILITY OF SUCH DAMAGES. In any event, the total liability of the Rightsholder and CCC (including their respective employees and directors) shall not exceed the total amount actually paid by User for the relevant License. User assumes full liability for the actions and omissions of its principals, employees, agents, affiliates, successors, and assigns.

12) Limited Warranties. THE WORK(S) AND RIGHT(S) ARE PROVIDED "AS IS." CCC HAS THE RIGHT TO GRANT TO USER THE

RIGHTS GRANTED IN THE ORDER CONFIRMATION DOCUMENT. CCC AND THE RIGHTSHOLDER DISCLAIM ALL OTHER WARRANTIES RELATING TO THE WORK(S) AND RIGHT(S), EITHER EXPRESS OR IMPLIED, INCLUDING WITHOUT LIMITATION IMPLIED WARRANTIES OF MERCHANTABILITY OR FITNESS FOR A PARTICULAR PURPOSE. ADDITIONAL RIGHTS MAY BE REQUIRED TO USE ILLUSTRATIONS, GRAPHS, PHOTOGRAPHS, ABSTRACTS, INSERTS, OR OTHER PORTIONS OF THE WORK (AS OPPOSED TO THE ENTIRE WORK) IN A MANNER CONTEMPLATED BY USER; USER UNDERSTANDS AND AGREES THAT NEITHER CCC NOR THE RIGHTSHOLDER MAY HAVE SUCH ADDITIONAL RIGHTS TO GRANT.

13) Effect of Breach. Any failure by User to pay any amount when due, or any use by User of a Work beyond the scope of the License set forth in the Order Confirmation and/or the Terms, shall be a material breach of such License. Any breach not cured within 10 days of written notice thereof shall result in immediate termination of such License without further notice. Any unauthorized (but licensable) use of a Work that is terminated immediately upon notice thereof may be liquidated by payment of the Rightsholder's ordinary license price therefor; any unauthorized (and unlicensable) use that is not terminated immediately for any reason (including, for example, because materials containing the Work cannot reasonably be recalled) will be subject to all remedies available at law or in equity, but in no event to a payment of less than three times the Rightsholder's ordinary license price for the most closely analogous licensable use plus Rightsholder's and/or CCC's costs and expenses incurred in collecting such payment.

14) Additional Terms for Specific Products and Services. If a User is making one of the uses described in this Section 14, the additional terms and conditions apply:

a) *Print Uses of Academic Course Content and Materials (photocopies for academic coursepacks or classroom handouts).* For photocopies for academic coursepacks or classroom handouts the following additional terms apply:

i) The copies and anthologies created under this License may be made and assembled by faculty members individually or at their request by on-campus bookstores or copy centers, or by off-campus copy shops and other similar entities.

ii) No License granted shall in any way: (i) include any right by User to create a substantively non-identical copy of the Work or to edit or in any other way modify the Work (except by means of deleting material immediately preceding or following the entire portion of the Work copied) (ii) permit "publishing ventures" where any particular anthology would be systematically marketed at multiple institutions.

iii) Subject to any Publisher Terms (and notwithstanding any apparent contradiction in the Order Confirmation arising from data provided by User), any use authorized under the academic pay-per-use service is limited as follows:

A) any License granted shall apply to only one class (bearing a unique identifier as assigned by the institution, and thereby including all sections or other subparts of the class) at one institution;

B) use is limited to not more than 25% of the text of a book or of the items in a published collection of essays, poems or articles;

C) use is limited to no more than the greater of (a) 25% of the text of an issue of a journal or other periodical or (b) two articles from such an issue;

D) no User may sell or distribute any particular anthology, whether photocopied or electronic, at more than one institution of learning;

E) in the case of a photocopy permission, no materials may be entered into electronic memory by User except in order to produce an identical copy of a Work before or during the academic term (or analogous period) as to which any particular permission is granted. In the event that User shall choose to retain materials that are the subject of a photocopy permission in electronic memory for purposes of producing identical copies more than one day after such retention (but still within the scope of any permission granted), User must notify CCC of such fact in the applicable permission request and such retention shall constitute one copy actually sold for purposes of calculating permission fees due; and

F) any permission granted shall expire at the end of the class. No permission granted shall in any way include any right by User to create a substantively non-identical copy of the Work or to edit or in any other way modify the Work (except by means of deleting material immediately preceding or following the entire portion of the Work copied).

iv) Books and Records; Right to Audit. As to each permission granted under the academic pay-per-use Service, User

shall maintain for at least four full calendar years books and records sufficient for CCC to determine the numbers of copies made by User under such permission. CCC and any representatives it may designate shall have the right to audit such books and records at any time during User's ordinary business hours, upon two days' prior notice. If any such audit shall determine that User shall have underpaid for, or underreported, any photocopies sold or by three percent (3%) or more, then User shall bear all the costs of any such audit; otherwise, CCC shall bear the costs of any such audit. Any amount determined by such audit to have been underpaid by User shall immediately be paid to CCC by User, together with interest thereon at the rate of 10% per annum from the date such amount was originally due. The provisions of this paragraph shall survive the termination of this License for any reason.

b) *Digital Pay-Per-Uses of Academic Course Content and Materials (e-coursepacks, electronic reserves, learning management systems, academic institution intranets).* For uses in e-coursepacks, posts in electronic reserves, posts in learning management systems, or posts on academic institution intranets, the following additional terms apply:

i) The pay-per-uses subject to this Section 14(b) include:

A) Posting e-reserves, course management systems, e-coursepacks for text-based content, which grants authorizations to import requested material in electronic format, and allows electronic access to this material to members of a designated college or university class, under the direction of an instructor designated by the college or university, accessible only under appropriate electronic controls (e.g., password);

B) Posting e-reserves, course management systems, e-coursepacks for material consisting of photographs or other still images not embedded in text, which grants not only the authorizations described in Section 14(b)(i)(A) above, but also the following authorization: to include the requested material in course materials for use consistent with Section 14(b)(i)(A) above, including any necessary resizing, reformatting or modification of the resolution of such requested material (provided that such modification does not alter the underlying editorial content or meaning of the requested material, and provided that the resulting modified content is used solely within the scope of, and in a manner consistent with, the particular authorization described in the Order Confirmation and the Terms), but not including any other form of manipulation, alteration or editing of the requested material;

C) Posting e-reserves, course management systems, e-coursepacks or other academic distribution for audiovisual content, which grants not only the authorizations described in Section 14(b)(i)(A) above, but also the following authorizations: (i) to include the requested material in course materials for use consistent with Section 14(b)(i)(A) above; (ii) to display and perform the requested material to such members of such class in the physical classroom or remotely by means of streaming media or other video formats; and (iii) to "clip" or reformat the requested material for purposes of time or content management or ease of delivery, provided that such “clipping” or reformatting does not alter the underlying editorial content or meaning of the requested material and that the resulting material is used solely within the scope of, and in a manner consistent with, the particular authorization described in the Order Confirmation and the Terms. Unless expressly set forth in the relevant Order Conformation, the License does not authorize any other form of manipulation, alteration or editing of the requested material.

ii) Unless expressly set forth in the relevant Order Confirmation, no License granted shall in any way: (i) include any right by User to create a substantively non-identical copy of the Work or to edit or in any other way modify the Work (except by means of deleting material immediately preceding or following the entire portion of the Work copied or, in the case of Works subject to Sections 14(b)(1)(B) or (C) above, as described in such Sections) (ii) permit "publishing ventures" where any particular course materials would be systematically marketed at multiple institutions.

iii) Subject to any further limitations determined in the Rightsholder Terms (and notwithstanding any apparent contradiction in the Order Confirmation arising from data provided by User), any use authorized under the electronic course content pay-per-use service is limited as follows:

A) any License granted shall apply to only one class (bearing a unique identifier as assigned by the institution, and thereby including all sections or other subparts of the class) at one institution;

B) use is limited to not more than 25% of the text of a book or of the items in a published collection of essays, poems or articles;

C) use is limited to not more than the greater of (a) 25% of the text of an issue of a journal or other periodical or (b) two articles from such an issue;

D) no User may sell or distribute any particular materials, whether photocopied or electronic, at more than one institution of learning;

E) electronic access to material which is the subject of an electronic-use permission must be limited by means of electronic password, student identification or other control permitting access solely to students and instructors in the class;

F) User must ensure (through use of an electronic cover page or other appropriate means) that any person, upon gaining electronic access to the material, which is the subject of a permission, shall see:

- a proper copyright notice, identifying the Rightsholder in whose name CCC has granted permission,
- a statement to the effect that such copy was made pursuant to permission,
- a statement identifying the class to which the material applies and notifying the reader that the material has been made available electronically solely for use in the class, and
- a statement to the effect that the material may not be further distributed to any person outside the class, whether by copying or by transmission and whether electronically or in paper form, and User must also ensure that such cover page or other means will print out in the event that the person accessing the material chooses to print out the material or any part thereof.

G) any permission granted shall expire at the end of the class and, absent some other form of authorization, User is thereupon required to delete the applicable material from any electronic storage or to block electronic access to the applicable material.

iv) Uses of separate portions of a Work, even if they are to be included in the same course material or the same university or college class, require separate permissions under the electronic course content pay-per-use Service. Unless otherwise provided in the Order Confirmation, any grant of rights to User is limited to use completed no later than the end of the academic term (or analogous period) as to which any particular permission is granted.

v) Books and Records; Right to Audit. As to each permission granted under the electronic course content Service, User shall maintain for at least four full calendar years books and records sufficient for CCC to determine the numbers of copies made by User under such permission. CCC and any representatives it may designate shall have the right to audit such books and records at any time during User's ordinary business hours, upon two days' prior notice. If any such audit shall determine that User shall have underpaid for, or underreported, any electronic copies used by three percent (3%) or more, then User shall bear all the costs of any such audit; otherwise, CCC shall bear the costs of any such audit. Any amount determined by such audit to have been underpaid by User shall immediately be paid to CCC by User, together with interest thereon at the rate of 10% per annum from the date such amount was originally due. The provisions of this paragraph shall survive the termination of this license for any reason.

c) *Pay-Per-Use Permissions for Certain Reproductions (Academic photocopies for library reserves and interlibrary loan reporting) (Non-academic internal/external business uses and commercial document delivery).* The License expressly excludes the uses listed in Section (c)(i)-(v) below (which must be subject to separate license from the applicable Rightsholder) for: academic photocopies for library reserves and interlibrary loan reporting; and non-academic internal/external business uses and commercial document delivery.

i) electronic storage of any reproduction (whether in plain-text, PDF, or any other format) other than on a transitory basis;

ii) the input of Works or reproductions thereof into any computerized database;

iii) reproduction of an entire Work (cover-to-cover copying) except where the Work is a single article;

iv) reproduction for resale to anyone other than a specific customer of User;

v) republication in any different form. Please obtain authorizations for these uses through other CCC services or directly from the rightsholder.

Any license granted is further limited as set forth in any restrictions included in the Order Confirmation and/or in these Terms.

d) *Electronic Reproductions in Online Environments (Non-Academic-email, intranet, internet and extranet).* For "electronic reproductions", which generally includes e-mail use (including instant messaging or other electronic transmission to a defined group of recipients) or posting on an intranet, extranet or Intranet site (including any display or performance incidental thereto), the following additional terms apply:

i) Unless otherwise set forth in the Order Confirmation, the License is limited to use completed within 30 days for any use on the Internet, 60 days for any use on an intranet or extranet and one year for any other use, all as measured from the "republication date" as identified in the Order Confirmation, if any, and otherwise from the date of the Order Confirmation.

ii) User may not make or permit any alterations to the Work, unless expressly set forth in the Order Confirmation (after request by User and approval by Rightsholder); provided, however, that a Work consisting of photographs or other still images not embedded in text may, if necessary, be resized, reformatted or have its resolution modified without additional express permission, and a Work consisting of audiovisual content may, if necessary, be "clipped" or reformatted for purposes of time or content management or ease of delivery (provided that any such resizing, reformatting, resolution modification or “clipping” does not alter the underlying editorial content or meaning of the Work used, and that the resulting material is used solely within the scope of, and in a manner consistent with, the particular License described in the Order Confirmation and the Terms.

15) Miscellaneous.

a) User acknowledges that CCC may, from time to time, make changes or additions to the Service or to the Terms, and that Rightsholder may make changes or additions to the Rightsholder Terms. Such updated Terms will replace the prior terms and conditions in the order workflow and shall be effective as to any subsequent Licenses but shall not apply to Licenses already granted and paid for under a prior set of terms.

b) Use of User-related information collected through the Service is governed by CCC's privacy policy, available online at www.copyright.com/about/privacy-policy/.

c) The License is personal to User. Therefore, User may not assign or transfer to any other person (whether a natural person or an organization of any kind) the License or any rights granted thereunder; provided, however, that, where applicable, User may assign such License in its entirety on written notice to CCC in the event of a transfer of all or substantially all of User's rights in any new material which includes the Work(s) licensed under this Service.

d) No amendment or waiver of any Terms is binding unless set forth in writing and signed by the appropriate parties, including, where applicable, the Rightsholder. The Rightsholder and CCC hereby object to any terms contained in any writing prepared by or on behalf of the User or its principals, employees, agents or affiliates and purporting to govern or otherwise relate to the License described in the Order Confirmation, which terms are in any way inconsistent with any Terms set forth in the Order Confirmation, and/or in CCC's standard operating procedures, whether such writing is prepared prior to, simultaneously with or subsequent to the Order Confirmation, and whether such writing appears on a copy of the Order Confirmation or in a separate instrument.

e) The License described in the Order Confirmation shall be governed by and construed under the law of the State of New York, USA, without regard to the principles thereof of conflicts of law. Any case, controversy, suit, action, or proceeding arising out of, in connection with, or related to such License shall be brought, at CCC's sole discretion, in any federal or state court located in the County of New York, State of New York, USA, or in any federal or state court whose geographical jurisdiction covers the location of the Rightsholder set forth in the Order Confirmation. The parties expressly submit to the personal jurisdiction and venue of each such federal or state court.

2020-01-2157 Published 15 Sep 2020

Fuel Dosing on a Diesel Oxidation Catalyst for After-Treatment System Heating on a Heavy-Duty Engine Powered by Polyoxymethylene Dimethyl Ethers

Alexander D. Gelner Technical University of Munich

Christian Pastoetter and Harald A. Beck MAN Truck and Bus SE

Martin Härtl and Georg Wachtmeister Technical University of Munich

Citation: Gelner, A.D., Pastoetter, C., Beck, H.A., Härtl, M. et al., "Fuel Dosing on a Diesel Oxidation Catalyst for After-Treatment System Heating on a Heavy-Duty Engine Powered by Polyoxymethylene Dimethyl Ethers," SAE Technical Paper 2020-01-2157, 2020, doi:10.4271/2020-01-2157.

Abstract

Polyoxymethylene dimethyl ethers (OME) are synthetic fuels, which offer the property of sustainability because the reactants of production base on hydrogen and carbon dioxide on the one hand, and the air pollution control in consequence of a soot-free combustion in a diesel engine on the other hand. High exhaust gas recirculation (EGR) rates are a promising measure for nitrogen oxide (NO_x) reduction without increasing particle emissions because of the resolved soot-NO_x trade-off. However, EGR rates towards stoichiometric combustion in OME operation reveals other trade-offs such as methane and formaldehyde emissions. To avoid these, a lean mixture with a combination of EGR and exhaust after-treatment with selective catalytic reduction (SCR) is useful. The limitation of urea dosing due to the light-off temperature of SCR systems requires heating measures. Besides electrical heating, fuel injection into the diesel oxidation catalyst (DOC) for an exothermic reaction is an effective method for a quick achievement of the catalyst working conditions. A slip of unburned or partially oxidized hydrocarbons (HC) in fossil diesel operation restricts this measure. Conducted investigations of a heavy-duty engine showed a reciprocal proportionality in OME operation between injection quantity and unburned fuel fragment slip over the DOC. Additionally, the NO oxidation increases with rising post injection quantities, whereas fuel dosing in diesel operation shows the opposite effect. These behaviors during OME operation enable potentials for further NO_x reduction in tailpipe emissions because of earlier urea dosing in SCR systems in addition to lower raw emission levels caused by high EGR rates.

Introduction

Taking into account the possibility of the production of synthetic fuels from renewable energy, tailored fuels from the group of polyoxymethylene dimethyl ethers (OME) can satisfy the requirements of both climate protection [1] and air pollution control and are a promising alternative to fossil diesel fuels [2]. An electricity based production of the educts methanol and formaldehyde, which are synthesized by hydrogen and carbon dioxide, is possible [3, 4, 5]. Their combustion in a conventional diesel engine is soot-free and therefore solves the soot-NO_x-trade-off. High exhaust gas recirculation (EGR) rates, even leading to stoichiometric conditions, are possible without the detection of soot formation in the exhaust [6, 7, 8, 9, 10, 11]. Although it is conceivable to use a combustion process in stoichiometric operations in combination with a three-way-catalyst [12], this approach is hampered by the declining efficiency of the combustion process and the increase of methane (CH_4) emission in this area [8, 13]. Nevertheless, high EGR rates lead to low raw emission levels of NO_x. Since the operation with OME shows good tolerability with this NO_x-reducing measure and also with decreasing rail pressure levels, simplification of the injection system and the after-treatment system is possible [13]. With a soot-free and low-NO_x combustion process, an after-treatment concept on the one hand without particulate filter and reduced complexity of the selective catalytic reduction (SCR) catalyst could meet the current emission regulation. On the other hand, the low raw emission levels have the potential to enable further tailpipe emission level reductions in combination with modern and future after-treatment technologies. Nevertheless, the operation temperature inside an SCR system is a prerequisite for the sufficient conversion of nitrogen oxides. The conversion depends on the activity of catalysts, but a light-off temperature with notable reduction of NO_x is always above 150°C [14]. For this reason, measures are necessary to achieve this starting temperature within a reasonably quick heating phase. In case of heavy-duty applications, high exhaust mass flows pose a challenge for solutions

with electrically heated catalysts because high electrical power is required. Another approach consists of dosing fuel into the diesel oxidation catalyst (DOC) in order to induce an exothermic reaction (so-called HC dosing or fuel dosing). The generated heat increases the temperature of the downstream after-treatment components until they reach their operating temperature. This measure is particularly promising in a scenario using OME without particulate filter, since the SCR system can be positioned closer towards the DOC. During diesel operation, slip of unburned respectively partially oxidized fuel fragments as consequence of fuel dosing at low exhaust temperatures restrict this measure. Additionally, an accumulation of soot in combination with unburned fuel fragments at the catalytic surface of the DOC - so-called face plugging - occurs in diesel operation [15].

The aim of this study is to characterize the behavior of OME in a fuel dosing application with a heavy-duty engine. It focuses on the temperature dependent slip of unburned fuel fragments over the DOC, especially on formaldehyde and methane, since these are known products of incomplete combustion of OME [7, 8, 13]. Formaldehyde is known for its toxic impact on the human body [16], while methane is considered harmful to the climate [17]. This work compares the results of the emission behavior of conventional diesel fuel under the same conditions as space velocity and exhaust temperature level to the behavior of OME. The first part of this study compares physical properties of the investigated fuels; the second part displays the research methodology, such as test engine, measurement technology setup and test procedure. The test procedure investigates the effect of fuel dosing on tailpipe emissions at several operating points. A detailed comparison of the different behaviors follows in the next part. An extensive discussion of the results with an outlook on the following research concludes the work.

Tested Fuels

Polyoxymethylene dimethyl ethers are oligomers with the structure CH_3-O-$(CH_2O)_n$-CH_3. The investigated fuel consists of a mixture of various OME_n with major percentages of n = 3 – 6 (OME_3: 47%, OME_4: 29%, OME_5: 17%, OME_6: 6%). In this work, the substitute name OME is used for this mixture, while diesel describes fuel according to the EN 590 standard [18] with a maximum content of 7% fatty acid methyl esters (FAME). Table 1 shows the properties of the investigated fuels. ASG Analytik Servicegesellschaft mbH, which also provided the fuel, determined the values of the used OME mixture. The appendix shows the respective standard of the measurement method used. Values for diesel come from the fuel EN 590 standard. The Cetane Number of OME exceeds the requirements of this standard (Cetane Number ≥ 51). Therefore, OME has a high ignitability. This advantage is used to simplify the injection system of common rail engines, since no pilot injection is needed in a wide operation range [13]. The oxygen content of OME is around 45%; the lower heating value (LHV) is thus about 2.2 times lower than the one of diesel. The higher density of OME reduces this relation to a volumetric diesel equivalent ratio of

TABLE 1 Properties of the investigated fuels. The values of OME are determined by ASG Analytik-Servicegesellschaft mbH, the values of diesel come from [19], if not specified in the standard EN 590 [18]

	OME	Diesel (EN 590)
cetane number	75.5	≥ 51
diesel equivalent in m^3/m^3	1.7	1
oxygen content in %	44.5 (m/m)	0 ≈ 0.8 (v/v) with max. 7 % FAME
sulfur content in mg/kg	< 5	≤ 10
lower heating value in MJ/kg	19.1	42.6
density (15°C at 1 bar) in kg/dm^3	1067	820 - 845
boiling range at 1 bar in °C	151.8 - 257.6	170 - 390
flash point at 1 bar in °C	64.5	> 55.0
cold filter plugging point in °C	-24	< -20 (winter) < 0 (summer)
kinematic viscosity in mm^2/s	1.183	2.0 - 4.5
lubricity - HFFR at 60°C in µm	435	≤ 460

$$\frac{LHV_{diesel}}{LHV_{OME}} \cdot \frac{\rho_{diesel}}{\rho_{OME}} \cong 1.7 \quad (1)$$

The boiling range and flash point of the investigated OME mixture are in the region of fossil diesel fuel, which facilitates storage and distribution. Since there is no standardization of the boiling range, the values of diesel are taken from [19], who have determined characteristic values of diesel fuel according to EN 590. For the same reason, the LHV of diesel from this publication is used to calculate the equivalent ratio. The Cold Filter Plugging Point of diesel according to EN 590 is divided into different classes for temperate climate zones. Therefore, the table lists limits of the summer and winter periods. The lubricity exceeds the requirement of the standard, while the kinematic viscosity is lower compared to the specification interval of the standard, which leads to smaller sauter mean diameters of the droplets during injection [20].

Methodology

Test Engine

An MAN D0834LFL79 heavy-duty diesel engine was used. The engine components are not specially adapted to OME operation, despite this, the nozzles of the injectors are modified for higher flows to compensate for the lower energy content of OME. Table 2 displays the attributes of the test engine.

An ABB MDM DN150 thermal dispersion mass flowmeter located in the intake path quantifies the air mass flow downstream of an air filter. A DFM DR 50.02 impeller counter measures the fuel consumption, followed by a fuel filter. A fuel cooler regulates a constant temperature of 35°C upstream of the high-pressure pump. A torque measurement flange connects the engine to a water operated brake on the output

TABLE 2 Attributes of MAN D0834LFL79

number of cylinders	4 inline
displaced volume	4580 cm^3
stroke	125 mm
bore	108 mm
engine power	162 kW
compression ratio	16:1
number of valves per cylinder	4
hydraulic nozzle flow rate of the injector	569 cm^3/30 s at 100 bar (diesel) 970 cm^3/30 s at 100 bar (OME)
charge	single-stage wastegate turbocharger with intercooler
exhaust gas recirculation	none
injection system	common rail (max. 1,800 bar)

TABLE 3 Properties of the diesel oxidation catalyst

carrier structure	Metal: CS®-structure
precious metal content	30 g/ft^3
gravimetric ratio: platinum: palladium	6:1
dimensions Metalit® matrix (diameter; length)	Ø=264 mm; l=50.8 mm
volume Metalit® matrix	2.78 dm^3
Metalit® shape	cylindrical
cell density	300 cells per square inch
open frontal area	82.17 % (*)

(*) assumption: Coating with 150 g/l and wash-coat density of 1.35 g/cm^3

side. An optical encoder provides the engine speed on the opposite side.

Exhaust After-Treatment

The engine in this test setup is equipped with a DOC, which consists of metallic monoliths in a row. Table 3 shows its properties. In this work, the number of monoliths varies between two and three. The number of monoliths defines the space velocity of the exhaust at the same operating point. Therefore, the investigation of the DOC behavior in dependence of the space velocity is possible under constant conditions, such as exhaust temperature upstream the DOC and raw emission levels. A thermocouple measures the exhaust temperature upstream of the DOC, which is simply referred to as exhaust temperature in the following. The additional thermocouple downstream of the DOC enables quantification of the temperature rise over the catalyst due to the exothermic reactions of unburned fuel fragments.

Exhaust Gas Analyzers

A flame ionization detector (FID) determines the unburned fuel fragments emissions. The common term total hydro carbons (THC) or short HC is misleading since it implies a chemical structure of solely hydrogen and carbon. The unburned fuel fragments of OME are considered to be mainly oxygen containing species; the term of volatile organic compounds (VOC) according to the council directive 1999/13/EC of the European Council [21] is therefore more appropriate. The Appendix shows the exact definition of this directive. The emissions quantified by the FID in this work are therefore referred to as VOC. A paramagnetic detector (PMD) is applied to measure the oxygen content of the exhaust gas. A fourier-transform infrared spectrometer (FT-IR) is calibrated to identify specific emissions as methane (CH_4), formaldehyde (CH_2O), nitrogen monoxide (NO) and nitrogen dioxide (NO_2). The detection of NO and NO_2 by the FT-IR enables direct measurement of these species in contrast to the recording of the differential of NO_x and NO with a chemiluminescence detector. A nondispersive infrared sensor (NDIR) quantifies the emission of carbon monoxide (CO). The sampling points for exhaust measurements are at a distance of approximately 45 centimeters upstream and downstream of the DOC. Figure 1 shows a schematic layout of the test bench.

Implementation of Fuel Dosing

Since the engine does not have an extra injector for fuel dosing, a late post injection (PoI) by the main injector is used to provide unburned fuel. The injection time of the PoI is set to a 120° crank angle after top dead center, since this is the value used in diesel particulate filter regeneration mode of the used data record. The diesel injection rate map in the Electronic

FIGURE 1 Schematic test bench layout.

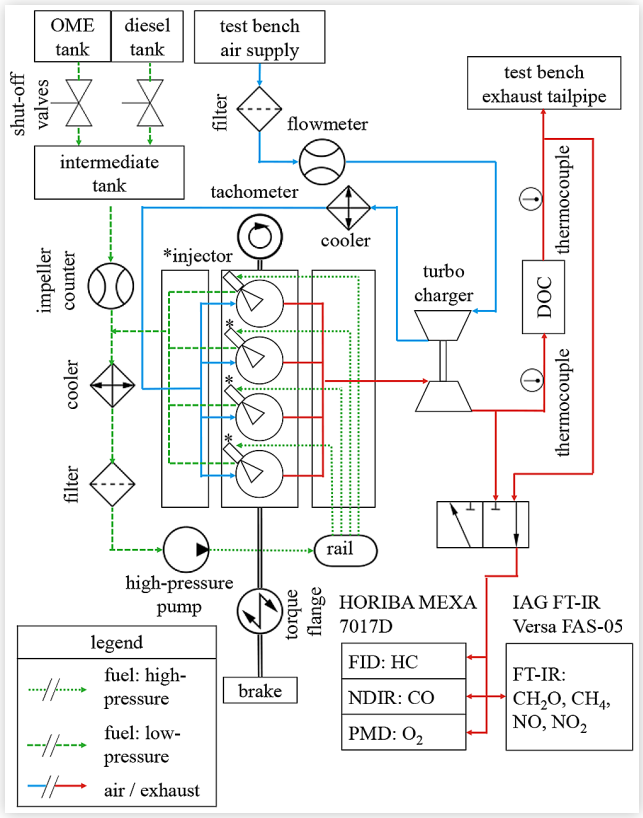

Diesel Control (EDC) is corrected with the factor of the volumetric energy equivalent to provide the same energy content with OME as in diesel operation during one post injection. The following desired injection quantities in this work are indicated in mg/str gravimetric diesel equivalent, which is abbreviated mg/str diesel-eq. or mg/str.

Test Procedure

The test run varied the operation points in direction of decreasing exhaust temperatures. This avoids accumulation of unburned components on the carrier matrix of the DOC, which may become detached in case of reverse direction and lead to measurement artifacts. Engine speed and torque specify the space velocity and exhaust temperature. The sum of the values indicated by the flowmeter in the air path and impeller counter in the fuel path predicts the exhaust massflow. This value results in the comparative value of space velocity, when divided by the catalyst volume and multiplied with the density of the exhaust. The authors consider a normal density of $\rho_{exhaust}$= 1.29 kg/m³or the calculation of the space velocity. The thermocouple upstream of the DOC measures the exhaust temperature. This temperature of 340°C and a space velocity of 30,000 1/h define the first investigated operation point during diesel operation at a speed of 1,450 rpm and a mean effective pressure (p_{me}) of 10.2 bar with a catalyst configuration of three monoliths. The following operating points reduce the exhaust temperature ϑ successively in steps of 20°C by reducing the engine torque. In order to keep the value of the space velocity stable, the engine speed increases to compensate for the lower mass flow resulting from the reduced main injection quantity and the lower charge pressure of the turbocharger due to the lower exhaust enthalpy. The last investigated point has an exhaust temperature of 180°C. Removing one monolith of the DOC increases the space velocity of the investigated operation points to 45,000 1/h. There is no difference in the test procedure for the variant with two monoliths. Since the application used for the engine during OME operation leads to comparatively lower exhaust temperatures, the investigated points in these runs differ in engine speed and torque in order to enable the same exhaust temperatures and space velocities as in diesel operation. The Appendix shows the engine speed and load of the investigated operating points.

Figure 2 shows a flow scheme of the test procedure. The first procedure uses OME in order to avoid measurement fragments in consequence of face plugging in diesel operation. A stabilization phase with a holding period of 300 seconds ensures a stationary temperature level inside the DOC. The test bench system switches to the sampling point upstream of the DOC to determine the raw emission level without fuel dosing. After this measurement with a duration of 60 seconds, the system switches to downstream of the DOC for recording of the tailpipe emissions with the same sampling time. The minimum desired quantity of the post injection (desqPoI), which can be set in the EDC, is 2 mg/str, while the maximum desired quantity is set to 5 mg/str.

FIGURE 2 Flow scheme of the test procedure.

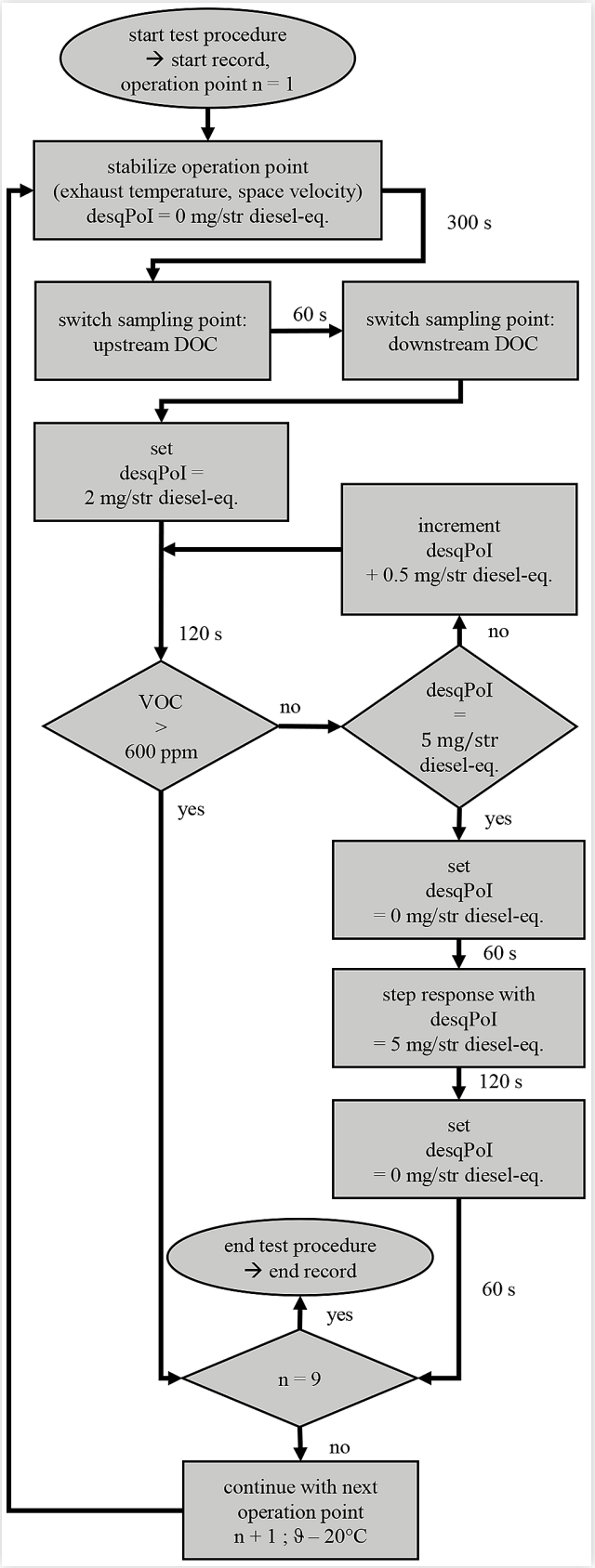

The authors set this maximum limit to avoid spray-wall-interaction due to the late start of injection of the PoI. The incremental step size is 0.5 mg/str. The incremental increase of the desired post injection quantity happens after a pause of 120 seconds to enable a stationary state. Before the increase of the quantity, the test system compares the FID value with the maximum allowed concentration of VOC emission, which is set to 600 ppm. If the VOC slip over the DOC reaches this level, the test system continues with the next operation point. If the emission is below the limit, this loop goes on until the maximum value of the PoI quantity is reached. A clear out by shutdown of the PoI for 120 seconds is followed by a step response measurement with the maximum desired quantity. After another duration of 60 seconds, the test system continues with the shutdown of the PoI and the next operation point. An emission measurement upstream of the DOC does not take place in the test procedure while the post injection is set. This avoids damage to the exhaust gas analyzers due to exposure to high amounts of unburned fuel fragments.

Results and Discussion

Additional Investigation of the CH_2O and CH_4 Unburned Fuel Fragments in OME Operation

Formaldehyde and methane occur under inadequate firing conditions as stoichiometric operation in a diffusive combustion process during OME operation [9, 13]. Since the post injection happens at a crank angle when the combustion is advanced in time, a remaining of a high formaldehyde concentration is likely: The formaldehyde formed during the so-called cold flame [22] at the beginning of the inflammation of the fuel of post injection requires temperatures of around 1,200 K for chemical decay. At temperatures below 1,000 K, CH_2O remains stable during an extended period of time [23]. Figure 3 shows a comparison of CH_2O and CH_4 emission levels upstream and downstream of the DOC with and without the PoI. The results clarify, that CH_2O and CH_4 remain because of incomplete combustion inside the combustion chamber or form in the region of the exhaust pipe upstream of the DOC like in the turbine of the turbocharger. The DOC therefore reduces both emissions, and the measured formaldehyde and methane during the test procedure is not a consequence of chemical decay of unburned OME components on the catalytic coat of the DOC. The knowledge of this fact is prerequisite for interpretation of the results of the presented investigations in this work. Figure 3 also indicates, that oxidation of methane inside the DOC requires higher exhaust temperatures or adapted coating mixtures, which is a commonly known issue [24].

FIGURE 3 Comparison of CH_2O and CH_4 emissions up-/downstream of the DOC with/without post injection at 45,000 1/h. Left side: Exhaust temperature of 260°C. Right side: 340°C.

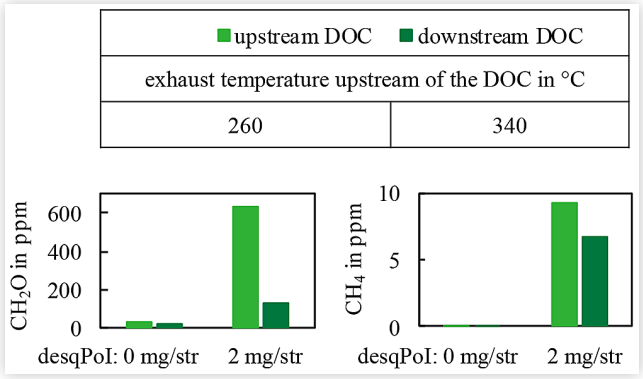

Unburned Fuel Fragments

The presentation focuses on two exhaust temperature levels. Figure 4 shows the emissions measured by the FID and declared as VOC at an exhaust temperature (ϑ) of 280°C. This figure also displays the emission levels of CH_2O and CH_4 and the temperature increase over the DOC (ΔT_{DOC}) as well as the desired quantity of post injection.

At a space velocity of 30,000 1/h, the effect of increasing quantities of post injection on the VOC emission is marginal. At 45,000 1/h, a different behavior between diesel and OME operation becomes visible: While the VOC emission level increases during diesel operation with a higher desqPoI, a decrease in OME operation is noticeable. Simultaneous measurements of the CH_2O level also show this behavior at both space velocities during OME operation.

Immediately after the start of the step response with the desqPoI = 5 mg/str at 1080 seconds, the emission level of the VOC jumps to a peak, followed by a decrease towards a lower level until the shutdown of the PoI. The CH_2O emission during OME operation shows the same behavior. These peaks and the comparison of upstream and downstream emissions in Figure 3 indicate that post injection leads to a bigger amount of unburned fuel fragments upstream of the DOC, especially of formaldehyde in the case of OME operation. This therefore increases the available exergy for heat increase downstream of the DOC in consequence of exothermic reaction at the catalytic surface. Figure 4 confirms this, since the rising PoI quantities lead to a temperature increase over the DOC. The reduction of the emission level, which immediately follows the peak after the increase of the desqPoI, can be explained as follows: Boundary conditions such as exhaust temperature, space velocity and quantity of unburned fuel fragments per stroke upstream of the DOC remain the same during the qPoI step. In addition, the PMD determines an oxygen content of > 9 % at every operating point with diesel and OME, so there is no global oxygen deficiency, which would slow down VOC oxidation. Therefore, a decreasing tailpipe emission level is

FIGURE 4 Comparison of emissions at an exhaust temperature of 280°C. Left side: Space velocity of 30,000 1/h. Right side: 45,000 1/h.

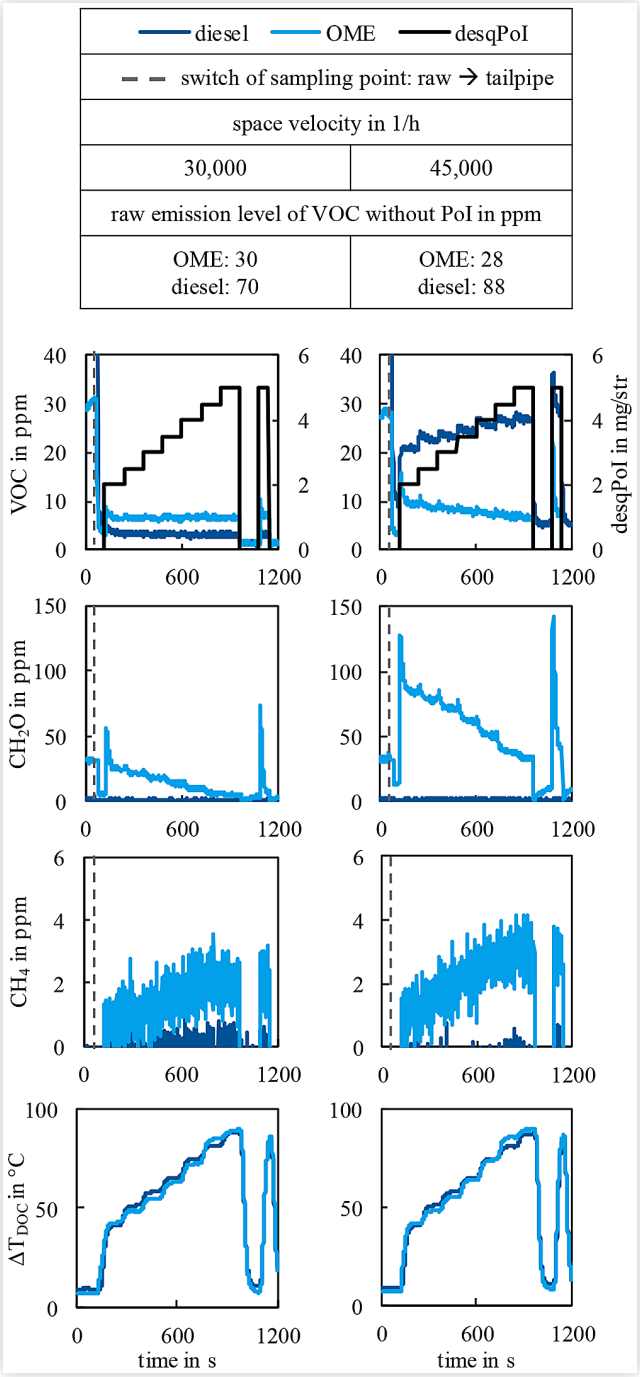

FIGURE 5 Comparison of emissions at exhaust temperature of 200°C. Left side: Space velocity of 30,000 1/h. Right side: 45,000 1/h.

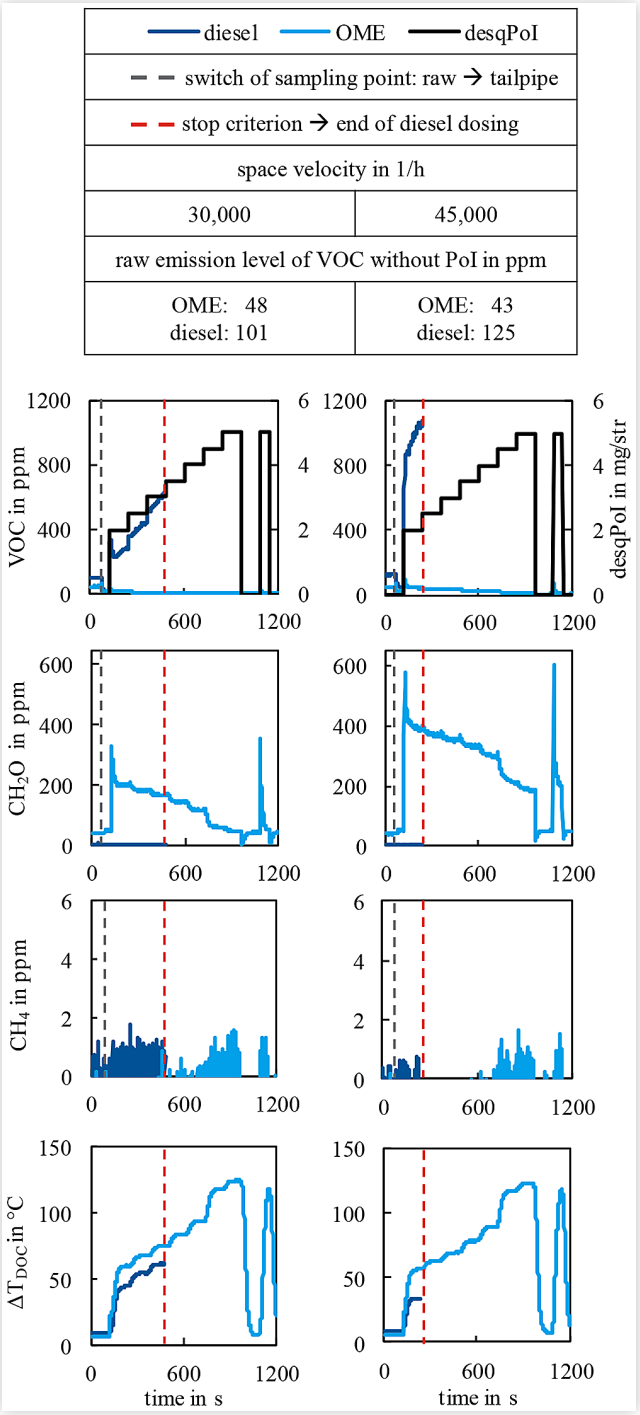

caused by a higher reactivity of the fragments inside of the DOC. Besides these boundary conditions, the local temperature of the catalytic surface of the DOC influences this reactivity. Therefore, the results confirm that post injection is likely to lead to higher surface temperatures and as a consequence to higher reactivity inside the DOC in diesel and OME operation.

Formaldehyde represents a part of the unburned fuel fragments in OME operation according to Figure 4 and Figure 5. *Zhang et al.* [25] and *Bai et al.* [26] confirm that formaldehyde oxidizes in a DOC with a platinum coated surface in high proportions. Therefore, the temperature rise over the DOC during OME operation at $\vartheta = 280°C$ is partly attributable to CH_2O oxidation. Figure 4 proves that, since the CH_2O emission level without the PoI upstream of the DOC is higher than downstream.

The methane emission in OME operations shows a proportional dependency. The measurement records a small

increase with a higher qPoI, while there are no CH_4 and CH_2O emissions in diesel operation. Although the level of methane emission is marginal during OME operation, the impact of the PoI is visible.

The small difference in the temperature increases over the DOC between the diesel and OME operations may be due to different causes. Pre-reactions inside the combustion chamber, the turbine of the turbocharger or the exhaust pipe and the engine speed influence the exergy that is available for conversion inside the DOC. Additionally, the nozzles of the OME injector contain larger holes in order to compensate the lower energy density. This measure affects the hydraulic behavior of the injector, especially in the ballistic range of the opening phase of the needle. Therefore, the relation between the duration of energizing and the injection quantity is nonlinear in a different area when compared to the diesel injector. The functional dependency of injected quantity to duration of energizing and rail pressure in this ballistic range of the OME injector is unknown. The adapted correction of the diesel injection rate map at the EDC with the factor of volumetric energy ratio is not sufficient to guarantee the same amount of injected energy with both fuels. A manual calibration of this map with the difference of values of fuel consumption with and without the PoI to reduce the difference between actually injected fuel quantity and the desqPoI is insufficient due to the inadequate measurement accuracy of the used impeller counter. Nevertheless, the temperature rise over the DOC gets bigger with every increase of the desqPoI at every investigated operating point with both fuels. Therefore, the injected quantity of the PoI increases with every step of desqPoI and the tendentious behavior of the emission levels are thus meaningful.

Figure 5 displays the measurement results at an exhaust temperature level of 200°C. The VOC and CH_2O emissions during OME operation show the same reciprocal relation to the desqPoI in both space velocities, as it is observed at ϑ = 280°C. In diesel operation, the increase of the desqPoI leads to a growing slip of VOC emission over the DOC. In contrast to the behavior at ϑ = 280°C, the VOC slip increases during the desqPoI step. Nevertheless, an increase of the desqPoI increases the $\Delta T_{DOC.}$ The test automation stops the fuel dosing during diesel operation at a desired quantity of 3 mg/str at 30,000 1/h, and at 2 mg/str at 45,000 1/h, because the VOC emission level reaches the limit of 600 ppm. The observed behavior of the methane emission increase in OME operation clearly does not occur at low exhaust temperature levels. At these operation points, no CH_2O or CH_4 emissions are verifiable during diesel operation.

Figure 6 shows the behavior of the VOC and CH_2O emissions during the shutdown of the PoI before and after the step response at 45,000 1/h. This illustration enlarges the section between 900 and 1,200 seconds in the right side of Figure 4 and Figure 5. The VOC emission level at ϑ = 280°C in diesel operation drops to the tailpipe emission level without the PoI in an exponential behavior, while in OME operation, the FID detects no VOC emission after the shutdown. However, the CH_2O emission drops to a lower level, followed by an increase towards the tailpipe emission level without the PoI. This is reproduced at ϑ = 200°C. At this temperature, the VOC emission during OME operation also show this behavior. As

FIGURE 6 Shutdown behavior of VOC and CH_2Oemissions at 280°C and 200°C at a space velocity of 45,000 1/h.

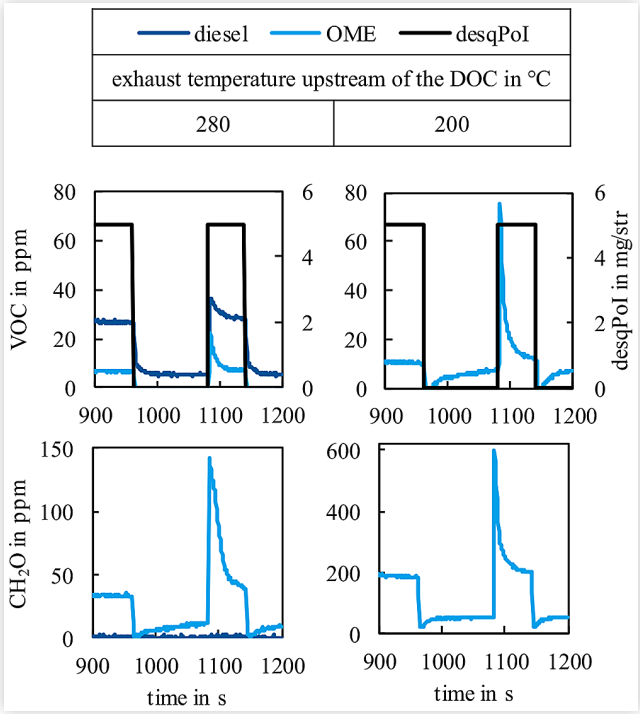

a step response due to the increase of the desqPoI to 5 mg/str, an emission peak appears, followed by an exponential drop towards the stationary level of the step-by-step increase that proceeded first. The CH_2O emission peak during OME operation is higher at 45,000 1/h, but decreases faster to the stationary level. This and the fact, that there is no peak during the step from the desqPoI = 4.5 mg/str to 5 mg/str, confirms the hypothesis of increasing surface temperatures due to the oxidation of formaldehyde.

The results shown in Figure 4, Figure 5 and Figure 6 sum up as follows: Increasing levels of post injection quantities lead to increasing temperatures over the DOC in all of the investigated operating points. At an exhaust temperature of 280°C and at a space velocity of 30,000 1/h, the desqPoI has no noticeable effect on the VOC emission levels during diesel operation, but still a decreasing influence on the CH_2O emission tailpipe levels in OME operation. This influence persists during OME operation at higher space velocities or lower exhaust temperatures. At these operating points, increasing desqPoI lead to higher VOC slip over the DOC in diesel operation, whereas the VOC tailpipe emission during OME operation show a decreasing behavior.

The summary of the observations leads to the following hypothesis: The applied post injections generate unburned fuel fragments, especially formaldehyde in the case of OME operation. These fragments lead to exothermic reactions inside the DOC, which increase the catalytic surface temperature. Higher post injection quantities lead to higher amounts of these fragments and therefore to more exothermic reactions. The increasing surface temperature of the DOC enables higher oxidation rates of the unburned fuel fragments. In case of OME operation, these effects result in decreasing tailpipe

emission levels of CH_2O and VOC in general in an inverse ratio to the quantity of post injection. This decrease is more pronounced in case of higher space velocities and lower exhaust temperatures. Whereas the reactivity increase due to a higher DOC surface temperature does not lead to an inverse ratio of the desqPoI and tailpipe emission level of VOC during diesel operation. *Hutter et. al.* used the effect of a catalytic surface temperature increase due to exothermic reaction of injected CO to enable methane oxidation in a TWC in a lean-burned natural gas engine [24]. Analogous to this study, one reason for the observed phenomenon of the reciprocal relation between CH_2O and VOC and the desqPoI in OME operation in this work, could be the higher oxidation reactivity of formaldehyde inside of the DOC compared to the reactivity of the unburned fuel fragments that appear in diesel operation. An additional observation on the behavior of the catalytic surface temperature and its distribution is useful, but not an integral part of this work. A consideration of integration of these temperature measurements in further investigations is reasonable.

Since the emission level decreases with a higher amount of injected fuel, the investigation of the stationary limit value of the maximum desired quantity of 5 mg/str is meaningful. The measure of fuel dosing in order to heat up the SCR system requires a maximum increase of the temperature over the DOC; therefore, investigations of the maximum desqPoI are expedient. The emission levels of VOC and CH_2O at the end of the last incremental step with the desqPoI = 5 mg/str at the time of 960 seconds in Figure 4 and Figure 5 show an approximation of the value in a stationary condition. Therefore, the arithmetic mean value of the last ten data points before the shutdown of the PoI defines this limit value. Figure 7 displays the limit value of VOC, CH_2O and CH_4 in diesel and OME operations for both space velocities for a desired quantity of post injection of 5 mg/str diesel-eq. for all investigated operation points. The limit value is stated for diesel operation down to an exhaust temperature of 220°C. At lower temperatures, the VOC emission reaches the upper limit of 600 ppm and the test automation shuts down the PoI. The VOC emission during diesel operation show an exponential behavior towards lower exhaust temperatures, which is also the case for CH_2O emission in OME operation. Figure 7 also indicates, that the methane emission at high temperatures during OME operation causes a rise in the VOC emission curve. At higher exhaust temperatures, the FT-IR also detects CH_4 emission in diesel operation, but still below the level of the OME operation.

Nevertheless, further investigations are necessary:

1. Depth of fuel penetration during post injection in order to restrict the quantity of the PoI to avoid fuel-liner-interaction.
2. Observations of an optical accessible combustion chamber for the investigation of methane and formaldehyde formation during OME operation.
3. Measurements of the heat distribution inside the DOC during fuel dosing operation.

However, the following must be taken into account: This study does not consider reactions of the observed emissions

FIGURE 7 Stationary limes of the emissions with desqPoI = 5 mg/str diesel-eq. Standard error of the mean is indicated, but invisible because of a value < 1 ppm for every datapoint.

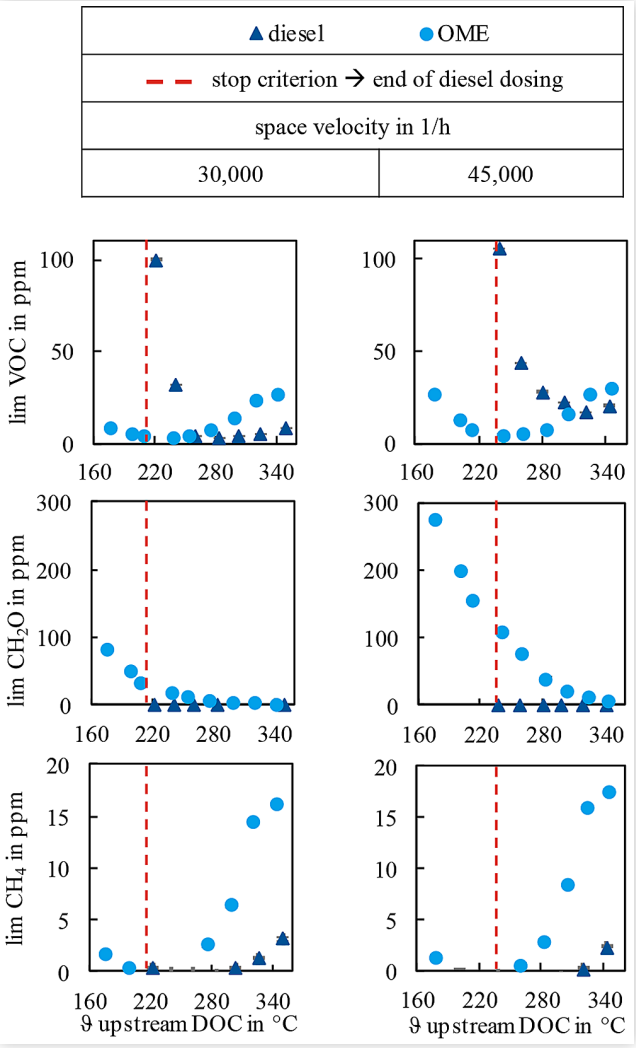

in the after-treatment components that follow downstream of the DOC. *Bertole* e.g. showed, that the injected ammonia in the SCR system increases formaldehyde oxidation [27]. The oxidation inside of an ammonia slip-catalyst will influence the tailpipe emission level as well. Since this study focuses on stationary exhaust temperature conditions, the results do not account for an application of dynamic engine operation. Therefore, it is possible that the experimental vehicle shows a different behavior with temporary varying exhaust mass flows, exhaust temperatures and quantities of post injection.

Effect on CO and NO Oxidation

In addition to the oxidation of unburned fuel fragments, there are also other reactions inside of the DOC. An analysis of the behavior of OME and diesel in fuel dosing also includes the consideration of the effect on the oxidation of carbon monoxide (CO) and nitrogen monoxide (NO). Figure 8

FIGURE 8 Comparison of CO emission and ratio of NO_2 to NO_x with fuel dosing at a space velocity of 30,000 1/h; diesel dosing stopped at the desqPoI = 3 mg/str because the VOC limit of 600 ppm was reached. Left side: Exhaust temperature of 280°C. Right side: 200°C.

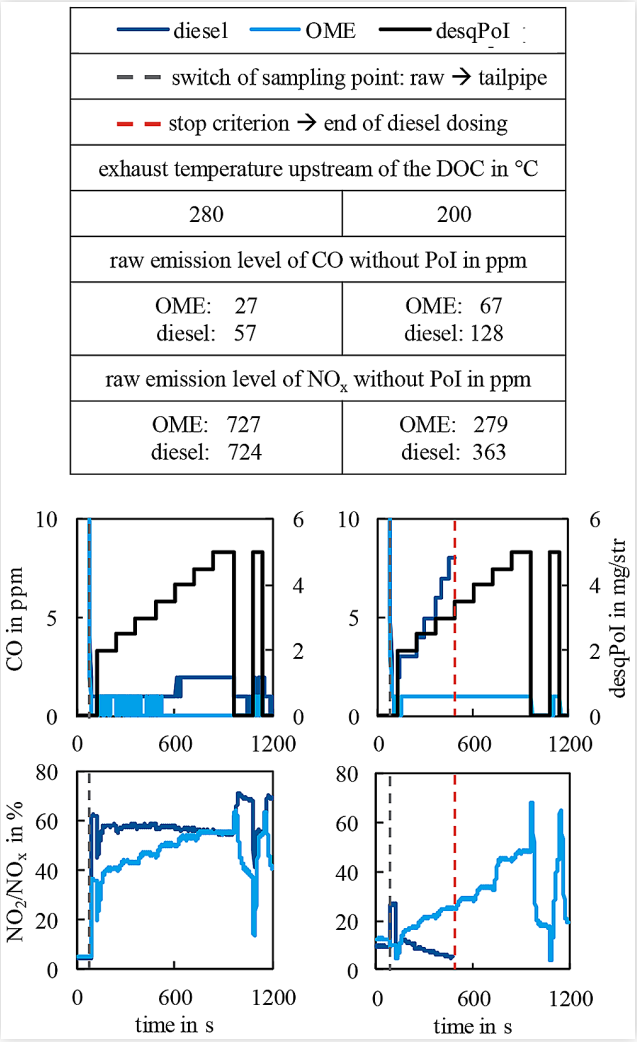

represents the effect of fuel dosing on CO and the NO_2-NO_x-ratio for the selected operating points with an exhaust temperature of 280°C and 200°C at a space velocity of 30,000 1/h. An increase of CO emission as consequence of fuel dosing is detectable, but especially in case of OME operation, it's negligibly small. However, the effect of fuel dosing on NO oxidation is clear. The reactions of VOC with oxygen occupy active centers on the catalytic surface. During diesel operation, fuel dosing leads to a decrease of NO oxidation in proportional dependency of the qPoI, whereas the VOC and especially formaldehyde oxidation increase the NO oxidation in OME operation. The level of NO_2/NO_x during OME operation behaves in an opposite direction than the emission level of CH_2O does during an increase or decrease of the desqPoI.

An inhibition of NO oxidation effects the reactions in the following SCR system. The so-called "fast SCR mechanism" is desirable for boosting NO_x reduction and requires a ratio of NO_2 to NO_x of 0.5 [28]. The increase of this ratio by oxidation of NO inside of the DOC is necessary due to values of < 0.1 for all operating points in the raw exhaust. Since fuel dosing is a measure to heat up the following SCR system in order to overcome the light-off threshold of NO_x-reduction, the resulting decrease of the NO_2-NO_x-ratio in diesel operation, especially at low exhaust temperatures, slows down the desired effect of NO_x-reduction by the fast SCR mechanism. Nevertheless, the tailpipe-NO_2-NO_x-ratio during OME operation without the PoI is lower compared to the level during diesel operation.

Conclusions and Outlook

Slip of VOC emission restricts the heating measure of fuel dosing in order to heat up the following after-treatment system by exothermic reaction inside of the DOC at low exhaust temperatures. While this slip increases with higher quantities of post injection in diesel operation, the investigations showed a reciprocal proportionality in OME operation, even at low exhaust temperatures as low as 180°C. Still, the late post injection of OME causes formaldehyde and methane slip over the DOC in dependence of the exhaust temperature level and space velocity. Nevertheless, the behavior enables potentials to keep the SCR system at operating temperature or shorten the warm-up phase without increasing the VOC slip with higher post injection quantities. Electrical heating of the catalytic surface could reduce the peak phase of VOC and especially CH_2O emissions after starting the PoI, in which the required heating of the DOC surface due to the oxidation of unburned fuel fragments, especially formaldehyde, takes place. With this measure, the VOC and especially CH_2O tailpipe emission levels decrease quicker. During diesel operation, the electrical heating must mitigate higher slip due to higher desired quantities of post injection. In OME operation, higher fuel dosing quantities support the reduction of tailpipe VOC and CH_2O emissions. Nevertheless, the rise of methane emission with increasing post injection quantities at higher exhaust temperatures causes an increase of VOC emission. Furthermore, the fuel dosing of OME intensifies NO oxidation on the catalytic surface of the DOC.

In order to evaluate the potential of OME regarding the reduction of tailpipe emissions of internal combustion engines, the following investigations are planned: The effect of exhaust in OME operation on the SCR system will be investigated. Furthermore, the presented potentials of fuel dosing with OME will be rated in combination with an electric heatable DOC carrier, and also during dynamic operation with a whole after-treatment configuration. These studies will be finalized by investigations on the effect of the removal of the particulate filter on particulate emissions and measurement of heat distribution in the following systems.

Contributions

Alexander D. Gelner is the main author of this work. He developed the experimental setup and the test procedure and

carried out the experiments. He analyzed the data and wrote the manuscript. Christian Pastötter supported the experimental setup, evaluation and discussion of results in this work and contributed review and consultation. Dr. Harald A. Beck supported in the chemical interpretation of the results and in reviewing. Dr. Martin Härtl and Prof. Dr. Georg Wachtmeister contributed to this work by reviewing and supervising. Mr. Alessandro Sommer, M.Sc. (TUM) and Mr. Christian Kastl (MAN Truck & Bus SE) supported the execution of the experiment.

Contact Information

Alexander D. Gelner
gelner@lvk.mw.tum.de

Acknowledgments

This study formed part of the "Sub-Zero-Emissions Dieselmotor" project, which is funded by the Bavarian Research Foundation. The project is carried out in collaboration with MAN Truck & Bus SE, VT Vitesco Technologies Emitec GmbH, Chair of Analytical Chemistry of TUM and Analytik Servicegesellschaft mbH. Their support is gratefully acknowledged. The authors also want to thank Dr. Dieter Rothe (MAN Truck & Bus SE), Dr. Eberhard Jacob and Mr. Dominik Pélerin, M.Sc. for consultation in this study.

Definitions/Abbreviations

CH_4 - methane

CH_2O - formaldehyde (IUPAC: methanal)

CO - carbon monoxide

desqPoI - desired quantity of post injection in $\frac{mg}{str}$ gravimetric diesel equivalent

DOC - diesel oxidation catalyst

EDC - electronic diesel control

EGR - exhaust gas recirculation

FAME - fatty acid methyl esters

FID - flame ionization detector

FT-IR - fourier-transform infrared spectrometer

HC - unburned fuel fragments

$LHV_{(n)}$ - lower heating value (of the component n) in MJ/kg

NDIR - nondispersive infrared detector

NO - nitrogen monoxide

NO_2 - nitrogen dioxide

NO_x - nitrogen oxides

OME - polyoxymethylene dimethyl ether

PMD - paramagnetic detector

p_{me} - mean effective pressure in bar

PoI - post injection

qPoI - quantity of post injection in mg/str diesel-equivalent

SCR - selective catalytic reduction

THC - total hydro carbons

VOC - volatile organic compounds

ΔT_{DOC} - temperature rise over the DOC in °C

ϑ - exhaust temperature upstream of the DOC in °C

$\rho_{(n)}$ - density (of the component n) in kg/m^3

References

1. Horowitz, C.A., "Paris Agreement," *Int. leg. mater.* 55(4):740–755, 2016, doi:10.1017/S0020782900004253.
2. Schemme, S., Samsun, R.C., Peters, R., and Stolten, D., "Power-to-Fuel as a Key to Sustainable Transport Systems - An Analysis of Diesel Fuels Produced from CO 2 and Renewable Electricity," *Fuel* 205:198–221, 2017, doi:10.1016/j.fuel.2017.05.061.
3. Burger, J., Siegert, M., Ströfer, E., and Hasse, H., "Poly(oxymethylene) Dimethyl Ethers as Components of Tailored Diesel Fuel: Properties, Synthesis and Purification Concepts," *Fuel* 89(11):3315–3319, 2010, doi:10.1016/j.fuel.2010.05.014.
4. Held, M., Tönges, Y., Pélerin, D., Härtl, M. et al., "On the Energetic Efficiency of Producing Polyoxymethylene Dimethyl Ethers From CO 2 Using Electrical Energy," *Energy Environ. Sci.* 12(3):1019–1034, 2019, doi:10.1039/C8EE02849D.
5. Zhang, X., Oyedun, A.O., Kumar, A., Oestreich, D. et al., "An Optimized Process Design for Oxymethylene Ether Production from Woody-Biomass-Derived Syngas," *Biomass and Bioenergy* 90:7–14, 2016, doi:10.1016/j.biombioe.2016.03.032.
6. Pellegrini, L., Marchionna, M., Patrini, R., Beatrice, C. et al., "Combustion Behaviour and Emission Performance of Neat and Blended Polyoxymethylene Dimethyl Ethers in a Light-Duty Diesel Engine," SAE Technical Paper 2012-01-1053, 2012, https://doi.org/10.4271/2012-01-1053.
7. Pellegrini, L., Marchionna, M., Patrini, R., and Florio, S., "Emission Performance of Neat and Blended Polyoxymethylene Dimethyl Ethers in an Old Light-Duty Diesel Car," SAE Technical Paper 2013-01-1035, 2013, https://doi.org/10.4271/2013-01-1035.
8. Härtl, M., Seidenspinner, P., Jacob, E., and Wachtmeister, G., "Oxygenate Screening on a Heavy-Duty Diesel Engine and Emission Characteristics of Highly Oxygenated Oxymethylene Ether Fuel OME1," *Fuel* 153:328–335, 2015, doi:10.1016/j.fuel.2015.03.012.
9. Barro, C., Parravicini, M., Boulouchos, K., and Liati, A., "Neat Polyoxymethylene Dimethyl Ether in a Diesel Engine; Part 2: Exhaust Emission Analysis," *Fuel* 234:1414–1421, 2018, doi:10.1016/j.fuel.2018.07.108.
10. Damyanov, A., Hofmann, P., Geringer, B., Schwaiger, N. et al., "Biogenous Ethers: Production and Operation in a Diesel Engine," *Automot. Engine Technol.* 3(1–2):69–82, 2018, doi:10.1007/s41104-018-0028-x.

11. Lumpp, B., Rothe, D., Pastötter, C., Lämmermann, R. et al., "Oxymethylene Ethers as Diesel Fuel Additives of the Future," *MTZ Worldw* 72(3):34–38, 2011, doi:10.1365/s38313-011-0027-z.
12. Ogawa, H., Nabi, N., Minami, M., Miyamoto, N. et al., "Ultra Low Emissions and High Performance Diesel Combustion with a Combination of High EGR, Three-Way Catalyst, and a Highly Oxygenated Fuel, Dimethoxy Methane (DMM)," in *SAE Technical Paper Series, CEC/SAE Spring Fuels & Lubricants Meeting & Exposition*, JUN. 19, 2000, SAE International, 400 Commonwealth Drive, Warrendale, PA, United States, 2000.
13. Pélerin, D., Gaukel, K., Härtl, M., Jacob, E. et al., "Potentials to Simplify the Engine System Using the Alternative Diesel Fuels Oxymethylene Ether OME1 and OME3−6 on a Heavy-Duty Engine," *Fuel* 259:116231, 2020, doi:10.1016/j.fuel.2019.116231.
14. Girard, J.W., Montreuil, C., Kim, J., Cavataio, G. et al., "Technical Advantages of Vanadium SCR Systems for Diesel NOx Control in Emerging Markets," *SAE Int. J. Fuels Lubr.* 1(1):488–494, 2009, https://doi.org/10.4271/2008-01-1029.
15. Nakano, K., Okano, H., Inoue, K., and Obuchi, A., "Study on the Prevention of Face-Plugging of Diesel Oxidation Catalyst (DOC)," in *SAE Technical Paper Series, WCX World Congress Experience*, APR. 10, 2018, SAE International400 Commonwealth Drive, Warrendale, PA, United States, 2018.
16. Fischer, M.H., "The Toxic Effects of Formaldehyde and Formalin," *The Journal of experimental medicine* 6(4–6):487–518, 1905, doi:10.1084/jem.6.4-6.487.
17. IPCC SYR TSU, "Climate Change 2014: Synthesis Report," 2015.
18. "DIN EN 590:2017-10, Kraftstoffe_- Dieselkraftstoff_- Anforderungen und Prüfverfahren; Deutsche Fassung EN_590:2013+A1:2017," Beuth Verlag GmbH.
19. Lautenschütz, L., Oestreich, D., Seidenspinner, P., Arnold, U. et al., "Physico-chemical Properties and Fuel Characteristics of Oxymethylene Dialkyl Ethers," *Fuel* 173:129–137, 2016, doi:10.1016/j.fuel.2016.01.060.
20. Li, D., Gao, Y., Liu, S., Ma, Z. et al., "Effect of Polyoxymethylene Dimethyl Ethers Addition on Spray and Atomization Characteristics Using a Common Rail Diesel Injection System," *Fuel* 186:235–247, 2016, doi:10.1016/j.fuel.2016.08.082.
21. THE COUNCIL OF THE EUROPEAN UNION, "COUNCIL DIRECTIVE 1999/13/EC of 11 March 1999 on the Limitation of Emissions of Volatile Organic Compounds Due to the Use of Organic Solvents in Certain Activities and Installations," 1999.
22. Pekalski, A.A., Zevenbergen, J.F., Pasman, H.J., Lemkowitz, S.M. et al., "Process Safety at Elevated Temperatures and Pressures," *Loss Prevention and Safety Promotion in the Process Industries*, Elsevier, ISBN 9780444506993:917–932, 2001.
23. Ashman, P.J., and Haynes, B.S., "Formaldehyde Formation in Small Gas Burners," *Combustion Science and Technology* 116–117(1–6):359–373, 1996, doi:10.1080/00102209608935554.
24. Hutter, R., de Libero, L., Elbert, P., and Onder, C.H., "Catalytic Methane Oxidation in the Exhaust Gas Aftertreatment of a Lean-Burn Natural Gas Engine," *Chemical Engineering Journal* 349:156–167, 2018, doi:10.1016/j.cej.2018.05.054.
25. Zhang, C., and He, H., "A Comparative Study of TiO2 Supported Noble Metal Catalysts for the Oxidation of Formaldehyde at Room Temperature," *Catalysis Today* 126(3–4):345–350, 2007, doi:10.1016/j.cattod.2007.06.010.
26. Bai, B., Qiao, Q., Li, J., and Hao, J., "Progress in Research on Catalysts for Catalytic Oxidation of Formaldehyde," *Chinese Journal of Catalysis* 37(1):102–122, 2016, doi:10.1016/S1872-2067(15)61007-5.
27. Bertole, C., "Formaldehyde Oxidation over Emission Control Catalysts," in *SAE Technical Paper Series, WCX World Congress Experience*, APR. 10, 2018, SAE International400 Commonwealth Drive, Warrendale, PA, United States, 2018.
28. GROSSALE, A., NOVA, I., TRONCONI, E., CHATTERJEE, D. et al., "The Chemistry of the NO/NO2-NH3 "Fast" SCR Reaction Over Fe-ZSM5 Investigated by Transient Reaction Analysis," *Journal of Catalysis* 256(2):312–322, 2008, doi:10.1016/j.jcat.2008.03.027.

Appendix

TABLE 4 Determined values of OME and the respective measurement method

	value	method
Cetane number	81	DIN EN 17155:2018
oxygen content in %(m/m)	45,3	DIN 51732:2014 mod.
sulfur content in mg/kg	<5	DIN EN ISO 20884:2011
lower heating value in MJ/kg	19,8	DIN 51900-2:2003 mod.
density (15°C at 1 bar) in kg/dm^3	1055,5	DIN EN ISO 12185:1997
boiling range at 1 bar in °C	118,7 - 266,8	DIN EN ISO 3405:2011
flash point at 1 bar in °C	57,5	DIN EN ISO 2719:2016
Cold Filter Plugging Point in °C	-18	DIN EN 116:2018
kinematic viscosity in mm^2/s	1,188	DIN EN ISO 3104:1999
lubricity - HFFR at 60°C in µm	440	DIN EN ISO 12156-1:2016

TABLE 5 Investigated operating points

	Diesel operation		OME operation	
Exhaust temperature upstream of the DOC in °C	Engine speed in rpm	Mean effective pressure in bar	Engine speed in rpm	Mean effective pressure in bar
340	1,450	10.15	1,350	11.75
320	1,510	8.65	1,420	10.15
300	1,570	7.55	1,480	8.95
280	1,620	6.55	1,550	7.55
260	1,680	5.5	1,610	6.3
240	1,730	4.55	1,650	5.35
220	1,800	3.7	1,750	3.85
200	1,850	2.9	1,810	3.3
180	1,910	2.05	1,860	2.2

Definition of Volatile Organic Compound According to 1999/13/EC

"Volatile organic compound (VOC) shall mean any organic compound having at 293,15 K a vapour pressure of 0,01 kPa or more, or having a corresponding volatility under the particular conditions of use. For the purpose of this Directive, the fraction of creosote which exceeds this value of vapour pressure at 293,15 K shall be considered as a VOC."

ISSN 0148-7191

Gelner, A. D.; Pang, G. A.; Weber, M.; Haisch, C.; Beck, H. A.; Härtl, M.; Jaensch, M.; Wachtmeister, G.: *Gaseous Emissions in Transient Cold-Start Operation of a Heavy-Duty Engine Fueled with Polyoxymethylene Dimethyl Ethers and Methods for After-Treatment System Heating*; Environmental Science: Advances (1), 2022, pp. 470-482. [198]

Gaseous emissions of a heavy-duty engine fueled with polyoxymethylene dimethyl ethers (OME) in transient cold-start operation and methods for after-treatment system heating

A. D. Gelner, G. A. Pang, M. Weber, C. Haisch, H. A. Beck, C. Pastoetter, M. Härtl, M. Jaensch and G. Wachtmeister,
Environ. Sci.: Adv., 2022, **1**, 470 **DOI:** 10.1039/D2VA00080F

Environmental Science Advances

ROYAL SOCIETY OF CHEMISTRY

PAPER

View Article Online
View Journal | View Issue

Cite this: *Environ. Sci.: Adv.*, 2022, **1**, 470

Gaseous emissions of a heavy-duty engine fueled with polyoxymethylene dimethyl ethers (OME) in transient cold-start operation and methods for after-treatment system heating†

Alexander D. Gelner, *[a] Genny A. Pang, [ac] Markus Weber, [a] Christoph Haisch, [a] Harald A. Beck,[b] Christian Pastoetter,[b] Martin Härtl, [a] Malte Jaensch [a] and Georg Wachtmeister[a]

Polyoxymethylene dimethyl ethers (OME) are promising e-fuels for diesel engines, combining carbon-neutral production and low-emission engine operation by virtue of soot-free combustion. The emissions of diesel engines fueled with OME and in blends with diesel have been studied extensively using single-cylinder research engines under laboratory conditions. Emissions from a series engine using an exhaust after-treatment system (ATS) – especially in cold-start operation – are largely unexplored. This study presents investigations conducted using a heavy-duty engine with ATS in a transient driving cycle including cold-start operation. Measurements from a Fourier transform infrared spectrometer (FT-IR) showed that formaldehyde and formic acid form the largest proportion of the monitored tailpipe exhaust emissions due to incomplete combustion in cold-start operation, as long as the catalysts are below their light-off temperature. Non-target screening using a mass spectrometer for online characterization of both gaseous and aerosol exhaust revealed that unburned OME accounts for the majority of gaseous emissions of heavy species in raw exhaust, independent of cold- or hot-start. The ATS removes OME in the exhaust equally in the cold and the hot run. Additionally, this study presents results with specific measures taken for ATS heating such as electrical heating and fuel dosing – demonstrating that electrical heating in combination with an early start of fuel dosing reduces nitrogen oxide (NO_x) emissions in the transient driving cycle by 64.9%, but at the cost of an increase in formaldehyde emission of 58.3%. A later start of fuel dosing avoids this increase and reduces NO_x emissions by 61.8%.

Received 27th April 2022
Accepted 16th June 2022

DOI: 10.1039/d2va00080f

rsc.li/esadvances

Environmental significance

OME is a sustainable e-fuel which burns soot-free and therefore helps to reduce the impact of diesel engines on the environment regarding climate change and air pollution due to black carbon emission. However, incomplete combustion of OME results in the formation of other pollutants such as formaldehyde. In order to avoid the emission of these species and the emission of nitrogen oxides, exhaust after-treatment is necessary but requires operation above the light-off temperature of the catalysts. This study contains investigations on gaseous emissions of a heavy-duty engine fueled with OME with a state-of-the-art after-treatment system in transient cold-start and hot operation. A conventional exhaust analysis system and a novel approach for non-target screening in order to observe secondary emissions besides the well-known products of incomplete OME combustion is used. Additionally, the study evaluates two methods for after-treatment system heating in order to reduce the period of inactive catalysts and therefore to minimize environmental impact of an OME engine.

Introduction

It is widely accepted that greenhouse gas emissions from fossil fuel combustion are considered a significant cause of anthropogenic climate change, which is a central challenge of the 21st century.[1] Therefore, substituting fossil fuels with energy from renewable sources like wind or solar power is considered an essential solution to avoiding greenhouse gas emissions.[2] Storage of these renewable energies *via* the electricity-based synthesis of so-called "e-fuels" enables the potential for

[a]*Technical University of Munich (TUM), Schragenhofstraße 31, Munich 80992, Germany. E-mail: gelner@tum.de*

[b]*MAN Truck & Bus SE, Vogelweiherstraße 33, Nuremberg 90441, Germany*

[c]*Universität der Bundeswehr München, Werner-Heisenberg-Weg 39, Neubiberg 85577, Germany*

† Electronic supplementary information (ESI) available. See https://doi.org/10.1039/d2va00080f

climate-neutral operation of existing and future internal combustion engines.[3] In addition to synthetic e-fuels having similar properties to their fossil fuel counterpart, some so-called "tailored fuels" offer advantages such as lower pollutant combustion. For example, oxygenated fuels burn with significant lower soot and particle emissions.[4] In the case of diesel engines, oligomers from the series of polyoxymethylene dimethyl ethers (OME) are among the most promising alternatives.[5] The synthesis process for producing OME is based on hydrogen – which can be produced by means of electrolysis from renewable energies – and carbon dioxide, which comes from either direct air capture, post combustion capture, or point sources.[6] The combustion of OME is soot-free[4,7–10] by virtue of the lack of intramolecular C–C bonds.[11] In addition to the harmful effect of soot on human health,[12] black carbon is also regarded as an accelerator of climate change.[13] Soot-free combustion resolves the trade-off between soot and NO_x that is typical of fossil diesel and paraffinic alternatives,[7,14,15] thus enabling the reduction of NO_x emissions through in-engine measures without increasing the level of particulate emissions by soot formation.[14,16] NO_x emissions are considered harmful to the respiratory tract[17] and are initiators of photochemical smog.[18] In combination with a state-of-the-art exhaust after-treatment system (ATS), OME-fueled engines offer the possibility of ultra-low pollutant emissions, which was demonstrated in a previous study by Gelner *et al.* on a heavy-duty engine in a stationary and transient test cycle.[19] As with conventional diesel operation, however, effectiveness of the ATS requires a system that is hot from engine operation. Due to successive adjustments to exhaust gas legislation, emissions in the so-called cold start – *i.e.* before the light-off temperature of the catalytic converters is reached – play an increasingly important role in passing emission tests.[20] Williams *et al.* demonstrated that most of the NO_x emissions were emitted during the first minutes of a driving cycle during cold-start operation.[21] Here both the oxidation of gaseous products of incomplete combustion, such as carbon monoxide or hydrocarbons by the diesel oxidation catalyst (DOC), and the reduction of NO_x by selective catalytic reduction (SCR) are inhibited. Whereas cold-start emissions from fossil or biodiesel have been studied in sufficient detail,[22–26] cold start emissions from OME operations remain uninvestigated. Härtl *et al.*,[4] Barro *et al.*[27] and Pélerin *et al.*[14] demonstrated formaldehyde (CH_2O) and methane (CH_4) emissions during incomplete OME combustion on a preconditioned single-cylinder research engine, which is why these emissions can also be assumed to occur during cold starts. Moreover, the results by Zengel *et al.*[28] and Elsener *et al.*[29] showed the formation of hydrogen cyanide (HCN) in the SCR system under the presence of CH_2O and NH_3. The results of Gelner *et al.* did not show any tailpipe emission of HCN with a hot ATS.[19] They assumed a combination of oxidative catalysts upstream and downstream of the SCR stage to be essential for avoiding the tailpipe emission of HCN because of the prior oxidation of CH_2O and the downstream oxidation of eventually formed HCN.

To keep the period of an inactive ATS as short as possible, various methods have been established to speed up heating of the ATS, which have been discussed by Gao *et al.* along with a discussion of their effectiveness.[30] Additionally, fuel dosing, in which the supply of unburned fuel to the DOC for catalytic combustion heats the downstream components of the ATS using the heat released from the exothermic reaction, is another effective method for reducing the period of inactive ATS.[31] Fuel dosing is restricted in diesel operation by a phenomenon known as face plugging. The resulting hydrocarbon (HC) emissions in combination with soot particles block the active centers of the DOC, and thus lead to inactivation of the catalytic surface.[32] Gelner *et al.* demonstrated the effectiveness of fuel dosing on a heavy-duty engine in OME operation using a DOC, but limited by a CH_2O slip.[31] In contrast to diesel operation, however, this slip is indirectly proportional to the injection quantity. Therefore, fuel dosing was considered to be a promising method for reducing the inactive ATS period due to soot-free combustion – and thus avoidance of face plugging – as long as the remaining ATS components are removing CH_2O slip.

This study investigates the gaseous emissions occurring in the homologation-relevant World Harmonized Transient Cycle (WHTC) driving cycle in an OME-fueled heavy-duty engine equipped with an ATS. The cold and hot cycles are compared in order to distinguish between cold-start-induced emissions and emissions that also occur at operating temperature. A custom-built mass spectrometer (MS) system was employed for supplementary non-target screening of gaseous emissions in order to identify any possible unknown substances in the exhaust which were not accounted for in the primary Fourier transform infrared spectrometer (FT-IR) concentration measurements of the exhaust. In addition, the MS employed was calibrated for quantitative OME concentration measurement at a higher sensitivity than the FT-IR used. Moreover, electrical heating of the DOC according to Maus *et al.*[33] was employed in combination with the fuel dosing suggested by Gelner *et al.*[31] The operating strategy was varied so as to enable evaluation of the effectiveness of various methods for reducing the length of the cold-start period.

Materials and methods

Fuel

OME are oligomers with different chain lengths and have the general structure of $CH_3–O–(CH_2O)_n–CH_3$, where n is the number of inner-molecular oxymethylene groups. The abbreviation OME_n indicates the respective chain length of the molecule. In this study, the fuel mixture used for the experiments contained several OME_n with major percentages of $n = 3$–6 (OME_3: 58%, OME_4: 29%, OME_5: 10%, OME_6: 2%). The proportion of shorter- or longer-chain OME was less than 1%. As additives, the fuel also contained 300 mg kg^{-1} each of butylated hydroxytoluene (BHT) as an antioxidant as well as a flow improver. This mixture will be simply abbreviated as OME in the remainder of this paper. ASG Analytik-Service AG (Germany) provided the OME fuel used and measured the property values. Table 1 in the ESI† contains these values and the respective standard of the measurement method used. The mixture fulfills the M DIN TS 51699 standard for OME fuel.[34] As

a reference, "diesel" describes fossil fuel according to the EN 590 standard[35] having a maximum content of 7% (v/v) fatty acid methyl esters (FAME). Table 1 presents the physico-chemical properties of the OME fuel mixture and presents a comparison of the properties with fossil diesel. The diesel values are largely from the fuel EN 590 standard. When the standard did not provide information about a specific property, this value was taken from Lautenschütz *et al.*[36] The oxygen content calculation was based on the assumption that the FAME content consists of oleic acid, with the respective values coming from Hoekman *et al.*[37]

Given an oxygen content of 45% (w/w), the OME mixture used had a reduced lower heating value (LHV) than fossil diesel. The higher OME density partially compensates this to a volumetric diesel equivalent ratio of

$$\frac{\mathrm{LHV_{diesel}}}{\mathrm{LHV_{OME}}} \cdot \frac{\rho_{\mathrm{diesel}}}{\rho_{\mathrm{OME}}} \approx 1.75 \quad (1)$$

The cetane number of OME exceeds the requirements of the EN 590 standard. The higher cetane number indicates excellent ignitability, which enables engine operation without pilot injection, as demonstrated in previous studies.[14,38] The boiling range of OME is similar to that of diesel, but with an initial start and end of boiling at lower temperatures. The flash point of OME surpasses the EN 590 value. The boiling range and flash point enable OME storage and distribution similar to that of fossil diesel. The lubricity of OME exceeds the requirement of the standard, while the kinematic viscosity is below the specification interval of the EN 590 standard. The sulfur content of OME is lower than 5 ppm, so it achieves the lower limit of the sulfur content determination standard. Furthermore, the OME mixture used contained an amount of 233 mg kg^{-1} CH_2O, which is a reactant in the synthesis process of OME.[39] The additive BHT prevents the decomposition of OME and therefore inhibits an increase in the CH_2O concentration in the fuel.[40]

Test engine

This study employed a MAN D2676LF51 heavy-duty six-cylinder diesel engine with two modifications besides the OME-adapted application of the electronic control unit of the state-of-the-art diesel operation:[1] the high-pressure pump was equipped with adapted seals which prevent swelling of the sealing material due to the different chemical polarity of OME,[2] the injectors in OME operation differed in nozzle geometry in order to compensate for the reduced LHV by a higher nozzle flow rate. The second modification prevented the need for higher injection durations on high-load points, which would have resulted in an increase in combustion duration and therefore in a reduction in efficiency.[41] Longer injection durations could also lead to interactions of the fuel jet with the lubricating film during the downward movement of the piston since the liner would be revealed. Moreover, the increase in nozzle flow rate enabled a reduction of rail pressure at low- and medium-load points – an important lever for decreasing NO_x emissions.[14,15] Table 2 illustrates the properties of the test engine used. The engine application was the same as in the previous study,[19] with a focus on a higher dynamic of the exhaust gas recirculation (EGR) valve.

After-treatment system and test bench setup

A modular twin-dosing system with an electrically heatable diesel oxidation catalyst (e-DOC), provided by VT Vitesco Technologies Emitec GmbH (Germany), was used for the ATS in this study. The catalysts were connected *via* flanges and pipes. Table 3 shows the properties of the ATS components in sequential downstream order. The e-DOC contained a separate heating disc in front of the platinum (Pt)-palladium (Pd)-coated structure of the DOC monolith. The heating disc had the same coating as the monolith. Two commercial heavy-duty vehicle batteries connected in series at 12 V and 220 Ah each supplied the e-DOC with electrical power. The resulting battery voltage of 24 V and the ohmic resistance of approximately 0.08 Ω resulted in an electrical current of about 300 A. The electrical power of the e-DOC was thus about 7.2 kW. A custom-built controller provided by VT Vitesco Technologies GmbH enabled the heating disc power supply to switch on and off. The designation of "twin dosing design" is derived from the structure of the ATS, which has components for NO_x reduction by means of SCR at

Table 1 Physico-chemical properties of the OME fuel mixture and fossil diesel. The values of diesel are from the standard EN 590[35] except from the LHV and boiling range, which are from Lautenschütz *et al.*[36] and the oxygen content, with the calculation using values from Hoekman *et al.*[37] This calculation assumes the FAME content to consist of oleic acid. ASG Analytik-Service AG measured the values for OME

	Diesel	OME
Oxygen content in % (w/w)	0–1[37] (with max. 7% (v/v) FAME)	45
Lower heating value in MJ kg^{-1}	42.6[36]	19.2
Density in kg m^{-3} at 15 °C	820–845	1057
Volumetric diesel equivalent ratio	1	1.75
Cetane number	>51	69
Boiling range in °C	170–390[36]	145–242
Kinematic viscosity in mm^2 s^{-1} at 40 °C	2.0–4.5	1.082
Lubricity – HFRR at 60 °C in μm	≤460	320
Flash point in °C	>55	65
Sulfur content in ppm	<10	<5
Formaldehyde content in mg kg^{-1}	—	233

Table 2 Properties of the test engine MAN D2676LF51. The injectors in OME operation have a higher nozzle flow rate to reduce the combustion duration at high-load points

Number of cylinders	6 (inline)
Bore	126 mm
Stroke	166 mm
Displacement	12419 cm^3
Compression ratio	18 : 1
Power	294 kW
Number of valves per cylinder	4 (2 inlet/2 exhaust)
Charge	Two-stage waste-gate turbocharger
Exhaust gas recirculation (EGR)	High-pressure & cooled
Injection system	Common rail (max. 1800 bar)
Hydraulic nozzle flow rate	Diesel: 1300 cm^3/30 s (at 100 bar)
	OME: 1835 cm^3/30 s (at 100 bar)

two different positions. In these subsystems, a doser injects aqueous urea solution as a reducing agent for the SCR reaction.

An EMITEC "GEN V" urea dosing pump provided delivery pressure for both dosers simultaneously. The urea dosage took place in an EMITEC "Universal Decomposition Pipe" (UDP) equipped with an EMITEC "JC-2" urea doser and a titanium dioxide (TiO_2) coated hydrolysis catalyst (Hyd), on which the conversion of urea to ammonia (NH_3) took place.[42] A downstream copper-zeolite (CuZe) SCR catalyst reduced NO_x *via* the reducing agent NH_3.[43] This catalyst was divided into three monolithic discs, thus enabling a modular catalyst volume increase or decrease. In the case of excess NH_3, the ammonia slip catalyst (ASC) oxidized this species selectively, thus avoiding the unselective oxidation of NH_3 to nitrous oxide (N_2O) in the downstream DOC,[44] which is desirable since N_2O is known to be a greenhouse gas with an enormous impact on climate change.[1] This DOC contained no heating disc. The downstream diesel particulate filter (DPF) was an uncoated Cordierite wall-flow filter. The second SCR system differed from the first in two major ways. First, the UDP in the second system was followed by a mixer for homogenization of the ammonia in the exhaust,[45] which was necessary given the usage of a different urea doser – an EMITEC "A^2-8" with varying spray targeting. The exhaust temperature was lower at the second SCR stage, which resulted in decreased decomposition of the injected urea.[45] Second, the second SCR catalyst had a larger volume than the one in the first stage, since it contained four monolithic discs instead of three. Moreover, the carrier structure differed slightly from that in the first system. Ideally, the second stage converts the remaining NO_x emissions. In contrast to the first SCR stage, the second stage had no ASC installed. The differences in the design of the two SCR stages resulted from the application to achieve the ultra-low NO_x emissions demonstrated in the previous study.[19]

Urea dosing was active in both SCR stages during the test cycles and considered the same starting temperatures as in standard diesel operation. The dosing strategy was based on ideal distribution between both stages in consideration of the temperature, the ammonia storage capacity, and the determined NO_x concentrations in the exhaust, which was similar to the experiments in the previous study.[19]

Fig. 1 shows a test bench setup scheme. The filtered air from the test bench air supply passes through an ABB MDM DN150 thermal dispersion mass flowmeter. This device determines the volumetric airflow for the calculation of the exhaust mass flow and the space velocity inside the catalysts, respectively. Downstream, another filter avoids contamination of the turbocharger compressor wheel. A two-stage turbocharger system with two intercoolers increases the boost pressure. The six-cylinder engine was equipped with an EGR valve, which controlled high-pressure EGR with intercooling. Two Type K thermocouples, each downstream of the hydrolysis catalysts, enabled monitoring of the exhaust temperature upstream of the respective SCR catalysts. Another thermocouple was installed upstream of the second DOC.

An IAG Versa FAS-05 FT-IR was set up for determining the concentration of the specific chemical species detected in emissions of the above-mentioned previous studies.[4,14,27] The chemical species include CH_4 and CH_2O. Additionally, the FT-IR was configured to measure methanol (CH_3OH), formic acid (CH_2O_2), HCN and several OME_n: dimethyl ether (DME or OME_0), dimethoxymethane (OME_1), and OME with a chain length of $n =$

Table 3 Properties of the ATS components provided by VT Vitesco Technologies Emitec GmbH in downstream order. The value of the Platinum Group Metals (PGM) density refers to the total quantity of the precious metal content. (*) The value of the open frontal area (OFA) is based on the following assumptions: coating of the DOC is 150 g dm^{-3}, coating of the UDP is 60 g dm^{-3} and coating of the SCR is 200 g dm^{-3}, the wash-coat density is 1.35 g cm^{-3} (**) Before the experiments of this study, the DPF had a mileage of about 500 km in diesel operation, but was regenerated in an oven at 500 °C for six hours

Component	Catalytic coating	PGM in g ft^{-3}	cpsi	Diameter in mm	Length in mm	Volume in dm^3	Carrier material	Carrier structure	OFA(*)
e-DOC	Pt, Pd (1 : 1)	35	N/A	285.8	101.5	6.51	Metal	300/600LS	82%
Hyd	TiO_2	—	N/A	174.6	60	1.43	Metal	300/600 LSPE	89%
SCR	CuZe	—	N/A	300	3 × 101.5	21.5	Metal	600 CS	79%
ASC	Pt	3	300	300	90	6.4	Metal	E300	78%
DOC	Pt, Pd (1 : 1)	35	300	300	150	10.6	Metal	300/600 LS	82%
DPF (**)	Uncoated	—	300	305	381	27.8	Cordierite	Symmetrical	83%
Hyd	TiO_2	—	N/A	174.6	60	1.43	Metal	300 PE	89%
SCR	CuZe	—	400	300	4 × 101.5	28.8	Metal	E400	77%

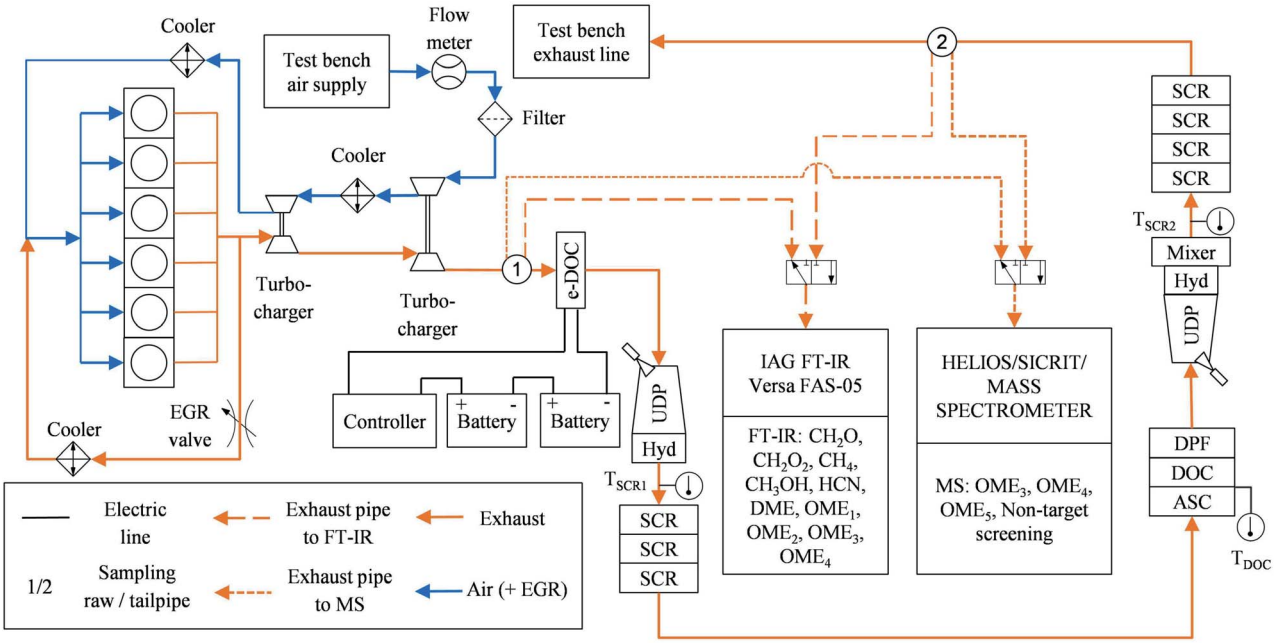

Fig. 1 Test bench setup.

2–4 (OME_2, OME_3, OME_4). Different OME in the exhaust indicate an incomplete combustion, as well as CH_3OH and CH_2O, since they are reactants in OME synthesis.[39] The FT-IR has a standard calibration. Therefore, the detection limits of the chemical species of interest are limited to the general specifications of the manufacturer. Table 2 in the ESI† lists the detection limits of interest. Two sampling points located downstream of the second turbocharger (raw exhaust) and downstream of the second SCR stage (tailpipe exhaust) were utilized for the exhaust samples analyzed using the FT-IR. A 3/2-way solenoid valve enabled switching between the two sampling points.

HELIOS/SICRIT/mass spectrometer

In addition to the FT-IR, the exhaust from the two sampling points was analyzed using the custom-built Mass spectrometer (MS) system described by Thaler *et al.*[46] In short, the MS was composed of a Thermo Fin Finnigan LTQ ion trap mass spectrometer by Thermo Fisher Scientific Inc. (Germany) with a commercially available highly efficient atmospheric ionization source named "soft-ionization by chemical reaction in transfer (SICRIT)" by Plasmion GmbH (Germany).[47] Directly upstream of the SICRIT ion source, a custom-built "high efficient light source for optical surface desorption (HELIOS)" infrared oven was used for evaporation of volatile particle components, thus enabling online detection of both gaseous exhaust species and volatile and semi-volatile aerosols or species absorbed on solid particles. The exhaust samples entered the HELIOS oven through stainless steel tubing heated to 191 °C and diluted by 20% with humidified nitrogen.

Fig. 2a shows a typical mass spectrum of the ambient temperature head space of the OME fuel mixture measured using the MS system. Major mass peaks were at m/z 154, 184, and 214, which correspond to OME_3, OME_4, and OME_5, respectively. These peaks were at [M + 18], where M is the molecular mass of the respective OME_n. The elemental composition of the [M + 18] signal was determined as [M + NH_4^+] with mass deviations below 2 ppm. NH_4^+-adducts were further confirmed by the [M + 22] signal corresponding to [M + ND_4^+] when measured with nitrogen humidified with deuterium oxide (D_2O). Fig. 1 in the ESI† contains this measurement by means of a different high-resolution mass spectrometer (Thermo LTQ Orbitrap XL) coupled with the SICRIT ion source.

Calibration of the HELIOS/SICRIT/MS system for OME was performed in the laboratory using samples of OME_3, OME_4, and OME_5 each, all supplied by ASG Analytik-Service AG. Two different methods were used to introduce known concentrations of each OME into the MS system. The first method utilized a syringe pump (Pico Plus Elite, Harvard Apparatus) for injecting each OME in liquid form into a vaporizer, which was built in-house and was similar to the one described by Herrmann *et al.*[48] The vaporized OME was diluted with humidified nitrogen obtained by bubbling nitrogen (purity 5.0) through a flask filled with distilled water. The nitrogen flow rate was controlled with mass flow controller (Vögtlin red-y smart controller GSC). The second method for introducing known concentrations of OME into the MS system involved the same syringe pump, but, instead of liquid OME the headspace of each OME from a headspace vial was injected into a stream of humidified nitrogen. The concentration of OME in the headspace was determined based on the vapor pressure of each OME as given by Boyd.[49] Both methods yielded consistent signals as measured by the MS system. The measured intensity at the respective mass peak for OME_3, OME_4 and OME_5 are shown in Fig. 2b, which shows the calibration coefficients along with the

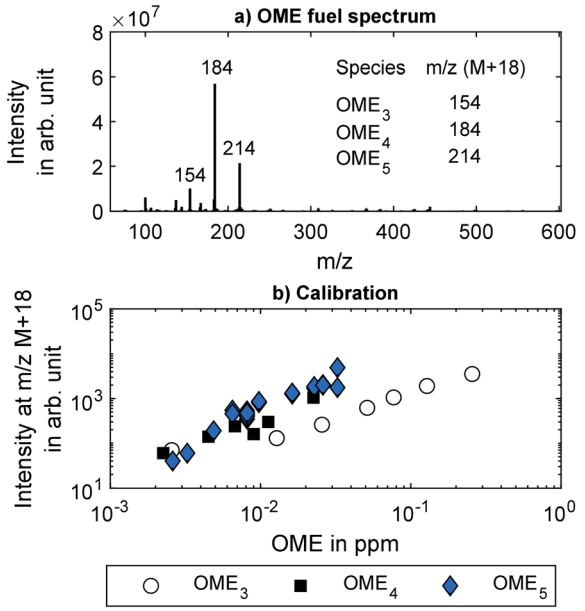

Species	ppm/intensity	σ
OME_3	$7.5471 \cdot 10^{-5}$	$2.1261 \cdot 10^{-5}$
OME_4	$3.5483 \cdot 10^{-5}$	$1.1881 \cdot 10^{-5}$
OME_5	$1.9514 \cdot 10^{-5}$	$1.4150 \cdot 10^{-5}$

Fig. 2 (a) Mass spectrum of OME fuel mixture. (b) Calibration results of the MS used for several polyoxymethylene dimethyl ethers. The calibration factor for each OME is also given, where σ describes the standard deviation of the calibration factor over the multiple measurements. The intensity is given in arbitrary units.

estimated uncertainty. These calibration coefficients were used to quantify the OME concentration in the engine experiments. No calibration was performed for OME_6 because its solid form at room temperature could not be introduced into the syringe pump, and its vapor pressure was too low to recover a sufficiently high concentration from a headspace vial. However, based on the high-resolution mass spectrometer measurements, the mass peak from OME_6 can be expected at m/z 244.

In the engine experiments, the HELIOS/SICRIT/MS system enabled non-target screening for unknown components in the exhaust samples that were not configured in the FT-IR. The MS system can detect only species with a mass-to-charge ratio over m/z 50, meaning that lighter chemical species such as CH_4 and CH_2O cannot be detected. The detection limit of the MS system for heavier species, such as OME, is lower than that of the FT-IR employed in this study. The detection limits of the MS system were found to be 20 ppb, 9 ppb, and 2 ppb for OME_3, OME_4 and OME_5, respectively, which are orders of magnitude lower than the detection limits of the OME concentrations using the FT-IR, as listed in Table 2 in the ESI†.

Test procedure

The test cycle used to investigate the cold-start emissions in OME engine operation was the WHTC, in accordance with UN/ECE Regulation No. 49.[50] The cycle starts at ambient conditions. Since the procedure stipulates that there must be no preconditioning, the various test runs were carried out over the course of several days. The ambient temperatures at all times were approximately 29 °C, with daily deviations of less than 1 °C. After the initial test run, the engine was shut off for a waiting period of ten minutes before starting the next run. In this study, the first and the second run are referred to as "cold" and "hot" runs, respectively. After each hot cycle, the engine performed a clearing out of the SCR system without urea dosage, so every cold run, including the initial one, started with empty ammonia storage of the catalysts. Test runs using the e-DOC start with immediate power supply of the heating disc after start of engine operation. After 20 minutes, the power supply was switched off.

For the application of fuel dosing, the engine used the engine control unit's DPF regeneration mode. In this case, a late post injection (PoI) at 120° crank angle provided fuel for the exothermic reaction at the DOC in a manner similar to the experiments in the previous study.[31] The quantity of PoI (qPoI) in gravimetric diesel equivalent was set to 15 mg/str, which corresponds to about 33.75 mg/str of OME.

During the hot run of the WHTC, both fuel dosing and the e-DOC power supply were switched off.

Since the modular ATS consists of monolithic discs connected *via* flanges and pipes, the heat losses were particularly higher than in a configuration with standard integration in a thermally insulated silencer. Therefore, the evaluation of the effectiveness in heating behavior is limited to qualitative statements in this study.

Results and discussion

OME concentration in engine exhaust determined *via* mass spectrometry

An initial investigation of the engine emissions during the WHTC was performed without applying any methods of ATS heating. In this context, Fig. 3 compares the concentration of OME_3, OME_4, and OME_5 in the engine exhaust during the cold and hot WHTC runs at the raw exhaust and tailpipe exhaust sampling positions, as determined by the MS system. The concentration of OME_3 was the lowest, with a maximum value of 5 ppm overall. OME_3 has the lowest boiling point of the monitored OME_n. For this reason, the evaporation tendency of OME_3 is expected to be higher, especially towards the end of the combustion. According to the property values determined by Lautenschütz *et al.*,[36] the Weber number decreases with increasing OME_n chain length. This dimensionless number describes the fuel droplet decomposition during the injection by putting the drag force and cohesion force on the interface of two different fluids in proportion. The decreasing Weber number indicates a reduced droplet decay with increasing OME_n chain length. The ignitibility is to be excluded as a causal factor because it increases with the chain length of OME_n.[36,51] The maximum values of the OME_4 and OME_5 concentrations were 36 ppm and 35 ppm, respectively. The difference between the cold and hot runs was marginal for all three species,

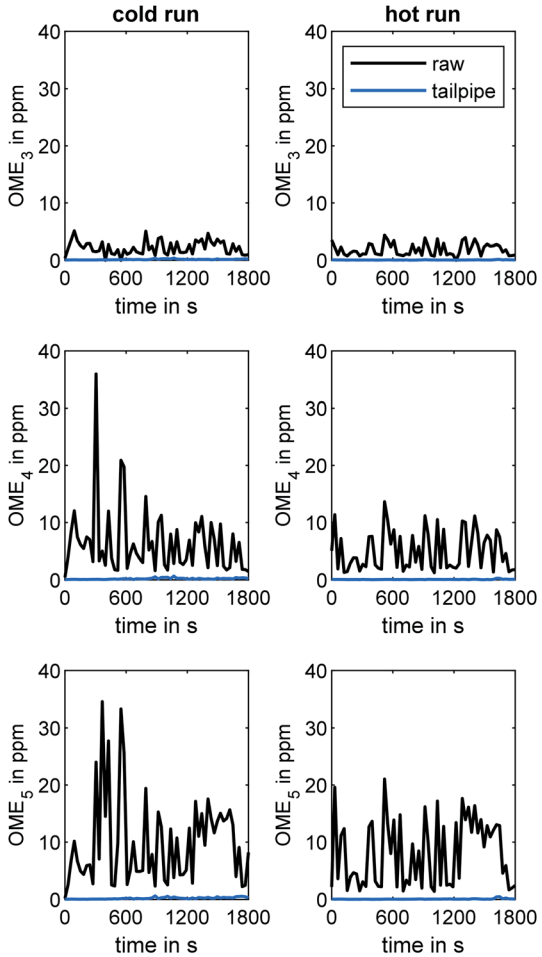

Fig. 3 Concentrations of OME_3, OME_4, and OME_5 in the engine exhaust during the WHTC cold and hot runs at the two sampling positions (raw and tailpipe sampling).

although the peak concentration of OME_4 and OME_5 in the raw exhaust was higher during the cold run. However, the difference between raw and tailpipe sampling is clearer than the difference between the cold and hot runs. Whereas the concentrations of all three OME species were in the range of several ppm in the raw exhaust, the concentrations did not exceed 1 ppm for any of the species when analyzed at the tailpipe position. Elsener *et al.* demonstrated the high hydrolysis activity of OME_3 on several catalytic surfaces.[52] Therefore, adsorption and reaction *via* hydrolysis or oxidation during the flow through the ATS was likely, since the ATS contained two TiO_2 catalysts and three Pt(-Pd)-coated catalysts.

Non-target screening

Fig. 4 shows the mass spectra at all times during the WHTC cold and hot test runs, presenting the results of the non-target screening analysis.

Like in Fig. 3, clear differences between raw and tailpipe emissions appear, whereas the differences between the cold and hot runs at both sampling positions were not clearly differentiable. At the raw exhaust position, intensity maxima are seen at

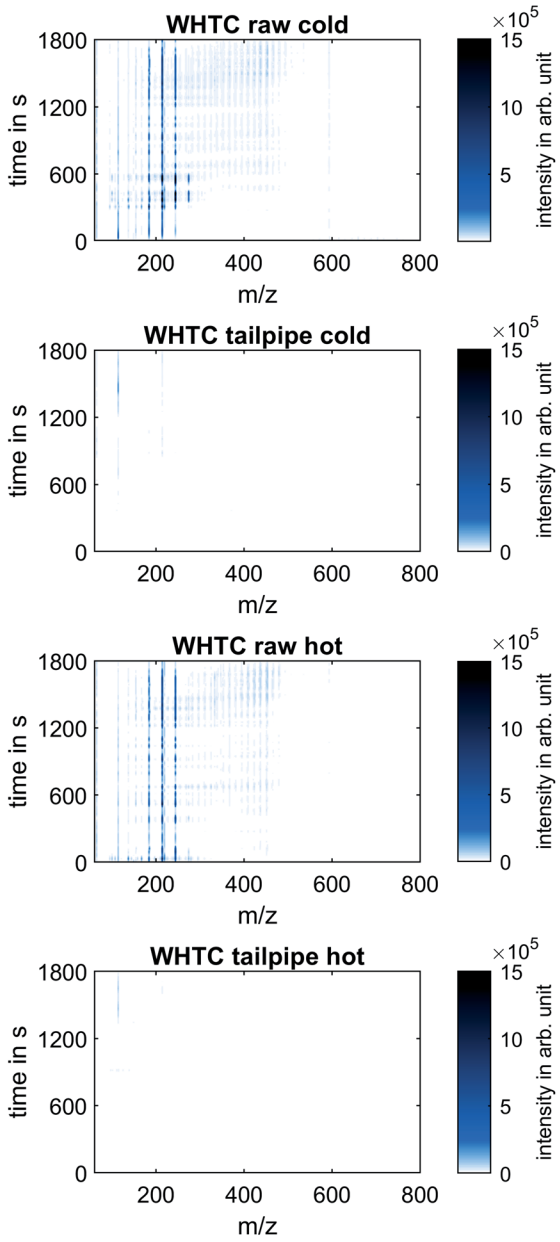

Fig. 4 Mass spectra of the non-target screening analysis with the maximum peaks of the sample from the raw exhaust shown at the *m*/*z* values corresponding to OME_4, OME_5, and OME_6. The intensity is given in arbitrary unit.

m/*z* 184, 214, and 244, suggesting that of OME_4, OME_5, and OME_6 formed the majority of the high-mass species in the exhaust gas. During the cold run, mass peaks also appeared at *m*/*z* 124 and *m*/*z* 274 in the raw exhaust, indicating the presence of OME_2 and OME_7 as well. In both the cold and the hot run, intensity peaks at *m*/*z* 114 stood out from the rest of the spectra at the tailpipe position towards the end of the WHTC, after approximately 1200 seconds. The high signal at *m*/*z* 114 was more pronounced in cold operation than in hot operation. In both cases, however, the maximum intensity of the *m*/*z* 114 trace was an order of magnitude lower than the signal intensity

of the mass peaks corresponding to unburned OME. Although the identity of the species generating the mass peak at m/z 114 was not able to be determined with the current MS system (a higher resolution mass spectrometer would be needed), the mass peak at m/z 114 has appeared in measurements in the same engine operated using fossil diesel fuel. Therefore, this substance is unlikely to be an unknown product of OME combustion, but further identification of this peak remains necessary. In summary, the mass spectra from both the cold and the hot runs, as well as both the raw exhaust and tailpipe exhaust sampling positions over the entire range of measured mass-to-charge ratios and measurement time, showed no signal intensities on a similar order of magnitude as the detected unburned OME in the raw exhaust. This result justifies the following focus on lightweight species known to occur in OME combustion, which include CH_2O, CH_4 and HCN as byproducts in exhaust after-treatment. The concentration of these species can be determined by means of the FT-IR.

Gaseous emissions determined *via* FT-IR

Fig. 5 presents the concentration of key species in the tailpipe exhaust measured with FT-IR during both WHTC runs. As already revealed by Gelner *et al.*, a higher EGR valve dynamic leads to CH_4 concentration peaks in the exhaust, due to the CH_4-NO_x-trade-off in an OME engine.[19] The CH_4 concentration peaks are more frequent during hot operation because the EGR valve remains closed during the cold-start operation. However, the integrated cycle result of the hot run regarding CH_4 concentration in the tailpipe exhaust is 7 ppm. Reduction of the concentration of CH_4 in future OME engine application would be desirable since CH_4 is a greenhouse gas.[1,53] CH_2O emission was also of interest in this study given its toxic effect on human health.[54] The effect of a hot ATS is clear from the results in Fig. 5. Whereas CH_2O appeared at concentrations of up to 41 ppm after a cold ATS during the cold run, the maximum value of the peak CH_2O concentration during hot operation was only 17 ppm. The WHTC cycle evaluation results were 9 ppm in cold operation and 1 ppm in hot operation. The exhaust concentration of CH_2O_2 – the first oxidation stage of CH_2O – exhibited the same behavior as seen with CH_2O, but at lower concentrations. The measured HCN concentration remained under 1.2 ppm in cold-start operation and was slightly lower in hot operation. The higher signal in the first part of the cold run may have been caused by the formation of small amounts of HCN due to residues of NH_3 on the SCR catalyst,[29] remaining after the clearing process prior to the test run. The effect of HCN formation might be more pronounced in repeated runs with cold-start operation occurring in road operation without clearing procedures. Furthermore, an investigation of intermediate products, as observed by Nuguid *et al.*,[55] would be necessary in order to generate a full assessment of the processes in the SCR system. However, since the HCN concentration signal was below the general FT-IR detection limit of 1.5 ppm provided by the manufacturer in Table 2 in the ESI†, the strategy of combining oxidative catalysts upstream and downstream of the SCR stage proved to be effective.

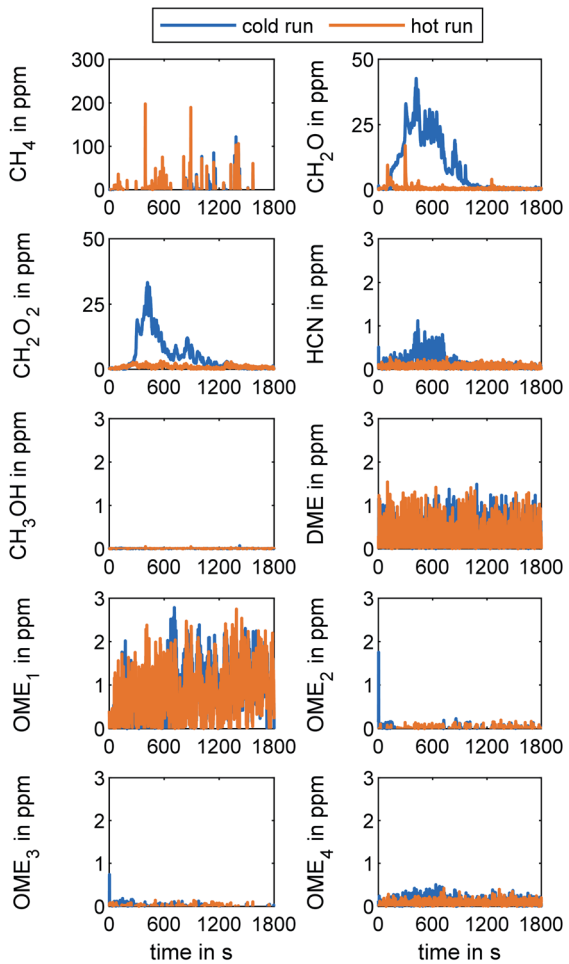

Fig. 5 Gaseous tailpipe emissions during WHTC cycle determined *via* FT-IR.

Regarding CH_3OH, DME, and OME_{1-4} as precursors of incomplete OME combustion, the tailpipe concentration was below 3 ppm regardless of cold or hot operation. This result agreed with the measurements using the MS system shown in Fig. 3. Gaiser *et al.* observed high concentrations of ethanol during OME combustion, as well as acetaldehyde and methyl formate.[56] The FT-IR used in this work did not include this species in the specific method, so further investigations regarding the products of incomplete OME combustion in addition to CH_4, CH_3OH, CH_2O, CH_2O_2, and OME_{0-6} will be necessary.

Since the concentration of CH_2O, CH_2O_2, and HCN in the exhaust were all higher in cold-start operation than in the hot run, methods for reducing the duration of the ATS heating period when the catalysts are below their light-off temperature are essential to reducing the overall concentration of these species during typical on-road engine operation. Furthermore, NO_x reduction *via* SCR also requires an operational hot system for urea dosing.

After-treatment system heating

Four cold runs of the WHTC comprised the current study on ATS heating methods. A run without an e-DOC served as

a baseline and enabled qualitative evaluation of the effectiveness of three different ATS heating methods. For the baseline run, the e-DOC was removed completely. The three runs using the electrical heating function of the e-DOC differed in PoI strategy: one run was without PoI, one run was with a PoI start at a temperature downstream of the first Hyd of $T_{SCR1} = 230$ °C, and one run had a later PoI start at a temperature of $T_{SCR1} = 280$ °C. The PoI ended at a temperature of the second SCR stage of $T_{SCR2} = 230$ °C. Fig. 6 depicts the results for the four runs using different ATS heating methods. The different path lengths to the respective catalysts delayed the heating effects of the various ATS heating methods. Whereas the energization of the e-DOC was noticeable by a temperature difference of 20 °C at the point of T_{SCR1} after 129 s, T_{SCR2} reached this value after 1146 s. After 635 s, the PoI with the threshold from $T_{SCR1} = 230$ °C started and the PoI with the threshold from $T_{SCR1} = 280$ °C started after 837 s. The run with the earlier PoI reached the termination criterion for the PoI ($T_{SCR2} = 230$ °C) after 1012 s, and the run with a later PoI did so after 1095 s. The run having only the e-DOC energized reached this temperature level after 1587 s. The run with lower temperature threshold for start of PoI generated a higher CH_2O slip through the ATS than the other runs. The CH_2O concentration of the run with a higher temperature threshold was at the level of the runs without PoI. In this run, at the beginning of fuel dosing, the temperature level upstream of the two DOCs was higher, so the catalytic conversion of CH_2O formed by PoI was higher.[31] A later start of fuel dosing thus reduced the length of the cold-start phase without additional CH_2O slip, albeit with a higher heating time than in a run with earlier start of PoI.

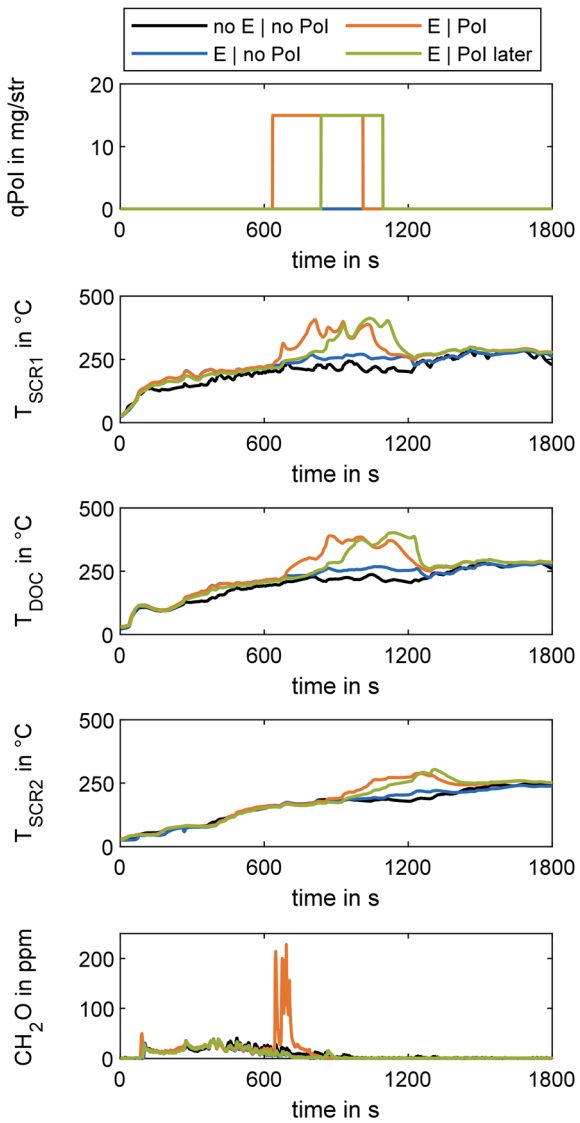

Fig. 6 Comparison of different ATS temperatures using different measures of ATS heating. qPoI is given in gravimetric diesel equivalent; temperatures of the catalysts determined *via* thermocouples; CH_2O determined *via* FT-IR at tailpipe position. e-DOC electrification starts with engine start and ends after 20 minutes. PoI starts at $T_{SCR1} = 230$ °C and 280 °C respectively. PoI ends at $T_{SCR2} = 230$ °C.

Table 4 Reduction of NO_x exhaust concentration during WHTC procedure due to the respective ATS heating method, as compared to the baseline measurement. The overall evaluation includes weighting of cold and hot run in accordance to UN/ECE R49[50]

NO_x emissions reduction in WHTC	Cold run	Overall evaluation
Without e-DOC	Baseline	Baseline
With e-DOC | No PoI	22.7%	47.7%
With e-DOC | PoI 230 °C	41.3%	64.9%
With e-DOC | PoI 280 °C	36.0%	61.8%

Table 4 shows the respective reduction of NO_x emission concentration levels for three different ATS heating methods. The reduction is provided in comparison to the baseline cold run and the overall evaluation of the WHTC for both baseline cold run and baseline hot run without ATS heating, respectively. The result of the WHTC evaluation, in mg kW^{-1} h^{-1}, was in accordance with UN/ECE R49.[50] This data enables evaluation of the effect of the ATS heating methods regarding NO_x reduction of the SCR system, due to higher efficiency and an earlier start of urea dosing.

Using e-DOC energizing and fuel dosing with a start of PoI at $T_{SCR1} = 230$ °C reduced the NO_x emissions by 41.3% as compared to the baseline cold run. Due to the higher temperature of the ATS at the start of the hot run, this reduced the overall NO_x concentration in the exhaust during the overall WHTC procedure by 64.9%. This reduction comes at a cost of a higher CH_2O concentration of 90.5% in the cold run and 58.3% overall, as compared to the baseline. A later start of fuel dosing enables a 36.0% reduction of NO_x as compared to the baseline cold run and a 61.8% reduction overall; the rise in CH_2O concentration is below 4.8% in comparison to the baseline cold run and below 0.1% in comparison to the overall evaluation and, therefore negligible. Single use of the e-DOC reduces NO_x emissions by 22.7% and 47.7% as compared to the baseline cold run and overall, respectively. Since the heat losses of the ATS in the modular configuration used in this work were higher than with a thermally insulated silencer, the advantages in a system ready for series production are assumed to be higher.

Conclusions and outlook

The present work contains experimental studies on the gaseous emissions and effectiveness of ATS heating measures during cold-start operation of a heavy-duty engine fueled with OME.

Measurements from the MS system of the concentration of different OME chain lengths in the raw and tailpipe exhaust enable evaluation of the effectiveness of the ATS in cold-start and hot-start operation. A non-target screening analysis performed using the same MS system suggests that no unknown heavy species derived from the combustion of OME were present in the exhaust gas at similar levels to the unburned OME. Concentration measurements of key species using the FT-IR reveal the differences between cold-start and hot-start transient operation. The comparison of the use of an electrical heatable DOC and fuel dosing clarifies the potential of methods to reduce the length of the cold-start phase. The results are summed up in the following conclusions:

In both the cold and hot operation during the WHTC, the concentration of OME_3, OME_4, and OME_5 measured with the calibrated MS system in the tailpipe exhaust do not exceed 1 ppm. The authors assume that adsorption, hydrolysis, and oxidation processes in the ATS are responsible for this result.

The non-target screening analysis *via* the MS system confirmed that the most dominant species in the exhaust are OME_n. No partially oxidized products were present in the exhaust at levels on the same order of magnitude. This result justifies a focus on the known pollutant emissions formed in OME exhaust such as CH_4 or CH_2O.

In both cold and hot operation, the tailpipe concentration of HCN remains below the given detection limit of the FT-IR used. Further experiments will be necessary in order to evaluate the processes during on-road operation, as well as using different SCR configurations. Differences in the performance of the CuZe catalysts used and SCR catalysts based on vanadium may occur in addition to differences due to different ammonia storage levels of the catalyst.

During cold-start operation, an engine fueled with OME primarily emits, besides NO_x, CH_2O and CH_2O_2 as long as the oxidation activity of the catalysts is inhibited. Further research on the formation processes of these species and in-engine methods for reducing the concentration of these species is necessary.

Fuel dosing in combination with an electrically heatable DOC is an effective method of shortening the cold-start phase in OME operation and enables earlier start of urea dosing and therefore NO_x reduction. An early start of fuel dosing with inhibited oxidation activity of the catalysts due to lower temperature leads to a CH_2O slip. Avoidance of the slip is possible by a later fuel dosing start but at the cost of a later NO_x reduction start.

By means of the configuration in this study, the NO_x emissions during a WHTC procedure are reduced by 64.9% using an e-DOC and fuel dosing, but with a CH_2O increase of 58.3%. With an increase in CH_2O emission of less than 0.1%, the NO_x reduction is 61.8%. Operation with the e-DOC without PoI enables a reduction in NO_x emission by 47.7%.

These conclusions are based on the experimental results of this work. Further studies will be necessary in order to validate the observed behavior and reduction potential with a thermally insulated ATS in a silencer. Furthermore, the potential of OME regarding NO_x reduction by way of an applied EGR strategy[19] and the increase in SCR performance by fuel dosing and electrical heating demonstrated in this work enable simplification of the ATS back to a one-stage SCR system, thus improving economic efficiency. Additionally, omission of the DPF by virtue of the low particle emission of an OME engine[57] reduces complexity and offers advantages in the cold-start phase with respect to ATS heating. Since the experiments in this study took place during summer at moderate ambient temperatures, further experiments with lower starting temperatures – *e.g.* temperatures below 0 °C – will be necessary for a holistic approach. Furthermore, the interactions of OME with components in contact with fuel should be investigated with regard to corrosion in long-term studies. Jin *et al.* observed increasing corrosion with increasing amounts of OME in a blend with methanol, palm oil and palm kernel oil.[58]

Author contributions

Alexander D. Gelner: conceptualization, data curation, formal analysis, investigation, methodology, project administration, validation, visualization, writing – original draft, writing – review & editing. Genny A. Pang: conceptualization, data curation, formal analysis, investigation, methodology, validation, writing – original draft, writing – review & editing. Christoph Haisch: conceptualization, funding acquisition, project administration, supervision, writing – review & editing. Harald A. Beck: validation, formal analysis, data curation, writing – review & editing. Christian Pastoetter: conceptualization, funding acquisition, project administration, supervision, writing – review & editing. Martin Härtl: funding acquisition, project administration, supervision, writing – review & editing. Malte Jaensch: writing – review & editing. Georg Wachtmeister: funding acquisition, project administration, supervision, writing – review & editing.

Conflicts of interest

The authors declare that they have no known competing financial interests or personal relationship that could have appeared to influence the work reports in this paper.

Definitions and abbreviations

ASC	ammonia slip catalyst
ATS	after-treatment system
BHT	butylated hydroxytoluene
CuZe	copper zeolite
DME	dimethyl ether (OME_0)
DOC	diesel oxidation catalyst

DPF	diesel particulate filter
e-DOC	electrically heatable diesel oxidation catalyst
FAME	fatty acid methyl esters
FT-IR	Fourier-transform infrared spectrometer
HELIOS	high efficient light source for optical surface desorption
Hyd	hydrolysis catalyst
LHV	lower heating value
MS	mass spectrometer
OFA	open frontal area
OME	polyoxymethylene dimethyl ethers
OME_1	methylal (dimethoxymethane)
OMEn	polyoxymethylene dimethyl ether of the chain length n
PGM	platinum group metals
PoI	post injection
ppm	parts per million
qPoI	quantity of post injection
SCR	selective catalytic reduction
SICRIT	soft-ionization by chemical reaction in transfer
UDP	Universal Decomposition Pipe
WHTC	World Harmonized Transient Cycle
σ	standard deviation

Acknowledgements

The research was part of the project "Sub-Zero-Emissions Dieselmotor", funded by the Bavarian Research Foundation (grant number AZ-1266-17). The project was carried out in collaboration with MAN Truck & Bus SE, VT Vitesco Technologies Emitec GmbH, Chair of Analytical Chemistry of TUM and ASG Analytik-Service AG. Their support is gratefully acknowledged. The authors also want to thank Dr Dieter Rothe, Dipl.-Ing. Florian Lindner (both MAN Truck & Bus SE) and Martin Elsener (Paul Scherrer Institute) for their support and consultation in this study.

References

1 *Climate change 2014: Synthesis report*, ed. Pachauri RK and Meyer L, Intergovernmental Panel on Climate Change, Geneva, Switzerland, 2015.
2 *Renewable Energy Sources and Climate Change Mitigation: Special Report of the Intergovernmental Panel on Climate Change*, ed. Edenhofer O, Pichs-Madruga R and Sokona Y, Intergovernmental Panel on Climate Change, 2012.
3 S. Schemme, J. L. Breuer, M. Köller, S. Meschede, F. Walman, R. C. Samsun, *et al.* H2-based synthetic fuels: A techno-economic comparison of alcohol, ether and hydrocarbon production, *Int. J. Hydrogen Energy*, 2020, **45**(8), 5395–5414.
4 M. Härtl, P. Seidenspinner, E. Jacob and G. Wachtmeister, Oxygenate screening on a heavy-duty diesel engine and emission characteristics of highly oxygenated oxymethylene ether fuel OME1, *Fuel*, 2015, **153**, 328–335.
5 S. Schemme, R. C. Samsun, R. Peters and D. Stolten, Power-to-fuel as a key to sustainable transport systems – An analysis of diesel fuels produced from CO 2 and renewable electricity, *Fuel*, 2017, **205**, 198–221.
6 M. Held, Y. Tönges, D. Pélerin, M. Härtl, G. Wachtmeister and J. Burger, On the energetic efficiency of producing polyoxymethylene dimethyl ethers from CO 2 using electrical energy, *Energy Environ. Sci.*, 2019, **12**(3), 1019–1034.
7 L. Pellegrini, M. Marchionna, R. Patrini, C. Beatrice, N. Del Giacomo, and C. Guido. Combustion Behaviour and Emission Performance of Neat and Blended Polyoxymethylene Dimethyl Ethers in a Light-Duty Diesel Engine, in, *SAE Technical Paper Series. SAE International400 Commonwealth Drive*, Warrendale, PA, United States, 2012, SAE Technical Paper Series.
8 L. Pellegrini, M. Marchionna, R. Patrini and S. Florio. Emission Performance of Neat and Blended Polyoxymethylene Dimethyl Ethers in an Old Light-Duty Diesel Car, in, *SAE Technical Paper Series. SAE International400 Commonwealth Drive*, Warrendale, PA, United States, 2013, SAE Technical Paper Series.
9 S. E. Iannuzzi, C. Barro, K. Boulouchos and J. Burger, Combustion behavior and soot formation/oxidation of oxygenated fuels in a cylindrical constant volume chamber, *Fuel*, 2016, **167**, 49–59.
10 A. Damyanov, P. Hofmann, B. Geringer, N. Schwaiger, T. Pichler and M. Siebenhofer, Biogenous ethers: production and operation in a diesel engine, *Automot. Engine Technol.*, 2018, **3**(1–2), 69–82.
11 H. Ogawa, N. Miyamoto, M. Yagi. Chemical-Kinetic Analysis on PAH Formation Mechanisms of Oxygenated Fuels. in: *SAE Technical Paper Series. SAE International400 Commonwealth Drive*, Warrendale, PA, United States, 2003, SAE Technical Paper Series.
12 C. J. L. Murray, A. Y. Aravkin, P. Zheng, C. Abbafati, K. M. Abbas, M. Abbasi-Kangevari, *et al.* Global burden of 87 risk factors in 204 countries and territories, 1990–2019: a systematic analysis for the Global Burden of Disease Study 2019, *Lancet*, 2020, **396**(10258), 1223–1249.
13 T. C. Bond, S. J. Doherty, D. W. Fahey, P. M. Forster, T. Berntsen, B. J. DeAngelo, *et al.* Bounding the role of black carbon in the climate system: A scientific assessment, *J. Geophys. Res.: Atmos.*, 2013, **118**(11), 5380–5552.
14 D. Pélerin, K. Gaukel, M. Härtl, E. Jacob and G. Wachtmeister, Potentials to simplify the engine system using the alternative diesel fuels oxymethylene ether OME1 and OME3−6 on a heavy-duty engine, *Fuel*, 2020, **259**, 116231.
15 D. Pélerin, K. Gaukel, M. Härtl, G. Wachtmeister. Nitrogen Oxide Reduction Potentials Using Dimethyl Ether and Oxymethylene Ether in a Heavy-Duty Diesel Engine, in, *SAE Technical Paper Series. SAE International400 Commonwealth Drive*, Warrendale, PA, United States; 2020, SAE Technical Paper Series.
16 S. Pöllmann, M. Härtl and G. Wachtmeister, Potential of miller timing with synthetic diesel fuels on a single cylinder heavy-duty engine, *Int. J. Engine Res.*, 2021, 146808742110436.

17 B. Gaston, J. M. Drazen, J. Loscalzo and J. S. Stamler, The biology of nitrogen oxides in the airways, *Am. J. Respir. Crit. Care Med.*, 1994, **149**(2 Pt 1), 538–551.
18 K. Li, L. Chen, S. J. White, K. Han, B. Lv, K. Bao, *et al.* Effect of nitrogen oxides (NO and NO 2) and toluene on SO 2 photooxidation, nucleation and growth: A smog chamber study, *Atmos. Res.*, 2017, **192**, 38–47.
19 A. D. Gelner, H. A. Beck, C. Pastoetter, M. Härtl and G. Wachtmeister, Ultra-low emissions of a heavy-duty engine powered with oxymethylene ethers (OME) under stationary and transient driving conditions, *Int. J. Engine Res.*, 2021, 146808742110479.
20 L. Yang, V. Franco, P. Mock, R. Kolke, S. Zhang, Y. Wu, *et al.* Experimental Assessment of NOx Emissions from 73 Euro 6 Diesel Passenger Cars, *Environ. Sci. Technol.*, 2015, **49**(24), 14409–14415.
21 R. Williams, J. Andersson, H. Hamje, P. Ziman, K. Kar and C. Fittavolini *et al.* Impact of Demanding Low Temperature Urban Operation on the Real Driving Emissions Performance of Three European Diesel Passenger Cars, in, *SAE Technical Paper Series. SAE International400 Commonwealth Drive*, Warrendale, PA, United States, 2018, SAE Technical Paper Series.
22 C. Dardiotis, G. Martini, A. Marotta and U. Manfredi, Low-temperature cold-start gaseous emissions of late technology passenger cars, *Atmos. Res.*, 2013, **111**, 468–478.
23 A. Broatch, B. Tormos, P. Olmeda and R. Novella, Impact of biodiesel fuel on cold starting of automotive direct injection diesel engines, *Energy*, 2014, **73**, 653–660.
24 M. Weilenmann, P. Soltic, C. Saxer, A.-M. Forss and N. Heeb, Regulated and nonregulated diesel and gasoline cold start emissions at different temperatures, *Atmos. Environ.*, 2005, **39**(13), 2433–2441.
25 A. S. Ramadhas and H. Xu, Cold start particle number, size and mass emissions from a CRDI diesel engine running on biodiesel blends in a cold environment, *Biofuels*, 2016, **7**(4), 353–363.
26 R. Suarez-Bertoa and C. Astorga, Impact of cold temperature on Euro 6 passenger car emissions, *Environ. Pollut.*, 2018, **234**, 318–329.
27 C. Barro, M. Parravicini, K. Boulouchos and A. Liati, Neat polyoxymethylene dimethyl ether in a diesel engine; part 2: Exhaust emission analysis, *Fuel*, 2018, **234**, 1414–1421.
28 D. Zengel, P. Koch, B. Torkashvand, J.-D. Grunwaldt, M. Casapu and O. Deutschmann, Emission of Toxic HCN During NOx Removal by Ammonia SCR in the Exhaust of Lean-Burn Natural Gas Engines, *Angew. Chem., Int. Ed. Engl.*, 2020, **59**(34), 14423–14428.
29 M. Elsener, R. J. G. Nuguid, O. Kröcher and D. Ferri, HCN production from formaldehyde during the selective catalytic reduction of NOx with NH3 over V2O5/WO3-TiO2, *Appl. Catal., B*, 2021, **281**, 119462.
30 J. Gao, G. Tian, A. Sorniotti, A. E. Karci and R. Di Palo, Review of thermal management of catalytic converters to decrease engine emissions during cold start and warm up, *Appl. Therm. Eng.*, 2019, **147**, 177–187.
31 A. D. Gelner, C. Pastoetter, H. A. Beck, M. Härtl, G. Wachtmeister Fuel Dosing on a Diesel Oxidation Catalyst for After-Treatment System Heating on a Heavy-Duty Engine Powered by Polyoxymethylene Dimethyl Ethers, in, *SAE Technical Paper Series. SAE International400 Commonwealth Drive*, Warrendale, PA, United States, 2020, SAE Technical Paper Series.
32 K. Nakano, H. Okano, K. Inoue, A. Obuchi Study on the Prevention of Face-Plugging of Diesel Oxidation Catalyst (DOC), in, *SAE Technical Paper Series. SAE International400 Commonwealth Drive*, Warrendale, PA, United States, 2018, SAE Technical Paper Series.
33 W. Maus, R. Brück, R. Konieczny and A. Scheeder, Electrically heated catalyst for thermal management in modern vehicle applications, *MTZ Worldw*, 2010, **71**(5), 34–39.
34 DIN/TS 51699 – Fuels – Polyoxymethylene dimethyl ether (OME): Draft German Standard.
35 *DIN EN 590:2017-10, Kraftstoffe_- Dieselkraftstoff_- Anforderungen und Prüfverfahren; Deutsche Fassung EN_590:2013+A1:2017*. Berlin: Beuth Verlag GmbH.
36 L. Lautenschütz, D. Oestreich, P. Seidenspinner, U. Arnold, E. Dinjus and J. Sauer, Physico-chemical properties and fuel characteristics of oxymethylene dialkyl ethers, *Fuel*, 2016, **173**, 129–137.
37 S. K. Hoekman, A. Broch, C. Robbins, E. Ceniceros and M. Natarajan, Review of biodiesel composition, properties, and specifications, *Renewable Sustainable Energy Rev.*, 2012, **16**(1), 143–169.
38 A. D. Gelner, R. Höß, A. Zepf, M. Härtl, G. Wachtmeister. Engine Operation Strategies for the Alternative Diesel Fuel Oxymethylene Ether (OME): Evaluation Based on Injection Rate Analyzer and 0D-/1D-Simulation, in, *SAE Technical Paper Series. SAE International400 Commonwealth Drive*, Warrendale, PA, United States, 2021, SAE Technical Paper Series.
39 J. Burger, M. Siegert, E. Ströfer and H. Hasse, Poly(oxymethylene) dimethyl ethers as components of tailored diesel fuel: Properties, synthesis and purification concepts, *Fuel*, 2010, **89**(11), 3315–3319.
40 I. Bogatykh, T. Osterland, H. Stein and T. Wilharm, Investigation of the Oxidative Degradation of the Synthetic Fuel Oxymethylene Dimethyl Ether, *Energy Fuels*, 2020, **34**(3), 3357–3366.
41 C. Barro, M. Parravicini and K. Boulouchos, Neat polyoxymethylene dimethyl ether in a diesel engine; part 1: Detailed combustion analysis, *Fuel*, 2019, **256**, 115892.
42 S. D. Yim, S. J. Kim, J. H. Baik, I. Nam, Y. S. Mok, J.-H. Lee, *et al.* Decomposition of Urea into NH 3 for the SCR Process, *Ind. Eng. Chem. Res.*, 2004, **43**(16), 4856–4863.
43 M. Koebel, M. Elsener and T. Marti, NO x -Reduction in Diesel Exhaust Gas with Urea and Selective Catalytic Reduction, *Combust. Sci. Technol.*, 1996, **121**(1–6), 85–102.
44 K. Kamasamudram, C. Henry, N. Currier and A. Yezerets, N 2 O Formation and Mitigation in Diesel Aftertreatment Systems, *SAE Int. J. Engines*, 2012, **5**(2), 688–698.

45 F. Birkhold, U. Meingast, P. Wassermann and O. Deutschmann, Modeling and simulation of the injection of urea-water-solution for automotive SCR DeNOx-systems, *Appl. Catal., B*, 2007, **70**(1–4), 119–127.

46 K. M. Thaler, L. Gilardi, M. Weber, A. Vohburger, Z. Toumasatos, A. Kontses, *et al.* HELIOS/SICRIT/mass spectrometry for analysis of aerosols in engine exhaust, *Aerosol Sci. Technol.*, 2021, **55**(8), 886–900.

47 J.-C. Wolf, M. Schaer, P. Siegenthaler and R. Zenobi, Direct quantification of chemical warfare agents and related compounds at low ppt levels: comparing active capillary dielectric barrier discharge plasma ionization and secondary electrospray ionization mass spectrometry, *Anal. Chem.*, 2015, **87**(1), 723–729.

48 F. Herrmann, B. Jochim, P. Oßwald, L. Cai, H. Pitsch and K. Kohse-Höinghaus, Experimental and numerical low-temperature oxidation study of ethanol and dimethyl ether, *Combust. Flame*, 2014, **161**(2), 384–397.

49 R. H. Boyd, Some physical properties of polyoxymethylene dimethyl ethers, *J. Polym. Sci.*, 1961, **50**(153), 133–141.

50 *Regulation No 49 of the Economic Commission for Europe of the United Nations (UN/ECE) – Uniform provisions concerning the measures to be taken against the emission of gaseous and particulate pollutants from compression-ignition engines and positive ignition engines for use in vehicles*; 2013.

51 L. Lautenschütz, D. Oestreich, P. Seidenspinner, U. Arnold, E. Dinjus and J. Sauer, Corrigendum to "Physico-chemical properties and fuel characteristics of oxymethylene dialkyl ethers" [Fuel 173 (2016) 129–137], *Fuel*, 2017, **209**, 812.

52 M. Elsener, D. Ferri, E. Jacob and O. Kröcher, Stability and reactivity of a polyoxymethylene dimethyl ether over typical catalysts of Diesel emission control: Manuscript in peer-review, *Top. Catal.*, 2022.

53 M. Etminan, G. Myhre, E. J. Highwood and K. P. Shine, Radiative forcing of carbon dioxide, methane, and nitrous oxide: A significant revision of the methane radiative forcing, *Geophys. Res. Lett.*, 2016, **43**(24), 12614–12623.

54 M. H. Fischer, The toxic effects of formaldehyde and formalin, *J. Exp. Med.*, 1905, **6**(4–6), 487–518.

55 R. J. G. Nuguid, M. Elsener, D. Ferri and O. Kröcher, Operando diffuse reflectance infrared detection of cyanide intermediate species during the reaction of formaldehyde with ammonia over V_2O_5/WO_3–TiO_2, *Appl. Catal., B*, 2021, **298**, 120629.

56 N. Gaiser, T. Bierkandt, P. Oßwald, J. Zinsmeister, T. Kathrotia, S. Shaqiri, *et al.* Oxidation of oxymethylene ether (OME0−5): An experimental systematic study by mass spectrometry and photoelectron photoion coincidence spectroscopy, *Fuel*, 2021, 122650.

57 A. D. Gelner, D. Rothe, C. Kykal, M. Irwin, A. Sommer, C. Pastoetter, *et al.* Particle emissions of a heavy-duty engine fueled with polyoxymethylene dimethyl ethers (OME), *Environ. Sci.: Atmos.*, 2022, (2), 291–304.

58 C. Jin, X. Liu, T. Sun, J. D. Ampah, Z. Geng, J. Ji, *et al.* Preparation and performance improvement of methanol and palm oil/palm kernel oil blended fuel, *Fuel Process. Technol.*, 2021, **223**, 106996.